Ground deformation associated with tunnelling and deep excavations in clay, with particular reference to London clay

Myrianthis, Michael L.

GROUND DEFORMATION ASSOCIATED WITH TUNNELLING AND DEEP EXCAVATIONS IN CLAY, WITH PARTICULAR REFERENCE TO LONDON CLAY

by

MICHAEL L. MYRIANTHIS

being a Thesis submitted to the Faculty of Science,
University of Durham for the fulfilment of the
Ph.D. degree.

DURHAM, ENGLAND 5th MAY, 1975.

ABSTRACT.

This work is mainly directed towards problems of ground stability and ground deformations caused by tunnelling and deep excavation in clay.

The particular question of surface settlement associated with soft ground tunnelling has been critically examined. Derivation of semi-empirical relationships has facilitated settlement prediction.

A detailed analysis has been carried out on the results of an extensive research programme of in-situ measurements aimed at determining ground movements created by

a) hand excavation of a 4.146m diameter shield-driven tunnel at a depth of 29.3m below ground surface, and

b) the excavation of a 6.1m long, 0.8m wide and 15m deep bentonite slurry-supported diaphragm wall.

Both engineering structures were situated in the stiff fissured, over-consolidated London Clay.

The stress-strain regime around the tunnel and behind the diaphragm wall was examined, and a theoretical analysis was attempted in order to provide an explanation for the actual performance of both structures during the early stages of construction.

ACKNOWLEDGEMENTS.

The work described in this thesis was carried out in the Engineering Geology Laboratories of the University of Durham under the direction of Dr. P.B. Attewell, Reader in Engineering Geology, whose help, constructive criticism and critical reading of the manuscripts are gratefully acknowledged. The author also expresses his debt to Dr. I.W. Farmer, Lecturer in Engineering Geology, particularly for his help during field-work in London.

The field measurement work outlined in the thesis was a team effort on Contract Research to the Transport and Road Research Laboratory of the Department of the Environment (British Government). The Contract Research was directed by Dr. P.B. Attewell and Dr. I.W. Farmer and the other members of the team were Mr. A.Gowland (Experimental Officer), Mr. J.C. Cripps and the author (both Research Students).

All these people participated in the field measurement programme. On the data processing side, Mr. J.C. Cripps was primarily responsible for the reduction of the raw inclinometer data reported in this thesis and further processed. Mr. A.Gowland performed the stress analysis computations reported in Figure 6.2.2. of the thesis and he also fitted the polynomial curve to Skempton's K_o curve also illustrated in Figure 6.2.2. The author was the person primarily responsible for the reduction of the surface and sub-surface settlement data.

The results of the Fleet Line tunnel measurements and the bentonite diaphragm wall measurement in Green Park were reported to T.R.R.L. under Report Nos. PBA/IWF/TRRL/1972/1 and PBA/IWF/TRRL/1973/1 respectively by Drs. Attewell and Farmer.

The author also wishes to acknowledge the help provided by Mr. A.E.Cobb during his laboratory work.

Thanks are due to Mrs. A.Taylor for her meticulous typing of the thesis.

Finally, thanks are due to his wife, Alice Mary, for her never-failing interest and encouragement throughout the research.

To my mother IRINI

CONTENTS

Chapter 7

STRESS PATH APPROACH FOR TUNNELLING IN LONDON CLAY

Chapter 8

STABILITY OF SLURRY TRENCHES IN CLAY

Chapter 9

GROUND MOVEMENTS CAUSED BY A DIAPHRAGM WALL EXCAVATION IN LONDON CLAY

SYMBOLS

Symbol	Represents	Reference
A	value of stress at boundary ($x \to \infty$)	eq.(1.2.9.)
A	rate of tunnel advance ($A = d\ell/dt$)	Chapter 1
A	coefficient with dimension of depth	eq.(2.4.1.)
A	a constant in equation (2.5.8.)	Chapter 2
A	pore pressure parameter	Chapter 5
A_o, A_1, A_2	coefficients in equation(2.5.17.)	Chapter 2
a	a = OFS/2	Chapter 1
a	ratio of R/R_o distance from tunnel centre over the tunnel radius	Chapters 6,7
a	a coefficient in equation (4.4.1.)	Chapter 4
B	breadth of the unsupported roof	Chapter 1
B	value of stress at boundary ($y \to \infty$)	eq.(1.2.10.)
B	pore pressure parameter	Chapter 5
B	width of a diaphragm wall or of a slurry trench	Chapter 8
B	width of Protodyakonov's arch	A.1
b	coefficient in equation (1.6.7.)	Chapter 1
b	a constant in equation (2.5.5.)	Chapter 2
b	slope of K_f-line	Fig. 5.6.5.
CU	consolidated undrained test	Chapter 5
CD	consolidated drained test	Chapter 5
$\overline{CU}$	consolidated undrained test with PWP measurement	Chapter 5
$\overline{CD}$	consolidated drained test with PWP measurement	Chapter 5
c	a constant in equation (2.5.9.)	Chapter 2
c	shear force due to shear resistance along a two-dimensional Coulomb wedge	eq.(8.2.2.)
c	shear force due to shear resistance along a three-dimensional Coulomb wedge	eq.(8.2.7.)
c'	cohesion intercept based on effective stresses	Chapters 1,5
c_u	total stress strength parameter (undrained shear strength)	Chapters 1,8
c_v	coefficient of consolidation	Fig.5.6.3.
c	cohesion	eq.(8.2.7.,8,9,10)

Symbol	Represents	Reference
D	original width (diameter) of a specimen	eq.(5.5.4.,5)
dε/dt	rate of extrusion	Chapter 1
dε/dt	rate of axial strain in triaxial compression tests	Chapter 5
d	shield bead width	Chapter 1
d	a constant in eq.(2.3.6.)	Chapter 2
$(ds/dt)_{max}$	maximum rate of settlement for points on the centre line of a tunnel above soffit level	eq.(4.4.1.)
E	Young's modulus	Chapters 1,9
ESP	Effective stress path	Chapter 5
F_1,F_2	constants in equation (1.2.16.)	Chapter 1
F	factor of safety against failure at the base of an excavation	Chapter 1
F.S.	factor of safety against shear failure	Chapter 8
$f_1(S)$	parametric expression of tangential(hoop) stresses	Chapter 1
$f_2(S)$	parametric expression of shear stresses	Chapter 1
f	length/depth ratio of a slurry trench	Chapter 8
G	a constant in equation (2.5.14.)	Chapter 2
H	height of the diaphragm wall or of the slurry trench	Chapters 8,9
H'	modified height of the slurry trench ($H' = H + \sqrt{2}$)	Chapter 8
H_a	critical height to which a slurry trench may be dug in cohesive soil without the sides falling in	Chapter 8
h	height of Protodyakonov's arch	A.1
h	horizontal movement of ground at face, per unit length of advance of the shield	Chapter 2
i	standard deviation on a normal probability curve, being the point of inflection distance on the surface settlement semi-profile	Chapters 1,2
J	horizontal movement of ground at the tunnel face per unit length of shield's advance	Chapter 1

Symbol	Represents	Reference
K	principal stress ratio or lateral stress ratio	Chapters 1,6,7,8,9.
K^*	elastic constant equal to $\sigma_z/2$ (in the maximum shear stress theory) and equal to $\sigma_z/\sqrt{3}$ (in the octahedral shear stress theory).	eq.(1.2.8.,11,12)
K_o	principal stress ratio based on effective stresses	Chapter 6
K	coefficient in equation (2.5.1.)	Chapter 2
K_A	active stress ratio	Chapter 8
K_P	passive stress ratio	Chapter 7
$K_A, K_B, K_C, K_{A'}, K_{B'}, K_{C'}$	specified stress ratios	Fig.7.4.1.
K_{in}	integration constant	Chapter 8
K_f-line	line through p_f' versus q_f	Chapter 5
LL	liquid limit	Chapter 5
L	original length of a specimen	Chapter 5
L	length of the slurry trench	Chapters 8,9
ℓ_o	length of shield	Chapter 1
ℓ_1	distance from the centre line on the harmonic settlement semi-profile	Chapter 2
ℓ_{inf}	point of inflection on the harmonic settlement semi-profile	Chapter 2
m	an exponent in equation (2.5.1.)	Chapter 2
N_c	a coefficient dependent on the dimensions of the excavation	Chapter 1
n	coefficient of viscosity	Chapter 1
n	an exponent of equation (2.5.8.)	Chapter 2
OFS	simple overload factor	Chapter 1
OFM	modified overload factor	Chapter 1
P	a probability of a sphere moving down in LITWINISZYN'S model	eq.(2.4.1.)

Symbol	Represents	Reference
P	hydrostatic force exerted by the suspension to the sidewall	eq.(8.1.2.,3)
PL	plastic limit	Chapter 5
PWP	pore water pressure	Chapter 5
P_o	disturbing force acting on the slurry trench sidewall	Chapter 8
p	$= (\sigma_1 + \sigma_3)/2$ or $(\sigma_v + \sigma_h)/2$	Chapter 5
p_f	p at failure	Chapter 5
Q	surface surcharge	Chapter 1
q_u	unconfined compressive strength of clay	Chapter 1
q	$= (\sigma_1 - \sigma_3)/2$ or $(\sigma_v - \sigma_h)/2$	Chapter 5
q_f	q at failure	Chapter 5
R	extent of plastic zone around a tunnel	Fig. 1.2.1.
R	distance from the tunnel centre	Chapter 1, eq.(6.2.1.)
R	tunnel radius	Chapter 2 & A.1
R	radius of shield	eq.(2.5.16.,17) & eq.(1.5.1.)
R	ratio of principal stresses σ_3/σ_1	eq. (5.4.2.)
R_o	external radius of the tunnel lining	eq.(1.5.10.) eq.(2.5.16.,17.)
R_o	tunnel radius	Chapter 1 & eq.(6.3.1.,2,4,5.)
R_f	ratio of principal stresses of failure $(\sigma_3/\sigma_1)_f$	eq.(5.4.2.)
s_{max}	maximum surface settlement	Chapters 1,2
s_{exp}	clay movement at tunnel soffit during exposure time (t_{exp})	Chapter 1
s_1	vertical settlement at any point of the harmonic semi-profile	Chapter 2
s_2	vertical settlement at any point of the linear profile	Chapter 2
s_o	absolute difference between s_1 and s_2	Chapter 2
s(X,Y)	settlement at (X,Y) point	eq.(2.4.3.)

Symbol	Represents	Reference
t	time	Chapter 1
t_{exp}	exposure time for an element of clay above the tunnel soffit	Chapter 1
t	relief behind the cutting edge	Chapter2
t_f	time required for failure under a triaxial $\overline{CU}$ or $\overline{CD}$ test	Chapter 5
U_o	void thickness related to Protodyakonov's arch	A.1
U_1	the de-coupled displacement at the crown of Protodyakonov's arch	A.1
U_R	radial displacement	Chapters 6,7
V_{surf}	volume of soil included within the surface settlement trough	Chapters 1,2
V_{exc}	theoretical volume of the excavated soil due to tunnelling	Chapters 1,2
V_ℓ	loss of ground	Chapters,1,2
$V_{\ell i}$	the -ith component of loss of ground	Chapters 1,2
V_θ	tangential displacement	Chapters 6,7
v	"look-up" of shield measured as extent of non-circularity on vertical diameter	eq.(1.5.9.)
W	weight of a three dimensional Coulomb wedge	eq.(8.2.2.,7)
W_1	strain energy before tunnelling	Chapter 6
W_2	strain energy after tunnelling	Chapter 6
W	strain energy due to tunnelling	Chapter 6
X_o	horizontal distance between the sidewall and the rupture plane	Chapter 8
Y_1	magnitude of the span of the settlement trough	Chapter 2
Y_2	forward extension of a settlement profile	Chapter 2
Y_3	magnitude of the transverse extension of settlement trough	Chapter 2
Z	axis depth i.e. depth from ground surface to tunnel axis.	Chapters 1,2
z	any depth below ground surface	Chapters 4,8,9
z_w	ground water level	Chapter 8
z_b	level of bentonite suspension	Chapter 8

Symbol	Represents	Reference
	GREEK	
α	= ds/dt rate of clay movement at the tunnel face.	Chapter 1
β	angle expressing the inclination to horizontal of a shear plane around a tunnel.	Chapter 2
γ	unit weight of the soil	Chapters 1,8
γ_w	unit weight of water	Chapter 8
γ_b	unit weight of bentonite suspension	Chapter 8
γ'	effective unit weight of clay (see MEYERHOF, 1972)	Chapter 8
γ_b'	effective unit weight of bentonite suspension (see MEYERHOF, 1972)	Chapter 8
δ	thickness of shield skin	A.1
δ_ℓ	horizontal ground deformation in a vertical plane parallel to the longitudinal axis of a diaphragm wall	Chapter 9
$\Delta\varepsilon_1$, $\Delta\varepsilon_2$, $\Delta\varepsilon_3$	increments of principal strain	eq. (5.5.2.,3)
$\Delta\sigma_1$ $\Delta\sigma_2$, $\Delta\sigma_3$	increments of principal stress	eq.(5.5.2.,3)
ΔL	increment of specimen length	Chapter 5
ΔD	increment of specimen diameter	Chapter 5
ΔV	volume change during consolidation	Chapter 5
ε	strain	
ε_{res}	residual relative displacement	eq.(1.6.6.,7)
θ	angle of the orientation of specimen's axis in respect to stratification	eq.(5.4.1.)
θ	angle defining a polar co-ordinate	Chapter 6
θ	inclination of a linear Coulomb-type rupture surface of an hypothetical wedge acting behind the trench	Chapter 8

Symbol	Represents	Reference
λ	factor in equation (A.1.1.)	A.1
ν	Poisson's ratio	Chapters 1,5,6, 7,9.
σ_v	overburden pressure	Chapter 1
σ_i	internal pressure applied in unlined tunnel wall for stabilization purposes	Chapter 1
$\sigma_{\theta max}$	maximum tangential (hoop) stress	Chapter 1
$\sigma_x;\sigma_y$	stresses in the x,y plane	Chapter 1
$\sigma_1,\sigma_2,\sigma_3$	principal stress	Chapter 1
σ_r	yield point of material for the case of uniaxial tension	Chapter 1
σ_3/σ_1	principal stress ratio	Chapter 5
σ_v/σ_f	stability ratio	Chapter 1
σ_1	stress due to the elastic element in the "Standard Linear Solid" (rheological model)	eq. (1.6.1.)
σ_2	stress due to the viscous element in the "Standard Linear Solid" (rheological model)	eq. (1.6.1.)
σ	total stress	eq. (1.6.1.)
σ_R	radial stress at distance R from tunnel's centre	Chapters 6,7
σ_θ	tangential stress at distance R from tunnel's centre	Chapters 6,7
σ	net effective lateral pressure acting on the sidewall of a slurry trench	eq. (9.6.1.)
$\tau_{\theta r}$	shear stress in polar co-ordinates	Chapter 1
τ_{xy}	shear stress in Cartesian co-ordinates	Chapter 2
$\tau_{R\theta}$	shear stress at distance R from tunnel centre	Chapters 6,7
$\Phi(x,y)$	stress function in Cartesian co-ordinates	Chapter 1
ϕ'	friction angle based on effective stresses	Chapters 1,5
ϕ	friction angle	Chapters 5,8

LIST OF FIGURES

FIG. 9.6.2.	Earth pressure distribution calculated from MEYERHOF'S (1972) approach. The K_o versus depth linear function is taken from COLE and BURLAND (1972).
FIG. 9.7.1.	Comparison between the actual (left) and the calculated (right) horizontal deformation profile. Borehole BH1.

LIST OF TABLES

INTRODUCTION

Ground movements may be differentiated between these which are attributed to natural causes (often with a strong geological control) and those which arise as a result of constructional activity. The first type of movement may be said to comprise:-

a) Ground movements due to non-elastic deformations,*

b) Ground movements due to earthquakes, or ground creep,

c) Ground movements due to natural ground compaction and consolidation, or due to natural changes in the groundwater level.

On the other hand, ground movements might be the result of the following artificial causes:

a) Mining**;

b) Tunnelling (rock or soft ground),

c) Deep excavations,

d) Deep foundations (pile driving);

e) Geotechnical processes (chemical treatment, vibroflotation, sand drains and so on);

f) Excessive pumping of water or withdrawal of oil,

g) Vibration of machinery or traffic vibrations;

h) Blast vibrations.

---

* Beneath heavy loads, plastic layers or layers which become plastic due to some disturbance, may squeeze outward, allowing surface settlement. Thus, clay may be extruded from beneath a structure, or sand and silt layers, unless drainage is provided, may become locally plastic and flow. (see TREFETHEN, 1960).

** Mainly mining subsidence which is an essentially downward movement of the ground surface due to the removal of large volumesof material underground. As a result, the weight of overlying rock may cause collapse and subsidence.

The aim of the present thesis is to examine ground deformation due directly to tunnelling operations and deep excavations in clay.

Ground movements can be described in every point of a three dimensional soil mass as a spatial vector, which may be resolved into three components one vertical, which is known as settlement, and two co-planar horizontal components. In the case of tunnelling, the horizontal components may be related to directions parallel and normal to the tunnel centre line, while in the case of deep excavations, these components have directions normal to the sidewall (the so-called ground deflection) and parallel to it.

The magnitude of the ground deformation vector is normally higher in the vicinity of the opening where the bulk of any ground loss takes place.

From both the practical and academic points of view the problem of ground movements due to tunnelling or mining has been treated with an emphasis on the surface settlement development rather than on the associated subsurface ground deformation. In this context, the main question was,and still is, the prediction of the magnitude and extent of the main parameters of the surface settlement trough, namely the amplitude of the maximum settlement and the magnitude of the settlement span. This trend is particularly illustrated in the State of the Art Report of PECK (1969) in which emphasis is given to the prediction of surface settlement and other movements associated with soft ground tunnelling and deep excavations.

During the last five years, however, the interest appears to be shifted towards the examination and analysis of subsurface ground deformation. This new trend would seem reasonably to be attributed to the following two main factors.

a) The necessity for recognition and understanding of the subsurface ground deformation regime as it directly affects the stability of the foundations of nearby buildings. Since the recent trend is to build more tunnels and rapid transit systems in urban areas, this factor is of particular importance.

b) The rapid improvement of more sophisticated instrumentation and measuring techniques for the analysis of the in-situ ground deformation. Nevertheless, most of the relevant literature is still concerned with surface settlement. This is probably understandable from the point of view of simple economics, since the establishment of a network of ground survey stations and precise levelling operations are far simpler and cheaper than the sinking of boreholes and the operation of continuous subsurface surveys with the aid of inclinometers, magnetic detectors and other instrumentation. Therefore, it is not surprising that during the last five years only sporadic, well-documented case histories for surface and subsurface ground deformation resulting from soft ground tunnelling and deep excavations have appeared in the literature.

Factors affecting ground movements

Examining those factors affecting the type, magnitude and extent of ground movements associated with soft ground tunnelling, one may single out as key factors the geological setting and the ground properties (particularly hydrological) of the site where the tunnel is driven.

Taking account of the particular character of the ground stress regime, the engineer choses the appropriate type of lining (concrete cast in situ, expanded lining, bolted pre-cast segments, and so on) and decides on the suitable method of excavation to be followed(hand-mined, digger shield, hand-mined shield, full face blasting, and so on). In the case of shield tunnelling, the particular type of shield and its structural features(such as the presence or otherwise of a bead, the jacking pressure, its length, the possible requirement for a diaphragm across the face when dealing with very soft soils lying beneath the water table) are factors having a particularly important control on the ground movements and consequential 'ground losses' around the shield. These ground losses taking the form of "face-take" or radial intrusions of the soil are essentially time-dependent deformations related to the geotechnical and rheological properties of the soil - and particularly, of course, to its drainage character - and to the rate of tunnel advance. ATTEWELL and FARMER (1974) have examined in some detail these ground losses associated with shield tunnelling in an overconsolidated stiff fissured clay.

PECK et al (1969) argue that the most difficult task during the construction of shield-driven tunnels is to prevent the movements of soil into the void behind the tailpiece of a shield before the void can be filled. Thus, in cohesionless soils the ground movement into the tail void may comprise two types: collapse of the sand at the crown, or inflow at the invert if the tunnel is below the ground water table, while in plastic clays or silts, the soil tends to squeeze radially into the annular space.

In the case of difficult soil conditions, or what are commonly termed "geologic anomalies" in the form of longitudinal variations of lithology and structure along the tunnel axis and centre line, mixed-face conditions, or unfavourable positions of any ground water table, ground stabilisation might be an effective way of preventing severe and unacceptable ground deformation. For soils having low cohesions, especially those beneath the ground water table, geotechnical processes of soil improvement are sometimes inevitable.

The most common types of such methods are the use of compressed air, grouting, ground water lowering, and ground water freezing.

Geotechnical processes, although very useful in ameliorating unfavourable soil conditions, must be used with care especially when the tunnel is driven beneath urban areas because it can happen that the stabilization of the ground around the tunnel may only be at the cost of inducing ground instability in the foundations of the nearby buildings. As BARTLETT and BUBBERS (1970) pointed out, in fissured ground care has to be exercised to ensure that grout at high pressure does not come into direct contact with the underside of foundations, with resultant heave and damage to the building. Also, in the case of ground water lowering, in addition to direct settlement, the possibilities of drawing down piles or of causing timber piles to rot have to be considered.

Another factor affecting ground deformation is the geometry of the tunnel, its depth and diameter. It has been found that, assuming the character of the transverse surface settlement profile above a tunnel to take the form of an error curve (considered in detail subsequently in this thesis), then the parameters of this curve are related to the dimensionless ratio: tunnel depth/tunnel diameter. This dimensionless ratio is a function of the standard deviation of the settlement curve (SCHMIDT, 1969, PECK, 1969, PECK et al, 1969) and is also a function of the maximum surface settlement (MYRIANTHIS, 1974 a,b) of the same curve.

Finally, some preliminary mention should be made of the influence exerted by the time factor on the ground deformation regime in soft ground tunnelling. This factor may be expressed as a function of the rate of soil deformation and the rate of tunnel advance. It is commonly acknowledged by the tunnelling engineer that the slower the rate of tunnel advance, the greater is the total soil intrusion for a given depth of tunnelling. For shield-driven tunnels, the problem lies in the accommodation of the time factor into the ground loss computations. Such a problem is considered in the present thesis.

As far as deep excavations are concerned, it may be argued that ground movements will always occur during construction whatever the effectiveness of the supporting system. These deformations usually take the form of:

a) An inward movement of the soil on the side walls,

b) An upward movement of the base of excavation - the well known bottom heave, and

c) A surface settlement resulting from the ground loss of the side walls.

The third type of movement is probably the most serious because it is the most likely to occur, and thus place at risk the foundations of the nearby buildings.

As in the case of soft ground tunnelling, the geological factor is dominant in the determination of ground deformation associated with deep excavations. This factor, together with the properties of the soil influence to some extent the choice of type of excavation and supporting system (braced, slurry-supported, timbering, and so on). The geometrical factor is also important for the stability of deep excavations. MEYERHOF (1972) pointed-out that the dimensionless ratio : depth/width of the structure is directly related to a stability factor in the case of slurry trenches in saturated clay.

Ground movements are also dependent on the particular details of construction and its historical progress, and upon the quality of workmanship.

Minimization of settlement and ground losses associated with deep excavations in soil may often be achieved if a trial part of the excavation is adequately instrumented in order to provide an early detection of the ground movement trend. This trend could in turn be interpreted in such a way as to promote possible alterations in the original design of the system provided that it has such an inbuilt flexibility.

<u>Damage to nearby buildings due to ground movements.</u>

Surface and subsurface ground movements and settlement due to soft ground tunnelling and deep excavation could cause damage to adjacent surface and subsurface structures. Surface settlement may result in differential settlement of the foundations of the building, while differential horizontal ground movement may distort piles and displace them from their original position. These movements would create a new and unknown distribution of load from the superstructure to the foundations. Surface heave may also endanger the foundations, creating conditions of surface ground compression which could possibly crush foundations, walls and roofs. In the case of shield-driven tunnels, the pressure exerted by the thrust rams may at least theoretically create a state of passive earth pressure at points ahead of and above the shield. If foundations of adjacent buildings are present in the vicinity of the range of influence of such tunnel pressures, there is a possibility of a completely new form soil-structure interaction - that of soil-foundation interaction.

For all these reasons special precautions are required* during design and construction for the minimization of the danger of damage.

* In the Civil Engineering Code of Practice No. 4 (1954) : Foundations, Part 5: 5.606 it is clearly stated that "In all cases where excavations are to be carried out in congested areas in close proximity to surrounding buildings and public highways, the excavation method adopted should be such as will provide adequate safeguard against settlement and damage to such buildings and highways...".

CHAPTER 1

GROUND STABILITY FOR TUNNELS IN CLAY

1.1 INTRODUCTION

The stability of soft ground tunnels can be examined with the aid of some semi-empirical criteria such as those expressed by the simple overload factor (OFS) and the modified overload factor (OFM).

The loss of ground around the opening is probably a major factor contributing to ground movements and surface settlements. Stability analysis indicates that the loss of ground is a function of OFS. Stability criteria in the form of critical stress ratios can also be formulated from special laboratory techniques such as extrusion tests. Finally, the incorporation of the time factor into any soft ground tunnelling stability consideration is a real necessity because stability is a dynamic phenomenon rather than a mere static concept. In fact, stability is a function of time dependent parameters such as the rate of tunnel advance, the rate of clay deformation around the opening and the rate of application of any internal stabilising pressure.

1.2. THE OVERLOAD FACTORS (OFS, OFM). FORMULATION OF A PLASTIC ZONE AROUND A TUNNEL.

DEERE et al (1969) proposed that the stability and the potential ground loss for a tunnel in clay might be expressed as a function of a "simple overload factor", OFS, which is the ratio of the overburden pressure, less any internal pressure (for instance, air pressure if it is applied), to the undrained shear strength of the clay for conditions in which the vertical and lateral pressures pre-existing in the ground are equal.

Thus,

$$OFS = \frac{\sigma_v - \sigma_i}{c_u} \qquad \text{.....(1.2.1.)}$$

where. σ_v is the overburden pressure,

σ_i is any internal pressure,

and c_u is the undrained shear strength of the clay.

The maximum tangential (hoop) stress according to the theory of elasticity equals twice the radial (vertical) pressure σ_v, for K = 1. Thus, one may define the "modified overload factor," OFM, as

$$OFM = \frac{\sigma_{\theta\ max} - 2\sigma_i}{q_u} \qquad \text{.....(1.2.2.)}$$

where

$\sigma_{\theta max}$ is the maximum tangential stress,

σ_i is any internal pressure,

and q_u is the unconfined compressive strength of the clay.

In essence, the maximum tangential stress is the major principal stress at the tunnel wall surface, and it is reasonable to assume that when σ_θ exceeds q_u some shearing take place to form a plastic annulus around the unsupported tunnel. The radius of the sheared annulus depends upon the magnitude of the ratio σ_θ/q_u.

Due to the very importance of the nature and extent of the "plastic annulus" around an unsupported tunnel, an attempt has been made via the theory of elasticity to define the radius of the plastic zone and the parameters influencing its amplitude.

SAVIN (1961) stated that if the stresses in a mathematically-defined region of stress concentration around a circular hole exceed a certain limiting value for a given material, the material in this region will be in a state of stress exceeding the limit of elasticity. Assuming, that this is the case and that the stress function $\Phi_1(x,y)$ which determines the stress state "beyond the limit of elasticity" in this zone is a hyperbolic function, then the stress function $\Phi_2(x,y)$ for the elastic range satisfies the bi-harmonic equation

$$\frac{\partial^4 \Phi_2}{\partial x^4} + 2\frac{\partial^4 \Phi_2}{\partial x^2 \partial y^2} + \frac{\partial^4 \Phi_2}{\partial y^4} = 0 \qquad \text{.....(1.2.3.)}$$

Assume further that tangential and shear stresses are given in a parametrical (S) form by

$$\sigma_\theta = f_1(S) , \quad \tau_{\theta r} = f_2(S) \qquad \text{.....(1.2.4.)}$$

are applied to the contour of the hole and satisfy the boundary conditions imposed by the limits

$$\left.\begin{aligned} &\lim_{S \to \infty} \sigma_\theta = \sigma_\theta(x,y) \\ &\lim_{\theta r \to \infty} \tau_{\theta r} = -\sigma_\theta\,(x,y) \end{aligned}\right\} \qquad \text{.....(1.2.5.)}$$

or,

$$\left.\begin{aligned} &\lim_{x \to \infty} \sigma_x = \sigma_1(x,y) \\ &\lim_{y \to \infty} \sigma_y = \sigma_2(x,y) \\ &\lim_{xy \to \infty} \tau_{xy} = \sigma_3(x,y) \end{aligned}\right\} \qquad \text{.....(1.2.6.)}$$

It is necessary to suppose that the function $\Phi_1(x,y)$, that is, the stress function for the range above the limit of elasticity, satisfies beyond the boundary conditions (equation 1.2.6.) the hyperbolic type equation

$$F_1\left(x,y, \frac{\partial^2 \Phi_1}{\partial x^2}, \frac{\partial^2 \Phi_1}{\partial y^2}, \ldots, \frac{\partial_1 \Phi_1}{\partial x}, \frac{\partial \Phi_1}{\partial y}\right) = 0 \qquad \text{.....(1.2.7.)}$$

which is known as the "plasticity condition".

The problem now consists of finding a bi-harmonic function $\phi_2(x,y)$ outside some unknown contour which surrounds the hole and separates the plastic from the elastic zone. In the meantime, at this contour the following conditions must apply

$$\frac{\partial^2\phi_1}{\partial x^2} = \frac{\partial^2\phi_2}{\partial x^2}, \quad \frac{\partial^2\phi_1}{\partial y^2} = \frac{\partial^2\phi_2}{\partial y^2} \quad \text{and} \quad \frac{\partial^2\phi_1}{\partial x\partial y} = \frac{\partial^2\phi_2}{\partial x\partial y} \qquad \text{...(1.2.8.)}$$

as well as the boundary conditions

$$\left.\begin{aligned} &\lim_{\substack{x\to\infty \\ y\to\infty}} \partial^2\phi_2/\partial x^2 = \sigma_2\,(x,y) \\ &\lim_{\substack{x\to\infty \\ y\to\infty}} \partial^2\phi_2/\partial y^2 = \sigma_1(x,y) \\ &\lim_{\substack{x\to\infty \\ y\to\infty}} \partial^2\phi_2\,/\partial x\partial y = \sigma_3(x,y) \end{aligned}\right\} \qquad \text{.....(1.2.9.)}$$

The "hyperbolic type" equation (1.2.7.) may be formulated as follows

$$\left[\frac{\partial^2\phi_1}{\partial x^2} - \frac{\partial^2\phi_1}{\partial y^2}\right]^2 + 4\left[\frac{\partial^2\phi_1}{\partial x\partial y}\right]^2 = 4K^{*2} \qquad \text{.....(1.2.8.)}$$

where K^* is a material constant defined as $K^* = \sigma_r/2$ in the maximum shear stress theory and $K^* = \sigma_r/\sqrt{3}$ in the octahedral shear stress theory. Note that σ_r is the yield point of the material in the case of uniaxial tension.

Assuming that a single normal pressure acts at the hole contour (the diameter of the tunnel): tunnel's circumference,

$$\left.\begin{aligned} \sigma_r &= -p \\ \tau_{r\theta} &= 0 \end{aligned}\right\} \qquad \text{.....(1.2.9.)}$$

and that the boundary conditions are.

$$\left.\begin{aligned} &\lim_{x\to\infty} \sigma_x = A \\ &\lim_{y\to\infty} \sigma_y = B \end{aligned}\right\} \qquad \text{.....(1.2.10.)}$$

the solution of equation (1.2.8.) is then given by

$$\Phi_1 (x,y) = K^* R^2 \ln (R/R_o) + \left(\frac{p+K^*}{2} \right) R^2 \qquad \text{.....(1.2.11.)}$$

where R_o is the tunnel radius and R is a distance from the tunnel centre. One may express the stress functions σ_x, σ_y, τ_{xy} and further, using a mathematical method known as the MUSKHELISHVILI formulation (see SAVIN 1961) it is possible finally to define the boundary of the plastic zone. This boundary is a circle with a radius given as follows.

$$R = R_o e^{\frac{A+p - K^*}{2K^*}} \quad , \quad \text{for } B = A \neq 0$$

and .....(1.2.12.)

$$R = R_o e^{\frac{p - K^*}{2K^*}} \quad , \quad \text{for } A = B = 0$$

i.e. no stress at infinity

The more complex case of normal and shear stresses applied at the contour of a circular hole (tunnel circumference) was examined by PARASYUK (see SAVIN 1961) who found that the boundary of the plastic zone is no longer a circle and that its radius is given under a rather complex notation.

Using the above results in a soil mechanics context and considering the case of a frictionless soil under $K_o = 1$, conditions, it is known that the yield state must satisfy TRESCA'S criterion of failure,

$$\sigma_1 - \sigma_3 = 2 c_u$$

This could be written as

$$\frac{\sigma_1 - \sigma_3}{2c_u} = a \qquad \text{.....(1.2.13.)}$$

where a = 1 at equilibrium.

Substituting $\sigma_1 = \sigma_v$ and $\sigma_3 = \sigma_1$ then,

$$a = \frac{\sigma_v - \sigma_1}{2c_u} = \frac{OFS}{2} \qquad \text{.....(1.2.14.)}$$

$a < 1$ means that no plastic zone will develop whereas

$a > 1$ means that a plastic zone will develop.

The radius of a developed plastic zone is given by equation (1.2.12.) in the case of (A = B = 0). Thus

$$R = R_o e^{\left[\frac{\sigma_v - \sigma_1}{2c_u} - \frac{1}{2}\right]}$$

or

$$R = R_o e^{0.5(OFS-1)} \qquad .....(1.2.15.)$$

This relationship has been plotted on a log-linear graph (see Figure 1.2.1.) for values of R_o ranging from 1m to 4.5m. Although the graph is self-explanatory, it must be emphasised that for the critical value of OFS = 6.28 (as defined by DEERE <u>et al</u> 1969) the extent of plastic zone is contained between the limits 14.5m $<R<$ 68m depending upon the respective value of the tunnel radius R_o. It should be noted, however, that for basic stability, OFS should not exceed 6 (PECK, 1969).

A detailed presentation of ten case studies has been given by PECK in his State of the Art Report. It was concluded that tunnelling can be carried out without undue difficulties in plastic clays if OFS$\leq$5. In shield tunnelling, if OFS is much greater than this, the clay is likely to invade the tailpiece too rapidly to permit satisfactory filling of the void with pea gravel or grout. For OFS values approaching 7, the shield may become unmanageable because of its tendency to tilt as it advances.

Using PECK'S op cit published data, a graph has been plotted relating the dimensionless ratio Z/2R (depth to diameter) to OFS for ten case studies. As is shown in Figure 1.2.2. a curve of the second degree describes the increase of OFS as Z/2R decreases. Taking into account the fact that shear strength may reasonably be assumed to increase linearly with depth (see Appendix 2a) the critical value of OFS for shallow depths could be even less than 6. As MUIR WOOD (1970) pointed out, this is only one condition for stability. DEERE et al (1969) emphasized the importance of the time of exposure of the face in a soil, the effective permeability of which is sufficiently low to permit appreciable variation in pore water distribution during the period of exposure. Immediately after excavation, the release of the ground sets-up negative pore pressures at the face which provide some measure of support so long as the condition persists and this negative pressure is assisted by the cohesion of the soil.

In a stiff, fissured clay such as London clay, the stability may depend less upon the strength of the clay mass, than upon the shear stresses developed at fissures. The orientation and inclination of the fissures should be taken into account because laboratory results indicate a significant difference in shear strength due to these factors (see MYRIANTHIS, 1973).

Nevertheless, for the question of crown stability in an unlined tunnel DEERE et al, op cit, provide a criterion based on BALLA'S analysis for a flat roof. This is that·

$$OFS = \frac{2\gamma z}{q_u} < \frac{2(F_1 - 2B\gamma F_2)}{c'} \qquad ....(1.2.16.)$$

where the unconfined drained compressive strength,

$$q_u = 2c' \tan (45^\circ + \phi'/2) \qquad ....(1.2.17.)$$

in which B is the breadth of the unsupported roof, c' and ϕ' are the effective shear strength parameters for the soil, and the constants F_1, F_2 are functions of the angle ϕ', as indicated by Figure (1.2.3.).

1.3 LOSS OF GROUND AND OFS.

The excavation of a tunnel in clay, under normal constructional and ground conditions, creates a symmetrical settlement trough at the ground surface. PECK et al (1969) suggest that the shape of the trough is nearly independent of the magnitude of the maximum settlement and that the settlement volume is equal to the volume of lost ground in the tunnel modified by any volume change in the subsiding mass.

More recently, PECK et al (1972) have stated that the maximum amplitude of the settlement curve can be estimated on the assumption that the volume of the settlement trough will be about one per cent of the volume of the tunnel (that is, the volume of the excavated soil). Under exceptionally good conditions and workmanship, the settlement may be as little as half of this amount. In contrast, volumes of settlement of up to 40% or 50% of the volume of the tunnel are not unknown (PECK et al, 1972).

The symmetrically-shaped settlement profile over a tunnel can adequately be approximated by a Gaussian error curve (see Chapter 2), and it has been shown in the literature that the shape of most settlement profiles conforms closely to it. From the properties of the Gaussian error function it is known that the surface settlement volume per unit advance of the tunnel is proportional to the product of i(the standard deviation on a normal probability curve, being the point of inflection on the surface settlement semi-profile) and s_{max} the maximum settlement on the error curve. Thus,

$$V_{surf} = \sqrt{2\pi}\, i\, s_{max} \qquad .....(1.3.1.)$$

Loss of ground however, must be related to the theoretical volume of the tunnel (V_{exc}),

$$V_{surf} = V_{\ell}\, V_{exc} \qquad .....(1.3.2.)$$

where V_{ℓ} is the ground lost

SCHMIDT (1969) examined variations in the loss of ground with the OFS value and with the soil properties under $K_o = 1$ conditions on the assumption of no volume change (that is $\nu = 0.5$). He concluded that

$$\text{For OFS} > 1, \quad V_\ell = \frac{3c_u}{E} e^{OFS-1} \qquad .....(1.3.3.)$$

$$\text{For OFS} \leq 1, \quad V_\ell = 3 \text{ OFS} \frac{c_u}{E} \qquad .....(1.3.4.)$$

where c_u is the undrained shear strength

and E is the Young's modulus.

Finally, he pointed out that the strength/modulus ratio for common soils varies within a fairly narrow range approximately bounded by the values 5×10^{-3} to 2×10^{-3}. This range is likely to be narrowed as more becomes known about the deformational behaviour of clay soils.

As is shown in Chapter 2, the Z/2R ratio (depth/diameter) is a function of the loss of ground (V_ℓ), and according to SCHMIDT'S results it might be a function of OFS, because $V_\ell = f(OFS)$. Indeed, SCHMIDT, op cit derived a graph giving the range of theoretical ground loss as a function of OFS for boundary values of the ratio c_u/E, as shown in Figure 1.3.1.

1.4. LABORATORY TECHNIQUES APPLIED TO GROUND STABILITY

Laboratory extrusion testing of clays and other soft ground materials has been suggested as a quick method of evaluating ground stability at a tunnel face. A feature of the model is that the direction of extrusion of material becomes perpendicular to the direction of stress application. Extrusion itself is by a combination of plastic deformation and shear. BJERRUM and EIDE (1956) determined the factor of safety against failure at the base of an excavation as,

$$F = N_c \frac{c_u}{\gamma h + Q}$$

where N_c is a coefficient dependent on the dimensions of the excavation,

c_u is the undrained shear strength of the soil,

γ is the unit weight of the soil,

h is the depth of the tunnel from the ground surface,

and Q is a surface surcharge.

If d is the hole diameter, they concluded that for $h/d > 4$, $N_c = 9$.

BROMS and BENNERMARK (1967) translated this idea in terms of a circular tunnel face where Z/2R is greater than 4. From a theoretical analysis of a semi-circular rotational failure at the face they deduced a value for $N_c = 6.28$.

They proceeded to reinforce their argument by a series of laboratory extrusion tests from which they derived a value for N_c in the region of 6 to 8. This adds a theoretical justification for the earlier practical observations of a critical value for OFS a little greater than 6.

A tunnel excavation would be stable therefore, if overburden pressure is less than six times the undrained shear strength of clay. Later work by ATTEWELL and BODEN (1971) stressed that the stability ratio which is based on simple stress-deformation criteria is incomplete. They argue that for practical considerations, the stress level of interest is not that of total failure but rather that of maximum acceleration of clay intrustion at a tunnel face. This occurs before the ultimate stress-deformation yield considered previously. The value for this new stability ratio is taken as $N_c = 0.45$.

BODEN (1969), PASCALL (1970), ATTEWELL and BODEN (1971), HARRISON (1971) and finally ATTEWELL and FARMER (1972) conducted a series of laboratory extrusion tests in order to simulate tunnelling. The basic testing programme was in almost all cases the same and consisted of two distinct parts.

The first part was an extrusion test using a constant rate of axial strain, while the second part was a series of extrusion tests using five constant stress steps loaded on the same sample and held on for approximately fifteen minutes each. The applied vertical stress and the amount of clay extrusion were measured in both tests with the addition of the axial deformation of the sample in the former case.

Investigations were carried out into the effects on the stability of the clay of varying moisture content and extrusion hole size. Other testing of a more standard form was also performed.

Atterberg limits were determined for each clay sample as was the undrained shear strength. ATTEWELL and BODEN (1971) plotted the variation of extrusion-based stability ratio with liquidity index for undisturbed laminated clay. They found a linear relationship to hold in the form that as the liquidity index increases, the stability ratio tends to decrease.

Figure 1.4.1. illustrates the cell for clay extrusion experiments with its geometrical elements, and some results of a typical constant axial strain rate test on a clay.

A more detailed analysis of a constant rate of axial strain test is given in Figure 1.4.2 while a graph is presented for the extrusion rate de/dt versus the stability ratio σ_v/σ_f. This graph comprises data on London clay and on stiff clay with different extrusion hole diameters used.

The basic feature in the interpretation of the combined curve (Figure 1.4.2.) is the series of values for critical overburden pressures such

as $\quad \sigma_v = \sigma_e(f)_{1,2.....5}$

In fact, $\sigma_e(f)_1$ is a value which is determined from the stress level corresponding to the point of departure of the pre-failure tangent from the extrusion curve. It shows, however, the stability value at the time when the clay is just starting to accelerate out of the hole.

Nevertheless, if the point of tangent interception is produced horizontally to meet the graph, the stability value $\sigma_{e(f)2}$ corresponds to a state where extrusion is visible but maximum acceleration has not yet been attained. On the other hand, $\sigma_{e(f)3}$ is the stability value which may be correlated with the maximum acceleration of extrusion. It is found from the point of intersection of the tangent angle bisector with the extrusion graph, while $\sigma_{e(f)4}$ is the stability value for the tangent intersection. It is actually a value corresponding to an event just after maximum acceleration.

Finally, $\sigma_{e(f)5}$ is determined from the point of departure of the post-failure tangent from the curve. It shows the value of the stability ratio when extrusion is attaining a more uniform velocity. Obviously, these $\sigma_{e(f)n}$ values can be expressed more consistently in a dimensionless way taking the ratio σ_v/σ_f which is a characteristic stability ratio.

1.5. TIME FACTOR AND GROUND STABILITY

It is usually accepted that the slower the rate of tunnel advance the greater is the total clay intrusion for a given depth of tunnelling. Indeed, the time factor is a governing parameter in the ground stability regime around a tunnel. The rate of tunnel advance determines in effect the time of exposure of any element of clay at or near to the tunnel face as well as around the opening.

For shield tunnelling, the problem lies in the accommodation of the time factor into the ground loss computations. MUIR WOOD (1970), in a quite precise manner, pointed out the main contributory factors for the determination of ground loss. Using MUIR WOOD'S op cit arguments as a framework, an attempt has been made by the author to modify and extend the concept, emphasizing the role of rate effects. The total ground loss might be expressed as the sum of ground losses

1) At the face
2) Behind the bead of the shield.
3) Along the shield, and
4) Behind the tail of the shield.

Thus,

$$V_{\ell} = V_{\ell_1} + V_{\ell_1} + V_{\ell_2} + V_{\ell_3} + V_{\ell_4} \qquad \text{.....(1.5.1.)}$$

The first factor of equation (1.5.1.) can be expressed in terms of the shield radius (R) and the horizontal movement of ground at the face per unit length of shield's advance (j).

Thus,

$$V_{\ell_1} = \pi R^2 j \qquad \text{.....(1.5.2.)}$$

This factor obviously is not time dependent. In order to incorporate the time factor it is necessary to define two basic rates, namely the rate of clay movement at the tunnel face ($\alpha = ds/dt$), and the rate of tunnel advance ($A = d\ell/dt$). Note that ℓ represents length measured in metres. Therefore,

$$j = \alpha / A \qquad \text{.....(1.5.3.)}$$

and

$$V_{\ell_1} = \frac{\pi R^2 \alpha}{A} \qquad \text{.....(1.5.4.)}$$

Equation (1.5.4.) expresses the ground loss due to the face take area.

Assuming a 180 degrees bead, the ground loss due to the radial take area is,

$$V_{\ell_2} = \frac{\pi \ell_o}{2} (2R - d) \simeq \pi \ell_o R \text{ because } d \ll 2R \qquad .....(1.5.5.)$$

where ℓ_o is the length of the shield only,

d is the bead width.

On this basis one could define the "exposure time" for an element of clay above the tunnel soffit as,

$$t_{exp} = \frac{\ell_o}{A} \qquad .....(1.5.6.)$$

During that time the clay movement is

$$s_{exp} = \frac{\ell_o \alpha}{A} \quad \text{or} \quad s_{exp} = \ell_o J \qquad .....(1.5.7.)$$

From equation (1.5.5.) and equation (1.5.7.) the ground loss could be expressed more accurately as,

$$V_{\ell_2} = \pi \ell_o^2 R \frac{\alpha}{A} \quad \text{or} \quad V_{\ell_2} = \pi \ell_o^2 RJ \qquad .....(1.5.8.)$$

Since the bead is relatively small, (something between 5 to 25mm according to European standards), one should expect that during the shield's passage there are two alternatives, i.e.. either,

$s_{exp} > d$ which means that the bead is closed,

or $s_{exp} < d$ which means that the bead is not closed.

In difficult soils the shield is often distorted so that its cross-section changes along its length. This results in some extra ground loss. The same, however, could happen when the shield is driven with its axis at an angle to the axis of the tunnel.

MUIR WOOD op cit, basing on SHIRAISHI'S (1968/69) paper, proposed that if a shield "crabs" or, on account of poor ground, is driven at an appreciable attitude, considerable settlement and ground losses are likely to occur.

Hence,

$$V_{\ell_3} = \frac{\pi \ell_o v}{8} \qquad \text{.....(1.5.9.)}$$

where

v is a "look-up" of shield measured as extent of out of plumb on vertical diameter.

Finally, a substantial ground loss usually occurred behind the tailpiece before, during and after the ground stabilization through grouting.

The estimation of that component of ground loss is probably the most difficult and speculative because many and different factors are affecting the nature and extent of ground movement behind the tailpiece.

First of all, the soil's nature, its stiffness, cohesion and moisture content are the dominant factors. Secondly, but not less important, is the type of temporary supporting system as well as the type of lining.

The time of unsupported ground exposure, the composition and effectiveness of grouting, the tunnel's depth and its location with respect to the groundwater level are no doubt some additional factors.

As a first approximation, it could be argued that for tunnels above the groundwater level, the loss of ground is given by

$$V_{\ell_4} = 2\pi R(R - R_o) \qquad \text{.....(1.5.10.)}$$

where R_o is the external radius of the lining,

and R is the radius of the shield.

Finally, it is then possible to express the volume of the total ground loss per unit length of tunnel, taking into account the partial ground loss values of relationships (1.5.4.), (1.5.6.), (1.5.9.) and (1.5.10.).

$$V_{\ell} = \pi R^2(\alpha/A) + \pi \ell_o^{\ 2} R(\alpha/A) + \frac{\pi \ell_o v}{8} + 2\pi R(R - R_o)$$

or,

$$V_{\ell} = \frac{\pi R \alpha}{A}(R + \ell_o^{\ 2}) + 2\pi \left(\frac{\ell_o v}{16} + R^2 - RR_o\right) \qquad .....(1.5.11.)$$

One should comment that the only unknown factors in relationship (1.5.11.) are The rate of clay movement at face, in other words α, and the "look-up" of the shield measured as extent of out of plumb on vertical diameter, i.e. v.

Since the latter factor could be determined in-situ, the problem arises with the first one.

With that point in view, the extrusion technique is a useful tool for the determination of the extrusion rate. Finally, it is possible to express the maximum surface settlement above a tunnel, taking into account rate effects. Thus, assuming that the volume of the surface settlement trough (V_{surf}) is equal to the total volume of ground loss (V_{ℓ}), and that the surface settlement curve follows a Gaussian error function,

$$V_{surf} = V_{\ell} \qquad .....(1.5.12.)$$

but as has been discussed previously (see equation 1.3.1.)

$$V_{surf} = \sqrt{2\pi}\, i\, s_{max}$$

Also, bearing in mind SCHMIDT'S (1969) equation,

$$\frac{i}{R} = \left(\frac{Z}{2R}\right)^{0.8}$$

it is possible to estimate the maximum settlement over a single tunnel by the combination of the latter relationships.

Thus,

$$\sqrt{2\pi}\, i\, s_{max} = \pi \left[R(\alpha/A)(R + \ell_o^{\,2}) + \frac{(\ell_o v}{8} + R^2 - RR_o) \right] \qquad .....(1.5.13.)$$

or

$$s_{max} = \frac{\sqrt{2\pi}/2 \left[R(\alpha/A)(R+\ell_o^{\,2}) + \frac{(\ell_o v}{8} + R^2 - RR_o) \right]}{i} \qquad .....(1.5.14.)$$

and since $i = R(\frac{Z}{2R})^{0.8}$, and $\sqrt{2\pi}/2 = 1.25$

Thus,

$$s_{max} = \frac{1.25 \left[(\alpha/A)(R+\ell_o^{\,2}) + \frac{(\ell_o v}{8R} + R - R_o) \right]}{(\frac{Z}{2R})^{0.8}} \qquad .....(1.5.15.)$$

Ground loss calculations have also been discussed by ATTEWELL and FARMER(1974).

1.6 RELATIONSHIP BETWEEN OFS AND TIME

Another problem of interest is the relationship (if any does exist) between the OFS and TIME. Such a relationship might be derived on the basis of rheological laws. For the case of saturated plastic clay or a stiff plastic clay, it is reasonable to adopt a visco-elastic behavioural mode which is represented by a Kelvin model. This is composed of an elastic element (spring) in parallel with a viscous element (dashpot), (see Figure 1.6.1.).

OBERT and DUVALL (1967) stated that the strain in the elastic element must equal the strain in the viscous element, the total stress σ, is the sum of the elastic stress σ_1 and the viscous stress σ_2. Thus, they proposed that the total stress is equal to

$$\sigma = \sigma_1 + \sigma_2 = E_1\varepsilon + 3\eta \qquad .....(1.6.1.)$$

Assume that at $t = 0$, when $\varepsilon = 0$, a constant stress σ_o is applied to the system. By integration of equation (1.6.1.) :

$$\varepsilon = \frac{\sigma_o}{E_1}\left[1-e^{\frac{E_1 t}{3\eta}}\right] \qquad .....(1.6.2.)$$

By adding in series with the Kelvin element a spring* in order to accommodate the instantaneous displacement, DEERE et al (1969) pointed that

$$\varepsilon(t) = \frac{\sigma}{E_2} + \frac{\sigma}{E_1}\left(1 - e^{-bt}\right) \qquad .....(1.6.3.)$$

Taking the limit,

$$\lim_{t \to \infty} \varepsilon(t) = \varepsilon_{ult} \qquad .....(1.6.4.)$$

where,

$$\varepsilon_{ult} = \sigma\left(\frac{1}{E_1} + \frac{1}{E_2}\right) \qquad .....(1.6.5.)$$

b is a coefficient with dimensions of inverse time.

Finally, taking $\varepsilon(t)$ as an arbitrary value of relative displacement of a tunnel wall, and further assuming that $\sigma = \sigma_v = \gamma h.$, i.e. the overburden pressure, then

$$\varepsilon_{res} = \frac{\sigma_v}{E} e^{-bt}$$

where,

ε_{res} is the residual relative displacement, or in other words, the remaining displacement that will occur after the removal of the external stress.

In fact, $\varepsilon_{res} = \varepsilon_{ult}^{-\varepsilon(t)}$ .....(1.6.6.)

Thus, $\sigma_v = \varepsilon_{res}^{Ee^{-bt}}$ .....(1.6.7.)

---

* This modified Kelvin model is called a "Standard Linear Solid".

Assuming, further, that an internal pressure is acting for the purposes of stabilization of the tunnel walls and that this pressure is given by a known function of time, i.e. $\sigma_{int} = f(t)$, then the OFS could be expressed as a function of time:

$$\text{OFS}\ (t) = \frac{\varepsilon_{res}\, Ee^{-bt} - \sigma_{int}(t)}{c_u} \qquad .....(1.6.8.)$$

The accuracy of the proposed relationship depends primarily upon the nature of the soil and its rheological properties and secondly upon the groundwater regime existing near the face and around the circumference. Maybe it is reasonable to suppose that the relationship in question is valid for short time domains, such as, for instance the time elapsed between the excavation and the installation of the early support of the tunnel.

CHAPTER 2

SURFACE SETTLEMENT CAUSED BY SOFT GROUND TUNNELLING

2.1 INTRODUCTION

Any cavity or tunnel excavation constitutes a discontinuity in the subsurface ground volume, and as a result disturbances occur in the state of stress and strain in the vicinity of the opening. As a consequence, this disorder causes deformations and displacements of the ground mass, these displacements being represented at the ground surface as a settlement phenomenon.

Many theories have been developed in an attempt to describe or model the actual mechanism of the ground movement in general and the surface settlement in particular. It is a natural fact that most of these theories are concerned with settlements due to mining operations rather than those due to tunnelling.

Unfortunately, the concept of settlement due to tunnelling has sometimes been treated consciously or unconsciously on the basis of the same assumptions and relationships which govern the mining phenomenon. It may be claimed that this is a groundless and rather dangerous oversimplification because, although the deformation mechanics of both tunnelling and mining follow approximately the same basic pattern, there are some substantial differences between them.

The main practical issue, however, is the transformation of the semi-empirical or purely theoretical concepts concerned with ground movements into handleable formulae expressing the major surface subsidence parameters with relation to the geological and geometrical elements of the underground opening. Nevertheless, the focus of attention in the present Chapter will be concentrated on the state of predictive art in subsidence due to soft ground tunnelling, with a brief reference to the generalized theoretical background.

2.2 REVIEW OF THE EXISTING BASIC CONCEPTS

The existing settlement theories have been developed primarily to explain ground movements created by longwall coal mining, and they could be classified into two main groups the so-called empirical concepts, and the elastic theory concepts.

The first group includes a) the mechanical approach which is related mainly to the pressure arch formation hypotheses, b) the stochastic hypothesis which will be examined separately later, c) laboratory models, which experimentally reproduce subsidence deformations with the aid of, for example, gelatine, and d) field data analysis such as the survey conducted by the British National Coal Board at 157 collieries and which resulted in the correlation and statistical treatment of the basic parameters involved.

The second group comprises the concepts of the classical theory of elasticity using various assumptions for the behaviour of the media. There is the linear elastic, the plastic or the viscoelastic approach. An outline of these concepts is illustrated in the following diagram

OUTLINE OF SUBSIDENCE MECHANISM CONCEPTS

SUBSIDENCE CONCEPTS

EMPIRICAL CONCEPTS

a) Mechanical (pressure arch)

SZECH, (1966, 1970)
AVERSIN, (1954)
LIMANOV, (1957)

b) Stochastic media

LITWINISZYN, (1953, 1956, 1957, 1957b)
SMOLANSKI, (1960)
BODZIONY and SMOLARSKI, (1960)
BODZIONI, LITWINISZYN and SMOLARSKI (1960)
LITWINISZYN and SMOLARSKI, (1962)
LITWINISZYN, (1964)
SWEET And BOGDANOFF, (1965)
SWEET, (1965)

c) Field data analysis

N.C.B. and co-workers

d) Laboratory models

WHETTON and KING, (1959)
HOFFMAN, (1964a, 1964b)
RANKILOR, (1970)

....

ELASTICITY THEORY CONCEPTS

a) Elastic approach

HACKETT, (1959, 1964)
BERRY, (1964, 1969, 1963)
BERRY and SALES, (1961)
SALAMON, (1964)
VOIGHT and SAMUELSON, (1969)

b) Plastic approach

DAHL, (1967)
PARISEAU and DAHL (1971)

c) Viscoelastic approach

IMAM, (1965)
BERRY, (1964)
MARSHALL and BERRY, (1966)

....

Major differences between the ground deformation in mining and tunnelling could be attributed to the following factors

a) The depth factor, which in the case of mining excavation is far greater than that for soft ground tunnelling.

b) Coal mining usually involves the disturbance of rocks, whereas most tunnelling in Britain takes place in soft ground.

c) Ground stabilization via compressed air, chemical injection, ground water freezing and ground water lowering is of little importance in mining operations, while for tunnelling in urban areas it is a major issue before and during construction.

d) Lining and support systems differ considerably in the two cases considered.

e) The majority of settlement profiles in tunnelling are subcritical (in mining subsidence terminology) in contrast to most coal mining long-wall faces.

f) Ground losses are very small in tunnelling while in mining they can reach appreciably high values.

2.3 SURFACE SETTLEMENT RESULTING FROM SHIELD TUNNELLING IN SOFT GROUND.

In order to define the magnitude of surface settlement due to shield tunnelling, some assumptions have to be made with respect to the main contributing factors and the nature and behaviour of the ground involved.

As a first approximation - and assuming non-dilating, non-bulking ground - it is reasonable to suggest that the volume of the settlement profile is the sum of the volume of material entering at the face plus the volume of the annular void behind the lining created by the tail-skin.

SZECHY (1970) also suggested taking into account the volume resulting from the void created by material compression within a PROTODYAKONOV de-coupled arch (see Appendix 1). It must be stressed, however, that SZECHY'S analysis primarily concerns cohesionless soils where arching phenomena (such as the formation of the de-coupled arch) are possible.

The second main assumption is that the ground density is independent of depth, and that the shear strength increases linearly with depth (see Appendix 2).

In fact, making the assumption that the volume of the soil mass, which is responsible for the loosening and thus the surface settlements, will mobilize in both cohesionless and frictionless materials the full shearing resistance along a rupture plane with inclination $(45+\phi/2)^{\circ}$ to the horizonta it is possible (excluding arching phenomena) to use the same analysis for any kind of soft ground tunnelling.

The geometrical arrangement of SZECHY'S op cit model is illustrated in Figures 2.1.1 and 2.3.2. The former Figure shows a transverse settlement profile (A) according to the model, and an actual measured profile (B) caused by the hand excavation of a 4.146m diameter shield driven tunnel at an axis depth of 29.3m in London clay.

A comparison between the model and the actual case history reveals good compatibility between the two. The predicted magnitude of the span of the settlement trough (Y_3) is equal to 64.45m*, while the measured span

---

* $Y_3 = 2(R\operatorname{cosec}\beta + Z\cot\beta)$, and $R = 2.07$m, $Z = 29.3$m, and $\beta = 45^{\circ}$ if $\phi = 0^{\circ}$ (undrained shear deformation).

is approximately equal to 70m. The latter exceeds the former by 8%. The forward extension (Y_1) of a settlement profile is equal to 29.3m according to the model, and 19m according to in-situ measurements (34.5% less).

Another interesting feature is the difference in the shape of the shear surface. A straight line inclined 45 degrees upwards is assumed from the model whereas a curved surface may be postulated from the measurements as shown in Figure 2.3.2 (Note that X1, Y1, Z1, are measurement stations for settlement and horizontal ground movement and are on the centre line of the tunnel, station X1 is actually slightly displaced - 0.85m - from the centre line).

Now, let us assume that the volume of the settlement trough is V_{surf} and let the maximum settlement be s_{max}. Although, the delimiting limbs of the settlement basin will be sigmoidal, as a first approximation it is possible to assume that they are straight and hence to regard the trough as a pyramid of height s_{max} and of rectangular cross-section (Y_2Y_3). This approximation (which is certainly valid in the case of a harmonic profile) is shown in Figure 2.3.3. Accordingly,

$$V_{surf} = \frac{1}{3} \text{ Base x Height} \quad \text{or,}$$

$$V_{surf} = \frac{4}{3} \left(R \operatorname{cosec}\beta + Z \cot\beta \right) Z \cot\beta \; s_{max} \qquad \text{..... (2.3.1.)}$$

Applying the fundamental hypothesis that the volume of the soil included in the surface settlement curve (V_{surf}) must be equal to the volume of soil lost at the end of the tunnel (V_{exc}) due to the excavation (no dilation in the intervening strata) one may write:

$$V_{surf} = V_{exc} \qquad \text{..... (2.3.2.)}$$

Thus, the maximum settlement could be expressed as,

$$s_{max} = \frac{3\,V_{exc}}{Y_2 Y_3} \qquad \text{.....}(2.3.3.)$$

or

$$s_{max} = \frac{V_{exc}}{2Z \cot\beta\,(R \operatorname{cosec}\beta + Z \cot\beta)} \qquad \text{.....}(2.3.4.)$$

The later equation is obviously an incomplete relationship and might be useful as a first approximation only because the prediction of settlement amplitudes at different planes along the profile would be inaccurate if based on the planar trough side concept.

Additionally, one could argue that inclinometer data suggest that this idea is not really acceptable. In order to overcome this difficulty, either a harmonic analysis can be used or the profile can be approximated to an error curve (the well known GAUSSIAN) along any section.

Nevertheless, another approach of the analytical expression for the transverse surface settlement profile is possible through the harmonic analysis. Figure 2.3.3. illustrates the harmonic analysis* of the settlement semi-profile, so that the profile is resolved into a linear component and into a harmonic component which can be approximated by a sine wave.

Let therefore s_1 be the vertical settlement at any point on the profile, and let s_2 be the same component on the linear profile. Finally, let s_o be the absolute difference between s_1 and s_2. The geometry of the arrangement indicates that,

$$\frac{s_2}{s_{max}} = \frac{\ell_1}{Z \cot\beta}, \text{ therefore } s_2 = \frac{\ell_1\, s_{max}}{Z \cot\beta} \qquad \text{.....}(2.3.5.)$$

---

* This concept is developed on the basis of P.B. Attewell's lecture notes (University of Durham, Academic year 1972-73).

Equation (2.3.5.) may be approximated to

$$s_2 \simeq d.s_{max} \sin \frac{2\ell 1}{Z\cot} \qquad .....(2.3.6.)$$

where d is a constant.

Accepting that the slope of the settlement profile is horizontal at the point (ℓ =0, Zcot β), the constant (d) may be designated as $d = \frac{1}{2\pi}$.

$$\text{Since} \quad s_1 = s_2 - s_o \qquad .....(2.3.7.)$$

it follows that the final relationship is of the form,

$$s_1 = s_{max} \left(\frac{\ell}{Z \cot\beta} - \frac{1}{2} \sin \frac{2\ell 1}{Z \cot\beta} \right) \qquad .....(2.3.8.)$$

The point of inflexion of this profile is defined by the maximum slope, i.e. $ds/d\ell = 0$ which gives a value of $\ell_{inf} = \frac{Z \cot\beta}{2}$

ATTEWELL and FARMER, (1972, 1974) based on SZECHY'S (1970) model developed an analysis assuming that the form of the axial and transverse settlement profiles can be approximated by the error function. They finally derived the following relationship for the maximum settlement,

$$s_{max} = \frac{9V_{exc}}{2\ Y_2.Y_3} \qquad .....(2.3.9.)$$

The latter equation is in fact a more refined form of equation(2.3.1.) and can be written more analytically as,

$$s_{max} = \frac{9V_{exc}}{4Z \cot\beta\,(R \operatorname{cosec}\beta + Z \cot\beta)} \qquad .....(2.3.10.)$$

2.4. THE STOCHASTIC THEORY OF GROUND MOVEMENTS AND SURFACE SETTLEMENTS

An important development took the form of a series of papers by LITWINISZYN concerned with stochastic theory as a tool for settlement prediction. LITWINISZYN (1953, 1956, 1957, 1957b) proposed an abstract model consisting of many layers of small uniform spheres in 3-dimensions or discs in 2-dimensions falling into "cages" in a random manner under the action of gravity. In fact, the removal of a single sphere leaves an empty space which is due to be occupied by another sphere which in turn creates a second void. The laws governing the upwards movement of voids or downwards movement of spheres are probabilistic. The translocation of a sphere from the point (X_2, Z_2) to X_1, Z_1) in a Cartesian plane is given by the diffusion-like differential equation

$$A \frac{\partial^2 P}{\partial X^2} - \frac{\partial P}{\partial Z} = 0 \qquad \text{.....(2.4.1.)}$$

where P is the probability of the sphere moving down
and A is the coefficient with the dimension of length.

The general solution to equation (2.4.1) is

$$P = s(X,Z) = \frac{1}{\left[4\pi A(Z_2-Z_1)\right]^{1/2}} \exp\left[-\frac{(X_2-X_1)^2}{4A(Z_2-Z_1)}\right] \qquad \text{.....(2.4.2.)}$$

where s(X,Z) is the settlement at (X,Z) point.

LITWINISZYN shows that equation (2.4.2.) takes the form of the well-known error curve

$$s = s_{max} \exp\left(\frac{-x^2}{2i^2}\right) \qquad \text{.....(2.4.3)}$$

where s_{max} is the maximum settlement,

i is the standard deviation, or the displacement of the point of inflexion on the settlement profile from the vertical centre plane of the disturbance, and

s the settlement in the point (X,Z).

It may be argued that the model has certain disadvantages due to the following reasons.

a) It completely ignores the stresses involved in the settlement mechanism.

b) As the spheres move always downwards there is no accommodation for upwards ground movements, such as heave for instance, which, it is claimed, sometimes occurs.

c) The model disregards the horizontal components of ground movements, so restricting its validity to settlement only.

d) It would be difficult to find a real geological material with the idealized properties of the uniform spheres as proposed. Even for the case of a granular soil the similarity is rather poor if a friction or apparent cohesion in water-bearing strata is taken into account. Also, as has been forcibly noted by BERRY (1969), from the mathematical point of view the model suffers by adopting the principle of superposition. Indeed, VOIGHT and PARISEAU. (1970) stressed that the experimental evidence obtained with sand as a mediumdoes not support the validity of superposition. BODZIONY, LITWINISZYN and SMOLARSKI (1960) suggested a delinearization of the concept. No doubt such a process would probably introduce complexities such as the necessary formation of constitutive laws.

It is accepted that every theory can only be judged by its performance when applied to actual practice. From that point of view, the stochastic concept does assume a certain validity. PECK ET AL (1969) pointed out that the symmetrically-shaped settlement profile over a tunnel may be approximated by the GAUSSIAN error curve not only on theoretical grounds but, more importantly, on the grounds of convenience and easy-to-use properties of the function, which is completely defined by the maximum settlement (s_{max}) and the standard deviation (i). The area under the curve (the settlement volume per unit advance) is given by

$$V_{surf} = \sqrt{2\pi}\, i\, s_{max} \qquad .....(2.4.4.)$$

and is a value of great importance for prediction of settlement especially in tunnels driven under urban areas. PECK (1969) supported the "stochastic theory" by presenting in a very analytical and critical manner case studies of tunnels in soft ground constructed and supported by various methods.

However, the main conclusion is that the error curve does fit reasonably well the majority of cases, thus greatly assisting the engineer in his calculations.

2.5. PREDICTION OF SETTLEMENT ASSOCIATED WITH SOFT GROUND TUNNELLING

The problem of settlement prediction consists of two quite separate parts. There is the question of the shape of the settlement trough, and the question of ground loss incurred during tunnelling. These questions are interrelated by common factors. For instance, knowledge of ground loss leads to the estimation of V_{surf}, which in turn is related to the main parameters of the settlement trough. Accepting the arguments of PECK (1969) and taking the "error function" as the most reasonable representation of the shape of a settlement curve, the problem is one of the designation of the standard deviation (i) or the maximum settlement (s_{max}) for the definition of the particular curve. By combining results from theoretical elastic analyses and model tests on the basis of stochastic theory, SCHMIDT (1969) derived a relationship relating the geometrical elements of the tunnel to the standard deviation

$$\left(\frac{i}{R} \right) = K\left(\frac{Z}{2R} \right)^{m} \qquad .....(2.5.1.)$$

where i is the standard deviation for a normal distribution of data,

K is a coefficient which is very close to unity

m is an exponent equal to 0.8

Equation (2.5.1.) is expressed independently of the type of soil. PECK (1969) confirmed indirectly the validity of SCHMIDT'S relationship by providing data for settlement over a number of tunnels. He concluded that the ratio i/R appeared to be greater in clay than in non-cohesive soils.

SCHMIDT'S op cit relationship is plotted (Figure 2.5.1.) in the same graph with a similar function derived from SZECHY (1970) if it is assumed* that the span of transverse settlement profile is equal to

$$Y_3 = 6i \qquad .....(2.5.2.)$$

Thus,

$$2(R \operatorname{cosec}\beta + Z \cot\beta) = 6i$$

Therefore

$$\frac{i}{R} = \frac{2}{3}\left(\frac{\operatorname{cosec}\beta}{2} + \frac{Z}{2R}\cot\beta\right) \qquad .....(2.5.3.)$$

The graph reveals that the functions are very close to one another for the limits of $1 < Z/2R < 9$. For the tunnel under consideration, $Z/2R = 7.07$ and $R = 2.07$. Therefore, the standard deviation is $i = 9.88$m on the basis of SCHMIDT'S (1969) equation, and $i = 10.24$m according to the SZECHY (1970) model.

---

*The assumption is quite reasonable because it is known from the properties of the normal probability curve that 99.7% of the volume per unit advance is contained within a transverse profile span between the limits of $-3i$ and $+3i$.

MUIR WOOD (1970) has pointed out the possibility that Schmidt's value of the ratio $\bar{i}/R$ might be fairly reliable for shield driven tunnels. In the derivation of his equation SCHMIDT assumed that volume changes in the subsiding mass can be neglected. PECK ET AL (1969) also argued that the equation can be used with confidence in predicting the width of the settlement troughs in clay, since the immediate soil displacements around a tunnel in clay takes place in an undrained condition and, thus, with little or no volume change.

In the context of ground loss, the percentage of the average settlement volume (V_{surf}) with respect to the theoretical volume, is a useful index of loss of ground.

Assuming that the theoretical volume of excavation per unit advance for a circular tunnel is

$$V_{exc} = \pi R^2 \qquad .....(2.5.4.)$$

The loss of ground might therefore be

$$V_\ell = bV_{exc} \quad \text{or} \quad V_\ell = b\pi R^2 \qquad .....(2.5.5.)$$

where b is a constant

π is 3.1415.

But according to the main hypothesis, which is a modified form of the mass conservation principle, the volume of the ground under the surface settlement trough (V_{surf}) is equal to the volume of loss of ground in the tunnel, (V_ℓ).

Thus,

$$V_{surf} = V_\ell \quad , \text{or} \ \sqrt{2\pi}\, i\, s_{max} = b\pi R^2 \quad \text{or}$$

$$\frac{s_{max}}{R} = \frac{b\ R}{\sqrt{2\pi}\ i}$$

or, $$\frac{s_{max}}{R} = \frac{CR}{i} \qquad \text{if } b\pi/\sqrt{2\pi} \text{ is written as C} \qquad .....(2.5.6.)$$

Taking into account SCHMIDT'S relationship,

$$\frac{s_{max}}{R} = d\left(\frac{Z}{2R}\right)^{-m} \qquad .....(2.5.7.)$$

where $d = C/K$

Taking logarithms of both sides of equation (2.5.7.), we have

$$\log\left(\frac{s_{max}}{R}\right) = \log d - m\log\left(\frac{Z}{2R}\right)$$

$$\text{or} \quad \log\left(\frac{Z}{2R}\right) = \frac{1}{m}\left[\log d - \log\left(\frac{s_{max}}{R}\right)\right]$$

$$\text{and} \quad \log\left(\frac{Z}{2R}\right) = \log\left[\frac{d}{\left(\frac{s_{max}}{R}\right)}\right]^{1/m}$$

finally,

$$\log\left(\frac{Z}{2R}\right) = \log\left[d\left(\frac{s_{max}}{R}\right)^{-1}\right]^{n}$$

where $1/m = n$.

Now taking antilogarithms,

$$\left(\frac{Z}{2R}\right) = d^{n}\left(\frac{s_{max}}{R}\right)^{-n}$$ for convenience we substitute

$d^n = A$, therefore,

$$\left(\frac{Z}{2R}\right) = A\left(\frac{s_{max}}{R}\right)^{-n} \qquad .....(2.5.8.)$$

Relation (2.5.8.) was proposed by MYRIANTHIS (1974a) and supported by the accompanied analysis of 40 case studies, (see Appendix 3).

Coefficient A and exponent n of relation (2.5.8.) take values depending upon the soil type where the tunnel is driven.

On the other hand, the equality of volumes indicate that a linear relationship must exist between V_{surf} and V_{exc}, since $V_{surf} = V_{\ell}$ and $V_{\ell} = bV_{exc}$. Indeed, the analysis of numorous case histories indicated (MYRIANTHIS op cit) that a relationship holds in the form of

$$V_{surf} = bV_{exc} + C \qquad .....(2.5.9.)$$

The coefficients b,C were determined through least squares regression techniques, and as in the case for maximum subsidence it was found that b and C depend a great deal upon the properties of the ground, as shown in Figures 2.5.4.,2.5.5. As expected, the coefficient b,which does represent a characteristic index of ground loss,is higher in the case of granular soils than for plastic clays.

PECK (1969) suggested that many but not all soft ground tunnels can be discussed with respect to loss of ground and settlement on the basis of four principal groupings of soils granular soils with no cohesion other than that imparted by capillarity, cohesive granular soils, non-swelling stiff to hard clays, and stiff to soft saturated clays.

The classification system adopted for the present thesis is more or less that of PECK op cit.

A graph of the dimensionless ratio Z/2R versus s_{max}/R has been plotted in Figures 2.5.2. and 2.5.3. for the case of stiff plastic clay and saturated plastic clay plus granular soil respectively. In general, the fitting for the fifteen cases of stiff plastic clay with the proposed equation (2.5.8.) is quite satisfactory. It appears that the pheonomenological relation

$$\frac{Z}{2R} = 9.35 \left[\frac{s_{max}}{R}\right]^{-0.41} \qquad .....(2.5.10.)$$

does reasonably represent the interrelationship between maximum settlement and tunnel geometry. The same behaviour could be claimed for the case of granular soil and for plastic clay, but with less satisfactory results.

Figures 2.5.2. and 2.5.3. indicate that there is a "critical" value for the ratio Z/2R, where the ratio s_{max}/R tends asymptotically to infinity. Obviously, this is a purely theoretical consideration attributed to the exponential nature of the proposed relationship, while in actual practice the maximum settlement is bound between certain upper limits imposed by the quality of workmanship and the implementation of ground stabilising processes.

Nevertheless, it is reasonable to accept that the deeper the tunnel, the more arching* and thus the less the surface settlement. On the other hand, the larger the tunnel cross-section (high values for R), the higher V_{cxc} and V_{surf} which in turn facilitate higher values of maximum settlement (s_{max}). However, the main argument in favour of the usefulness is of any relationship such as these proposed for settlement prediction is that they are primarily addressed to design engineers as a first quick estimation of the extent and amplitude of settlement due to soft ground tunnelling. However, practical and safety reasons bound the upper and lower limits for values of the ratios Z/2R and s_{max}/R. In that respect, arguments concerning, for example, an asymptotic behaviour for the functions involved, are of a rather academic value. Finally, it is worthwhile noting that the ratio Z/2R, in contrast to the case of stiff plastic clay, varies within a small range of values in the case of granular soils, while the ratio of s_{max}/R varies quite widely. The latter is compatible with the

---

*GETZLER et al(1968) in a series of experiments studied the loads on a rigid underground structure supported by a flexible base when a uniformly distributed static load acts on the ground surface. The aim of the experimental programme was the detection of any arching involved and the connection with the other factors which influenced the underground structure. The results obtained reveal that the amount of arching tends to increase but there is more or less asymptotic behaviour towards an ultimate level of arching when the depth of the structure increased. In a more refined analysis GETZLER et al(1970) also confirmed the existence of arching which again increases asymptotically with the depth/width ratio of the underground structure.

nature of granular soils.

A rather linear relationship between V_{surf} and V_{exc} appears in Figures 2.5.4. and 2.5.5. which include case history data. The quality of fit of the actual data reasonably justifies the proposed linear equation (2.5.9.). This relationship is of particular importance because it provides a first approximation of the volume under the settlement curve per unit advance from estimates of the theoretical volume of tunnel excavation V_{exc}. Also, an estimate of a mean value for loss of ground is possible from the graphs of Figures 2.5.4. and 2.5.5. (the latter with more reservations). A plot of Z/2R versus the loss of ground V_ℓ is illustrated in Figure 2.5.6. where, for reasons that are not immediately apparent, there is a strict demarcation between cases in granular soils above and below the ground water table. The curve fitting for the cases of saturated plastic clay is less successful, while there is no correlation at all for the cases of stiff plastic clay. A Z/2R versus V_ℓ relationship is to be expected because

$$V_\ell = (V_{surf}/V_{exc}) \times 100 \ \% \qquad \text{.....(2.5.11.)}$$

Taking into account that,

$$V_{surf} = \sqrt{2\pi}\ s_{max}\ i \qquad \text{.....(2.5.12.)}$$

it follows that equation (2.5.11.) can be written

$$V_\ell = \frac{\sqrt{2\pi}}{\pi} \left(\frac{s_{max}}{R}\right)\left(\frac{i}{R}\right) \qquad \text{.....(2.5.13.)}$$

Substituting $(\frac{s_{max}}{R})$ and $(\frac{i}{R})$ from relationships (2.5.8.) and (2.5.1.) respectively,

$$V_\ell = G\left(\frac{Z}{2R}\right)^{m+n} \qquad \text{.....(2.5.14.)}$$

where G is a constant equal to $\frac{\sqrt{2\pi}}{\pi}\ K\ A^{-n}$

Since $m = 0.8$ from equation (2.5.1.) and $n = 0.0574$ from Figure 2.5.3. it follows that,

$$V_{\ell} = G\left(\frac{Z}{2R}\right)^{0.857} \qquad \text{.....(2.5.15.)}$$

Equation (2.5.15) can be approximated by a linear relationship for the narrow domain of values

$$0 < Z/2R < 5$$

Finalising the above analysis, it is worth noting that the phenomenological relationships have been extracted under the dominant assumption that the loss of ground is a function of the square of the tunnel radius.

This is obviously a debateable point and particularly if MUIR WOOD'S (1970) analysis is taken into consideration. According to that concept, the loss of ground into a shield-driven tunnel may entail the following contributory factors

a) At the face, computed as $V_{\ell 1} = \pi R^2 h$ with normal limits (0.1-?)%,

b) behind the cutting edge or bead of the shield $V_{\ell 2} = 2\pi Rt$, with normal limits (0.1 - 0.5)%,

c) along the shield, $V_{\ell 3} = \pi \ell_o v/8$, with normal limits (0 - 1)%,

d) behind the tail of the shield $V_{\ell 4} = \pi R(R - R_o)$ with normal limits (0 - 4)%.

where R is the radius of the shield ,

R_o is the external radius of the lining,

t is the relief behind the cutting edge ,

v is the "look up" of shield measured as extent of out-of-plumb on vertical diameter,

ℓ_o is the length of shield,

h is the horizontal movement of ground at face, per unit length of advance of shield.

Thus the total amount of ground loss may be expressed as:

$$V_{\ell} = \frac{\pi \ell_o v}{8} + 2\pi\, t\, R + \pi R(R - R_o) + \pi h R^2 \qquad .....(2.5.16.)$$

The second factor of equation (2.5.16.) is linearly related to tunnel radius and takes normal limits of 0.1 - 0.5.% The third and fourth factors of the same equation are functions of the square of tunnel radius and have normal limits of 0.1 - over 4%. The first factor is apparently radius-independent.

Adoption of the hypothesis that $V_{\ell} = f(R^2)$ seems to be justified since it accounts for over 4% of the ground loss, while the hitherto ignored linear relationship $V_{\ell} = f(R)$ accounts for only 0.5%. Because the above analysis has so far totally ignored the radial loss of ground (linearly related to tunnel radius), it must be stressed that the latter becomes an all important factor for tunnels with small diameters where the face-take area ($\sim\pi R^2$) is very small. However, for greater precision, the basic hypothesis of $V_{\ell} = b\pi R^2$ should really be replaced by a linear polynomial of the second degree:

$$V_{\ell} = A_o + A_1 R + A_2 R^2 \qquad .....(2.5.17.)$$

but this would tend to sacrifice simplicity for extra - and questionably - more accuracy.

Besides the stochastic approach of LITVINISZYN more recently an attempt has been made by FOLYAN et al (1970) towards the use of decision theory as a tool for settlement prediction. In a case study involving settlements, the reliability of settlement predictions for San Francisco Bay mud was reported to fall within ± 20% of the actual settlement. FOLYAN op. cit. stated that probabilistic procedures provide a framework that can assist the engineer to organize, accumulate, interpret and evaluate experience. They can become a distinct aid in Soil Mechanics and Foundation Engineering if properly applied.

2.6 THE DEVELOPMENT OF SURFACE SETTLEMENT PROFILES DURING SOFT GROUND TUNNELLING.

Early knowledge of time-dependent ground movements in the soil mass above and around a tunnel is vital because it could lead to a rough estimate of the deformation of tunnel walls as a function of the predicted earth response. It has been shown that ground deformations which take place in the vicinity of a tunnel are ultimately reflected at the surface by the formation of a settlement trough. The implication of the time factor in the genesis and progression of surface and sub-surface ground movements due to tunnel advance is a complicated problem. Two possible alternatives are available in order to study this effect a rheological or a phenomenological approach. The latter can draw conclusions from the detailed study of a given number of case histories (the more the better) ignoring the actual mechanisms which create the observed ground behaviour. As for the rheological approach, DEERE et al (1969) refer to these laws in a tunnelling context. They state that "since these laws are mathematical approximations of the real behaviour under specified simple conditions, the effect of certain conditions that have little influence on the behaviour under simple conditions, but may have greater influence under more complex conditions, may not be adequately accounted for. For this and other reasons, it is not likely that predictions on this base are accurate".

This comment is very true for tunnelling, where excavation complexities and ground conditions may often vary over a distance of a few metres. However, in a phenomenological context, and in the light of a very simple analysis of six available case studies, (see Table 2.6.1.) an attempt has been made to relate the progression of the surface settlement curve with the tunnel advance. The results indicate the existence of such a relation MYRIANTHIS (1974b).

A typical surface settlement profile appears in Figure 2.6. 1. and it shows a fair agreement with the normal probability curve. The standard deviation (i) is located 15m from the tunnel's centre line and the curve is converging towards the point of zero settlement at a distance of more than 35m. This distance is reasonably comparable with the 45m distance which might be expected from the properties of the normal probability curve (3i = 45m).

Figure 2.6. 2. illustrates how the evolution of the profile relates to the position of the shield, from the same graph there is evidence that ground movements originate when the plane of the shield face is located over 20m from the datum plane. Thus, at a distance of 20m (tunnel approaching) the s_{max} is 8% of the measured s_{max} in the final profile, 23% at 10m and 47% during shield passage. The calculation is based on the assumption that s_{max} has reached its maximum when the shield is located 36m away from the datum point. Of course, small movements may continue on the surface over a longer period of time and in that case the limit of 36m seems arbitrary.

Nevertheless, it might be claimed that these small movements do not greatly influence the safety of any overlying structures since such amplitudes of movement could effectively be absorbed without any drastic differential settlement in the foundation of a building.

The second graph in Figure 2.6. 1. is a relationship between the s_{max} and the tunnel advance. As far as cases 5 and 6 are concerned in Figure 2.6.3., this relationship takes the form of a modified normal distribution function.

However, the point of inflexion on the settlement development profile occurs when the tunnel advance is zero, that is, during shield passage, the non-symmetric right hand part of the curve being attributed to the slow convergence until an ultimate s_{max} is reached.

Data in Table 2.6.1. have again been plotted in a semi-dimensionless manner in an attempt to normalize the s_{max} parameter. It is to be expected from the equation (2.5.8.) that the ratio s_{max}/R increases as Z/2R decreases, as shown in Figure 2.6.1. From the same graph it could be argued that in almost all cases the ratio s_{max}/R converges for practical purposes when the tunnel advance is between 40 to 50m away from the point in question, and also that the ground disturbances start when the tunnel approaches to within a distance of -15 to -10m. Another feature of this particular graph is that cases 2, 4, 5 and 6 reasonably approximate to a normal probability curve, but in case 3 there is no point of inflexion at all.

Finally, it may be noted that the points of inflexion seem to develop at a distance of between 0 and +10m with an apparent tendency to move towards the zero as the ratio Z/2R increases. Nevertheless, the above analysis indicates that the graph of s_{max}/R versus the tunnel advance can be approximated to a modified normal distribution function with the point of inflexion lying between 0 and 10m along the tunnel advance axis. Clearly, there is a need for more case studies to be examined in order to confirm or modify the implied trend. Until then, the above conclusions must serve as general guidelines only.

CHAPTER 3

DESCRIPTION OF IN-SITU MEASUREMENTS

3.1 INTRODUCTION

The present Chapter *describes the methods of in-situ measurements which formed part of a research programme aimed at determining ground deformations caused by hand excavation of a 4.15m external diameter shield driven tunnel at an axis depth of approximately 30m in London clay.

3.2 DESCRIPTION OF THE WORKING SITE

The section of the tunnel chosen for detailed observation was the initial length of the northbound North tunnel starting from the working access shafts at Green Park station (Figure 3.2.1.). This tunnel forms part of the stage one contract let by London Transport Executive for the new Fleet Line comprising 2¾ miles of a 4m diameter double tunnel from the Strand to Trafalgar Square station via Green Park and Bond Street to Baker Street station, where it will take over the existing 11 miles of the Stanmore Branch of the Bakerloo line.

The northbound North section was chosen because, with the exception of a short length of tunnel in Regents Park, it is the only part of the new line passing through ground that is relatively unaffected by other services, surface structures or surface cover, excluding some recent site concrete. The ground comprises mainly blue and brown London clay over-lain by a thin layer of sand/gravel.

3.3 IN-SITU MEASUREMENT METHODS

As was stated by ATTEWELL and FARMER (1972 1974) the choice of instrumentation was governed by the need to obtain a sufficiently high degree of

* Most of the description in this Chapter is taken from Attewell & Farmer (1972)

accuracy to record the small surface and subsurface movements expected to result from the tunnel excavation, whilst at the same time retaining sufficient simplicity to permit a large number of observations to be recorded over the short time period during which the instrumented ground was under the influence of the tunnel excavation.

The instrumentation for the tunnel is described in the next part (3.4.) of the present Chapter where it can be seen that vertical surface movements were monitored using a precise Cooke level at stations established along three lines normal to the tunnel centre line and approximately 9m apart (see Figure 3.2.2.). The design of the TBM (temporary bench mark) at Green Park is shown in Figure 3.3.1. together with the design of the actual survey stations. A detailed scale layout (cross-section) of the boreholes and inclinometer access tubes with the exact position of each magnetic ring as initially located on each tube is illustrated in Figure 3.3.2.

For safety precautions with respect to possible water inflow at the tunnel during construction it was decided that the centre line boreholes should be terminated 1.5m above soffit level. Similarly, the nearest encroachment of borehole X2 to the springline is approximately the same. It would appear that the borehole arrangement is well designed for the work that was undertaken. Equally, it could be argued that there were two drawbacks

a) The tubes in boreholes X2, Y2, Z2, X3, Y3 not in the centre line were not extended below the tunnel axis level. To some extent this inhibited the measurement of the complete ground movement pattern around the tunnel and specifically below the invert horizon.

b) In retrospect, it would undoubtedly have been very useful if a borehole had been placed at a horizontal distance greater than 10m from the tunnel centre line in order more precisely to demark the boundaries between the 'disturbed' and the undisturbed' ground.*

3.4 INSTRUMENTATION

In order to detect sub-surface horizontal and vertical ground movements through the 100mm diameter boreholes, inclinometers and settlement gauges were used. The Soil Instruments torpedo inclinometer incorporating a digital read out has a resolution of ± 1m horizontal deflection computing to ±0·1mm. It operates inside an aluminium access tube grouted into the borehole. A clay-cement grout designed to have a three months strength equal to that of the surrounding clay infills the annulus between borehole wall and tube. The borehole tube itself has four keyways dividing the tube's circumference into four equal parts. Two diametrically opposed keyways were located parallel to the longitudinal axis of the tunnel, while the other two were at right angles to it. Nevertheless a set of readings comprised one run up and one run down each tube at 4 x 90° settings in order to give maximum accuracy of readings in two orthogonal directions. Readings were taken at every meter of torpedo travel down the tube. As HANNA (1973) has pointed out, the precision of inclinometer measurements may differ significantly from the precision of the inclinometer system as a whole. The main factors affecting any observations are.

a) possible spiralling of the casing, check tests eliminated this possibility,

b) a lack of repeatability of the reading position,

c) the sensitivity and therefore dependence of the inclinometer to temperature and humidity change,

and finally,

* There were, however, practical on-site difficulties which tended to militate against adopting this course of action.

d) the skill of the observer.

In order to detect vertical ground movements, an electrical borehole settlement system was provided which comprised four or more magnetic rings located at various depths in each borehole and located on the outside of the aluminium access tube. The accuracy of these measurements was estimated at ± 1mm and attempts were always made to restrict the taking of these readings to a single observer in order to limit the personal error. These settlements were measured from the surface by the use of an audible 'bleeper' relay unit which was lowered down the hole on the end of a steel tape. As the moving relay probe entered the magnetic field created by the rings, closed contact was established and the ring position established by audible note. Four measurements were taken - entering and leaving the magnetic field on both the up and down runs - and the average of these four measurements was taken. The vertical surface settlements (accuracy ± 0.1mm) were monitored using a COOKE S440 precise level at stations established along three lines normal to the tunnel direction of advance. The readings of the surface movements and settlements were obtained by precise levelling, triangulation and trilateration surveying to the caps of the access tubes and to other stations forming a surface grid. Use was also made of the NPL Mekometer for precise inter-station distance measurements.

Daily surveys and instrument readings were taken for approximately 25 days after which it had been estimated that the ground disturbance would cease. During that period, the tunnel advance was observed with precision, thus making it possible subsequently to correlate the measured ground movements as a function of face advance or, in effect, as a function of time.

CHAPTER 4

GROUND DEFORMATIONS ASSOCIATED WITH SHIELD TUNNELLING IN LONDON CLAY.

4.1 INTRODUCTION

The present Chapter attempts to describe the ground disturbance which occurs during shield tunnelling in the overconsolidated stiff fissured London Clay.*

In particular, an effort is made to define the main factors which might affect the form and the magnitude of the recorded ground movement. Due recognition is made of the influence of time in the tunnelling process.

4.2 VERTICAL SURFACE AND SUBSURFACE GROUND MOVEMENTS

Typical surface (continuous lines) and subsurface (broken lines) settlements measured by precise levelling and by the settlement ring relay system are shown in Figures 4.2.1. to 4.2.4. The vertical settlement development profiles relate to boreholes X1, Y1 Z1, which lie above the tunnel centre line.+ Similarly, vertical settlement development profiles are shown for a series of vertical planes parallel to the tunnel centre line. In this case, the settlements were monitored for different depths in the boreholes X2, X3, Y2, Y3 and Z2.

All the above Figures take the form of graphs where the abscissa represents the distance between the particular borehole and the plane of the face of the shield. The tunnel advance is denoted by the letter "A" and is measured in metres in a direction parallel to the tunnel centre line. The ordinate represents vertical settlement denoted by the letter "s" and measured in mm. Each curve refers to a particular depth. All the curves

---

*Much of the description in this Chapter and some of the comment is taken from ATTEWELL & FARMER (1972), report to T.R.R.L.

+X1 was slightly displaced (0.85m) from the centre line.

have been drawn in by eye as best fits to the data points and it is to be expected that maximum vertical surface and subsurface settlements will have occurred in boreholes X1, Y1, Z1 above the tunnel centre line.

The graphs in Figures 4.2.1., 4.2.2. and 4.2.3. indicate that when the shield face is exactly below the particular borehole (or when A = zero metres) the settlement development curve tends to its point of inflexion. They also show that the maximum value of surface and subsurface settlement coincides with tunnel advance distances of 10 to 20 metres beyond the borehole point under consideration. In order to normalize the settlement development curve for the boreholes X1, Y1 and Z1, graphs are shown in Figure 4.2.5. to relate s/s_{max} versus A/z (tunnel advance/depth). From these graphs it is clear that the maximum settlement s_{max} has occurred for values of A/z ranging between 1/3 to 2/3. Another graph in Figure 4.2.6. illustrates the development of maximum s_{max} and ultimate s_{ult}* settlement with depth. It is evident from these graphs that settlement increases with depth, and if the trend of the relationship holds, then by extrapolation the amplitude of settlement at soffit level may be approximated to a value of 22mm. Figures 4.2.1., 4.2.2., 4.2.3. and 4.2.5. point to the fact that there is some apparent uplift of the ground above the soffit following the occurrence of maximum settlement.

We may note two points. First, significant uplift occurred only for the X1 and Z1 boreholes, while for Y1 there is less firm evidence. Second, the accuracy of the measurements is estimated at ± 1mm, while the recorded uplift is 3mm for X1 and 2mm for Z1, being more or less within the range of error in measurement. Alternatively, taking for granted that the uplift really did occur it may be argued that they are some reasons for justifying such a ground behaviour. These are discussed in Chapter 6 in some detail.

---

*Ultimate settlement s_{ult} is the magnitude of surface settlement when the tunnel advance is over 70m beyond the particular cross-section.

Vertical settlements at boreholes X2, X3, Y2, Y3 and Z2 which are laterally displaced from the tunnel centre line are, for obvious reasons, of reduced amplitude. This settlement reduction with lateral distance from the tunnel centre line is reflected by the form of the transverse settlement trough (see Figure 4.2.4.) which conforms quite reasonably to a normal probability curve with its point of inflexion 50% further displaced from the centre line than would be predicted on the basis of SCHMIDT'S (1969) equation (see Chapter 2.). ATTEWELL and FARMER (1974) argue that such a discrepancy might be explained at least qualitatively from the measurement evidence of some post-shield contraction and consequential extension of horizontal and vertical tunnel axes respectively.

These deformations could be partially responsible for the flattening tendency at the base of the maximum surface settlement trough, which probably is an attenuated manifestation of the uplift effect mentioned earlier.

HANSMIRE and CORDING (1972) reported on the performance of a soft ground tunnel on the Washington metro bored in river terrace deposits of Pleistocene age. Soils in the top heading were partially cemented sand and gravel and silty sand. The remainder of the heading consisted of clayey and silty zones, with shear strengths of an order of 72 kN/m^2. The contractor used a 6.4m diameter shield, and sand-cement-bentonite grout was pumped behind the poling plates after completion of each shove. The authors stressed that the typical subsurface settlements measured by extensometers indicated that two-thirds of the movement occurred over the shield. The remaining one-third occurred within about six shoves after the tail passed the instrument. Only one-third of the surface settlements could be attributed to movements over the shield and the remaining two-thirds occurred behind the tail. The delay in the total development of the surface settlement appeared to be related to the change from a three-dimensional to a two-dimensional displacement geometry as the tunnel heading was advanced. A surface point is influenced not only by deep movements immediately beneath the surface point but also by the deep movements several shoves ahead of and behind the point.

4.3 HORIZONTAL SUBSURFACE GROUND MOVEMENTS

The inclinometer records were presented in a manner somewhat similar to the settlement development curves. The curves take the form of a series of continuous records of horizontal deflection with depth, each graph being related to a particular tunnel advance with respect to the position of the inclinometer tube.

In Figures 4.3.1. and 4.3.2. deflection both in the direction of tunnel advance parallel to the line of advance and transversely towards the tunnel centre line in a direction normal to the line of advance are registered as a positive displacement.

On the line of the tunnel (Figure 4.3.1.) significant movement did not occur until the tunnel face approached within 5m of the inclinometer boreholes. This is confirmed by the X1 record but not by the Y1 and Z1 records.

Horizontal transverse displacement profiles are shown in Figure 4.3.2. Boreholes Z1 and Y1, being on the plane of symmetry, were not subjected to any movement normal to the direction of tunnel advance. Borehole X1 was offset 0.845m from the tunnel centre line and monitored a fairly uniform 5mm movement towards the centre line at the base of the hole 1.5m above the soffit. From the same Figure boreholes X2, Y2 and Z2 confirm this deformation trend, indicating a uniform and apparently localized component of deformation towards the tunnel opening at axis level of between 6 and 8mm for X2 and Y2 and 2 to 3mm for Z2. Figures 4.3.1. and 4.3.2. reveal that the horizontal deflection did reduce rapidly towards the ground surface.

Finally, the horizontal ground movement parallel to the tunnel axis above soffit level, and as related to the tunnel advance, can be explained by the compression exerted at the face through the actions of the shield rams when shoving off the last ring of lining segments. This thrust alters the state of active pressure of the clay in front of the face to one of passive pressure. Thus, noting that for the tunnel in question up to ten 50 tonnes rams may have been used to a maximum 50% power so exerting a total thrust of 250 tonnes, it seems reasonable to expect a local movement in the direction of tunnel advance rather than an intrusive decompressional movement towards the face.

WARD (1970) published data from measurements on subsurface movements during the construction of the Victoria Line in London Clay. Two sets of observations of the convergence of the London Clay towards the tunnel were made by means of sleeved rods anchored at one end in the clay and which extended to nearby underground structures where reference points were established. A set of lateral convergence measurements at the axis level of the approaching tunnel were made with reference to an existing parallel tunnel at the same level and 8.3m clear of the tunnel under construction. The results are in good agreement with the present findings. This is not very surprising because WARD op cit describes a tunnel which, from the point of view of construction and ground conditions, is quite similar to the tunnel considered in the present thesis. His second set of axial convergence measurements were made at three points at axis level in front of the face of the same tunnel. Results of this set indicate a very small axial displacement of 1.27mm close to the edge of the face compared with the displacement of 17.2mm at the axis. This implies a strong dome-like shearing of the clay at the face as it intrudes.

4.4. TIMING THE SHIELD'S DRIVE AND INTERRELATING IT TO THE GROUND MOVEMENT PATTERN.

The particular constructional conditions are certainly one of the major factors which affect the stability of the soil in the vicinity of a tunnel. Ground loss, surface and subsurface settlements and ground movements are influenced by the excavation method chosen and the manner in which the stabilization has been achieved. The tunnel under discussion was of the hand-excavated, shield-driven circular type, with a radius of 2.073m (external shield radius), lying at an average depth of 29.6m to axis level in London clay. The length of the shield was 2.36m and that of the tail-piece was 0.915m, giving a total length of 3.275m. On the outside of the cutting edge of an upper 180 degrees bead of 6.5mm thickness was provided in order to facilitate guidance and to reduce friction on the skin as the shield was pushed forward off the last ring of lining support. Some features of the shield, with the configuration of the major ground loss areas around it, are shown in Figure 4.4.1 and the graph of tunnel advance versus time is shown in Figure 4.4.2. Although some difficulty arose when estimating an average rate of tunnel advance, it seemed reasonable also to include the halt periods in order to achieve a more representative overall rate. Calculations on that basis gave an average rate of advance of 0.134m/h or 2.23 mm/min. Also, as shown in Figures 4.2.1., 4.2.2. and 4.2.3., calculations with respect to the average maximum deformation rate of an element of clay directly above the soffit produced the value of 0.005 mm/min. ,(ATTEWELL & FARMER,1972).

It is also possible to generate from these three Figures a family of curves* representing the change in rate of settlement as a function of tunnel advance. These curves are shown in Figure 4.4.3. and it may be concluded that for the borehole X1 the rate of settlement maximizes at the time of passage of the tunnel face beneath the borehole. In the case of boreholes

*This was an idea developed by the author and adopted by ATTEWELL and FARMER(1972). The calculation and plotting of the curves (Fig.4.4.3) was carried out by the author.

Y1 and Z1, the maximum settlement rates occurred when the shield was 5 to 10 metres away from the borehole in question. The curves are sensibly symmetrical about the particular tunnel advance point zero for X1, about 5m for Y1 and about 10m for Z1. This symmetry reveals that there is little or no phase shift in the settlement curve for the different ground horizons.

Finally, by plotting the maximum for each of the above curves versus depth and then expressing them as a function of time, it is possible in Figure 4.4.4. to express the maximum rate of settlement as a function of depth. This Figure indicates the "settlement velocity" of a clay column on the centre line of the tunnel above soffit level. The curve appears to follow a hyperbolic form which may be approximated by the analytical expression,

$$z = \frac{a}{(ds/dt)_{max}} \qquad \text{.....(4.4.1.)}$$

where z is a depth below ground,

a is a coefficient with dimensions L^2T^{-1}, mm^2/min,

and $(ds/dt)_{max}$ is the maximum rate of settlement for points on the centre line of the tunnel above soffit level.

From the estimated average deformation rate of clay at the soffit (0.005 mm/min) it follows that an element of clay requires 1300 minutes in order to reach the skin of the shield after deforming through a distance of 6.5mm. It is estimated that 1300 minutes corresponds in terms of tunnel advance to a distance of 2.9m. Consequently, the element of deforming soil does in fact reach the tailpiece because the length of shield and tail (2.36 + 0.915m) is obviously greater than this estimated distance of 2.9m. Thus, frictional shearresistance between clay and tailskin occurs over 41 percent of the total length of the tailpiece provided that the average clay deformation rate is uniform during the passage of the shield and tail.

In order to present a vectorial representation of ground movements for the two major planes of symmetry which lie vertically along the tunnel axis and vertically normal to it, it was decided to combine the results of the surface settlement survey, the inclinometer and the magnetic settlement ring records. Since inclinometer readings of horizontal deflection were taken every metre of depth and magnetic rings were installed at 6m intervals along the inclinometer access tube (see Chapter 3), it was necessary by using the vertical settlement development profiles to extrapolate and thus present a relationship between settlement and depth for different positions of the tunnel face. The extrapolated conversion curves are given in Appendix 4. By using these relationships it is possible to combine both the vertical and horizontal components of ground movement for the different stages of tunnel advance.

Figures 4.4.6. to 4.4.8. show the state of ground deformation in a vertical plane along the tunnel centre line during the tunnel advance. The direction and inclination of the vectors representing ground deformation - for a level just above soffit - possibly indicate a limited frictional shear resistance between clay and shield skin, confirming the validity of the earlier calculations. Also, it may be deduced from the state of these vectors that ground movement <u>in the direction of tunnel advance</u> takes place when the face is 8 to 10 metres away from the particular point of measurement. At such a distance from the tunnel face, the injected grout will be offering a degree of set resistance, and the clay deformation will be a direct result of frictional shear resistance between the soil and the grout rather than between the soil and the shield/tailskin.

BARTLETT and BUBBERS (1970) presented a simplified qualitative concept of ground movement ahead of a shield driven in stiff clay (see Figure 4.4.5.). The main assumption in their approach is that the ground is incompressible or, in terms of their model, there is no change in the area of each grid segment.

The boundary of the zone of movement ahead of the face is projected upwards at 45° to the horizontal and the vertical lines above the top of the shield generally remain vertical. With the exception of the heave development, the actual figures of longitudinal ground movement profiles tend to agree in principle with the above concept.

Early ground disturbance appears in Figure 4.4.6. where the face is 10 metres behind the borehole Z1 and a strong horizontal deflection of ground in the direction of the shield advance is indicated particularly in the upper horizons. At the 2 to 5 metres horizon above the soffit, the soil predominantly settles without any horizontal deflection, and boreholes Y1 and X1 just begin to register the presence of the shield. When the tunnel face arrives at borehole Z1, the same pattern is repeated for borehole Y1 (see Figure 4.4.6.) while at Z1 the horizontal deflection in the middle to upper soil horizons seems to decrease. In the horizon immediately above soffit level, the soil behaves as if it were under the influence of the action of the thrust from the shield. Finally, some peculiarity rises in the ground disturbance in borehole Y1 when the face is exactly coincident with it. Above soffit level, the clay moves in a direction contrary to that of the tunnel drive. This behaviour has vanished to some extent (see Figure 4.4.7.) as the vector of ground deformation rotates about its axis and re-orientates towards the direction of advance. Such a feature is not, however, the case for horizons just above soffit level where the movement increases in amplitude, probably due to the exceptionally large halt period when the tunnel face was boxed for 125 hours, as it was below the borehole Y1 and as shown in Figure 4.4.2. Thus, it may be argued that the clay during the halt period has deformed to the extent of exceeding the elastic limit.

Ground movements at right angles to the tunnel axis are considered at different stages of face advance. This is shown in Figures 4.4.9., 4.4.10. and 4.4.11 (note that the left hand side of Figure 4.4.9. illustrates the scaled layout of the boreholes with the exact position of each magnetic ring being marked.

In order to avoid confusion, the movements detected in the pair of boreholes X2,Y2 and Z2,X3 have been presented jointly by taking the mean value of each pair of curves for horizontal or vertical movement versus depth for the same point of advance in time (that is, same face position). The right hand side of Figure 4.4.9. depicts the state of the subsurface disturbance when the face is approaching the particular clay cross-section but is at a standoff distance of 5 to 10 metres. The left hand side of Figure 4.4.10 illustrates the clay deformation when the face is exactly underneath the ground cross-section, while the right hand side of the Figure relates to the face position 10 metres ahead of the cross-section. Both Figures reveal an increasingly radial "intrusion-like" trend which is eliminated in a zone defined by distances of 10-15m in the vertical axis and 5-7m in the horizontal axis.

Borehole Y3 results show that the clay is moving predominantly downwards. More generally, the horizontal component of ground movement reverts to zero over a distance of roughly 4 to 4.5 tunnel radii.

Finally, Figure 4.4.11 shows the clay motion situation when the tunnel face is 20 and 30m ahead of the ground cross-section in question.

The magnitude of the soil deformations is likely to increase steadily over a face advance of 30m, but the horizontal deflection towards the cavity seems to have decayed as the shield was retracted beyond the cross-section.

CHAPTER 5

LABORATORY TESTING PROGRAMME.

5.1 INTRODUCTION

In the present Chapter, a brief account of the strength properties of London Clay is given by reviewing the extensive data published by various authors. For the express purposes of theoretical stress analysis some laboratory tests were conducted on samples of clay taken from the site of the tunnel which is the subject of the present thesis. The test results are reported and discussed.

5.2. BRIEF REVIEW ON THE NATURE AND MORPHOLOGICAL CHARACTERISTICS OF LONDON CLAY.

a. Geology The clay which underlies most of central London is a stiff, fissured, overconsolidated, blue-grey clay. It was called "London Clay" by W. Smith in 1812. The sediments were laid down under marine conditions in the Eocene period, and subsequently the Claygate beds, followed by the Bagshot, Bracklesham and Barton beds were deposited.

These were all predominantly sandy beds with occasional clay layers. However, uplift and erosion in the late Tertiary and Pleistocene epochs have removed most of the overlying beds and half to two thirds of the London Clay itself, in only a few areas do any of the overlying beds remain (BISHOP *et al*, 1965).

Following each period of down-cutting, terrace gravels were deposited by the River Thames. The alluvium which overlies the Flood plain gravels is a recent post-glacial material and contains Neolithic as well as Roman remains.

The amount of material removed by erosion varies from place to place. SKEMPTON and HENKEL (1957) quote a pre-consolidation load of 2145 kN/m^2 for the central London area, suggesting a removal of 170-230m of material.

The London Clay itself consists of a lower sandy clay varying from 0-3m thick and known as the basement bed. This is overlain by a blue-grey clay varying from 30-170m thick and which is the London Clay proper. Finally, near to the surface is the brown and somewhat weathered clay, varying from 0-10m in thickness.

The sands and gravels mentioned earlier overlie the London Clay in many areas, as does alluvium near the Thames and soft marsh clay and peat near the sea. The upper layer is yellowish-brown in colour near to the surface but becoming grey-brown at depth due to oxidation of the iron salts in the blue clay, probably when the ground water level was low.

WARD <u>et al</u> (1959) have suggested that the structure of London Clay on a regional scale takes the form of a very gentle syncline with some minor folding in places, although dips of more than three degrees are rare.

The geology in the vicinity of the site in question, namely Green Park corner, is of some complexity.* This is generally confirmed in the geological map of central London drawn by SKEMPTON and HENKEL (1957).

Strata description from borehole No. 23 at the Green Park construction site ** helps, however, to remove some of the ambiguities as far as the ground profile is concerned

---

* ATTEWELL (1974): personal communication

** Data records from borehole No. 23 were taken from ATTEWELL and FARMER (1972), and FARMER (1972-73) personal communication.

Depth	Soil description.
1.67 - 2.13m	Yellow brown sandy clay (firm)
2.13 - 5.48m	Medium brown clay. Stiff with thin blue-grey traces on fissure surfaces. Medium density of fissuring. Fissures tight, of small extent oblique to sub-vertical plane. Smooth or slight slick degradation.
5.48 - 10.00m	Unlaminated dark brown grey slightly silty clay, very stiff but fissured.
10.00 - 14.02m	Thinly laminated dark brown grey slightly silty clay with some thin partings of pale fine sand, very stiff but fissured. Fissure density medium to high. Fissures as above.
14.02m	Claystone nodule.
14.02 - 20.00m	Degradation of fissure surfaces to pale grey.
20.00 - 32.00m	Thinly laminated dark brown-grey fissured clay with some fine sand partings and occasional clay stone nodules.

b. Mineralogy. BROOKER and IRELAND (1965) have published the results of X-ray diffraction tests aimed at the determination of the mineralogical composition of London Clay. Percentages of the main minerals are as follows.

Quartz	15%
Chlorite and Kaolinite	35%
Illite	35%
Montmorillonite	15%

c. Microstructure. TCHALENKO (1968) studied the microstructure of London clay from several localities and depths using petrographic thin sections under the polarizing microscope. Measurements of the birefringence ratio β^*, indicated variation in values in the range of 0.35-0.65 denoting strong

---

* β is the ratio of the minimum to the maximum light intensity transmitted through crossed polars as the thin section is rotated on the stage. Therefore β is a modulus of particle re-orientation, i.e. $\beta \neq 0$ corresponds to perfect orientation and $\beta = 0$ to random orientation.

particle parallelism in the horizontal plane. The ratio was found to increase at shallow depths due to a disruption of the original matrix. Another interesting feature observed was the existence of primary and secondary microshear surfaces.

d. Macrostructure. A significant contribution to the classification of macrostructural features came from SKEMPTON et al (1969) who distinguished the five main types of structural discontinuities on a macro-scale·

i) Bedding Where in general, there is no lithological change the bedding appears as a "discontinuity with a gently undulating surface having a somewhat rough or bumpy texture".

ii) Joints. Predominantly vertical (at Wraysbury site) between 0.3 to 1.2m high and up to 6m long, with a pronounced trend in two orthogonal directions of N60^{o}W and N30^{o}E. They are plane in surface, matt in texture with occasional small steps.

iii) Sheeting Surfaces of moderate size are approximately 320cm^2 at the Edgwarebury site, dipping at angles of between 5^{o} and 25^{o} in a southerly direction. They are smooth in surface with a plane shape.

iv) Fissures At depths of 10-12m these are planar or conchoidal fractures up to 15cm in size with a matt surface texture. Their number per unit volume increases and their size decreases as the upper surface of the clay is approached. Usually they lie horizontally and almost parallel to bedding.

v) Faults: Sometimes they contain some gouge clay (5-10mm in the case of the fault at Wraysbury).

5.3 REVIEW OF THE STRENGTH PROPERTIES OF THE LONDON CLAY.

It is well known that London clay has been the subject of some quite thorough studies by a number of authors. With respect to its strength properties, attention is frequently concentrated on the question "Which factors and to what extent do these factors influence the shear strength of the clay under consideration"?

HOOPER and BUTLER (1966) derived and consequently treated numerical data on the shear strength of London clay from a statistical point of view. Their results are quite interesting because they indicate that the triaxial shear strength/depth profile obtained for any given site depends upon the sampling procedures employed. It is also shown that the frequency distribution of triaxial test strengths corresponding to a given depth may be represented by the classical Gaussian curve. Therefore, assuming a Gaussian population distribution of shear strength, it is possible to estimate the number of samples required at any specific clay level to give a mean sample shear strength which falls within specified limits of the population mean strength.

Referring to the undrained properties of stiff fissured clays, MARSLAND (1971) outlined the factors which might affect these properties estimated from in-situ loading tests. The factors are

i) The mineralogical composition, strength and type of discontinuities present in the clay.

ii) The forces and restraints imposed on the ground around the test levels by different mechanical arrangements adopted for the tests. MARSLAND (1972) investigated further this factor from results of in situ plate tests in lined and unlined boreholes in highly fissured London clay at

Wraysbury near London airport. The basic conclusion from this work was that there was no significant difference between tests made in unlined and lined portions of boreholes and this suggests that the degree of restraint imposed by standard borehole linings has no measurable influence on the results of plate tests in highly fissured clay. MARSLAND op cit emphasized that these conclusions only applied to the particular test conditions, and that it will be necessary to make further investigations on this particular problem.

iii) Dimensions of the test equipment and in particular the relative dimensions of the loaded plate and the spacing of the fissures in the clay.

iv) The reduction in stress and the accompanying strains which occur in the clay during drilling and insertion of the test equipment.

v) The interval of time between drilling the hole and loading the plate.

vi) The rate of penetration during loading.

More attention was given to the time factor, that is the interval of time between sampling and testing in MARSLAND (1973), where the variation in the stress strain curves - obtained from tests on 38,75 and 125mm diameter specimens prepared from adjacent block samples at different times after sampling - is given. Also, the opening of fissures due to the reduction of external atress during excavation, sampling and storage is intimated as being a factor attributing to the "softening" phenomenon.

The opening of fissures is a well-known feature of tunnelling where, as soon as the face is excavated, examination of the clay in the walls of the tunnel shows that the fissures start to develop and open.

The operational strength of fissured clays was examined by LO (1970) who analysed data reported in the literature. As a first approximation, the fissure strength may be taken as the residual strength of the clay, while the intact and fissure strength could provide the upper and lower bound values respectively of the strength that can be measured by any type of test on any size of sample. LO op cit, considering a clay with a system of fissures randomly distributed - and assuming that the size of the specimen is increased from an initial value - suggested that the following probability of occurrences will be correspondingly increased

i) the number of fissures included in the sample,

ii) the probability of having fissures critically orientated to the applied stress system,

iii) the probability of having larger fissures;

iv) the probability of having large fissures critically orientated,

v) the probability of coalescing adjacent cracks in the proximity of the potential failure plane.

Finally, LO developed an equation for the strength-size relationship which contains two parameters describing the intensity of fissuring of the clay. Based on the proposed equation, the operational strength, or the strength of the soil mass in the field might be predicted.

The stress path method presented by LAMBE (1967) and extended by LAMBE and WHITMAN (1969) comprises a major approach to stability and deformation analysis in soil mechanics. Data concerning the shear strength of London clay being selected from the literature and presented in a stress path manner is shown in Figure 5.3.1. The left hand graph of this Figure illustrates the effective stress paths (ESP) as they are defined by the test results of several authors using different techniques and specimen diameters. The right hand side of the same Figure visualizes the total stress paths (TSP), while K_f-lines for peak and residual strength were drawn together. Both K_f-lines were derived from data published by SKEMPTON et al (1969).

Although, by definition, the axes in two-dimensional stress space are

$p = \frac{1}{2} (\sigma_1 + \sigma_3)$ and $q = \frac{1}{2} (\sigma_1 - \sigma_3)$ corresponding to the hydrostatic and shear stress components respectively, a modified basis was used in the present thesis. The use of σ_1 or σ_v versus σ_3 or σ_h bears the advantage of simplicity and provides a quick and direct assessment of the state of stresses in the Clay.

5.4 INDEX PROPERTIES AND RESULTS FROM UNCONSOLIDATED UNDRAINED (UU) TRIAXIAL COMPRESSION TESTS.

Site investigation results from borehole no. 23 at the Green Park working site for the Fleet Line Tunnel revealed the following index properties.

Depth m	Moist. cont. %	LL %	PL %	Bulk density Mg /m^3
3.7 - 4.1	28	80	32	1.920
17.2 - 17.7	26.5	75	29	1.935
27.3 - 27.7	26	70	27.5	1.970
31.5 - 32.0	25	76	33	1.935

For the employment of the elastic-plastic approach, and in order to define the state of stress around the tunnel in question, it was necessary to use shear strength values and elastic modulus values from "representative" samples. Accordingly, specimens were prepared from samples taken at the depth of the tunnel axis (30m) at the tunnel face.

The samples comprised two groups collected from two directions (vertical and horizontal) with respect to ground surface, so giving a loading facility for two different inclinations on a particular fabric of fissures.

Undrained triaxial compression tests on 38mm diameter specimens were conducted and results indicated (see Figures 5.4.1., 5.4.2. and 5.4.3.) that the shear strength was 67% higher in the horizontal samples than for the vertical samples. WARD et al (1965) reported similar percentage differences as a function of orientation ranging between 30% and 62% for undrained tests on London clay. AGARWAL (1967) also noticed the same effect. BISHOP (1966) proposed a relationship for the variation of undrained shear strength (c_u) with respect to sample orientation θ

$$c_u = c_{u\ vert.} \quad (1 - a\sin^2\theta)\ (1 - b\sin^2 2\theta) \qquad .....(5.4.1.)$$

where a and b are constants.

For confining pressures near to the overburden pressure existing at axis depth (30m), the stress ratio $R = \sigma_3/\sigma_1$ has been plotted against strain and is shown in Figure 5.4.4. It can be seen that the curve for horizontal samples underlies that for vertical, and both have the parabolic shape already suggested by BRETH et al (1973)

Although BRETH et al were concerned with test results on sand, they observed that the plotted curves of strain against stress ratio σ_3/σ_1 showed a parabolic trend with strain becoming excessively high as the stress ratio approached the failure stress ratio $(\sigma_3/\sigma_1)_f$. That observation eventually led to formulation of an analytical expression for the function $(\sigma_3/\sigma_1) = f(\varepsilon)$ which is

$$\varepsilon(\sigma_3/\sigma_1) = a + \frac{b}{(R - R_f)} + \frac{c}{(R - R_f)^2} + \quad .. \qquad .....(5.4.2.)$$

where

ε is the axial or lateral strain at any value of the ratio (σ_3/σ_1).

σ_3 is the minor principal stress,

σ_1 is the major principal stress,

R_f is R at failure stress,

a,b,c are parameters depending on the observed stress-strain characteristics of the material.

Another interesting feature revealed in Figure 5.4.4. is that the stress ratio (σ_3/σ_1) at failure is approximately 0.60. It is worth noting that the K_o ratio may be determined through Jaky's relationship

$$K_o = 1 - \sin \phi' \qquad .....(5.4.3.)$$

derived from tests on granular material, although the expression

$$K_o = 0.95 - \sin \phi' \qquad .....(5.4.4.)$$

has been found to be more applicable to cohesive soils (BROOKER and IRELAND, 1965). As will be seen in a later part of the present Chapter, the effective friction angle based on the effective stresses was found to be equal to $\phi' = 19^o$. Therefore substituting the value of $\phi' = 19^o$ for equation (5.4.4.) results in a K_o value equal to 0.62. This particular K_o value is reasonably compatible with the experimentally-defined ratio of principal total stresses at failure $\sigma_3/\sigma_1 = 0.60$, although K_o is defined as the ratio of the principal effective stresses σ_3'/σ_1'.

5.5. POISSON'S RATIO MEASUREMENT DURING TRIAXIAL UNDRAINED TESTS.

Poisson's ratio may be evaluated from the ratio of the lateral induced strain to axial inducing strain during a triaxial compression test with axial loading.

In order to evaluate the variation of Poisson's ratio with strain, 38mm diameter specimens were prepared from samples which were collected from the working face of the tunnel in two main directions (horizontal and vertical) with respect to ground surface. The tests were performed in the unconsolidated undrained triaxial compression mode and a provision was made for Poisson's ratio measurement during the various stages of loading. This was achieved with the use of an electronic linear variable differential transformer, wired via a carrier amplifier demodulator system to an auto potentiometric chart recorder. The displacement on this recorder was carefully calibrated beforehand and several times subsequently. Poisson's ratio was recorded during compression for the two sets of tests for the different sample orientation and for the several cell pressures.

An initial value of Poisson's ratio was taken as 0.5 on the assumption that the clay is an elastic isotropic material. Thus

$$\begin{aligned} \varepsilon_2 &= \frac{1}{E}\left[\sigma_2 - \nu(\sigma_3 + \sigma_1)\right] \\ \varepsilon_3 &= \frac{1}{E}\left[\sigma_3 - \nu(\sigma_1 + \sigma_2)\right] \\ \varepsilon_1 &= \frac{1}{E}\left[\sigma_1 - \nu(\sigma_2 + \sigma_3)\right] \end{aligned} \qquad \text{.....(5.5.1.)}$$

Assuming that in the triaxial stress field, the strain is $\Delta\varepsilon_2 = \Delta\varepsilon_3$ and that $\Delta\varepsilon_1$ is caused by stresses $\Delta\sigma_2 = \Delta\sigma_3$ and $\Delta\sigma_1$, it follows that Poisson's ratio is given by the relationship,

$$\nu = \frac{\Delta\sigma_2\,\Delta\varepsilon_1 - \Delta\varepsilon_2\,\Delta\sigma_1}{\Delta\sigma_2(\Delta\varepsilon_1 - 2\Delta\varepsilon_2) + \Delta\sigma_1\Delta\varepsilon_1} \qquad \text{.....(5.5.2.)}$$

Thus, under hydrostatic compression and <u>before</u> any shearing occurs $\Delta\sigma_2 = \Delta\sigma_1$ and as a consequence equation (5.5.2.) becomes

$$\nu = \frac{\Delta\sigma_2(\Delta\varepsilon_1 - \Delta\varepsilon_2)}{2\Delta\sigma_2(\Delta\varepsilon_1 - \Delta\varepsilon_2)} = 0.5 \qquad \text{.....(5.5.3.)}$$

During the early range of strain, LAMBE and WHITMAN (1969) argue that Poisson's ratio varies with strain. This is shown to have occurred during the test programme described herein. It is shown however, in Figure 5.5.1. for vertically orientated samples that Poisson's ratio steadily increases up to a given value of strain - which is controlled by a particular confining pressure - and when it does exceed a critical value, the ratio decreases gradually (see also Table 5.5.1.). On the other hand, for the results for the horizontally oriented samples graphed in Figure 5.5.1. it appears that Poisson's ratio* increases almost inversely with strain.

The observed behaviour of the vertically oriented sample may be attributed to some plastic deformation behaviour beyond a critical elastic limit.

Figures 5.4.1.and 5.4.2. illustrate the stress-strain curves for both vertical and horizontal samples,pointing out the difference in stiffness between them. This difference presumably combined with the rather extensive plastic behaviour for the vertical samples provides an explanation for the strain-Poisson's ratio relationship, for both cases. Undoubtedly, further research is required to distinguish between these possible causes of the difference in results mentioned above. Nevertheless, these results are influenced by many other factors as the elastic anisotropy, the overconsolidated nature of the clay, the orientation of the fissures fabric, the high K_o value (~ 1.65) existing at that depth, the stress path and the rate of strain.

However, the test results have clearly shown that variations of Poisson's ratio during triaxial compression are practically negligible.

Poisson's ratio might also depend upon the stress path. Figure 5.5.2. illustrates the plotted variation of Poisson's ratio with the stress ratio σ_3/σ_1. It is evident that an asymptotic decay of the ratio emerges as the stress ratio decreases from values of 1.0 to 0.5 (for vertical samples) and

---

*Assuming that the original length of the specimen is L and the original width is D, and further assuming that the variation in width is ΔD and the variation in length is ΔL, then the Poisson's ratio by definition is

$$\nu = \frac{-\Delta D/D}{\Delta L/L} \qquad .....(5.5.4.)$$

1.0 to 0.3 or 0.4 (for horizontal samples).

5.6 UNCONSOLIDATED UNDRAINED ($\overline{UU}$) AND CONSOLIDATED UNDRAINED ($\overline{CU}$) TRIAXIAL TEST RESULTS.

Two further sets of triaxial compression tests were carried out. These comprised unconsolidated undrained and consolidated undrained, both with pore water pressure measurements. The second set was necessary in order to define the shape of the failure envelope in terms of the effective stresses.*
The first set consisted of tests on 98mm diameter samples taken from the depth of 25m in a borehole drilled into the London Clay at a site in Regent's Park. A rather small nominal strain rate 5.5×10^{-3} mm/min. was used to allow the development of pore pressures during loading. In all the undrained and consolidated undrained tests, filter paper strips attached to the perimeter of the test cylinders were used to accelerate drainage during consolidation ($\overline{UU}$ tests) and to equalize the pore pressure during shearing (both $\overline{UU}$ and $\overline{CU}$ tests). The stress-strain and pore water pressure relationships for the $\overline{UU}$ tests are shown in Figure 5.6.1. It will be seen that the specimens failed at strains of about 2% while the pore pressures reached their peak a little earlier. Failure was usually of a brittle nature along one or more shear planes. Finally, for each specimen the pre-shear effective stress has been given. The effective stress path for a sample taken from 25m depth has been evaluated from the results of the $\overline{UU}$ triaxial tests as shown in Figure 5.6.2.

Also on this Figure has been plotted a stress path for the same element of clay predicted from the Kirsch equations (see Chapters 6 and 7). In terms

---

*According to BISHOP and HENKEL (1964), if the pore pressure is measured during the undrained test on saturated cohesive soils, the effective stresses at failure can be determined. It will be found, however, that for saturated clays both the σ'_1 and σ'_3 are independent of the magnitude of the cell pressure applied. Hence only one effective stress circle is obtained from these tests and the shape of the failure envelope in terms of effective stress cannot be determined. Consolidated undrained or dtrained tests are used for the latter purpose.

of total stress, $\sigma_\theta = \sigma_h = \sigma_1 = 1100$ kN/m^2 and $\sigma_R = \sigma_v = \sigma_3 = 498$ kN/m^2. For effective stress evaluation, the $\Delta u \cdot \varepsilon$ curve in Figure 5.6.1 at a confining pressure $\sigma_3 = 605$ kN/m^2 was used. Assuming elastic ground deformation up to 0.5% strain (Figure 5.6.1), a Δu value of 221 kN/m^2 may be taken for the computation of effective stresses $\sigma_1' = \sigma_\theta - \Delta u = 879$ kN/m^2 and $\sigma_3' = \sigma_R - \Delta u = 277$ kN/m^2. The experimental and theoretical stress paths show reasonable compatibility over the restricted length of the latter.

In the case of the consolidated undrained tests, the following procedure was adopted:

a) A cell pressure of 70 kN/m^2 was applied initially and kept constant for a period of time (usually two to three hours).

b) The pore pressure was then measured and noted. The cell pressure was increased to 140 kN/m^2 and after a few hours, the pore pressure was again measured. Each step of pore pressure measurement was followed by "equalisation" between the back pressure and the cell pressure, and a measurement of the pore pressure parameter "B". Since "B" was not equal to unity, the term "equalisation" can therefore be somewhat misleading with respect to parameter pressure.

c) The cell pressure was then increased to 210 kN/m^2 and left for a few hours. After a new "equalisation" between cell pressure and pore pressure the parameter "B" was measured.

d) The cell pressure was increased to 280 kN/m^2 and left overnight. It was found that the value of "B" finally obtained was nearly equal to one (in fact between 0.95 and 0.98).

e) After this consolidation with back pressure in the pore water circuit so that any air remaining might be dissolved, the volume change circuitry was then connected and the pore water volume changes recorded through a series of suitably spaced readings. Consolidation was theoretically completed when no significant movement of the water level in the measuring burette occurred (see BISHOP and HENKEL, 1964). Figure 5.6.3. illustrates the relationship between the volume change and the square root time ($\sqrt{t}$) for a 38mm diameter sample during consolidation under an all around pressure (radial and end drainage). The same Figure 5.6.3 incorporates the calculation for an estimate of the coefficient of consolidation c_v which was found to equal 0.14 mm^2/min. Basing on that value and taking the value of the coefficient n equal to 40.4 (see BISHOP and HENKEL, 1964, page 125) the time required for failure under the particular triaxial stress field was found to be t_f = 86 hours. It is worth noting that this time is based on drained conditions and it might therefore be expected that in undrained tests the corresponding value of t_f would be much less. Indeed, the time to failure was in the order of 18 to 24 hours.

The stress-strain relationships for the consolidated undrained triaxial tests on 38mm diameter specimens are shown in Figure 5.6.4. where it appears that failure has occurred at strains considerably less than those in the case of unconsolidated undrained tests. The same differences are evident for the pore pressure.

On the basis of these results, Mohr envelopes in terms of effective stresses have been drawn in Figure 5.6.5. From these, it would appear that the friction angle based on the operative effective stresses is 19 degrees and the cohesion intercept similarly based on the operative effective stresses is 10.57 kN/m^2. In the same figure the K_f line has been drawn together with the slope angle b, and the ordinate axis intercept a.

Another feature of this suite of tests was a special set of five consolidated undrained triaxial compression experiments with pore pressure measurement on 38mm diameter specimens and with a different rate of strain for each loading. All specimens were taken at a depth of ~22.5m and the common pre-shear effective stress was equal to 450 kN/m^2. The rates of strain used were 1.20, 2.44, 5.50, 15.2 and 76.2 (all x 10^{-3}) mm/min.

The relationship between the pore pressure parameter A and the axial strain has been plotted in Figure 5.6.7. These graphs are plotted from the results of $\overline{CU}$ triaxial tests on 38mm diameter specimens and for different rates of axial strain.

The effect of the rate of strain on the pore pressure parameter A is self evident and could perhaps be attributed to the dependent of A on both the total stress path and the strain, as pointed out by LAMBE and WHITMAN(1969). Thus, taking into account the fact that all specimens were from the same depth, it is reasonable to accept that a different rate of axial strain influences considerably the development of pore pressures and therefore alters the stress paths accordingly.

The stress-strain characteristics of this set of $\overline{CU}$ triaxial tests are shown in Figure 5.6.6., from which it would also seem that the deviator stress at failure depends upon the rate of axial strain. Such a dependence was reported for the first time by BISHOP and HENKEL (1964) but with respect to a different material.

To conclude this set of results a graph has been drawn in Figure 5.6.8. between the deviator stress at failure and the rate of strain. Although this graph does not provide a conclusive trend, it appears, however, that there is an exponential relationship between the rate of axial strain ($d\varepsilon/dt$) and the deviator stress at failure $(\sigma_1-\sigma_3)_f$ such that an increase in $d\varepsilon/dt$ implies a decrease in the quantity $(\sigma_1-\sigma_3)_f$. Clearly, further tests are required in order to verify this trend which might be of some importance in tunnelling applications where the rate of clay deformation is functionally related to the rate of tunnel advance (see Chapter 1) and both rates exert an influence on the overall tunnel stability.

CHAPTER 6

THE STRESS-STRAIN REGIME AROUND A CIRCULAR TUNNEL DURING THE EARLY STAGES OF CONSTRUCTION.

6.1 INTRODUCTION

Using the classical elasto-plastic approach, a simple analysis may be carried out upon the stress regime around a circular tunnel, the results of that analysis being correlated with the tunnel advance. The resulting theoretical ground deformations predicted on that basis may then be compared with the in-situ measurements as a check on the validity of the concepts built into the theory.

6.2 STRESS-DEFORMATION DISTRIBUTION AROUND THE TUNNEL

Any tunnelling operation results in a re-distribution of the stress regime in the surrounding ground and produces a new unknown state of stress.

Using the classical methods in elastic theory, it is possible to estimate the new state of stress with an accuracy which depends primarily on the elastic properties of the soil and its deviation from elastic behaviour when it is subjected to tensile or compressional loading.

In the present work, Kirsch's equations (see DEERE et al, 1969) are employed for their convenience and simplicity. As is to be expected from the theory of elasticity, the soil is considered to be an incompressible material*(no volume change) with Poisson's ratio equal to 0.5. Of course, it may be argued that during loading this ratio possibly undergoes considerable variation from the 0.5 value. Thus, before employing the classical elastic approach for the determination of stresses and strains

---

* in the undrained state.

around the tunnel in question, some laboratory tests* were carried out in order to check the possible deviations of Poisson's ratio from the value of 0.5. These tests are described in Chapter 5 and the results have shown that variations of Poisson's ratio are not a practical issue.

During and after the excavation, Poisson's ratio for the over-consolidated stiff clay is neither constant nor does it correspond to a situation of constant volume. Such an assumption is valid only for short term deformation and it would be preferable after CHRISTIAN (1968) to adopt a slightly smaller value of say 0.48 for the purpose of any calculations. In fact, the value proposed by CHRISTIAN op cit for Poisson's ratio is in good agreement with the experimental results outlined in Chapter 5.

For the evaluation of stresses around the opening, the familiar Kirsch equations were used for a biaxial case problem** (see DEERE et al, 1969).

$$\sigma_R = 0.5\,\sigma_v \left[(1 + K)(1 - a^2)+(1 - K)(1 + 3a^4 - 4a^2\cos 2\theta)\right]$$

$$\sigma_\theta = 0.5\,\sigma_v \left[(1 + K)(1 + a^2) - (1 - K)(1 + 3a^4) \cos 2\theta\right]$$

$$\tau_{R\theta} = (K - 1)(1 - 3a^4 + 2a^2) \sin 2\theta \qquad \text{.....(6.2.1)}$$

$$\sigma_y = \nu(\sigma_R + \sigma_\theta) \qquad \text{.....(6.2.2.)}$$

where $a = R_o/R$

R_o is the hole radius,

R is the radial distance from the centre of the hole to any point in the clay mass,

K is the coefficient of earth pressure at rest;

σ_R is the radial stress at distance R

σ_θ is the tangential stress at distance R,

$\tau_{R\theta}$ is the shear stress at distance R

and θ is an angle defining a polar co-ordinate, the horizontal axis through the centre of the tunnel defines the case $\theta = 0^o$

---

* UU triaxial compression tests on 38mm diameter specimen.

** Assuming an infinite ground mass.

SKEMPTON (1961) provided data which related the undisturbed horizontal and vertical stresses of London Clay. A polynomial curve was fitted by GOWLAND (1974)*to those data and this function of K_o with depth was interlaced with equation 6.2.1. to compute suites of stress for different points around the tunnel. It may be noted that COLE and BURLAND (1972) referring to the same overconsolidated stiff clay deduced a similar relationship from the data of SKEMPTON op cit. and BISHOP et al (1965). Their graph suggests, however, that values obtained from BISHOP et al are generally higher than those obtained by SKEMPTON, but that they take a similar trend to that of Figure 6.2.1.

The computer programme written by A. Gowland and referred to above, was used to calculate the stresses and deformations around the opening within a region up to 5 tunnel radii and for discrete points at every 0.2 radius and every 10 degrees. From the computer output, contours of normalized principal stress have been plotted for the vertical plane along with the longitudinal tunnel axis and the plane of the tunnel's cross section. (Figure 6.2.2.).

Although the information on the graph is self explanatory, note should be taken of the dramatic change in the stress regime at a vertical height above soffit of approximately 1 to 1.5 tunnel radii which approximately

---

* GOWLAND, personal communication.

corresponds to a vertical distance of 4 to 5 metres. A further change in the trend of the contours is evident at a horizontal distance of one tunnel diamter (4m.). It also appears from the curves that the maxima of ratios σ_3/σ_1 and $\nu(\sigma_1 + \sigma_3)/\sigma_1$ occur at a tunnel axis level. This is simply a reflection of the dominant horizontal major principal stress in the overconsolidated clay prior to disturbance.

It is useful to attempt to correlate the configuration of the principal stress ratios σ_3/σ_1 for the plane of the tunnel cross-section with the earlier experimental curves which relate Poisson's ratio to the stress ratio σ_3/σ_1 for the same clay (see Figure 5.5.2.). However, it would appear from superimposing the experimental values that it might be reasonable to replace the contours of equal principal stress ratio with contours of equal Poisson's ratio. Consequently, by choosing from the family of curves in Figure 5.2.2. the particular curve having a confining pressure equal to 760 kN/m^2 (a horizontal test sample and a confining pressure which is a reasonable approximation to the calculated horizontal stress existing at the depth of 29m), it is possible to convert the principal stress ratios to Poisson's ratio values. The contour for σ_3/σ_1 = 0.45 corresponds approximately to the ν = 0.45 contour. This particular Poisson's ratio value is that found at the failure stage of the sample under UU triaxial compression conditions. The most important results seem to be that the contour of σ_3/σ_1 = 0.45 defines the limits of the shear strength for the overconsolidated clay when the opening has been created.

The general problem of evaluating the stress regime around a shield driven tunnel is of some complexity since the stresses surrounding the circular cross-section are a function of shield position. However, as soon as the face reaches a given cross-section of the clay, the ground moves radially inwards in order to fill the bead annulus (in the present case of thickness 6.5mm). The intrusion is terminated when the clay touches the shield surface. Noting that the bead thickness is quite small, it follows that the inward movement of the clay may well be restricted during that particular phase of the excavation. Therefore, since the associated strains are also small it is not unreasonable to assume that the deformation is mainly elastic in character and that this quasi-elastic deformation persists until the 3.275m long shield and tail clear the given cross section.

Before any grouting operations took place behind the erected lining segments over the measurement length of the Fleet Line tunnel there was a further 1.20m of unsupported annulus behind the tailpiece into which the soil can move. This total unsupported length amounted to 3.275 + 1.20 = 4.475m so giving to the clay a real facility for more radial intrusion.

It has been suggested that the average rate of tunnel advance is 2.23 mm/min and so it follows that the unsupported length of 2.115m corresponds to 15.8 hours of exposure time, during which the clay at the cross-section could move in an unrestricted manner.

On the basis of the average maximum deformation rate of the clay (at the soffit) of 0.005 mm/min the further movement amounts to 4.7mm. This latter deformation facility may well have created strains of amplitudes beyond the elastic regime and therefore have introduced a form of "plastic release zone" around the tunnel.

DEERE <u>et al</u>, (1969) suggested that for a circular tunnel driven in an elastic-plastic medium the criterion for the development of a plastic zone around the opening is

$$\sigma_v - \sigma_i = c_u \qquad \text{.....(6.2.3.)}$$

where

σ_v is the overburden stress,

σ_i is the internal pressure,

and

c_u is the undrained shear strength of the soil.

The stress field in the soil is supposed to be one of uniform compression, and for a frictionless soil the radius of the plastic zone around the tunnel is given by the equation

$$R = R_o e^{\frac{\sigma_v - \sigma_i}{2c_u} - 0.5} \qquad \text{.....(6.2.4.)}$$

where R_o is the hole radius.

Inside the plastic region the volume is assumed to be constant (Poisson's ratio is everywhere equal to 0.5). By using equation 6.2.4. it was found that the extent of the plastic zone was approximately 1.5 tunnel radii. This is in basic agreement with the change in the stress regime for the same distance as shown in Figure 6.2.2. Inside the plastic region the radial and hoop stresses are given by the equations.

$$\sigma_R = \sigma_i + 2c_u \ell n\,(R/R_o)$$

$$\sigma_\theta = \sigma_R + 2c_u = \sigma_i + 2c_u\left[1 + \ell n(R/R_o)\right] \qquad \text{.....(6.2.5.)}$$

A possible objection to the adoption of the 'plastic zone' concept could be the fact that the equations describing the plastic stress state are based on the K = 1 assumption, while for the clay in question the K values greatly exceed unity. There are, however, no analytical solutions outside the hydrostatic state and so as an approximation it is necessary to use the equations 6.2.5. The results of this exercise with respect to soffit, axis and 45^o elevation are shown in Figure 6.2.3.

Progress of the shield may be considered in two stages

a) the time which has elapsed between the appearance of the face of the shield and the end of the tailpiece at a particular clay cross-section, and

b) the time which has elapsed between the tailpiece retreat and the first contact grouting operation.

During the first phase of the excavation, the clay is assumed to behave elastically, the radial and tangential stresses within the plastic region being drawn by broken lines. In essence, during that phase, there is no plastic zone at all. For the second phase of the excavation, an elasto-plastic behaviour has been adopted and the stresses inside the plastic region were given by the continuous lines.

The stress situation at the springline resembles that described by KASTNER (1962) for the distribution of secondary stresses adjacent to a circular tunnel where a pseudo-plastic stress state is applied. It should be noted that in the second phase of excavation, due to the limited time during which the clay is allowed to deform freely, it is quite possible for the real plastic state not to develop fully, so giving way to a rather pseudo-plastic stress situation instead.

It may be argued that there is a third phase of ground movement which is characterized by the setting of the grout. During the stiffening progress, the inward incursion of the clay is progressively resisted to create a changing stress situation around the tunnel.

Any attempted specification of that new stress is a matter of speculation, but it is worthwhile to note that the clear trend for some uplift of the ground above the soffit as recorded in boreholes X1, Y1, Z1 (see Figures 4.2.1., 4.2.2., 4.2.3.) for the tunnel advance over 10 metres may be explained on the basis of this changing ground-lining interaction effect (see ATTEWELL and FARMER, 1974).

6.3 STRAIN ENERGY RELEASE DURING TUNNELLING.

Changes in the status of stress and the resulting ground movements due to tunnelling in an elastic medium may be interpreted in terms of the release of strain energy due to the excavation. Conceptually, the variation of the strain energy stored in the ground is the potential factor which drives the ground disturbance.

The theory of elasticity provides the means of estimating the variation of strain energy that results from tunnelling in an annulus of ground with radius R ($R \gg R_o$). Thus, considering a deep unlined tunnel with an internal radius R_o, surrounded by an homogeneous, isotropic and tectonically undisturbed ground, it is necessary to find analytical expressions for the pre-existing strain energy which is stored in the ground due to the hydrostatic stress field in addition to the new state of strain energy which is established after the tunnel drive.

The difference between these two values should express the amount of energy which has been released during tunnelling. This change of strain energy is important since it provides the triggering mechanism for the development of ground movements which might be associated with any excavation.

The examination of that particular problem has attracted the attention of various authors, notably JAEGER and COOK (1969) who presented some relationships connecting the internal radius of the tunnel, the radius of the annulus, the elastic parameters of the surrounding ground and the hydrostatic stress, with the strain energy before and after tunnelling.

Prior to driving the tunnel, the strain energy per unit length stored in an annulus of radius $R(R \gg R_o)$ due to the hydrostatic stress of the medium is,

$$W_1 = \frac{\pi(1+\nu)(1-2\nu)}{E}\sigma_v^2 (R^2 - R_o^2) \qquad \text{.....(6.3.1.)}$$

and after the tunnel is driven it becomes

$$W_2 = \frac{\pi(1+\nu)\sigma_v^2\left[(1-2\nu)R^4 + R^2R_o^2\right]}{E(R^2 - R_o^2)} \qquad \text{.....(6.3.2.)}$$

where,

ν is Poisson's ratio of the ground,

E is Young's modulus of the ground,

σ_v is the hydrostatic stress of the ground ($\sigma_v = \gamma Z$),

R_o is the internal radius of the tunnel,

R is the radius of the annulus,

W_1 is strain energy before tunnelling,

W_2 is strain energy after tunnelling,

and W is strain energy due to tunnelling.

Obviously, the change in strain energy due to tunnelling is given by $W_2 - W_1$,

$$W = W_2 - W_1 \qquad \text{.....(6.3.3.)}$$

JAEGER, op cit using the same pattern of calculations, also proposed a relationship giving the displacement (U_R) induced at R by driving the tunnel.

Thus,

$$U_R = \frac{2(1+\nu)(1-\nu)\,\sigma_v R_o^{\,2} R}{E(R^2 - R_o^{\,2})} \qquad \text{.....(6.3.4.)}$$

An attempt has been made, however, to apply the above formulae to the tunnel in question and to find out the strain energy and displacement as a function of distance from the tunnel centre which, for convenience, is expressed by the dimensionless ratio R/R_o.

It is evident that the relationship involved includes terms which normally might be affected by the ratio R/R_o, by the overburden pressure $\sigma_v = \gamma Z$, by Young's modulus, and by Poisson's ratio. Therefore, in an attempt to improve the basis of the analysis it was decided to accommodate into the calculations the functions.

$$\begin{aligned} \sigma_v &= f(R/R_o) \\ E &= f(R/R_o) \end{aligned} \qquad \text{.....(6.3.5.)}$$

making the no-volume change assumption, that is by supposing that Poisson's ratio is equal to 0.5 or-in order to avoid null terms- 0.48. The value of 0.48 seems to be justifiable on the basis of the laboratory test results. These results are presented in Chapter 5 of the thesis.

Values for the variation of Young's modulus with depth for the same clay were provided by MARSLAND(1973) who conducted triaxial compression tests on 98mm diameter specimens.

Finally, entering the radius of the tunnel as R = 2.035m, some calculations were carried out (tabulated in the Table 6.3.1.) and the graphs are presented in Figure 6.3.1.

As shown in Figure 6.3.1. the strain energy due to tunnelling (the difference in energy between the states of before and after tunnelling) increases significantly where the ratio R/R_o approaches unity from the value of 4 tunnel radii, while for values over 4 there is a more or less uniform relationship between strain energy and distance from tunnel centre. As the ratio R/R_o approaches the value of 14.5 - which approximately corresponds to the ground surface - the strain energy appears to be very small, just enough in fact to satisfy the few millimetres of surface settlement. On the other hand, the employment of the displacement formula leads to very interesting results when the predicted function of displacement versus depth is compared with the actual relationship measured in the research boreholes.

Figure 6.3.2. shows the two curves on the same graph for comparison purposes. It is apparent that the two curves are compatible with one another - subject to some deviations in the vicinity of the opening - when the estimated

("theoretical") curve implies higher settlements than those actually measured. It may be argued that this behaviour is quite expected because the "theoretical" curve completely ignores the ground stabilisation processes and the early lining erections which drastically reduce further displacements.

Finally, both curves in Figure 6.3.2. do change their slopes in a quite marked manner at a point where the distance from tunnel centre is about 8m. This approximates to the value 4 for the ratio R/R_o.

6.4 GROUND DEFORMATION IN THE VICINITY OF THE TUNNEL

Post tailpiece and pre-grouting clay deformations were reported by ATTEWELL and FARMER (1972) after the completion of a micrometric measurement programme conducted in situ in the tunnel under question. The observations were carried out through grout holes in a newly-erected ring of cast iron lining segments just off the tailpiece 30 minutes after the shield shove. It is believed that the results represent the state of clay deformability at that time. The thickness of the annular void between the lining and the clay was accurately measured for eight different points around the circumference.

Noting that the actual void annulus might have been slightly distorted from its original circular cross-section to an elliptical one due to the lining's own weight distortion, a simple calculation results in an expression for the theoretical void annulus as a function of the elevation angle. ATTEWELL and FARMER op cit. subtracted the actual from the theoretical values to estimate the absolute value of clay displacement for each of the eight positions under consideration.

On the basis of those data, a graph was prepared illustrating the absolute radial displacement of the clay versus the angle (Figure 6.4.1.).

It should be noted that the graph constitutes a major deviation from the expected configuration of clay displacement around the opening, according to the earlier concept of WARD and THOMAS (1965).

It is usually accepted that once a tunnel has been constructed it tends to become distorted so that its horizontal diameter is increased and its vertical diameter is correspondingly reduced. This mode of deformation is termed "squatting". As DRUCKER (1943) pointed out, where the vertical loading exceeds the active lateral pressure the horizontal diameter increases until it has built-up a sufficient lateral passive resistance from the ground. WARD and THOMAS (1965) showed that the diameters of continuously lined circular tunnels in the horizontally bedded London clay become shorter in the vertical direction and lengthened horizontally, during which time a uniform circumferential thrust - equivalent to the full overburden pressure acting hydrostatically - was slowly mobilized, and that this effect occurred irrespective of the method of construction.

These observations are in some conflict with the results of the measurements outlined a little earlier, where the clay seemed to be thrust upwards at the soffit while converging at axis level. Nevertheless, ATTEWELL and FARMER (1972) carried out in situ measurements of moisture content changes in the clay at the tunnel face in order to check the pore water situation which was an important element appearing in the interpretations of WARD and THOMAS op cit.

However, the moisture content calculations for samples of clay taken at different depths into the clay and across the tunnel face in cruciform configuration produced inconclusive results which neither supported nor rejected the large suction pressure arguments of WARD and THOMAS.

It is worth noting that MUIR WOOD (1969, 1971) measured ground movements of an airfield runway during the construction of a cargo tunnel at

Heathrow airport. His records of tunnel deformation showing that there was a small increase in tunnel diameter was in some disagreement with the measurements of WARD and THOMAS (1965) where for the Victoria line, the horizontal diameter increased and the vertical diameter decreased.

However, such discrepancies between observations for different tunnels in the same soil lend a certain degree of impetus towards a theoretical interpretation, and the use of elastic theory - although not entirely satisfactory - is at this stage probably valid.

The modified elastic displacement equations for the biaxial stress field may be written after DEERE et al (1969) as.

$$U_R = \frac{\sigma_v}{2E}(1+\nu)\left[\frac{R_o^{\,2}}{R}\left[(1+K)+4(1-K)(1-\nu)\cos 2\theta\right] - \frac{R_o^{\,4}}{R^3}(1-K)\cos 2\theta\right] \qquad \text{.....(6.4.1.)}$$

$$V_\theta = \frac{2\sigma_v}{E}(1+\nu)(1-K)\left[2R_o^{\,2}/R + R_o^{\,4}/R^3\right]\sin 2\theta \qquad \text{.....(6.4.2.)}$$

where U_R is the radial displacement,

V_θ is the tangential displacement,

σ_v is the overburden pressure,

E is Young's modulus for the clay,

ν is Poisson's ratio of the clay,

K is the ratio σ_h/σ_v for the clay in its undisturbed state,

R_o is the tunnel radius,

R is the radial distance from tunnel axis,

and θ is the polar co-ordinate angle with the vertical axis representing $\theta = 0^\circ$.

Values for the radial displacement have been plotted as a function of the dimensionless ratio R/R_o in Figure 6.4.2. This particular graph contains a family of curves representing different angles θ^* for the domain defined by $0^o < \theta < 90^o$. This elastic treatment tends to indicate that for axis level the radial displacements are greater than those displacements at soffit.

It may, therefore, be concluded that, taking into account the K_o variation with depth for the London Clay and using elastic theory, it is possible to predict reasonable values for the radial displacements.

The figures that emerge from the theory directly support the values actually measured <u>in situ</u>. For comparative reasons, the radial displacements predicted by elastic theory for $R = R_o$ and for the first quadrant of the circumference are plotted in the same graph in Figure 6.4.3. as the results of the <u>in situ</u> measurements. Although there is a consistent difference of 25 mm between the theoretical and measured curves the reasonable concordance in the shape of both curves suggests that the analysis proposed above produces a reasonable answer with respect to the form of the displacement distribution as a function of angular elevation (θ) around the tunnel. It must be acknowledged, however, that the result is strongly dependent on the elastic assumption whereas we know that non-linear stress-strain behaviour must occur. One thing must be stressed and that is that inside measurements of lining deflection do not necessarily reflect the true deformation of the ground, particularly soon after erection of the segments.

---

*Note that for technical reasons the graphs illustrated in Figure 6.4.2. calculated under the assumption that horizontal axis represents $\theta = 0^o$.

CHAPTER 7

STRESS PATH APPROACH FOR TUNNELLING IN LONDON CLAY

7.1 INTRODUCTION.

The present Chapter attempts to describe the employment of stress path theory in order to interpret the stress on an element of clay at

a) the tunnel axis level, and

b) the tunnel soffit level.

Both elements are taken at a distance of 0.2 tunnel radii from the free cut surface, of a circular shield driven tunnel in the London clay. The tunnel radius is 2.035m. The approach is based on total stresses and its validity is necessarily restricted to the time that elapses between the creation of the excavation and before grouting. Pore pressure and possible volume change phenomena associated with the excavation are neglected.

7.2 STRESS-PATH ESTIMATES DERIVED FROM THE ELASTIC-PLASTIC ANALYSIS

Stress paths for the ground elements defined earlier and which deform during the tunnelling process can be described with the aid of elastic-plastic analysis using equations 7.2.2. for the elastic case and equation 7.2.3. for the plastic stage of ground deformation* (see DEERE et al, 1969).

$$\sigma_R = 0.5\,\sigma_v \left[(1 + K)(1 - a^2) + (1 - K)(1 + 3a^4 - 4a^2 \cos 2\,\theta)\right]$$

$$\sigma_\theta = 0.5\,\sigma_v \left[(1 + K)(1 + a^2) - (1 - K)(1 + 3a^4) \cos 2\,\theta\right]$$

where $a = R/R_o$ .....(7.2.2.)

and

$$\sigma_R = \sigma_1 + 2c_u \ell n\, a$$

$$\sigma_\theta = \sigma_1 + 2\,c_u(1 + \ell n a)$$ .....(7.2.3.)

It may be argued that for both ground elements in question, the radial and hoop

*The analysis performed in Chapter 6 has indicated that ground and constructional conditions could satisfy the criterion for the formation of a plastic zone around the opening.

stresses are coincident with principal total stresses or

$\sigma_\theta \simeq \sigma_v$ and $\sigma_R \simeq \sigma_h$ (tunnel axis level), and

$\sigma_\theta \simeq \sigma_h$ and $\sigma_R \simeq \sigma_v$ (tunnel soffit level).

Equations 7.2.2. and 7.2.3. are employed for a distance from the tunnel centre equal to $a = R/R_o = 1.2$. The choice of that particular distance was governed by the desire to be very close to the tunnel circumference, avoiding in the meantime the free surface where for $a = R/R_o = 1$, then $\sigma_R = 0$ at both axis and soffit level.

For the element of clay at axis level (K = 1.65) it was found* that $\sigma_\theta \simeq \sigma_v = 813$ kN/m^2, $\sigma_R = \sigma_h = 168$ kN/m^2 (elastic state of stress) and $\sigma_\theta \simeq \sigma_v = 1034$ kN/m^2, $\sigma_R = \sigma_h = 212$ kN/m^2 (plastic state of stress). For the element of clay at soffit level (K = 1.70), the respective values are $\sigma_R \simeq \sigma_v = 160$ kN/m^2, $\sigma_\theta = \sigma_h = 760$ kN/m^2(elastic state of stress) and $\sigma_R \simeq \sigma_v = 137$ kN/m^2, $\sigma_\theta = \sigma_h = 669$ kN/m^2 (plastic state of stress). As the initial principal stress ratios K are known, one could presumably reconstruct the hypothetical stress path for these clay elements producing a rather general but comprehensive idea of stress mobilization during tunnelling. However, before tunnelling, the undisturbed clay is represented in two -dimensional stress space (σ_v,σ_h) by the points A (axis level) and A' (soffit level) where the corresponding principal stress ratios+

---

* The calculation of the stresses due to the plastic state are based on values for the undrained strength. These were obtained from laboratory results of unconsolidated undrained triaxial compression tests on specimens of 38mm in diameter taken from the tunnel face (29m in depth) in two main directions coinciding with the principal axes. The results show that

$c_u = 411$ kN/m^2 when the deviator stress is applied parallel to the ground surface

$c_u = 266$ kN/m^2 when the deviator stress is applied vertical to the ground surface.

+ These K ratios are estimated from SKEMPTON(1961) and by GOWLAND'S (1974) personal communication to the author.

are $K_A = 1.65$ and $K_{A'} = 1.70$ (see Figure 7.2.1.).

As soon as the excavation has been created, the clay moves towards a stress state represented by the point B (axis level) and B' (soffit level) where the respective K values are $K_B = 0.20$ and $K_{B'} = 4.75$. Both points B and B' correspond to the elastic stress state due to tunnelling, and were calculated using equation 7.2.2. The values of K_B and $K_{B'}$ indicate that there is a trend for the ground to undergo active stresses (tunnel axis)and passive stresses (tunnel soffit), where a considerable vertical stress relief seems to occur accompanied by minor changes in the horizontal stress.

Further stress change occurs due to the formation of a plastic zone around the opening and the new plastic state of stress is marked by points C (axis level) and C' (soffit level) and by the K ratios $K_C = 0.20$ and $K_{C'} = 4.80$ respectively. For the element of clay at axis level it may be argued that the stress difference from the elastic to plastic state is quite considerable while the point C lies on the experimentally-defined TRESCA-line (see Figure 7.2.1.) being therefore at failure.

On the other hand the stress difference from the elastic to plastic state for the element of clay at soffit level is very small and remote from the TRESCA-line* (see Figure 7.2.1.). The K ratio for that element equals $K_{C'} = 4.80$ and this indicates a further stress change towards a passive state of stress. Perhaps this passive state of stress is to some extent responsible for the earlier mentioned (see Chapters 4 and 6) apparent upwards movement of the clay at soffit level as was detected from the instrumented boreholes, and from <u>in-situ</u> measurements on the deformation of the unlined clay annulus surrounding the shield.

---

*This line has defined according to TRESCA'S failure criterion, having an analytical expression

$$\sigma_v = \sigma_h + 2c_u$$

7.3. THE SOIL-GROUT INTERACTION.

For the tunnel in question, a 1 1 water-cement grout was injected at low pressures behind the newly constructed lining. GORDON (1974) has referred to the soil-grout interaction pointing out that grout initially is virtually incompressible and will tend to flow, but as its shear strength is increased with time and is compressed by the converging clay, the grout will tend to bleed and shrink. The bleed water will drain into the clay, facilitating the softening phenomenon, and the remaining grout will gain stiffness with time while some reduction in volume occurs.

During the first stage of grouting, the clay continues to deform at a very slow rate. As soon as the stiffness of the grout converges to the value of the clay's stiffness, the latter is subject to radial recompression tending to restore its original stress field.

For all of the above reasons it is difficult to reproduce - in a stress path manner - the clay-grout interaction bearing also in mind the fact that the degree of clay alteration due to intrusion of bleed water into the clay-grout interface is completely unknown.

7.4. MOBILIZED EARTH PRESSURE DURING SHIELD TUNNELLING.

Before tunnelling, the clay element at tunnel axis level is at an undisturbed stress state under K_o conditions. As soon as the face approaches the clay starts to move and at the same time undergoes a redistribution of stress towards a state of active earth pressure, say K_1, (see Figure 7.4.1.).

As the face advances forward, the clay moves to infill the bead volume. This movement ceases when the bead is closed. It is worth noting that the probability of the bead's closure is governed mainly by the rate of clay deformation. ATTEWELL and BODEN (1971) proposed a laboratory method for the calculation of that rate of deformation under tunnelling conditions,(see Chapter 1).

However, during this time interval, the clay is tending progressively towards smaller K values, say K_2. The time elapsed $(t_2 - t_1)$ is equal to the average exposure time for the clay element during passage of the shield. Exposure time may be defined by the ratio · length of shield plus the tailpiece/rate of tunnel advance.

Due to bead closure - which is the case for the clay tunnel in question - the radial convergence of clay is restricted by the shield-skin. Probably a small amount of friction and larger K values are developed to a condition K_3.

When the tailpiece clears the cross-section and the lining has been installed, the clay is in relatively inactive state until the injection of grout.

The first stage of grouting is characterized by a strong clay-grout interaction resulting in a passive earth pressure built up during the setting time $(t_4 - t_3)$.

Finally, as the grout tends towards its ultimate value of stiffness, the clay tends towards an ultimum value of earth pressure (K_{ult}).

It must be stressed that this probably over-simple analysis is limited to the case of a clay element at tunnel axis level. It will be appreciated that the stress situation at soffit is even more complicated. The nature of the analysis is essentially qualitative because it is particularly difficult and probably impractical to assess quantitatively by theoretical means the mobilized earth pressure both during construction and in the long term. Such an appraisal could probably be achieved experimentally by the <u>in-situ</u> installation of earth pressure cells at strategic points on the circumference of the newly-installed lining. Even in that case the question of early earth pressure mobilization - before the installation of any lining - must remain one of basic speculation. A programme of research for the determination of the creep properties for London Clay from specimens recovered at these particular depths would facilitate such analyses.

CHAPTER 8

STABILITY OF SLURRY TRENCHES IN CLAY

8.1 FACTORS AFFECTING STABILITY

A slurry trench is defined as an excavation supported by a slurry based on the technique of bentonite suspension.

The main factors contributing to the stability of slurry trenches may be summarised as follows

a) The slurry properties.

b) The ground properties.

c) The position of the water table and the level of bentonite.

d) The degree of slurry penetration into the ground and the resulting modification of the shear strength and effective stress parameters of the ground.

e) The geometrical configuration of the trench.

f) The effects of arching and the transfer of pressures by shear.

g) Electrical phenomena associated with the slurry.

a) Effect of slurry properties

RENAU (1972) states that the specific weight of the bentonite suspension and the increase of this weight by non-colloidal particles in suspension has a major effect on trench stability. It will in fact be shown in Section 8.2 that the so-called stability factor, determined by Coulomb wedge analysis, is a function of the unit weight of the slurry. Another factor affecting the flow properties of slurry is the water/solids ratio.

CARON (1973) classified the primary and secondary factors affecting the characteristic properties of bentonite suspensions and water/cement grouts as shear resistance, viscosity and yielding time. Figure 8.1.1. illustrates some grout properties.

b) Ground properties

Ground properties are also important, particularly the unit weight, undrained shear strength, and friction angle. These factors determine the stability factor, the safety factor and the shape and extent of the disturbed or deforming ground area behind the trench. On the other hand the K_o and K_A coefficients determine the degree of earth pressure mobilisation in the ground inside the hypothetical Coulomb wedge.

c) The position of the water level and the level of bentonite

The influence of that factor in the overall trench stability can be illustrated by considering (FARMER, 1974)* the "actual forces" acting on the trench sidewall. Thus the total horizontal force in saturated soil having a ground water level at a depth z_w where $H > z_w$ (H is the height of the wall) is given by:

$$P_o = K_A \left[\gamma \, z_w \, (H - \tfrac{1}{2}z_w) + (\gamma - \gamma_w)(H - z_w)^2 \right] + \tfrac{1}{2}\gamma_w \, (H - z_w)^2 \quad ..(8.1.1.)$$

where K_A is the coefficient of active earth pressure

γ is the density of the soil

γ_w is the density of water

This force will be reduced by the total hydrostatic force exerted by the suspension and in the case of a bentonite slurry is given by.

$$P = \tfrac{1}{2} \, \gamma_b \, (H - z_b)^2 \quad ....(8.1.2.)$$

where z_b is the level of bentonite suspension,

γ_b is the density of the suspension.

---

* FARMER(1974), personal communication.

d) Slurry penetration

The significance of slurry penetration depends on the type of the soil. Thus, as pointed out by ELSON (1968), in soils with intermediate permeability, the formation of an impermeable filter cake is assumed at the interface between slurry and soil. On the other hand, in highly permeable soils, the slurry penetration is of great important and must be taken into account. ELSON op cit argues that penetration of the mud into the soil is due to negative pore pressures induced by soil dilation and shearing. This negative pore pressure will serve to increase the shearing strength of the soil. LA RUSSO (1963) reported that in such a soil a radius of penetration up to 17m from the trench centre line is possible.

e) Trench geometry

The effect of trench geometry has been considered by many authors, notably MEYERHOF (1972) and PRATER (1973). MEYERHOF examined the lateral earth pressure and the short term stability of a slurry trench in saturated clay, extending the solution for the stress distribution around a shallow cylindrical cut. This solution supplies an equation for the net horizontal pressure at any depth.

$$\sigma = (\gamma' - \gamma_b')z - 2c_u \qquad .....(8.1.3.)$$

where γ' is the effective unit weight of clay

and γ_b' is the effective unit weight of bentonite suspension

and in that solution the critical height of stable trench sidewall is given by·

$$H_{cr} = \frac{4c_u}{\gamma' - \gamma_b'} \qquad .....(8.1.4.)$$

MEYERHOF op cit suggested, however, that the value 2 in equation (8.1.3.) and the value 4 in equation (8.1.4.) are likely to be replaced by a value of earth pressure coefficient defined according to the equation.

$$K = 2\left[\ln(2D/B + 1) - 1\right] \qquad .....(8.1.5.)$$

where D/B is the dimensionless ratio of depth/width, as shown in Figure 8.1.2.a.

Finally, in another study, PRATER (1973) related the depth/length ratio of a slurry trench to the inclination of a linear Coulomb-type rupture surface of an hypothetical wedge acting behind the trench. This relationship is of the form:

$$f = \frac{\cos\theta}{\tan^2\theta - 1} = \frac{L}{H} \qquad \ldots\ldots(8.1.6.)$$

where f is the length/depth ratio. The above relationship is illustrated in Figure 8.2.4.

f) Arching and stress transfer effects.

The effects of arching and transfer of earth pressure by shear are of great importance as they entail a decrease of earth pressure both vertically between the soil below the trench bottom and the guide walls at the top and also horizontally across the sub-soil adjacent to the panel excavated. A useful discrimination between arching and stress transfer by shear will be considered in Section 8.3. RENAU (1972) suggested that the arch action is in fact three dimensional and vault-like. The vault action consists of a re-distribution of stresses in the soil mass caused by the movements of the trench walls. Figure 8.1.2.b provides a schematic configuration of horizontal arching in a rigidly sheeted vertical cut with fixed upper edge and yielding lower edge, and of vertical arching behind a flexible bulkhead. Both cases were reported by TERZAGHI (1941) and appeared in TSCHEBOTARIOFF (1951).

g) Electrical phenomena

Another interesting feature of a slurry is the development of electrical phenomena in the suspension. The suspension as a system (bentonite and water) is electrically neutral with the negative charges on the clay surfaces completely balanced by the positive charge of the exchangeable cations in water. The difference in ion concentration between the suspension and the surrounding soil could initiate movement of water by osmosis. This osmotic pressure, although small in magnitude, may be an additional factor contributing to the stability of slurry trenches.

Finally, in addition to these key factors, some secondary factors influence stability. These include the method of construction, the rate of excavation and its relationship to the rate of soil deformation at the slurry/soil interface, and the possible lubrication of slip planes caused by loss of fluid through the wall cake and aided perhaps by swelling caused by the action of large horizontal forces which exist within stiff fissured clays. This latter point was noted by PULLER (1974) in the case of London Clay.

8.2. DERIVATION OF THE CRITICAL DEPTH (H_{cr})

One of the classical problems in foundation engineering is the determination of the maximum depth which corresponds to the limit equilibrium conditions of an unsupported vertical cut in a cohesive soil. COULOMB (1773) posed and solved the problem assuming the existence of a rupture surface behind the cut which separates the slipping material from the undisturbed material.

Although Coulomb admitted in principle the idea of a curved failure surface, he based his calculation on the assumption of a triangular wedge. By a simple resolution of forces acting on that wedge he stated that the greatest or critical depth (H_{cr}) to which a trench could be dug in cohesive soil without the sides falling in would be determined by the equation

$$H_{cr} = \frac{4c_u}{\gamma} \cot\theta \qquad \text{where, } \theta = \left(\frac{\pi}{4} - \frac{\phi}{2}\right) \qquad \text{.....(8.2.1.)}$$

Using Coulomb's main analysis, an attempt will be made to derive an equation for the critical depth in the case of a slurry-supported trench both for case of a plane triangular wedge and a three dimensional prismatic wedge. The soil behind the trench is assumed to be perfectly plastic with an undrained yield strength c_u in shear, while the unit weight of soil and the bentonite suspension are treated as depth-independent variables.

8.2.1. TWO DIMENSIONAL COULOMB WEDGE ANALYSIS IN PURELY COHESIVE SOIL.

A simple analysis of the stability of a slurry-supported wedge can be obtained by resolution of forces (Figure 8.2.1.) along the rupture surface.

$$W\sin\theta - C - P\cos\theta - W\cos\theta\tan\phi = 0 \qquad \text{.....(8.2.2.)}$$

The weight, hydrostatic force, and cohesive resistance (all per unit length) are given as:

$$W = \gamma H^2/2\tan\theta\ , \quad P = \gamma_b H^2/2\ , \quad C = c_u H/\sin\theta.$$

Substituting values of W, P and C in equation 8.2.2., re-arranging, and finally solving for H we have

$$H = \frac{2c_u}{\gamma(\cos\theta\sin\theta - \cos^2\theta) - \gamma_b\sin\theta\cos\theta} \qquad \text{.....(.8.2.3)}$$

Taking into account the fact that

$$\cos\theta\sin\theta - \cos^2\theta = 0.5\tan\theta$$

it follows that.

$$H = \frac{2c_u}{\dfrac{\gamma}{2\tan\theta} - \sin\theta\cos\theta} \qquad \text{.....(8.2.4.)}$$

At failure, a critical value of the angle θ, say θ_{cr}, will correspond to a critical value of height H_{cr}. Minimization of height implies maximization of the denominator in equation 8.2.4. This is satisfied for the value $\theta = \frac{\pi}{4}$.

Therefore,

$$H_{cr} = \frac{4c_u}{\gamma - \gamma_b} \qquad \text{.....(8.2.5.)}$$

Equation 8.2.5. is a modification of the original Coulomb relationship and it provides a higher value for H_{cr} as a result of the unit weight decrease $(\gamma - \gamma_b)$.

NASH and JONES (1963) have suggested that the ratio $4c_u/H(\gamma - \gamma_b)$ must be taken as a factor of safety. One may argue that this analysis ignores possible tension cracks in the clay which reduce the factor of safety.

Equation 8.2.5. may also be written in the form

$$\left(1 - \frac{\gamma_b}{\gamma}\right) = \frac{4c_u}{\gamma H_{cr}} \qquad \text{.....(8.2.6.)}$$

This function is expressed in Figure 8.2.2. where a quick appraisal of the critical depth (H_{cr}) is feasible provided that the properties of the clay and the bentonite are known.

8.2.2. THREE DIMENSIONAL COULOMB WEDGE ANALYSIS IN PURELY COHESIVE SOIL

In the three dimensional analysis, the triangular wedge (see Figure 8.2.1.) is transformed to a triangular prism as is shown in Figure 8.2.3. It is obvious that the difference between a two- and three-dimensional analysis is the consideration by the latter of a cohesive resistance acting at both ends in a direction parallel to the rupture plane.

Using the same static arguments as previously, it is possible to write the limit equilibrium equation along the rupture plane as:

$$P\cos\theta - W\sin\theta + C + C_o = 0 \qquad \text{.....(8.2.7.)}$$

Taking into account the fact that.

$W = L\gamma H^2 \cot\theta/2,$

$P = L\gamma_b H^2/2,$

$C = H^2 \cot\theta c/2$

$C_o = LHc/\sin\theta,$

it follows that. $P\cos\theta = \gamma LH^2 \cos\theta/2 - LHc/\sin\theta - H^2 c \cot\theta/2$.....(8.2.8.)

Expressing the stabilising force as force/unit length:

$$P/L = \gamma H^2/2 - 2Hc/\sin 2\theta - H^2 c/L \sin\theta \qquad .....(8.2.9.)$$

Introducing PRATER'S (1973) dimensionless factor,

$$f = \text{length/depth} = L/H$$

$$P/L = \gamma H^2/2 - Hc\,(2/\sin 2\theta - (1/f)\sin\theta) \qquad .....(8.2.10.)$$

PRATER op cit argues that critical equilibrium is obtained when:

$$\frac{d(P/L)}{d\theta} = 0 \qquad .....(8.2.11.)$$

The fulfillment of this condition reveals a critical value of factor (f):

$$f = \frac{\cos\theta}{\tan^2\theta - 1} \qquad .....(8.2.12.)^*$$

Figure 8.2.4. illustrates the relationship between the angle θ with the ratio f. Using this ratio f, an attempt will be made - as for the two-dimensional case - to express the stability factor as a function of the unit weight ratio.

Rewriting equation 8.2.10., it follows that·

$$\gamma_b H^2/2 = \gamma H^2/2 - Hc\,(2/\sin 2\theta - (1/f)\sin\theta) \qquad .....(8.2.13.)$$

Substituting equation 8.2.12. for 8.2.13., we have:

$$H_{cr} = \frac{4c_u}{(\gamma - \gamma_b)} \; \frac{\tan^2\theta}{\sin 2\theta} \qquad .....(8.2.14.)$$

and finally.

$$(1 - \frac{\gamma_b}{\gamma}) = \frac{4c_u}{\gamma H_{cr}} \; \frac{\tan^2\theta}{\sin 2\theta} \qquad .....(8.2.15.)$$

---

*see also equation 8.1.6.

This relationship is plotted in Figure 8.2.5. and it will be noted that for a given value of the ratio (γ/γ_b) the stability factor increases as theta (θ) decreases. For the particular value of the ratio $\gamma/\gamma_b = 1$, the stability factor is independent of the angle (θ) and is equal to zero. This extreme condition corresponds to a purely hypothetical case where $\gamma = \gamma_b$ and is described by the limit

$$\lim_{\gamma_b \to \gamma} \frac{4c_u}{\gamma H_{cr}} = 0 \qquad \text{.....(8.2.16.)}$$

The practical implication of equation 8.2.15. is clear for it permits - at the design stage - the estimation and therefore the optimization of the stability factor and, in effect, the critical height H_{cr} for different values of the ratio γ/γ_b and for various inclinations of the shear plane.

<u>Application</u>

As will be seen in some detail in the next Chapter, the deep excavation in question was a 6.1m long, 0.8m wide and 15m deep bentonite slurry-supported diaphragm wall, excavated in the stiff, fissured over-consolidated London Clay.

According to NASH and JONES (1963), the factor of safety of that trench will be.

$$F.S. = \frac{4c_u}{H(\gamma - \gamma_b)} = \frac{4 \times 150 \text{ kN/m}^2}{15\text{m } (2-1) \text{ Mg/m}^3} = 4$$

where

c_u = 150 kN/m^2 *
H = 15m
γ = 2 Mg/m^3
γ_b = 1 Mg/m^3
L = 6.1 m
B = 0.8m.

If no effective stress changes take place, and the excavation is open only for a matter of days, then $c = c_u$ and $\phi = 0$, hence the inclination of the shear surface must be $\theta = 45^{\circ} + \phi/2 = 45^{\circ}$.

8.3 NORMAL STRESS TRANSFER IN SLURRY TRENCHES.

One of the dominant factors contributing to the stability of slurry trenches in cohesive soil is the effect of the transfer of earth pressures in the form of shear stresses.

Despite its importance, this factor is rarely referred to explicitly in the literature. Almost all stability analyses do, however, mention the ground arching effect.

TSCHEBOTARIOFF (1951, 1973) made a useful discrimination between these two ground functions. While conceptually they both involve some transfer of pressures by discrete shear they do differ radically in that arching pre-supposes the existence of "two rigid boundaries" able to withstand the mobilized earth pressure. In the case of slurry trenches, the guide wall at the top and the soil below the trench bottom could probably be considered as "rigid boundaries". Nevertheless, for deep excavation in purely cohesive soil ($\phi = 0^{\circ}$) it is perhaps more accurate to regard stability from the standpoint of stress-transfer rather than in terms of arching.

Stability analyses which take arching into account should be primarily concerned with cohesionless material where the friction angle is the key factor determining the magntiude of earth pressure. Such analyses have been introduced by various authors and notably by SCHNEEBELI (1964), PIASKOWSKI and KOWALEWSKI (1965) and HUDER (1972). In the present section an attempt will be made to present schematically the forces acting on a ground element in the cross-section (Figure 8.3.1.) of a three dimensional Coulomb wedge (Figure 8.2.3.). These forces are

a) The weight of the soil element,

$$dW = \gamma L \left[(X_o - \cot\theta dz) + \tfrac{1}{2} \cot \theta dz \right] dz \qquad .....(8.3.1.)$$

b) The hydrostatic force exerted by the bentonite suspension,

$$dP = \gamma_b \, L \, z \, dz \qquad \ldots\ldots(8.3.2.)$$

c) The force due to shear resistance along the rupture plane is:

$$dC = L \, c \, \frac{dz}{\sin\theta} \qquad \ldots\ldots(8.3.3.)$$

d) The force due to shear resistance along both ends is:

$$dC_o = c \left[(X_o - \cot\theta \, dz) + \tfrac{1}{2} \cot\theta \, dz \right] dz \qquad \ldots\ldots(8.3.4.)$$

The equation determining stability of the soil element with dimensions (L, X_o, dz) may be obtained by a resolution of the forces parallel to the rupture plane

$$dC + dC_o + \cos\theta \, dP + (\sigma_v + d\sigma_v)(X_o - \cot\theta dz) \, L \sin\theta - \sin\theta dW - \sigma_v X_o L \sin\theta = 0 \qquad \ldots\ldots(8.3.5.)$$

Substituting dC, dC_o, dW and dP for equation 8.3.5. and neglecting differentials of the second order and differential products, it follows that

$$\frac{d\sigma_v}{dz} + \frac{1}{H-z}\left(\frac{2c}{\sin 2\theta} + \gamma_b z \right) + \frac{c}{L\sin\theta} - \gamma - \frac{\sigma_v}{H-z} = 0 \qquad \ldots\ldots(8.3.6.)$$

The latter equation is a typical linear, first order differential equation of the form

$$\frac{dy}{dx} + P(x)y = Q(x) \qquad \ldots\ldots(8.3.7.)$$

and its solution offers the appropriate integrations:

$$\sigma_v = -\frac{2c}{\sin 2\theta} \, \frac{z}{H-z} - \frac{\gamma_b}{2} \, \frac{z^2}{H-z} + \tfrac{1}{2}\left(\frac{c}{L\sin\theta} - \gamma \right)(H-z) + \frac{K_{in}}{H-z} \qquad \ldots\ldots(8.3.8.)$$

where K_{in} is the integration constant, which is determined by the boundary* conditions of the problem. This relationship (equation 8.3.8.) is an

---

*Admittedly from the mathematical point of view there are some difficulties in arriving at the boundary stresses, especially for z=H where all the acting forces apparently coincide to a single point.

expression of the normal stress transfer effect in the form of a function $\sigma_v = f(z)$, with parameters the length of the trench (L) and the properties of the ground(c, γ) and the bentonite suspension (γ_b).

CHAPTER 9

GROUND MOVEMENTS CAUSED BY A DIAPHRAGM WALL EXCAVATION IN LONDON CLAY

9.1. INTRODUCTION

The structure under investigation was a 6.1m long, 0.8m wide and 15m deep slurry-supported diaphragm wall excavated in a stiff, fissured, over-consolidated clay (London Clay) forming one side of a proposed square access shaft to an underground railway tunnel. A new method of construction had been adopted which carried out the excavation in three stages using the B.W. Longwall Drill system with reverse circulation of bentonite. The depth of the excavation, its method of construction and its proximity to adjacent underground structures necessitated the design of a ground monitoring system in order to register ground movements associated with the excavation. The in-situ measurement programme was aimed at the determination of lateral soil deformations and surface and subsurface settlements. This was achieved through measurements in instrumented boreholes.

Some of the results of the project are reported by FARMER and ATTEWELL (1973). However, in the present Chapter these results will be presented in a more detailed manner while a post-construction earth pressure analysis will be developed in order to predict the shape and magnitude of the recorded ground deformations. This analysis consists of two different approaches, namely,

I. A semi-empirical approach derived from a combination of TERZAGHI and PECK (1967) trapezoidal earth pressure distribution modified by the hydrostatic pressure due to bentonite suspension, and

II An elastic theory approach developed by MEYERHOF (1972).

9.2 THE WORKING SITE.

The site of construction was in central London (Green Park corner) and its geology was of some complexity (Attewell, 1974)*. Nevertheless, the major part of the excavation was in overconsolidated,stiff,fissured London Clay. The site plan, geology and soil properties are illustrated in Figure 9.2.1.

9.3 METHOD OF CONSTRUCTION

The operational process for the excavation of the bentonite-supported diaphragm wall, using the B.W. Long wall drill, and the B.W. Support and excavation system, is schematically presented in Figure 9.3.1. The Figure is taken from the journal 'Ground Engineering' (1971) and illustrates the arrangement for the mud circulation system, which links the BWN-5580 submersible drilling unit with a slurry separation and treatment plant.

The excavation was constructed in three panels (Figure 9.4.1.). The sequence of excavation was Panel A first, followed by Panels B (left hand) and Panel C (centre). Figure 9.3.2. visualizes the excavation progress which was rather irregular and relatively slow, with long halt periods, especially as far as panels A and B are concerned. This feature,caused by machine breakdown,was undesirable from both financial and geotechnical points of view, the financial impact of constructional delays being self-evident, while the geotechnical aspect could be understood in terms of yield and softening of ground surrounding the diaphragm wall. The latter situation could eventually lead to potentially unstable ground situations.

9.4 MONITORING SYSTEM.

In order to monitor lateral soil deformations and vertical surface and sub-surface settlements, four boreholes (BH1, BH2, BH3 and BH4) were installed

---

*ATTEWELL, personal communication.

at distances of 0.6m, 2.1m, 4.1m and 6.1m from the edge of the excavation. The four boreholes lay on a plane which intersects the plane of the wall at right angles, at its centre point, as is shown in Figure 9.4.1. Borehole BH1 was 18m deep being 0.6m from the sidewall, while the other boreholes were only 10m deep. Vertical surface movements were monitored using a Cooke S440 precise level to an established bend mark. A complete surface level survey was usually carried out once a day and at frequent intervals during critical periods of excavation. Horizontal subsurface movements were monitored using a Mark II Soil Instruments inclinometer with digital read-out computing to 0.1mm horizontal displacement over a metre vertical length. Inclinometer access tubes with orthogonal guide keyways were located parallel to and normal to the longitudinal plane of the diaphragm wall. Vertical subsurface movements were measured at magnetic rings located at approximate 3m intervals (for BH1) along the inclinometer access tubes. Vertical settlements and inclinometer readings were measured to an accuracy of $\pm$ 0.1mm. Subsurface vertical settlements were measured with $\pm$ 1mm of error.

9.5 OBSERVED BEHAVIOUR DURING CONSTRUCTION.

From the results settlement development profiles in a vertical plane normal to and passing through the wall centre line and at different depths in BH1 were computed and are presented in Figure 9.5.1. The pattern of settlements in this Figure indicates that

I. A maximum settlement occurred at the depth of 7.5-8.0m, approximately one half of the total height of the wall,

II It appears that the ground was relatively slow - in general - to respond to the excavation since the major settlement occurred between the 18th and 20th day from the beginning of the construction. This conclusion is not entirely justified since the BH1 is in front of panel C (see Figure 9.4.1.) whose excavation started on the 17th day (see Figure 9.3.2.). It is, therefore, reasonable to accept that the ground in BH1 is virtually unaffected by the excavation of panels A and B, while the ground behind panel C is not slow to respond during the excavation of that particular panel.

III.

During the limited time interval of six days, i.e. 20th to 26th, there is no significant variation of the pattern of settlements. This statement is reinforced by the shape of the graph for the maximum settlement versus depth as shown in Figure 9.5.2.

This graph shows that a maximum settlement occurs at a depth approximately 8m. This might have been related to the progress of excavation in panel B and maybe in panel C,where long stand-up periods at the particular level of 9m may have affected the nearby clay in a way permitting the possible occurrenceof vertical consolidation.

Another interesting feature documented in Figure 9.5.1. is that the particular subsurface horizon of 16.9m (note that the maximum height of the wall is 15m) moves in a way that confirms the existence of a bottom heave trend. Finally, a transverse surface settlement profile is illustrated in Figure 9.5.3. It is interesting to note that the maximum value of the ratio

$$\frac{\text{distance from excavation}}{\text{maximum depth from excavation}} = 0.3$$

while the maximum value of the ratio

$$\frac{\text{settlement}}{\text{maximum depth from excavation}} = 0.02\%$$ Nevertheless, PECK (1969),

referring to case studies of deep excavation - long walls - using standard soldier piles or sheet piles braced with crossbracing or tiebacks, found that for conditions of average workmanship the respective ratios are equal to

2.0 and 1%. It could be argued, therefore, that bentonite-supported excavations surpassed the traditional constructional methods providing limited extension of the surface settlement profile (15% of the value obtained by the latter methods), and very limited magnitude of maximum settlement.

The evolution of lateral deflection profiles in time is taken from FARMER and ATTEWELL (1973) and is illustrated in Figure 9.5.4. The recorded maximum deflection is 16mm for BH1, 6mm for BH2, 2.6mm for BH3 and 0.0mm for BH4. These maxima occurred at depths of 5m for BH1, and 6m for BH2 and BH3. It is obvious that BH4 lies out of the disturbed ground zone. Combining vertical and horizontal soil movements for BH1, a two-dimensional vectorial representation is attempted in Figure 9.5.5. similar to that presented by FARMER and ATTEWELL (1973). In the lower part of that Figure, the slope of the ground deformation vector (ϕ_o) is plotted against depth (z). Both graphs of this Figure indicate that the horizontal component of the vector is more evident at depths of 2~6m while the vertical component dominates at depths below 10m. A schematic representation of maximum horizontal ground deflections in each borehole is shown in Figure 9.5.6.

Following an estimation - by an approximate extrapolation - of depths where ground deflection is zero for BH1, 2, 3 and 4, a scaled diagram has been drawn (Figure 9.5.7.) where the disturbed ground zone appears to be of parabolic shape. The parabola intersects the ground surface at a point displaced 6.2m from the edge of the sidewall. A characteristic feature of this parabola is its slope of 45 degrees at the point of maximum height of the wall. Nevertheless, it must be stressed that this pattern of ground-affected area is only a rough approximation of real situation. The quantitative consideration of the parabolic profile is highly speculative, but it is reasonable to accept the qualitative nature of this line of demarcation for the ground deformed zone.

9.6 POST-CONSTRUCTION EARTH PRESSURE ANALYSIS

Various attempts have been made to calculate the earth pressures responsible for the recorded sidewall deformation during the excavation. FARMER and ATTEWELL (1973) suggested that the sidewall of the wedge was similar to a yielding retaining wall flexibly supported by the bentonite suspension, and that is subject - during excavation - to the resultant stress equal to the difference between the trapezoidal earth pressure distribution suggested by TERZAGHI and PECK (1967), and to the hydrostatic pressure exerted by the bentonite suspension. This distribution is shown in Figure 9.6.1. Although trapezoidal earth pressure distribution is in use for design purposes in braced excavations, it was probably assumed by the authors that the deformation mechanism of a slurry trench is comparable to that of a braced excavation if one accepts that each level of bentonite suspension "constitutes" an equivalent strut at that level. Therefore, the slurry method could be equivalent to a bracing system with "continuous" struts, i.e. struts placed in such a succession as if no sidewall was left uncovered On the other hand, MEYERHOF (1972) examined the lateral earth pressure of a slurry trench in saturated clay and proposed that the net lateral pressure at depth (z) is given by.

$$\sigma_\ell = (K_o\gamma - \gamma_b)z \qquad \text{.....(9.6.1.)}$$

The pressure profile calculated from equation 9.6.1. is shown in Figure 9.6.2. together with the linear variation in K_o with depth (for London Clay) as proposed by COLE and BURLAND (1972) in a similar analysis.

Nevertheless, MEYERHOF'S relationship is very reasonable because during excavation under bentonite it is probably sufficient to say that lateral earth pressure is replaced by the supporting hydrostatic pressure of the bentonite suspension. As this support pressure is applied immediately following excavation, the deformation measured initially at the borehole represents the relaxation of the soil at that position in a mainly horizontal direction as a result of the replacement of the original horizontal constraining pressure ($K_o\gamma z$).

9.7 PREDICTED HORIZONTAL GROUND DEFORMATION

Two displaced positions of borehole BH1 have been selected for analysis, the position of 9.11.72. (FARMER and ATTEWELL, 1973), when the central panel was just finished and concreted, and a "final" horizontal deformation profile taken at 27 . 1.73. (ATTEWELL and FARMER, 1972). These horizontal deformation profiles are illustrated in Figure 9.7.1. A considerable time-dependent deformation appears for the later BH1 profile at depths between 10m and 15m, while the ground appears to be stable at depths between 1 to 10 metres.

This apparent stress relief over the lower one third of the diaphragm wall might be attributable to bad workmanship. There appears to have been some trench collapse prior to concreting which was delayed due to machine failures and contract difficulties..

In order to predict the horizontal deformation profile near the sidewall of the diaphragm wall two different approaches were used. The first is that proposed by MEYERHOF (1972) who, using elastic theory results, calculated the radial deformation at any depth (z) for a deep cylindrical cut in clay as

$$\delta_\ell = \frac{(1+\nu)\ \sigma_\ell\ B}{2E} \qquad \text{.....(9.7.1.)}$$

where the net lateral pressure is,

$$\sigma_\ell = (K_o\gamma - \gamma_b)z \qquad \text{.....(9.7.2.)}$$

Substituting equation 9.7.2. for equation 9.7.1

$$\delta_\ell = \frac{(1+\nu)(K_o\gamma - \gamma_b)z\ B}{2E} \qquad \text{.....(9.7.3.)}$$

Using the relationship of K_o versus depth, of COLE and BURLAND (1972), a Poisson's ratio equal to $\nu = 0.48$ and a Young's modulus for London Clay equal to 60 MN/m^2 (after MARSLAND, 1971), a calculation for soil deflection versus depth was obtained (see Table 9.7.1.) and is shown in Figure 9.7.1. One could comment that the proposed profile fails to reproduce the shape and magnitude of the actual profile as it is developed just after the excavation (9.11.72.). Another approach is that considered by MYRIANTHIS (1974c) where the influence area of the relaxed zone is assumed equivalent to the area bounded by a typical 45 degrees Coulomb wedge (as in the stability analysis developed in Chapter 8). The magnitude of the deformation will depend on the extent of the relaxed zone, determined by the amount of any arching or stress-transfer, and the pressure gradient in this zone. Accordingly, excluding arching or stress-transfer phenomena (see Chapter 8) the deflection must be given as.

$$\delta_\ell = \frac{\sigma_\ell (H-z)}{E} \qquad \text{.....(9.7.4.)}$$

This relationship is in fact another form of Hooke's law and is obviously valid for elastic deformations only.

As for the variation of the net effective horizontal stress with depth the stress distribution developed by FARMER and ATTEWELL (1973) was adopted, as is shown in Figure 9.6.1.

The calculations were based on the stated elastic properties, i.e. $E = 60\ MN/m^2$ and $\nu = 0.48$, while the unit weight of the clay was taken as 2 Mg/m^3 and the unit weight of the bentonite suspension was taken as 1 Mg/m^3. (For the detailed calculation see Table 9.7.2.).

The deformation profile resulting from the calculation was in good agreement with the actual profile measured at 9.11.72., having a peak deformation of 14.5mm at 4m depth instead of the actual 16.0mm at 5m depth. The shape of the predicted profile is also in accordance with that of the actual profile, while it decays more rapidly towards the value of zero horizontal deformation.

CONCLUSIONS.

A theoretical analysis supported by case studies of soft ground tunnelling has revealed that there is :-

a) an exponential relationship between the ratio of maximum surface settlement to tunnel radius and the tunnel geometry expressed by the ratio of depth to diameter,

b) a linear relationship between the theoretical volume of soil excavated and the volume of soil within the surface settlement curve as defined by an error function, and

c) a relationship taking the form of a modified normal distribution function between the dimensionless ratio maximum surface settlement/tunnel radius and the tunnel advance expressed in units of length.

It is also concluded that a relationship can be formulated between the loss of ground due to tunnelling or the maximum surface settlement and the time factor (the latter factor takes the form of the rate of tunnel advance, and the rate of clay deformation).

The transverse surface settlement profile can be approximated to a normal probability curve having a maximum surface settlement equal to 6mm and a point of inflection at an approximate distance of 15m from the tunnel centre line. This latter distance exceeds that displaced from that predicted by an empirical relationship between depth, diameter and inflexion distance as formulated by PECK (1969). The apparent basal flatness of the settlement curve may perhaps be attributed to quite strong lateral decompression upon excavation. It has been further postulated (ATTEWELL and FARMER, 1972) that such lateral decompression may cause some re-consolidation at soffit and invert leading to the apparent uplift at depth which attenuates towards ground surface.

For the tunnel in question, the study of ground deformations in a vertical plane along the tunnel centre line indicates that the clay predominantly subsides in a vertical manner but it also deflects horizontally towards the direction of tunnel advance for points in front of the shield. As the shield clears the vertical line of reference, an apparent retraction of the horizontal component of the movement occurs, while settlement does continue gradually behind the shield until ground stabilization by grouting is achieved.

A cross-sectional view of the ground deformations reveals that, as might be expected, the main component of the ground motion vector is a vertical one. Ground deformation occurs for a distance of 5 tunnel radii either side of the centre line. This is in some disagreement with theoretical expectations on the assumption of the formation of a 45 degrees inclined hypothetical shear failure plane defining boundaries of the disturbed from the undisturbed ground. Following retraction of the shield, a substantial clay motion continues while the tunnel advances a distance of 30m beyond the reference point.

Results from <u>in-situ measurements</u> of the deformability of a clay annulus just off the tailpiece of the shield tend to show that a major inward clay movement takes place at the axis level, while outward motion appears at soffit and invert. Consequently, a reduction of the horizontal diameter and an increase of the vertical diameter should be expected. These results are confirmed by elastic deformation analysis which take into account the high values of K_o existing at depth in London Clay. However, these findings tend to contradict the results of previous investigations for similar tunnelling and ground conditions- results which suggest (from <u>lining</u>

deformation measurements) - that the clay 'squats' vertically when it is decompressed.

Ground movement records taken during the excavation of a bentonite-supported diaphragm wall have indicated that

a) consequential surface settlement of the ground was of negligible magnitude and extent,

b) the magnitude, extent and development of horizontal ground deformation is more pronounced than the vertical deformation. A maximum deflection of 16mm was observed at a depth of 5m (one third of the total height of the wall), while a maximum vertical settlement of 6mm was recorded at a depth of 7.7m. Also, a limited trend for bottom heave formation was detected.

c) the deformed ground zone (on a vertical plane normal to the longitudinal axis of the wall) appeared to be of parabolic form.

d) Post-construction earth pressure analysis has revealed that a semi-empirical approach to ground deformation is generally satisfactory since it reproduces the shape and magnitude of the actual ground deflection profile. On the other hand, elastic theory has failed to confirm the actual ground deformation trends.

REFERENCES.

AGARWAL, K.B. (1967) The influence of size and orientation of samples on the undrained strength of London clay. Unpublished Ph.D. thesis, University of London.

ARMENTO, W.J. (1972) Criteria for lateral pressures for braced cuts. Proc. Specialty Conf. on Perf. of Earth and Earth-supported structures. Vol. 1, part 2, pp. 1283-1302. Purdue Univ. Lafayette, Indiana, U.S.A.

ATTEWELL, P.B. and BODEN, B. (1971) Development of stability ratios for tunnels drive in clay. Tunnels and Tunnelling, Vol.3, No. 3 pp 195-8.

ATTEWELL, P.B. and FARMER, I.W. (1972) Determination and interpretation of surface and subsurface ground movements during construction on a tunnel in London clay. Report for Transport and Road Research Lab. Ref. No. PBA/IWF/TRRL/1972/I Contract No. ES/LN/842/101.

ATTEWELL, P.B. (1973) Soft ground tunnelling in urban areas. Lecture No.10, Regional Meeting of the Engineering Group of BGS., University of Durham, England. pp 35-38.

ATTEWELL, P.B. and FARMER, I.W. (1973) Ground movements caused by a diaphragm wall excavation in London clay. Report for Transport and Road Research Lab. Ref. No. PBA/IWF/TRRL/1973/1.Contract No. ES/LN/842/101.

ATTEWELL, P.B. and FARMER, I.W. (1974) Ground deformations resulting from shield tunnelling in London Clay. Can. Geotech. Jnl.,Vol II, pp 380-395.

BALLAS, see MUIR WOOD, A.M. (1970).

BARTLETT, J.V. and BUBBERS, B.L. (1970) Surface movements caused by bored tunnelling. Proc. Conf. on Subway Constr. Budapest III, 5, pp 513-539.

BERRY, D.S. (1960) An elastic treatment of ground movement due to mining. Jnl. Mech. and Phys. of Solids. Part I, Vol 8, No. 4, Nov.1960 pp 280-292.

BERRY, D.S. and SALES, T. (1961) Elastic treatment of ground movement due to mining. Jnl. Mech. & Phys. of Solids. Part 2, Vol 9, No. 1, Feb. 1961, pp 52-62.

BERRY, D.S. (1963) Ground movement considered as an elastic phenomenon. The Mining Engineer, No. 37, pp 28-39.

BERRY, D.S. (1964) The ground considered as a transversely isotropic material. Int. Jnl. Rock Mechanics Min. Sci., vol I, pp 159-169.

BERRY, D.S. (1964) A discussion of the stochastic theory of ground movement. Rock Mech. & Eng. Geol. Vol 2, pp 213-227.

BERRY, D.S. (1964) A theoretical elastic model of the complete region affected by mining a thin seam. Proc. 6th Symp. on Rock Mech., Rolla. pp 310-329.

BISHOP, A.W. and HENKEL, D.J. (1964) The measurement of soil properties in the triaxial test. London, E. Arnold.

BISHOP, A.W., WEBB, D.L. and LEWIN, P.I. (1965) Undisturbed samples of London clay from the Ashford common shaft . strength effective stress relationships. Géotechnique, Vol 15, pp. 1-30.

BISHOP, A.W. (1966) The strength of soils as Engineering materials. 6th Rankine lecture, Géotechnique, Vol 16, pp. 89-130.

BISHOP, A.W. and LITTLE, A.L. (1967) The influence of the size and orientation of the sample on the apparent strength of the London clay at Maldon, Essex. Proc. Geotech. Conf., Oslo, pp. 89-96.

BISHOP, A.W. (1972) Shear strength parameters for undisturbed and remoulded soil specimens. Stress-strain behaviour of soils. Edited by Parry, R.H.G. Foulis and Co., Ltd., Oxford, England, pp. 3-58.

BJERRUM, L. (1967) Mechanisms of progressive failure in slopes of overconsolidated plastic clay and clay shales. Jnl. Soil Mech. Found. Div., Proc. ASCE, Vol 93, No. SM5, Part I, pp 1-49.

BODEN, J.B. (1969) Site investigation and subsequent analysis for shallow tunnels. M.Sc. Eng.Geol.Adv.Course Dissertation, University of Durham, England.

BODZIONI, J., LITWINISZYN, J. and SMOLARSKI, A. (1960) New research into rock masses treated as media characterized by stochastic equations. 3rd Int. Conf. on Strata Control, Paris, pp 137-150.

BODZIONI, J. and SMOLARSKI, A.Z. (1960) Experimental investigations of loose bodies from the aspect of the theory of the stochastic medium. Bull. de l'Academie Polonaise des Sciences. Vol 8, pp 139-144.

BRETH, H., SCHUSTER, E. and PISE, P. (1973) Axial stress strain characteristics of sand. Jnl. Soil Mech., Found. Div., Proc. ASCE, Vol 99, No. SM8, pp 617-632.

BROMS, B.B. and BENNERMARK, H. (1967) Stability at vertical openings, Jnl. Soil Mech, Found. Div., Proc. ASCE, Vol 93, No.SM1, pp 71-94.

BROOKER, E.W. and IRELAND, H.O. (1965) Earth pressure at rest related to stress history. Can. Geotech. Jnl. Vol 2, No. 1, pp 1-15.

CARON, C. (1973) Un nouveau style de perforation la boue autodurcissable, Annales IT BTP, serie Materiaux No. 47, Nov.73, No.311, pp 12,22, 26, 38.

CHRISTIAN, J.T. (1968) Undrained stress distribution by numerical methods. Jnl. Soil Mech. Found. Div.,Proc. ASCE, Vol 94, No.SM6,pp 1333-1346.

COLE, K.W. and BURLAND, J.B. (1972) Observation of retaining wall movements associated with a large excavation. Proc. 5th European Conf. Soil Mech. Found. Eng., Madrid, Vol 1, pp.445-453.

COSTET, J. and SANGLERAT, G. (1969) Cours pratique de Mecanique des sols. Dunod, Paris, pp 357-359.

COULOMB, C.A. (1773) Essai sur une application des regles de maximis et minimis a quelque problemes de statique relatifs a l'architecture, Mem. Math. Phys. (divers Savans). vol 7, p. 343.

DAHL, H.D. (1967) Mine subsidence as a problem in Coulomb plasticity. M.Sc. thesis, Pennsylvania State University, U.S.A.

DEERE, D.U., PECK, R.B., MONSEES, J.E. and SCHMIDT, B. (1969) Design of tunnel liners and support systems. Report for the U.S. Dept. of Transportation. OHSGT, Contract 3-0152.

DRUCKER, M.A. (1943) Determination of lateral passive soil pressure and its effect on tunnel stresses. Jnl. Franklin Inst. pp 499-512.

ELSON, W.K. (1968) An experimental investigation of the stability of slurry trenches. Géotechnique, Vol. 18, No. 1, pp 37-49.

FARMER, I.W. and ATTEWELL, P.B. (1973) Ground movements caused by a bentonite-supported excavation in London clay. Géotechnique. Vol XXIII. No. 4, pp 576-581.

FOLYAN, J.I., HOEG, K. and BENJAMIN, J.R. (1970) Decision theory applied to settlement predictions. Jnl. Soil Mech. Found Div., Proc. ASCE, Vol 96, No. SM4, pp 1127-1141.

GETZLER, Z., KOMORNIK, A. and MAZURIK, A. (1968) Model study on arching above buried structures. Jnl. Soil Mech. Found. Div., Proc. ASCE, No. SM5, pp 1123-1141.

GETZLER, Z., GELLART, M. and EITAN, R. (1970) Analysis of arching pressures in ideal elastic soil. Jnl. Soil Mech. Found. Div., Proc.ASCE, Proc. paper 7431, pp 1357-1372.

GOLDER, H.Q. (1948) Measurement of pressure in timbering of a trench in clay. Proc. 2nd Int. Conf. Soil Mech. & Found. Eng. Vol 2, pp 76-81.

GORDON, T. (1974) The stress field and displacements associated with soft ground tunnels. M.Sc. thesis, Univ. of Durham.

HACKETT, P. (1959) An elastic analysis of rock movement caused by mining. Trans. Inst. Min, Eng. Vol 118, Part 7, Apr.1959, pp 421-433.

HACKETT, P. (1964) Prediction of rock movement by elastic theory compared with in-situ measurement. Rock Mech. & Eng. Geol. Supplementum I, 1964, pp 88-102.

HANNA, T.H. (1973) Foundation instrumentation. Series on rock and Soil Mechanics. Vol 1, 1971/73 No. 3, Trans. Tech. Publ. Page 192.

HANSMIRE, W.H. and CORDING, E.J. (1972) Performance of a soft ground tunnel on the Washington metro. Proc. 2nd North Amer. Rapid Excavation and Tunnelling Conf. Chicago, Illinois, Vol 1, AIME, Chapter 23, pp 371-390.

HARRISON, A (1971) Extrusion testing of remoulded clays applied to stability problems in soft ground tunnelling. M.Sc.Eng.Geol. Adv.Course Dissertation, University of Durham, England.

HOFFMAN, H. (1964a) Subsidences in a stratified, true-to-scale model, in relation to friction, direction of work and rate of working. Mitteilungen aus dem Markscheidewesen.

HOFFMAN, H. (1964b) The effects of direction of working and rate of advance on the scale-deformation of a self loaded stratified model of a large body of ground. Proc. 4th Symp. on Strata Control and Rock Mech. New York, 14pp

HOOPER, J.A. and BUTLER, F.G. (1966) Some numerical results concerning the shear strength of London clay. Géotechnique, Vol XVI, pp 282-304.

HUDER, J. (1972) Stability of bentonite slurry trenches with some experience in Swiss practice. Proc. 5th European Conf.Soil Mech. & Found. Eng. Madrid, 1972, pp 517-522.

IMAM, H.I. (1965) A viscoelastic analysis of mine subsidence in horizontal laminated strata. Ph.D. thesis, University of Minnesota, Minneapolis, U.S.A.

JAEGER, J.C. and COOK, N.G.W. (1969) Fundamental of Rock Mechanics, Methuen, London. pp 441-445.

KASTNER, H. (1962) Statik des Tunnel-und Stollenbaues. Springer-Verlag, Berlin, Gottingen, Heidelberg.

KING, J. and WHETTON, J. (1958) Mechanics of mining subsidence. Colliery Engineering, July 1958, pp 285-288.

LAMBE, W.T. (1967) Stress path method. Jnl. Soil Mech. Found. Div. Proc. ASCE, Vol 93, No. SM6 pp 309-331.

LAMBE, W.T. and WHITMAN, R.V. (1969) Soil Mechanics. John Wiley and Sons, Ltd,, London.

LA RUSSO, R.S. (1963) Wanapurn developemtn - slurry trench and grouted cut-off. Proc. Symp. Grouts and Drilling Muds in Engineering Practice. pp 196-201 - Butterworth, London.

LITWINISZYN, J. (1953) The differential equation of displacement of rock masses. Bull. de l'Academie Polonaise des Sciences, Vol 1, pp 38-40.

LITWINISZYN, J. (1956) Application of the equations of stochastic processes to mechanics of loose bodies. Archivum Mechaniki Stosowanej. Vol 8, pp 393-411.

LITWINISZYN, J. (1957) Fundamental properties of the mechanics of stochastic media. Proc. 3rd Congr. Theor. & Appl. Mech. Bangalore, pp 93-110.

LO, K.Y. (1970) The operational strength of fissured clays. Géotechnique, Vol 20, No. 1, pp 57-74.

MARSLAND, A. and LOUDON, A.G. (1963) The flow properties and yield gradients of bentonite grouts in sands and capillaries. Proc. Symp. Grouts and drilling muds in Eng. practice. 3, London, Butterworth, pp. 15-21.

MARSLAND, A. (1971) Large in situ tests to measure the properties of stiff fissured clays. Proc. 1st Australia-NewZealand Conf. on Geomech. Melbourne, Vol 1, pp 180-189.

MARSLAND, A. (1972) Clays subjected to in situ plate tests. Ground Engineering, Vol 5, No. 6, Nov. 1972, pp 24-26, 29-31.

MARSLAND, A. (1973) Laboratory and in situ measurements of the deformation moduli of London clay. B.R.S. current paper CP 24/73, England.

MARSHALL, G.J. and BERRY, D.S. (1966) Calculation of the stress around an advancing longwall face in viscoelastic ground. Proc. 1st Cong. Int. Soc. Rock Mech. Vol II, pp 379-384.

MEYERHOFF, G.G. (1972) Stability of slurry trench cuts in saturated clay. Proc. specialty Conf. on performance of Earth and Earth supported structures. Vol 1, Part 2, pp 1451-1466.

MORETTO, O. (1969) State of stress at rest in preconsolidated clays. Proc. 7th Int. Conf. Soil Mech. & Found. Eng. Main session 4, pp 357-359.

MORGENSTERN, N.R. (1963) Discussion. Proc. Symp. Grouts and drilling muds in Engineering practice. London, Butterworth, pp 233.

MUIR WOOD, A.M. (1969, 1971) see HANNA, T.H. (1973).

MUIR WOOD, A.M. (1970) Soft ground tunnelling. Proc. TUNCON 70, Johannesburg, Vol 1, pp. 167-174.

MYRIANTHIS, M.L. (1973) The effect of fissures on the shear strength of blue London clay. Bull. Geological Soc. of Greece. Vol X,No.2 pp 97-107.

MYRIANTHIS, M.L. (1974a) Quelques relations phenomenologiques sur le tassement d'un terrain de faible resistance surmontant un tunnel. Annales de l'ITBTP. Seri sols et fondation No 317, pp 117-128.

MYRIANTHIS, M.L. (1974b) The development of surface subsidence profiles during soft ground tunnelling. Proc. 2nd Int. Cong. of Eng. Geology. Sao Paulo, Brazil, Vol 2, Theme VII No. 4.

MYRIANTHIS. M.L. (1974c) Analysis of the ground deformations associated with the excavation of a deep trench supported by bentonite slurry. (in Greek) Technica Chronica. 571, No. 1, pp 71-82.

NADAI see SAVIN, G.N. (1961).

NASH, J.K.T.L. and JONES, G.K. (1963) The support of trenches using fluid mud. Proc. of the Symp. on Grouts and Drilling Muds in Engineering Practice. London, Butterworth, pp 177-180.

OBERT, L. and DUVALL, W.I. (1967) Rock Mechanics and the design of structures in Rock. John Willey, 1959, New York. pp 162-169.

PASCALL, D. (1970) Extrusion testing of clays applied to soft ground tunnelling. M.Sc.Eng. Geol. Adv.Course Dissertation, Univ. of Durham, England.

PIASKOWSKI, A. and KOWALEWSKI, Z. (1965) Application of thixotropic clay suspensions for stability of vertical sides of deep trenches without strutting. Proc. 6th Int. Conf. Soil Mech. and Found. Eng. Vol 2 and 3, Montreal, Canada, 1965.

PECK, R.B. (1942) Earth pressure measurements in open cuts, Chicago, Illinois Subway. Proc. ASCE, 1942, Vol 68, No. 6, pp 900-928.

PECK, R.B. HANSON, W.E. and THORNBURN, T.H. (1947) Foundation Engineering, John Wiley, 13th Edition, 410 pages.

PECK, R.B., DEERE, D.U., MONSEES, J.E., PARKER, H.W. and SCHMIDT, B. (1969) Some design considerations in the solution of underground support systems. Final Report for the U.S. Dept. of Transportation, Washington, D.C. Contract No. 3-0152.

PECK, R.B. (1969) Deep excavations and tunnelling in soft ground. State of the Art Volume, 7th Int. Conf. Soil Mech. and Found. Eng. Mexico City, pp. 225-290.

PECK, R.B., HENDRON, A.J. Jr. and MOHRAZ, B. (1972) State of the art of soft ground tunnelling. Proc. 2nd North American Rapid Excavation and Tunnelling conf. Chicago, Illinois, Vol 1, Chapter 19, pp 259-286.

PRATER, E.G. (1973) Die Gewolbewirkung der Schlitzwande. Der Bauingenieur, 48, pp 125-131, Springer-Verlag.

PULLER, M.J. (1974) Slurry trench stability - theoretical and practical aspects. Ground Engineering, Sept. 1974, Vol. 7, No. 5, pp 34-36.

RANKILOR, P.R. (1970) An approach to the simulation of mining subsidence phenomena in an elastic layered model. Quart. Jl. Eng. Geol., Vol 3, pp 55-63.

RENAU, F. (1972) see PULLER, M.J. (1974).

SADLEIR, N.A. and DOMINIONI, G.C. (1963) Underground structural concrete walls. Proc. Symp. on Grouts and Drilling muds, in Engineering Practice. Vol 25, London, Butterworth, pp 189-193.

SALAMON, M. (1963, 64) Elastic analysis of displacements and stresses by mining seam on reef deposits. Jnl. South African Inst. Min. and Metal. Part 1, vol 64, Nov. 1963, pp 128-149, Part 2, Vol 64, Jan. 1964 pp 197-218, Part 3, Vol 64, Mar.1964, pp 468-500, Part 4, Vol 65, Dec. 1964, pp 319-341.

SCHMIDT, B. (1969) Settlements and ground movements associated with tunnelling in soil. Ph.D. thesis, Univ. of Illinois, Urbana, Illinois, U.S.A.

SCHNEEBELI, G. (1964) La stabilite des tranchees profondes forees en presence de boue. La Houille Blanche, No. 7, pp 815-820.

SCHOFIELD, A.N. and WROTH, C.P. (1968) Critical state soil mechanics. McGraw-Hill, New York, U.S.A.

SHIRAISHI, S. (1968/69) Recent major shield driven tunnels through soft ground in Japan. Soils and Foundations. Vol 9(3), p. 16.

SKEMPTON, A.W. and HENKEL, D.J. (1957) Tests on London clay from deep borings at Paddington, Victoria and the South Bank. Proc. 4th Int. Conf. Soil Mech. and Found. Eng., Vol 1a, No. 25, pp 100-106.

SKEMPTON, A.W. (1961) Horizontal stresses in overconsolidated Eocene clay. Proc. 5th Int. Conf. Soil Mech. & Found. Eng., Paris, Vol 1, pp 351-357.

SKEMPTON, A.W., SCHUSTER, R.L. and PETLEY, D.J. (1969) Joints and fissures in the London clay at Wraysbury and Edgeware. Géotechnique, Vol. 19, No. 2, pp 205-217.

SOM, N.N. (1968) The effect of stress path on the deformation and consolidation of London clay. Unpublished Ph.D. thesis, University London, England.

SWEET, A.L. (1965) Validity of stochastic model for predicting subsidence. Jl. Eng. Mech. Div., Proc. ASCE, Vol 91, No. EM6, proc. paper 4573, pp 111-128.

SWEET, A.L. and BOGDANOFF, J.L. (1965) Stochastic model for predicting subsidence. Jl. Eng. Mech. Div., Proc. ASCE, Vol 91, No. EM2, Proc. paper 4292, pp 22-45.

SZECHY, K. (1967) The Art of Tunnelling. Publ. Akademiai Kiado, Budapest.

SZECHY, K. (1970) Surface settlements due to the shield tunnelling method in cohesionless soils. Conf. on Subway Construction, Budapest, 1970, pp 615-625.

TCHALENKO, J.S. (1968) The microstructure of London clay. Q. Jl. Eng. Geol., Vol I, pp 155-168.

TERZAGHI, K. (1941) General wedge theory of Earth pressure. Trans. ASCE, pp 68-97.

TERZAGHI, K. (1943) Theoretical Soil Mechanics. John Wiley & Sons, New York,

TERZAGHI, K. (1946) Introduction to tunnel geology. In R.V. PROCTOR and T.L. WHITE (1968) Rock tunnelling with steel supports. Youngstown printing co., U.S.A., 292 pages.

TERZAGHI, K. and RICHART, F.E. (1952) Stresses in rock above cavities, Géotechnique, Vol 3, 2, p. 57.

TERZAGHI, K. and PECK, R.B. (1967) Soil Mechanics in Engineering Practice, Wiley Int., 2nd Edition, 729 pages.

TREFETHEN, J.M. (1960) Geology for Engineers, Van Nostrand Co., London, page 405

TSCHEBOTARIOFF, G.P. (1949) Large scale earth pressure tests with model flexible bulkheads. Final report Bureau of Yards and Docks, U.S. Navy, Princetown University, January 1949, 272 pp.

TSCHEBOTARIOFF, G.P. (1951) Soil Mechanics, Foundation and Earth Structures, Mc-Graw Hill, New York, 655 pp.

TSCHEBOTARIOFF, G.P. (1973) Foundations, Retaining and Earth Structures, Mc-Graw Hill, New York.

VEDER, C. (1963) Excavation of trenches in the presence of bentonite suspensions for the construction of impermeable and load-bearing diaphragms. Proc. Symp. on Grouts and Drilling Muds in Engineering Practice. Vol. 24, London, Butterworth, 181 pp.

VOIGHT, B. and PARISEAU, W. (1970) State of predictive art in subsidence Engineering, Jl. Soil Mech. Found. Div., Proc. ASCE, Vol.96, No. SM2, pp 721-750.

WARD, W.H. (1970) Yielding of the ground and the structural behaviour of linings of different flexibility in a tunnel in London Clay. B.R.S. Current Report CP: 34/70, England.

WARD, W.H., SAMUELS, S.G. and BUTLER, E. (1959) Further studies of the properties of the London Clay. Géotechnique, Vol 9, No.2.

WARD, W.H. and THOMAS, H.S.H. (1965) The development of earth loading and deformation in tunnel linings in London Clay. Proc. 6th Int. Conf. Soil Mech. Found. Eng., Montreal, Vol 2, pp 432-436.

WARD, W.H., MARSLAND, A. and SAMUELS, S.G. (1965) Properties of the London Clay at Ashford common shaft, in situ and undrained tests. Géotechnique, Vol 15, No. 4, pp 321-344.

T A B L E S

TABLE 2.6.1. Above Tunnelling in various soils

Below Records for the tunnel advance and the dimensionless ratio s_{max}/f for six case studies of tunnelling.

TABLE NR 1

NUMBER	CASE	REFERENCE	DEPTH TO TUNNEL AXIS (m)	DIAMETER 2R (m)	Z/2R	ULTIMUM Smax/R x10^{-3}	SOIL CONDITIONS
1	NAGOYA UTILITY TUNNEL (point A)	B SCHMIDT 1969	745	410	182	2585	SILTY SAND ABOVE THE GROUND WATER LEVEL N= 10 - 40
2	same (point B)	do	do	do	do	2341	do
3	SAN FRANCISCO BART MARKET STR	R B PECK S FILES 1968	1730	525	330	2061	SILTY CLAY WITH SANDY LENSES
4	TOKYO HANEDA 1968	B SCHMIDT 1969	1029-1135	660	156-172 (164)	3454	SAND BELOW THE GROUND WATER LEVEL
5	TYNESIDE TUNNEL UK 1973	P B ATTEWELL 1973	730	202	365	762	LAMINATED CLAY
6	TUNNEL IN LONDON CLAY 1972	ATTEWELL & FARMER (1972)	2930	414	710	289	OVERCONSOLIDATED STIFF FISSURED CLAY

TABLE NR 2

TUNNEL ADVANCE (m)	S_{max} (mm)	S_{max}/R x 10^{-3}
CASE NR 1		
-3	50	243
1	200	975
5	375	1829
8	412	2009
11	500	2439
34	530	2585
CASE NR 2		
-6	265	129
-2	530	260
2	1000	487
14	3650	1785
18	4450	2175
30	4800	2341
CASE NR 3		
-5	75	286
0	225	858
12	405	1545
24	465	1774
39	540	2061
CASE NR 4		
0	8	242
75	32	969
100	48	1454
125	74	2242
150	90	2727
210	106	3212
330	114	3454
CASE NR 5		
-5	110	108
-2	165	163
0	290	287
5	620	613
10	700	693
40	770	762
CASE NR 6		
* -20	05	024
-10	142	068
0	285	137
10	442	213
20	507	244
36	600	289

* The minus sign in tunnel advance means that the tunnel approaching

TABLE 5.5.1.

Poisson's ratio measurement during triaxial undrained tests on 38mm diameter samples, collected in two main directions, parallel and normal to stratification.

	Deviator stress $\sigma_1-\sigma_3$ kN/m^2	Principal stress σ_1 kN/m^2	Principal stress ratio σ_3/σ_1 -	Poisson's ratio r -	strain ε %
a)	σ_3 = 490 kN/m^2	sample orientation	vertical		
	0.0	490	1	0.500	0.0
	26	516	0.94	0.499	0.13
	50	540	0.90	0.498	0.26
	-	-	-	0.498	0.39
	74	564	0.86	0.497	0.52
	89	579	0.84	0.496	0.65
	170	660	0.74	0.493	1.18
	260	750	0.65	0.490	1.70
	333	823	0.59	0.486	2.23
	400	890	0.55	0.486	2.75
	448	938	0.52	0.488	3.28
	484	974	0.50	0.492	3.80
	506	996	0.49	0.496	4.33
	499	989	0.49	0.502	4.85
b)	σ_3 = 650 kN/m^2	sample orientation	vertical		
	0.0	650	1	0.500	0.0
	78	728	0.89	0.499	0.13
	106	756	0.85	0.498	0.26
	128	778	0.83	0.498	0.39
	-	778	-	0.497	0.52
	-	778	-	0.496	0.65
	196	846	0.76	0.493	1.18
	251	901	0.72	0.490	1.70

306	956	0.67	0.487	2.23
357	1007	0.64	0.484	2.75
391	1041	0.62	0.482	3.28
421	1071	0.60	0.481	3.80
433	1083	0.60	0.481	4.33
451	1101	0.59	0.480	4.85
463	1113	0.58	0.479	5.38
475	1125	0.57	0.478	5.90
488	1138	0.57	0.478	6.95
497	1147	0.56	0.475	8.00
497	1147	0.56	0.475	9.05
499	1149	0.56	0.473	10.1

c) σ_3 = 700 kN/m^2 sample orientation : vertical

0.0	700	1	0.500	0.0
13	713	0.98	0.499	0.13
17	717	0.97	0.498	0.26
26	726	0.96	0.498	0.39
47	747	0.93	0.497	0.52
60	760	0.92	0.495	0.65
168	868	0.80	0.491	1.18
249	949	0.73	0.486	1.70
318	1018	0.68	0.481	2.23
387	1087	0.64	0.475	2.75
431	1131	0.61	0.470	3.28
446	1146	0.61	0.464	3.80
479	1179	0.59	0.462	4.33
489	1189	0.58	0.459	4.85
488	1188	0.58	0.457	5.38

d) σ_3 = 780 kN/m^2 sample orientation vertical.

0.0	780	1	0.500	0.0
56	836	0.93	0.499	0.13
91	871	0.89	0.498	0.26
130	910	0.85	0.498	0.39
163	943	0.82	0.498	0.52
184	964	0.80	0.497	0.65
291	1071	0.72	0.497	1.18
378	1158	0.67	0.496	1.70
440	1220	0.63	0.495	2.23
496	1276	0.61	0.494	2.75
537	1317	0.59	0.494	3.28
568	1348	0.57	0.493	3.80
596	1376	0.56	0.492	4.33
614	1394	0.55	0.492	4.85
623	1403	0.55	0.490	5.38
634	1414	0.55	0.493	5.90
641	1421	0.54	0.496	6.95

e) σ_3 = 400 kN/m^2 sample orientation horizontal

0.0	400	1	0.498	0.0
72	472	0.84	0.497	0.13
89	489	0.81	0.497	0.26
113	513	0.77	0.496	0.39
145	545	0.73	0.495	0.52
182	582	0.68	0.495	0.65
307	707	0.56	0.492	1.18
426	826	0.48	0.489	1.70
541	941	0.42	0.487	2.23
651	1051	0.38	0.484	2.75
743	1143	0.34	0.482	3.28
804	1204	0.33	0.479	3.80
825	1225	0.32	0.482	4.33

f) σ_3 = 440 kN/m^2 sample orientation horizontal.

0.0	440	1	0.500	0.0
67	507	0.86	0.499	0.13
69	509	0.86	0.498	0.26
89	529	0.83	0.498	0.39
119	559	0.78	0.497	0.52
143	583	0.75	0.497	0.65
250	690	0.63	0.494	1.18
372	812	0.54	0.493	1.70
494	934	0.47	0.491	2.23
598	1038	0.42	0.490	2.75
679	1119	0.39	0.489	3.28
760	1200	0.36	0.487	3.80
823	1263	0.34	0.486	4.33
870	1310	0.33	0.485	4.85
905	1345	0.32	0.484	5.38
922	1362	0.32	0.483	5.90
898	1338	0.32	0.480	6.95-
811	1251	0.35	0.481	8.00

g) σ_3 = 620 kN/m^2 sample orientation horizontal

0.0	620	1	0.500	0.0
72	692	0.89	0.499	0.13
104	724	0.85	0.498	0.26
135	755	0.82	0.498	0.39
156	776	0.79	0.497	0.52
180	800	0.77	0.497	0.65
281	901	0.68	0.495	1.18
380	1000	0.62	0.493	1.70
477	1097	0.56	0.491	2.23
564	1184	0.52	0.489	2.75
626	1246	0.49	0.487	3.28
682	1302	0.47	0.485	3.80
715	1335	0.46	0.483	4.33
729	1349	0.45	0.481	4.85

735	1355	0.45	0.479	5.38
731	1351	0.45	0.477	5.90

h) $\sigma_3 = 760\ kN/m^2$ sample orientation horizontal.

0.0	760	1	0.500	0.0
6	766	0.99	0.498	0.13
26	786	0.96	0.498	0.26
65	825	0.92	0.497	0.39
87	847	0.89	0.496	0.52
128	888	0.85	0.495	0.65
255	1015	0.74	0.493	1.18
363	1123	0.67	0.488	1.70
464	1224	0.62	0.483	2.23
593	1353	0.56	0.479	2.75
635	1395	0.54	0.474	3.28
713	1473	0.51	0.471	3.80
764	1524	0.49	0.462	4.33
780	1540	0.49	0.459	4.85
833	1593	0.47	0.453	5.38
813	1573	0.48	0.447	5.90

TABLE 6.3.1.

Calculation of strain energy release and vertical ground displacement due to tunnelling, according to relationships proposed by JAEGER and COOK (1969).

Distance from Tunnel centre	Young's Modulus	Strain energy			Vertical Displacement
R/R_o	E *	W_1	W_2	W_2-W_1	U
	$x10^2 kN/m^2$	$x\ 10^5 kN$			mm
2	280	2.14	30.38	28.24	38.0
3	262	5.19	24.91	19.72	21.1
4	243	8.79	25.62	16.83	14.8
5	224	12.53	27.24	14.71	11.3
6	205	16.10	28.89	12.79	9.1
7	187	18.98	29.91	10.93	7.5
8	168	21.04	30.22	9.18	6.3
9	149	21.86	29.34	7.48	5.4
10	131	21.00	26.73	5.73	4.5
11	112	18.55	22.77	4.22	3.8
12	93	14.32	17.06	2.74	3.1
13	75	8.45	9.81	1.36	2.2
14	51	2.64	3.02	0.38	1.3

Where the strain energy before tunnelling (W_1) the strain energy after tunnelling and the vertical displacement of the soil (U) are given by equation

$$W_1 = \frac{\pi(1+\nu)(1-2\nu)}{E}\ \sigma_v^2\ (R^2 - R_o^2)$$

$$W_2 = \frac{\pi(1+\nu)\ \sigma_v^2 \left[(1-2\nu)R^4 + R^2 R_o^2\right]}{E(R^2 - R_o^2)}$$

and

$$U_R = \frac{2(1+\nu)(1-\nu)\ \sigma_v R_o^2 R}{(R^2 - R_o^2)\ E}$$

note that R = 0.48 and R_o = 2.035m (tunnel radius)

*E (Young's modulus) has been taken from MARSLAND (1973)

TABLE 9.7.1

Calculation of the earth pressure acting behind the diaphragm wall (see Chapter 9) and the ground deformation in borehole BH1 according to the elastic theory approach (MEYERHOF, 1972) and the semi-empirical approach (FARMER and ATTEWELL, 1973 and MYRIANTHIS, 1974c).

Depth z in metres	Earth pressure kN/m^2		Ground deformation, mm	
	Elastic Theory approach	Semi-empirical approach	Elastic theory approach	Semi-empirical approach
1	22	20	0.22	4.66
2	58	40	0.58	8.66
3	104	60	1.03	12.00
4	156	80	1.53	14.66
5	210	70	2.07	11.66
6	264	60	2.60	9.00
7	316	50	3.11	6.66
8	364	40	3.59	4.66
9	408	30	4.02	3.00
10	446	20	4.40	1.66
11	478	10	4.71	0.66
12	504	0	4.97	0.0
13	525	-10	5.18	-0.33
14	543	-20	5.35	-0.33
15	555	-30	5.47	0.0

where

$B = 0.8m$

$\gamma = 2 Mg/m^3$

$\gamma_b = 1\ Mg/m^3$

$H = 15m$

$\nu = 0.48$ (see Chapter 5)

$E = 60\ MN/m^2$ (after MARSLAND, 1971)

K_o = values taken from COLE and BURLAND, 1972.

F I G U R E S

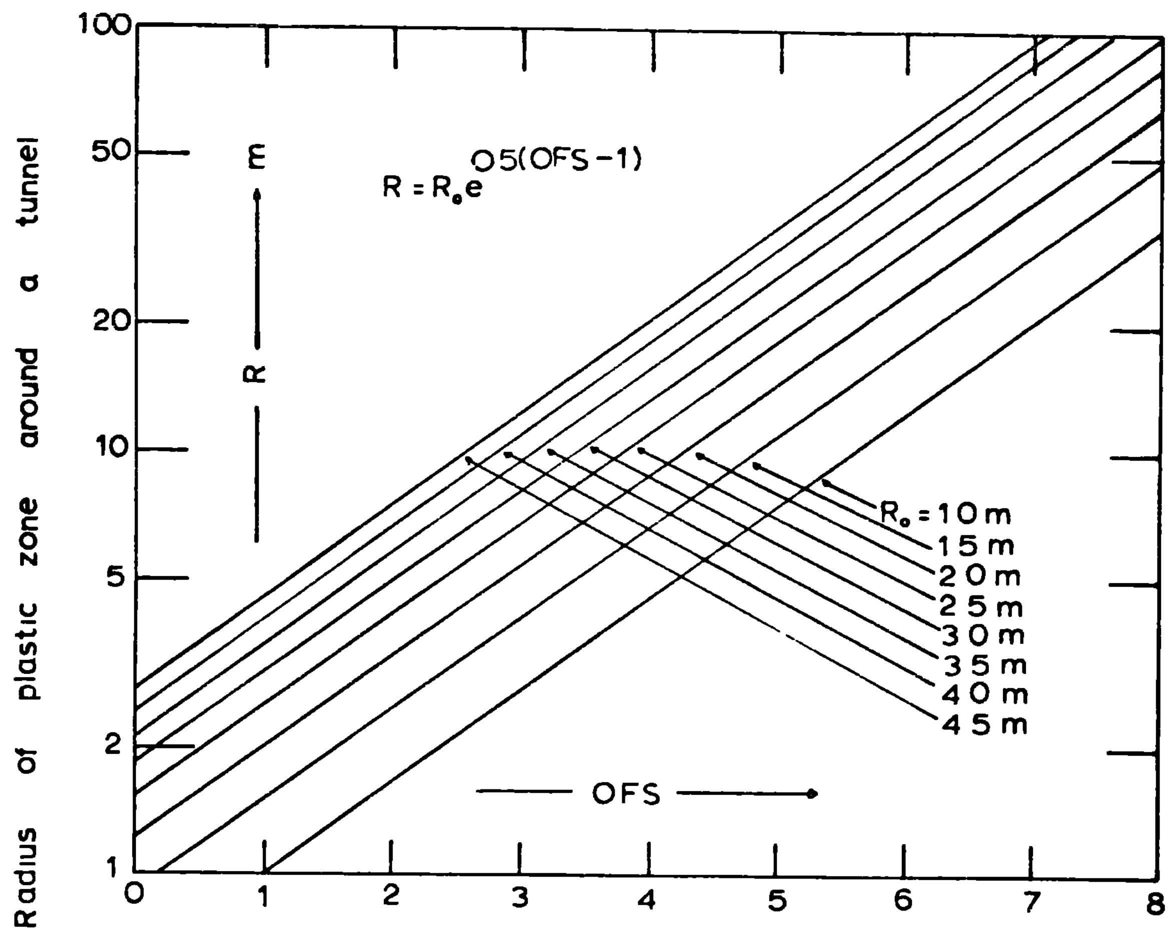

FIG 1.21 Relationship between the extent of a plastic zone around a tunnel (R), and the OFS, for various tunnel radii (R_o)

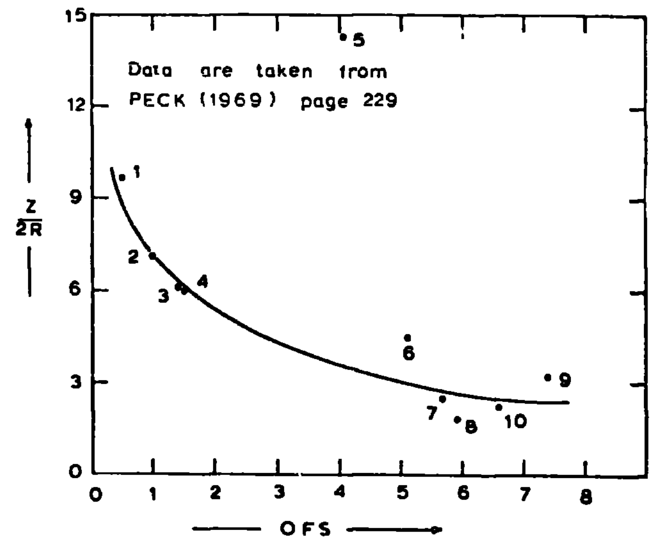

FIG 12 2 Relationship between Z/2R and OFS

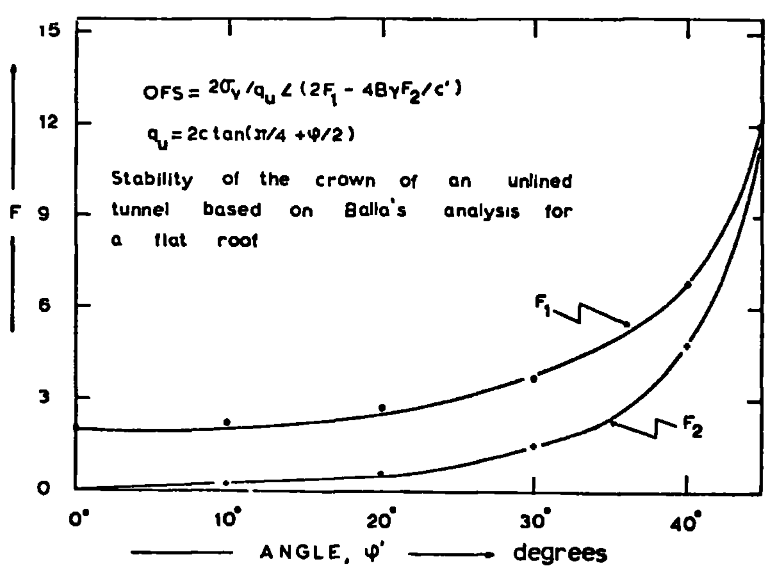

FIG 12 3 Relationship between the coefficients (F), and the friction angle based on effective stresses (φ')

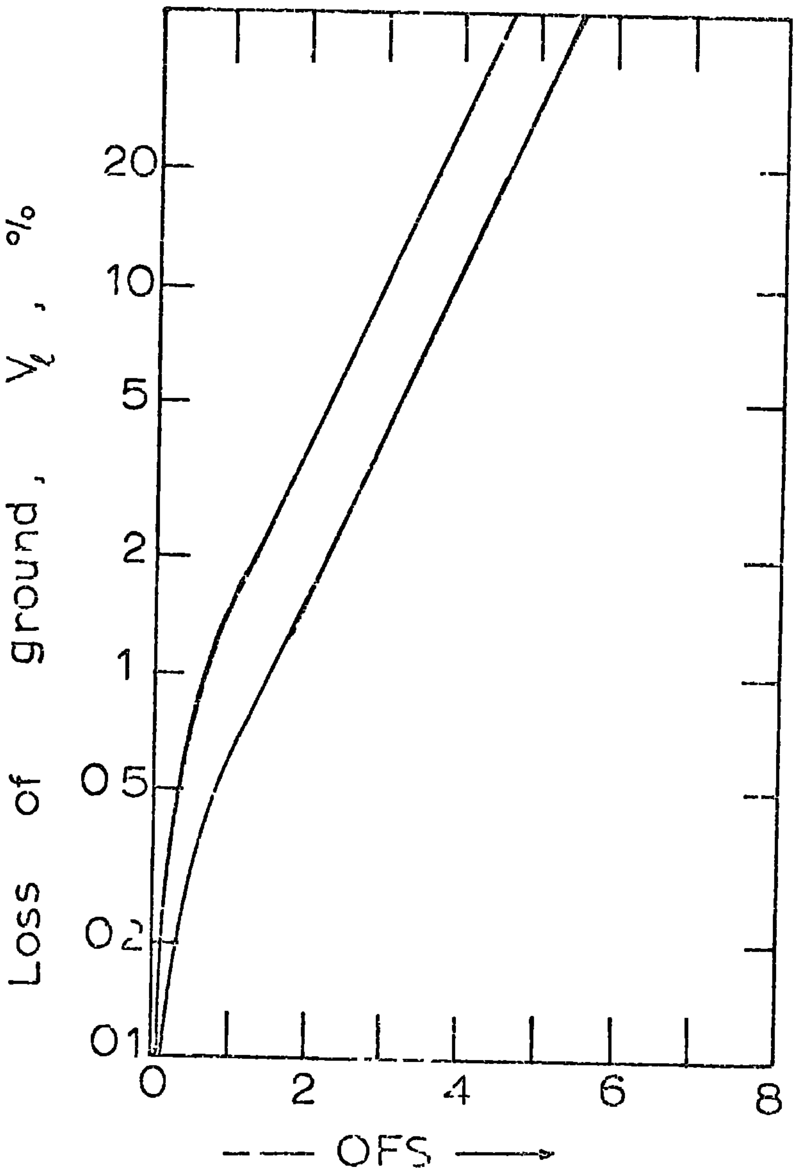

FIG 13 1 Ground loss associated with tunnelling in clay After, SCHMIDT (1969)

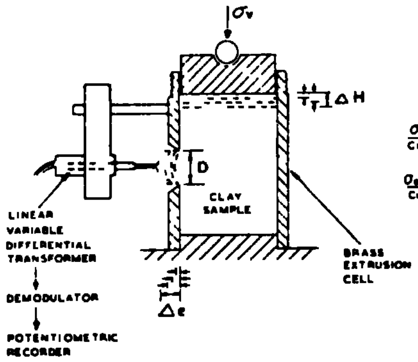

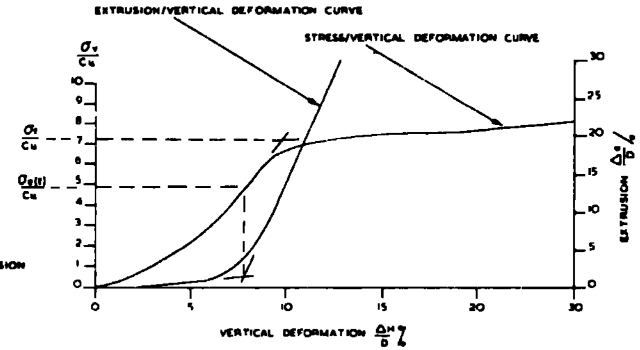

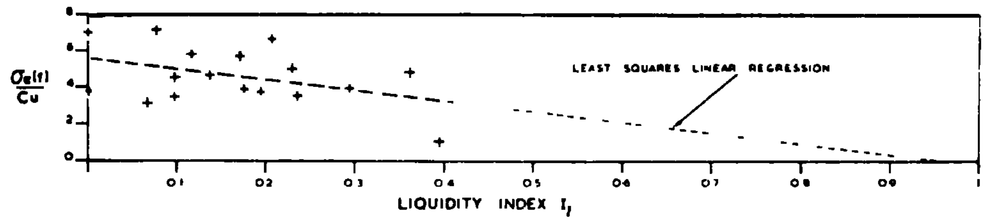

FIG. I.4.I. Above (left): Outline of extrusion cell parameters. Above (right) Typical combined vertical stress/vertical deformation and extrusion/vertical deformation curves.
Below: Variation of extrusion-based stability ratio liquidity index, for undisturbed laminated clay.
After, **ATTEWELL and BODEN (I97I).**

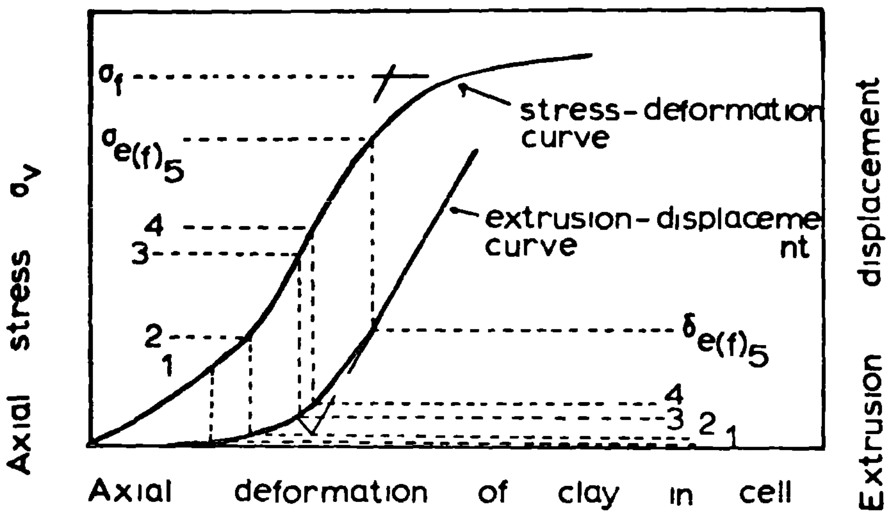

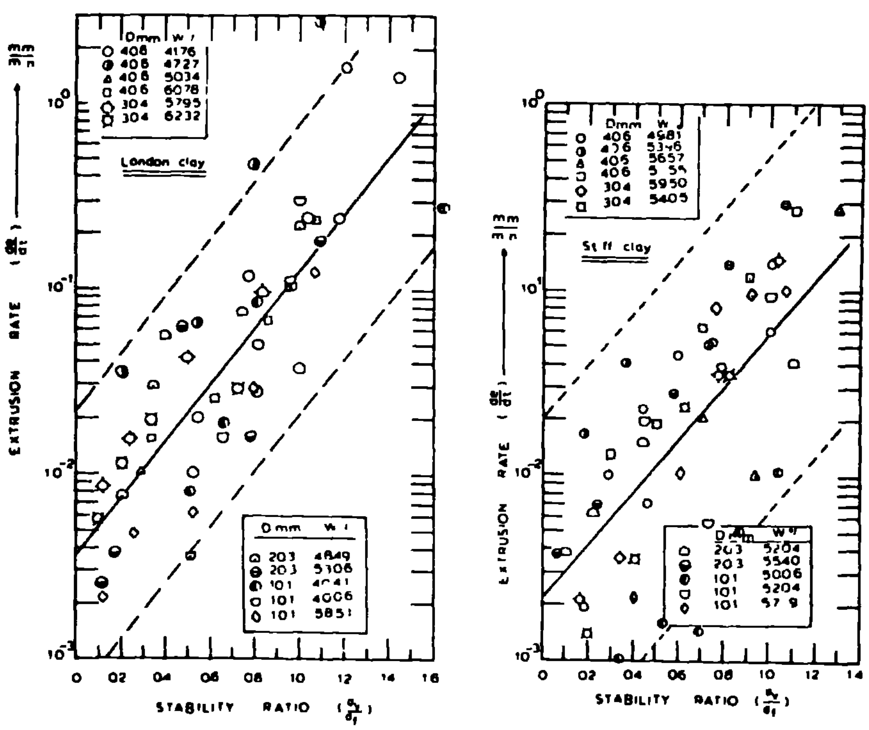

FIG. I.4.2. Above: Use of constant strain-rate extrusion tests to define critical stability ratios.

Below: Relationships between extrusion rate and stability ratio.

After, [illegible] and PARKER (1972)

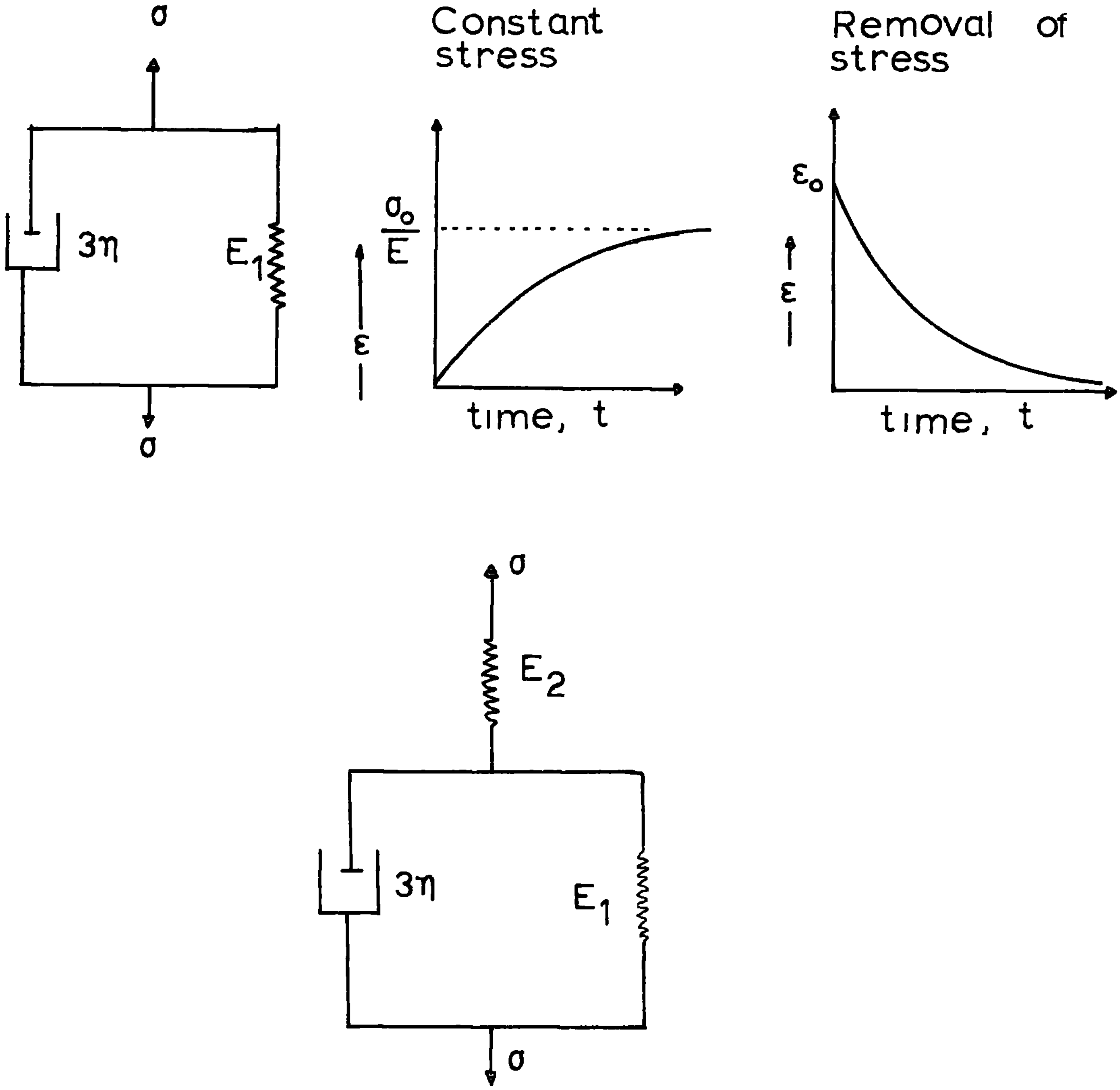

FIG. I.6.I. Characteristics of rheological models.
Above a Kelvin material, after OBERT and DUVALL (1967). Below: a modified Kelvin material.

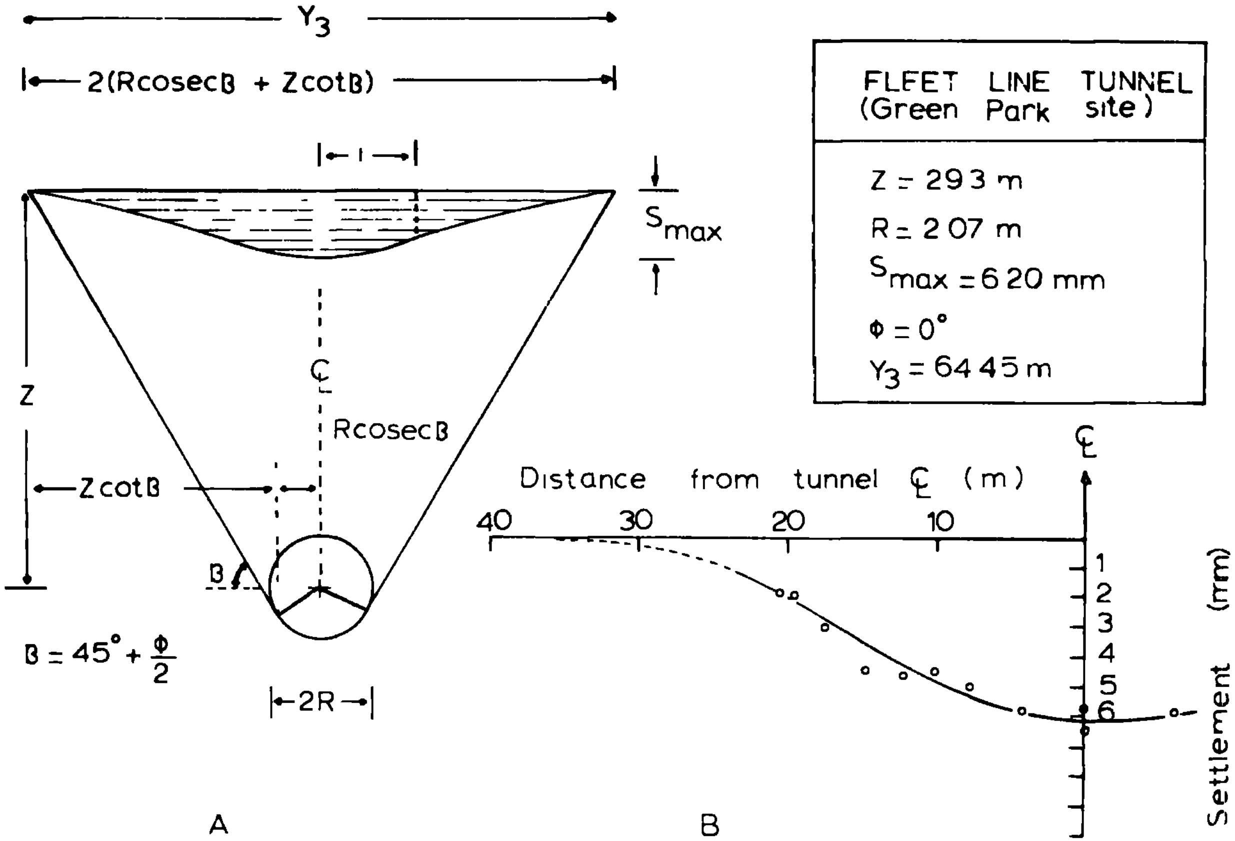

FIG 2 31 Transverse settlement profile

A SZECHY'S, (1970) model

B Actual semi-profile

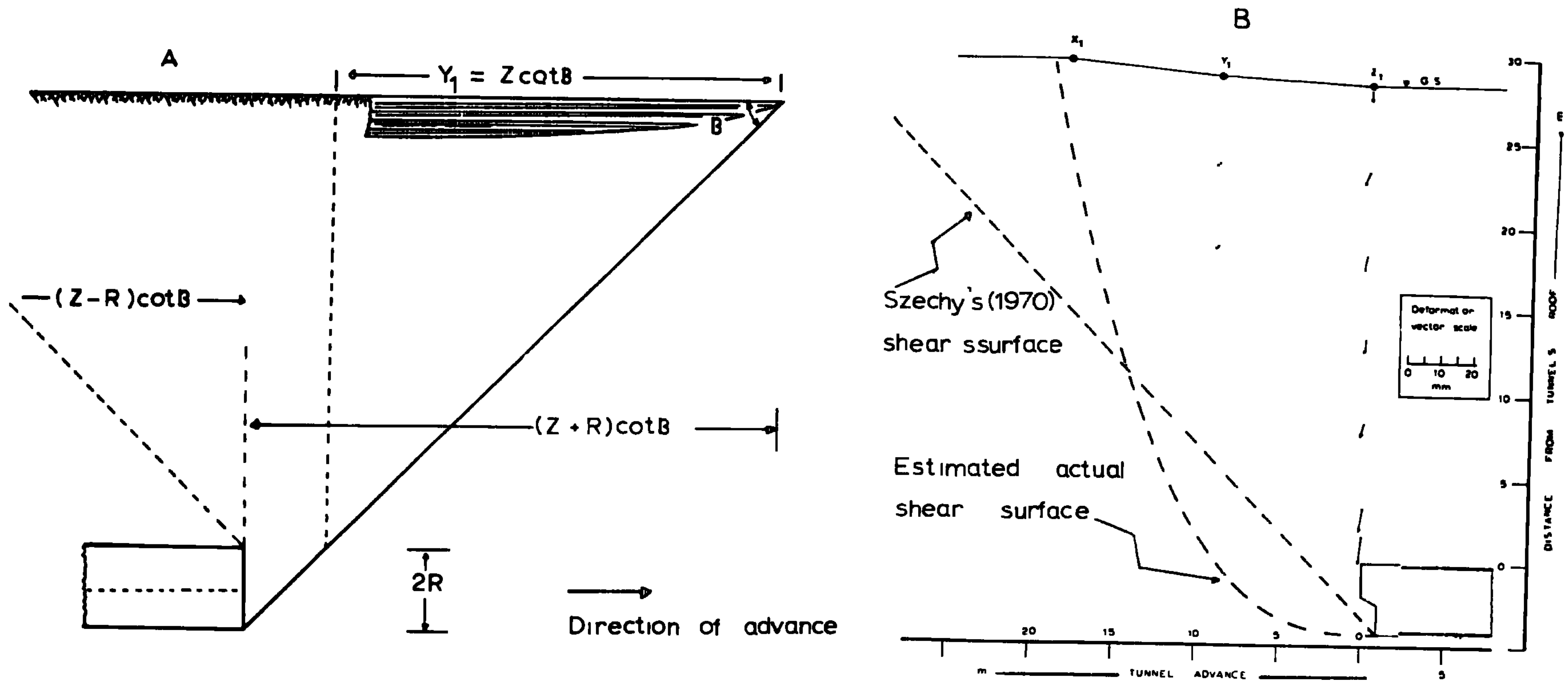

FIG 2 3 2 Centre line settlement profile

A SZÉCHY 'S, (1970) model

B Estimated actual profile

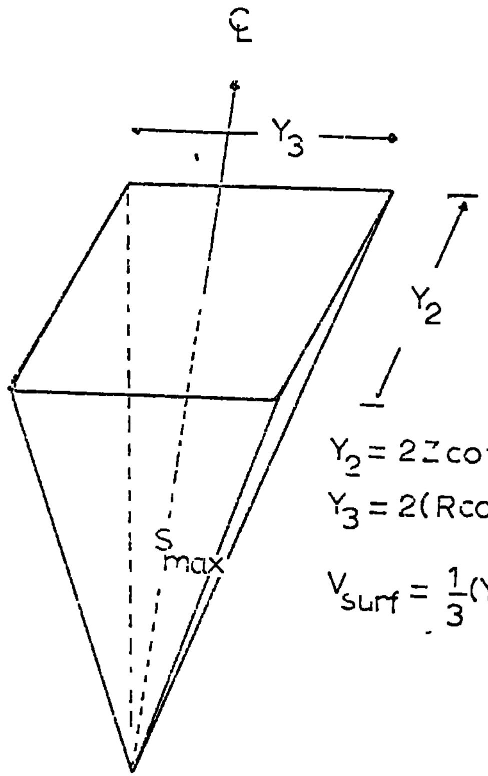

$$Y_2 = 2Z\cot B$$

$$Y_3 = 2(R\operatorname{cosec}B + Z\cot B)$$

$$V_{surf} = \frac{1}{3}(Y_2 Y_3)S_{max}$$

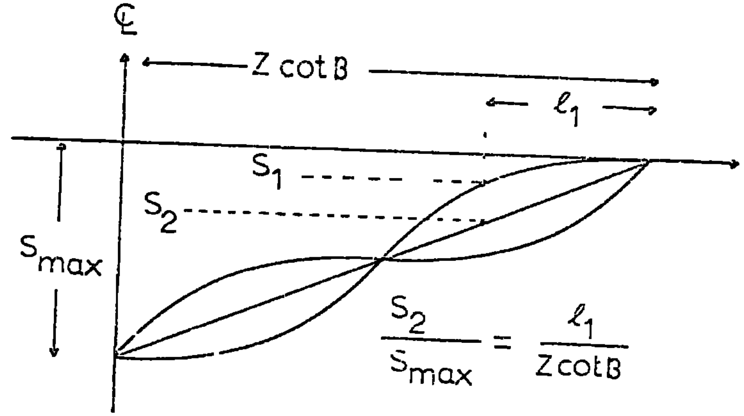

$$\frac{S_2}{S_{max}} = \frac{\ell_1}{Z\cot B}$$

$$S_2 = \frac{\ell_1 S_{max}}{Z\cot B} = dS_{max}\sin\left[\frac{2\ell_1}{Z\cot B}\right]$$

Fig. 2.3.3. Linear(left) and Harmonic (right) settlement transverse profile

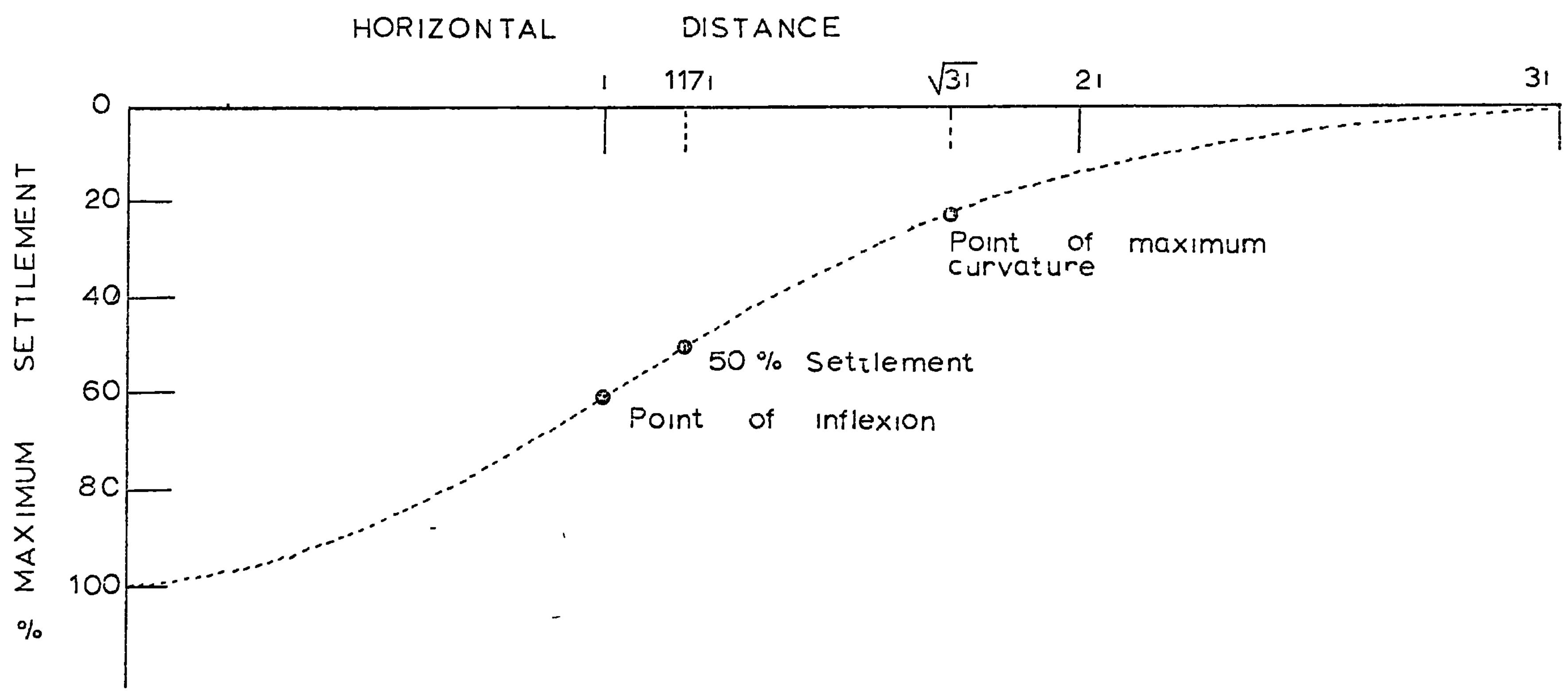

Fig. 2.3.4. Characteristics of settlement semi-profile
-After ATTEWELL and FARMER (1972).

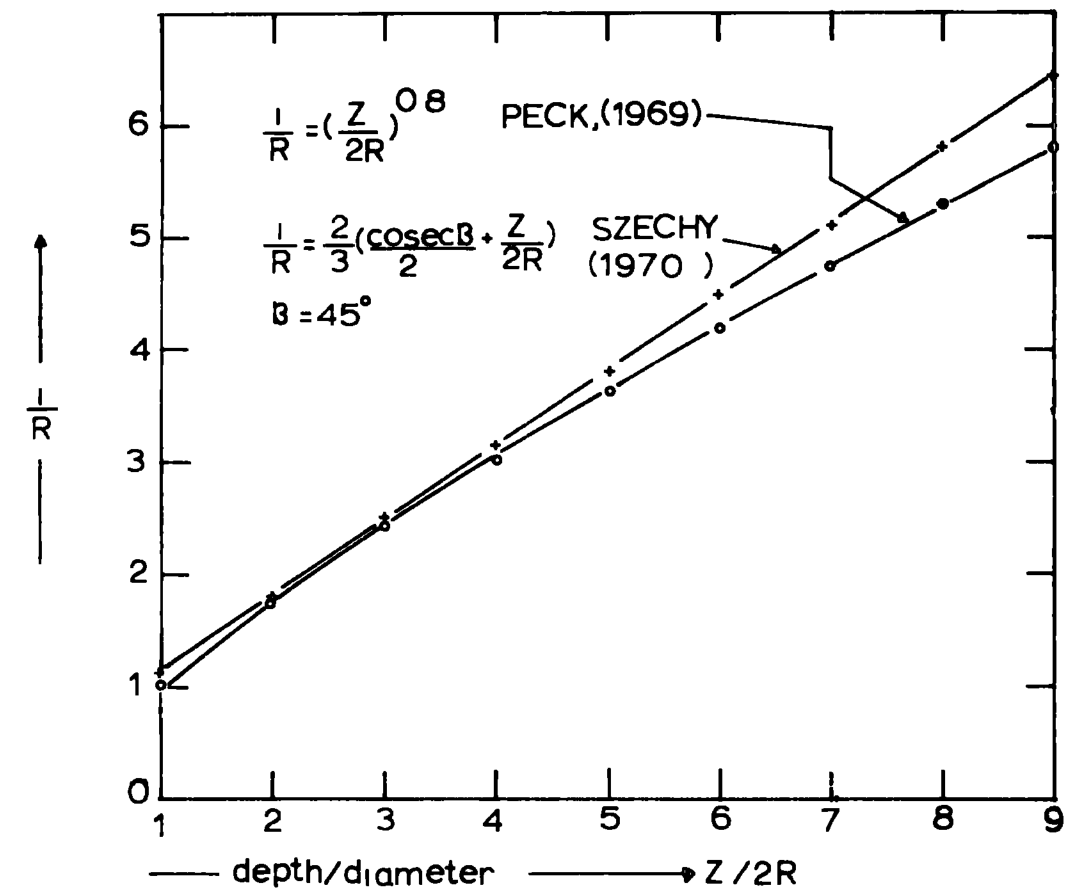

FIG 2 51 Relationship between $\frac{1}{R}$ and $\frac{Z}{2R}$

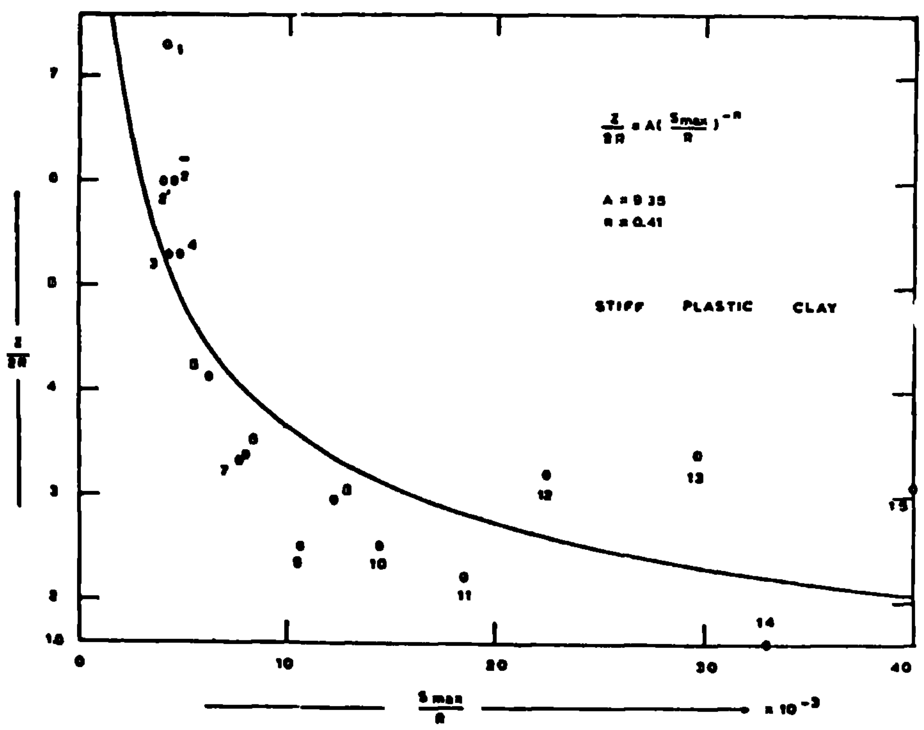

FIG. 2.5.2. Relationship between Z/2R and s_{max}/R for tunnels in stiff plastic clay.

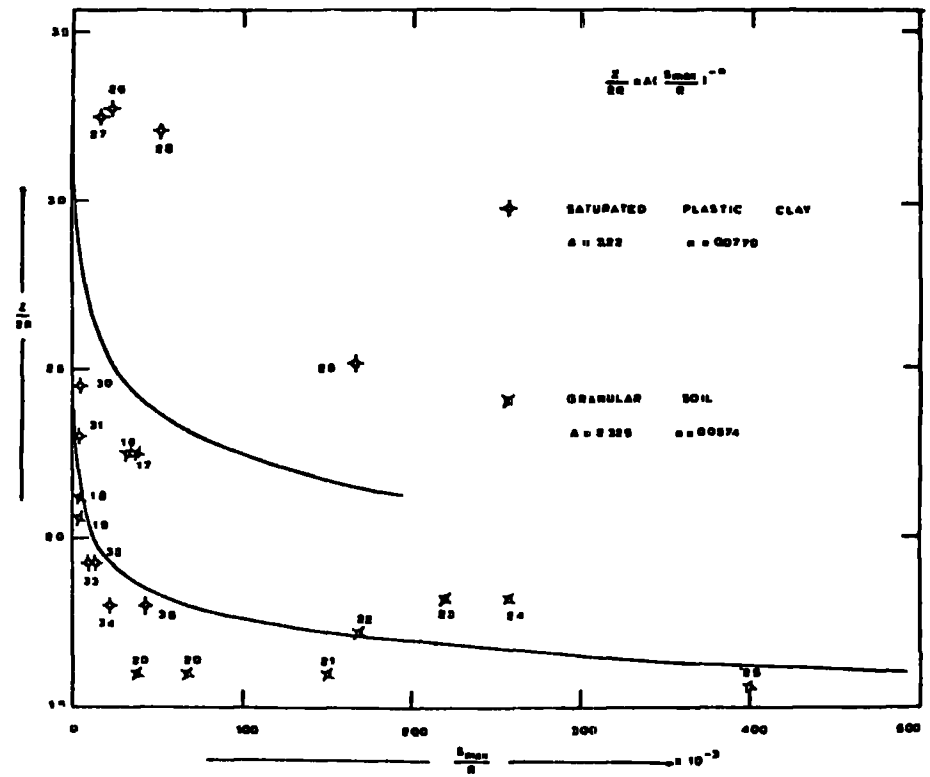

FIG. 2.5.3. Relationship between Z/2R and s_{max}/R for tunnels in saturated plastic clay and granular soil.

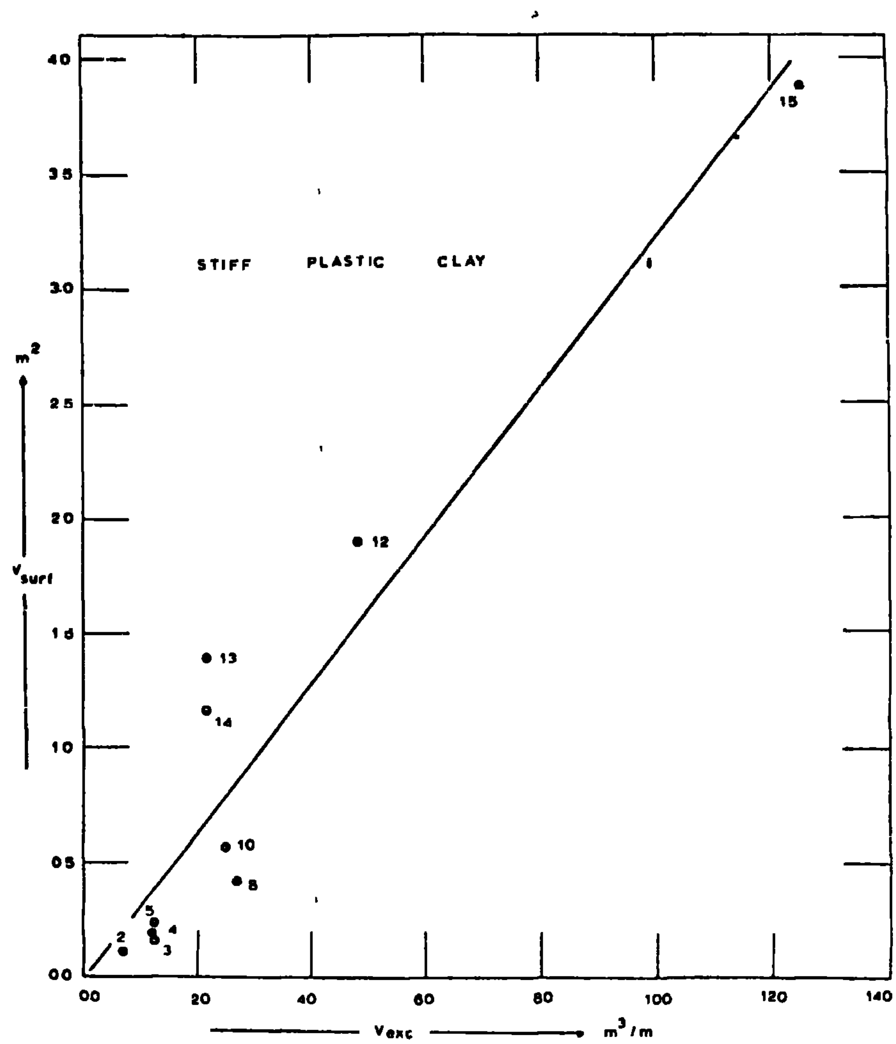

FIG. 2.5.4. Relationship between the excavated volume of soil (V_{exc}) and the volume included within the surface settlement trough, for tunnels in stiff plastic clay.

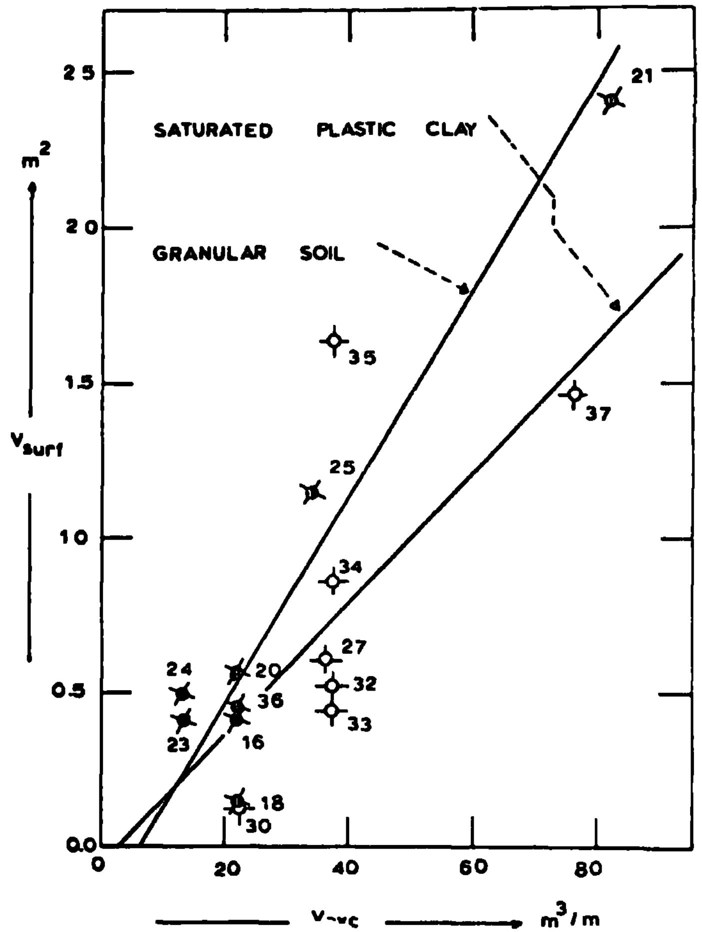

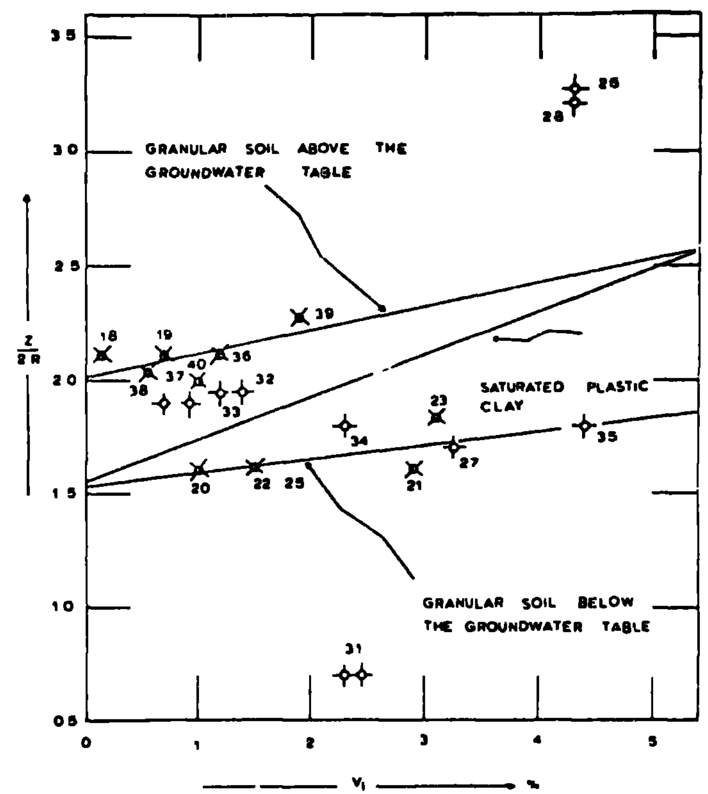

FIG 2 5 5 (left) Relationship between V_{surf}, and V_{exc} for saturated plastic clay and granular soil

FIG 2 5 6 (right) Relationship between the ratio Z/2R and the loss of ground (V_l)

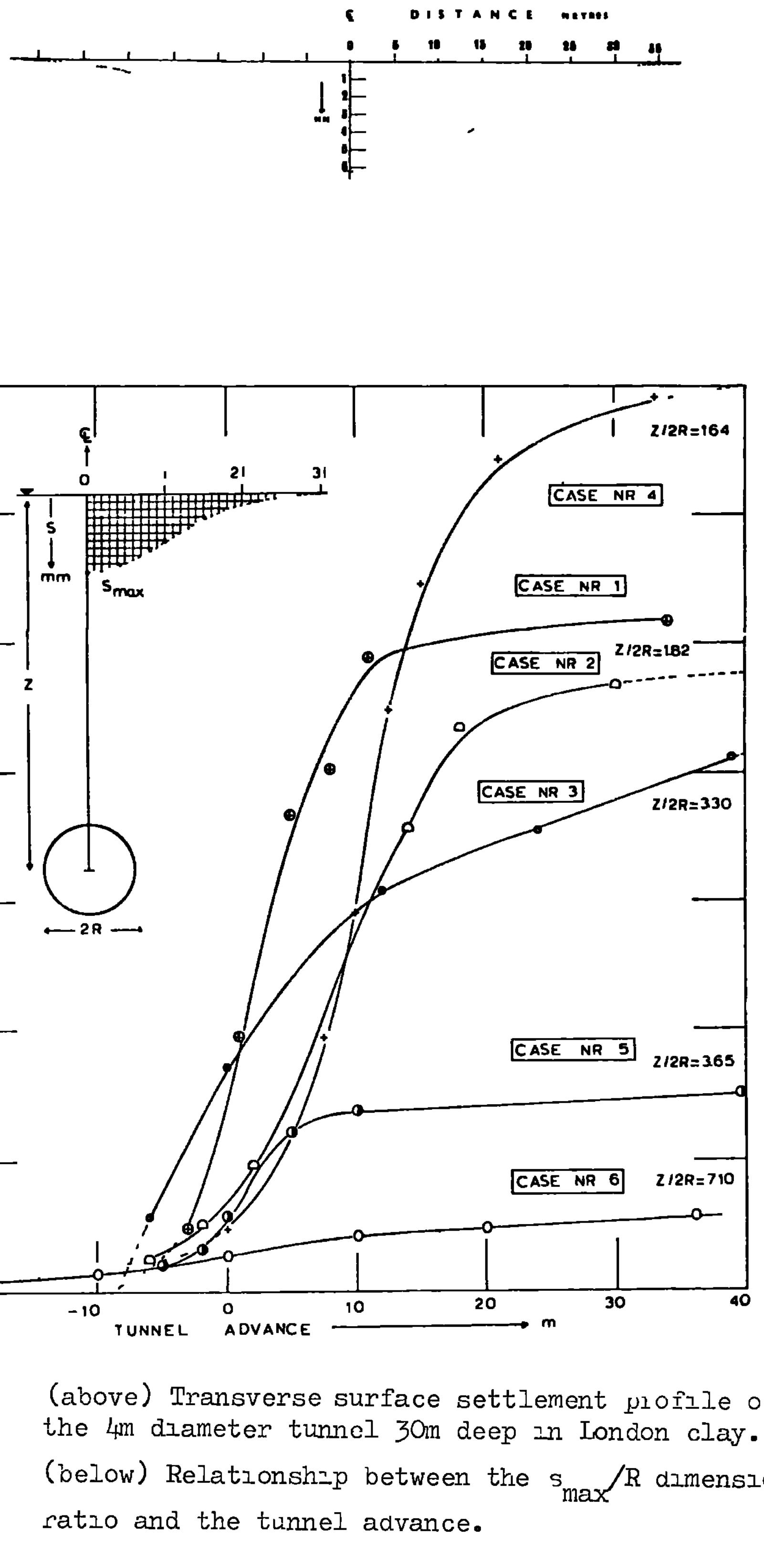

FIG. 2.6.1 a. (above) Transverse surface settlement profile of the 4m diameter tunnel 30m deep in London clay.

b. (below) Relationship between the s_{max}/R dimensionless ratio and the tunnel advance.

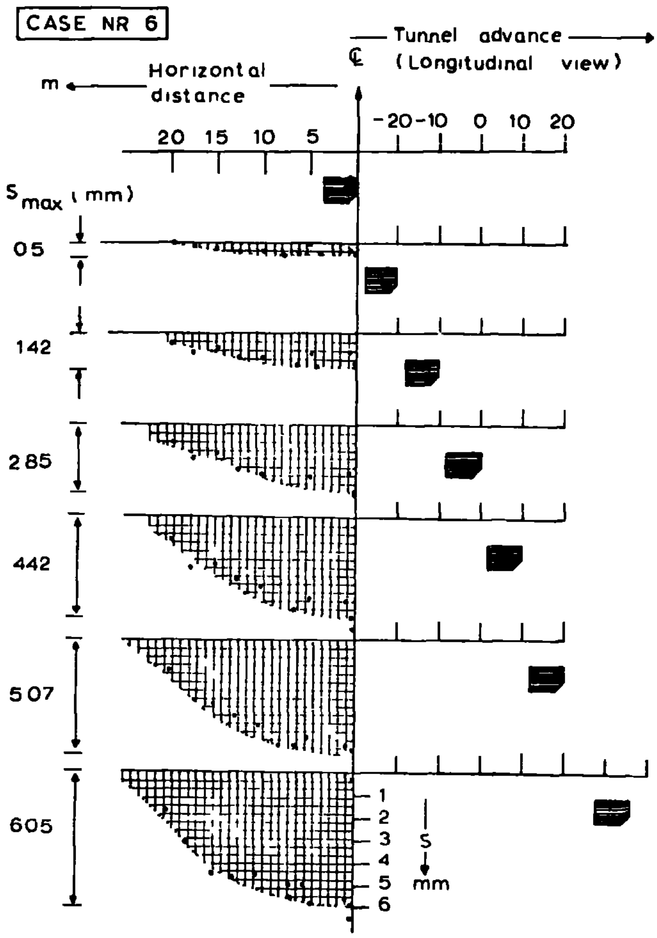

FIG.2.6 2

The development of the surface settlement transverse profile as a function of tunnel advance.

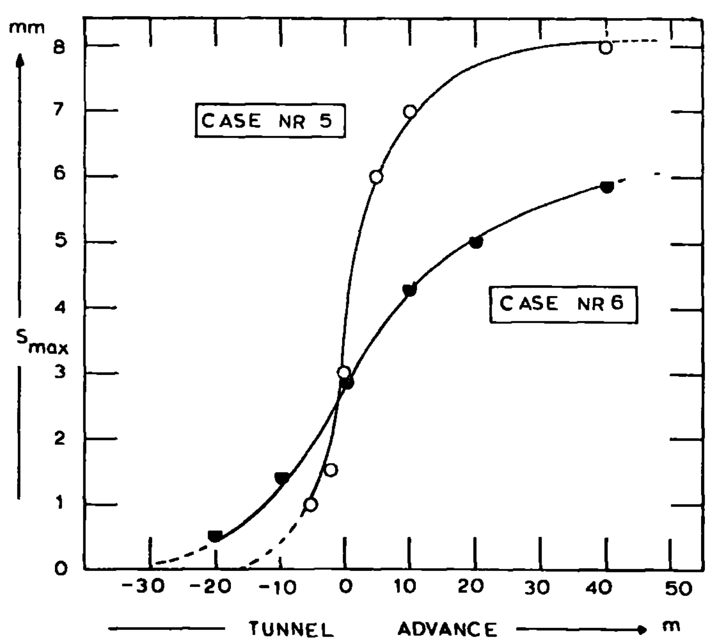

FIG. 2.6 3.

Relationship between the s_{max} (max. settlement) and the tunnel advance.

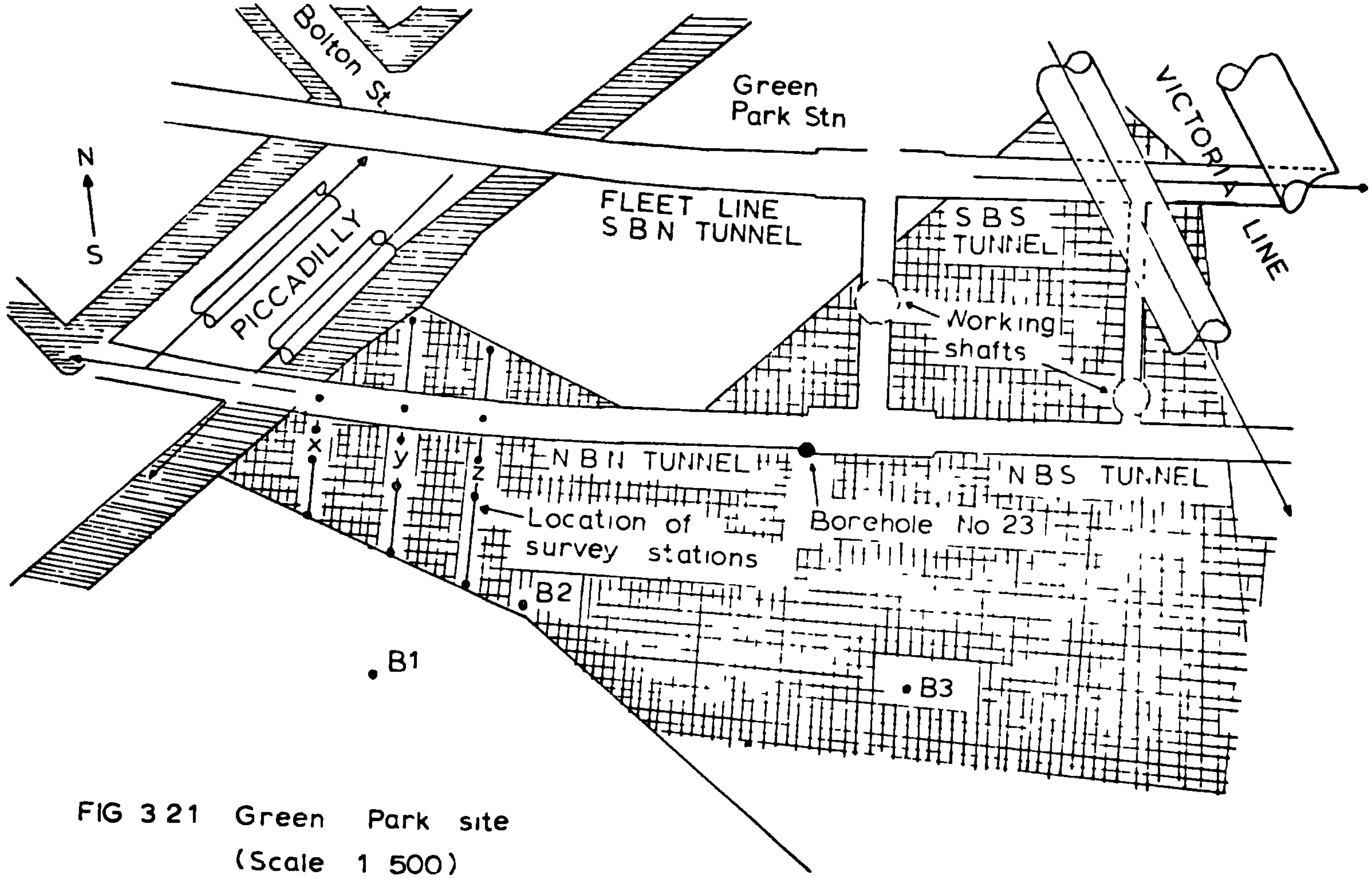

FIG 3 21 Green Park site
(Scale 1 500)
(Redrawn from ATTEWELL and FARMER (1972)

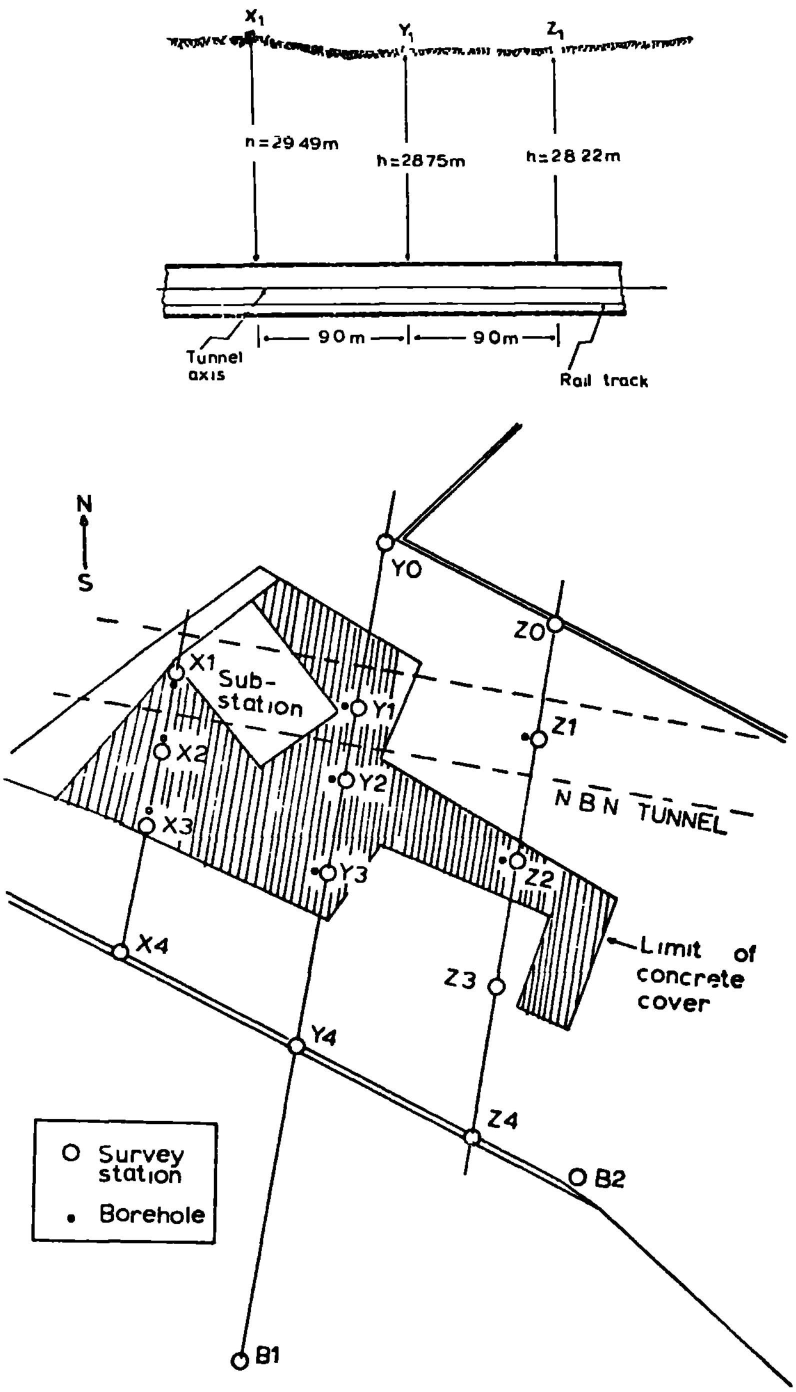

FIG 3 2 2 Above Longitudinal view of borehole arrangement (Not to scale)
Below Location of boreholes and survey stations (Scale 1 200)

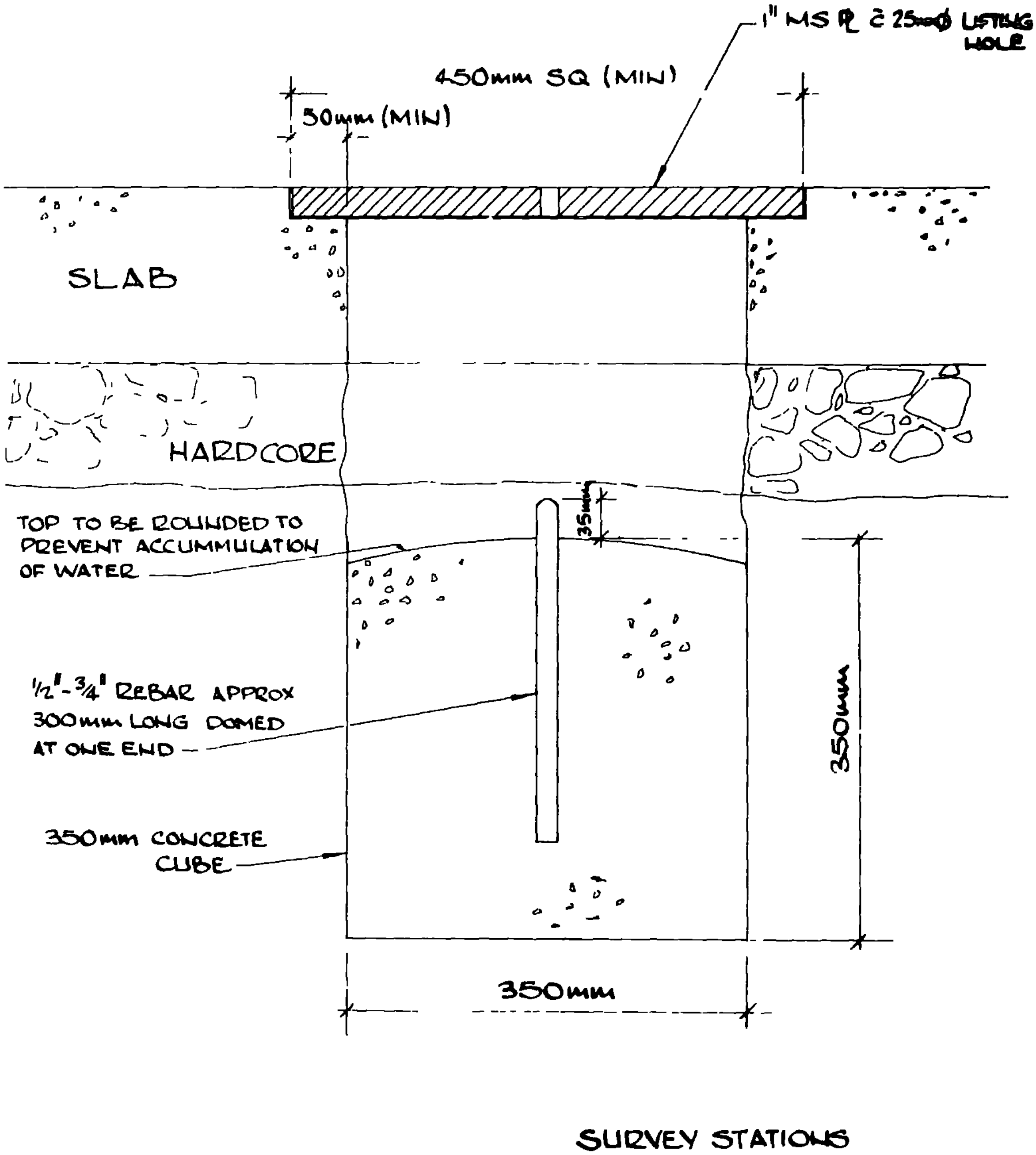

Fig. 3 3.1 a Design of survey stations.

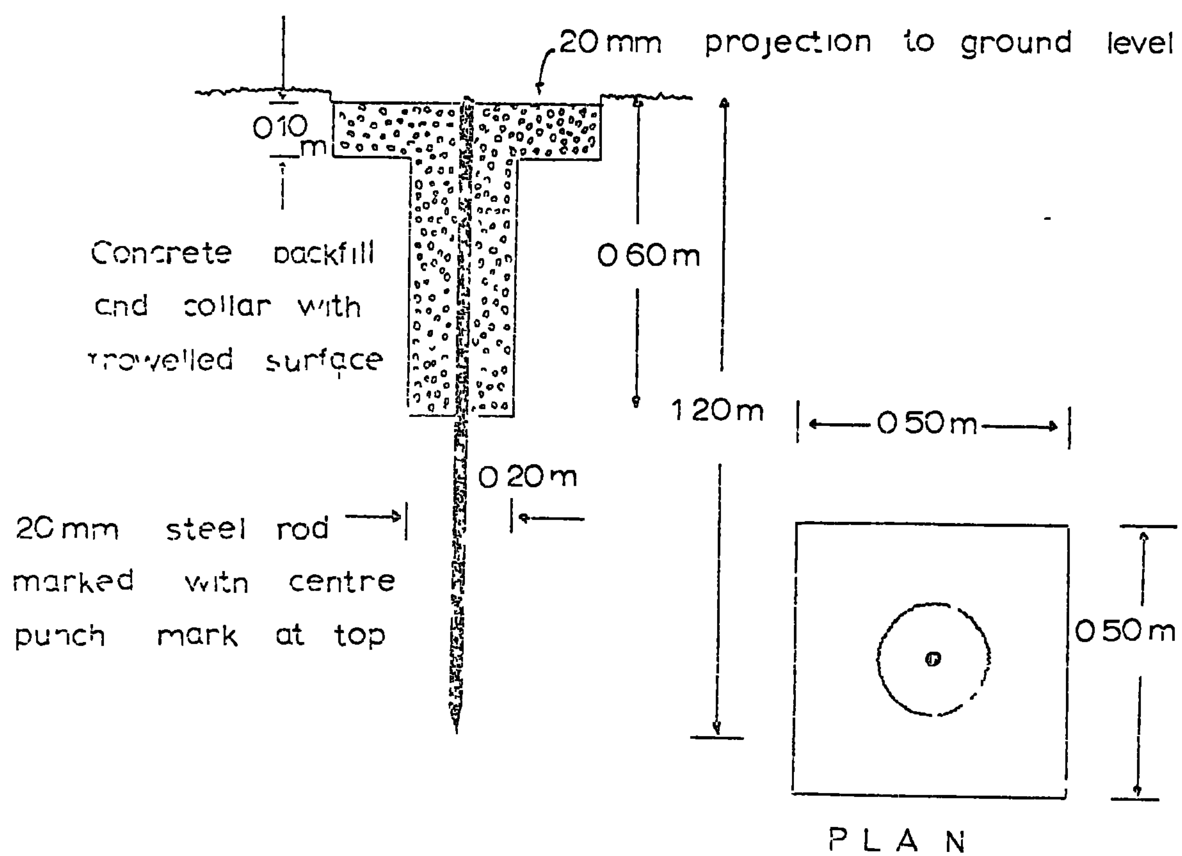

Fig. 3.3.1.b Design of the temporary ground survey station.

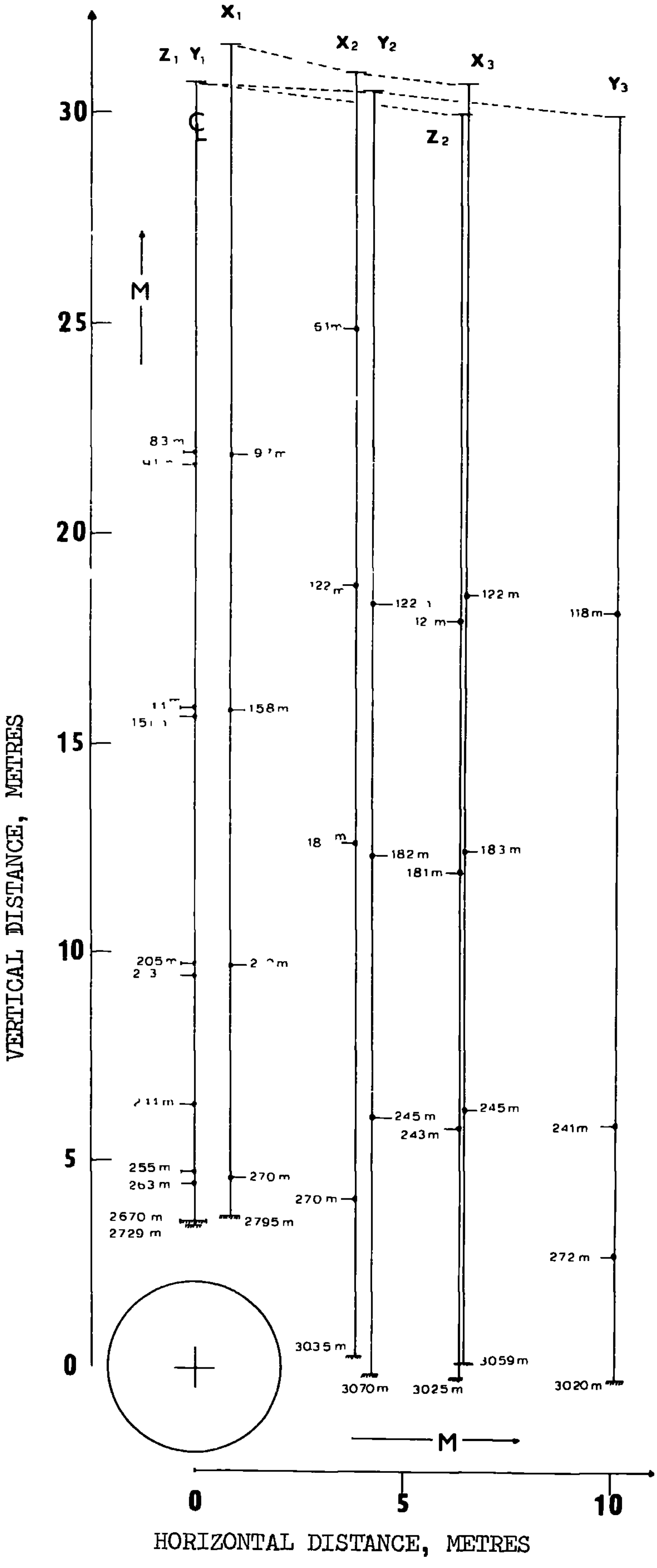

FIG. 3.3.2. Scaled layout (cross-section) of the boreholes and inclinometer access tubes with the exact position of each magnetic ring as initially located on each tube.

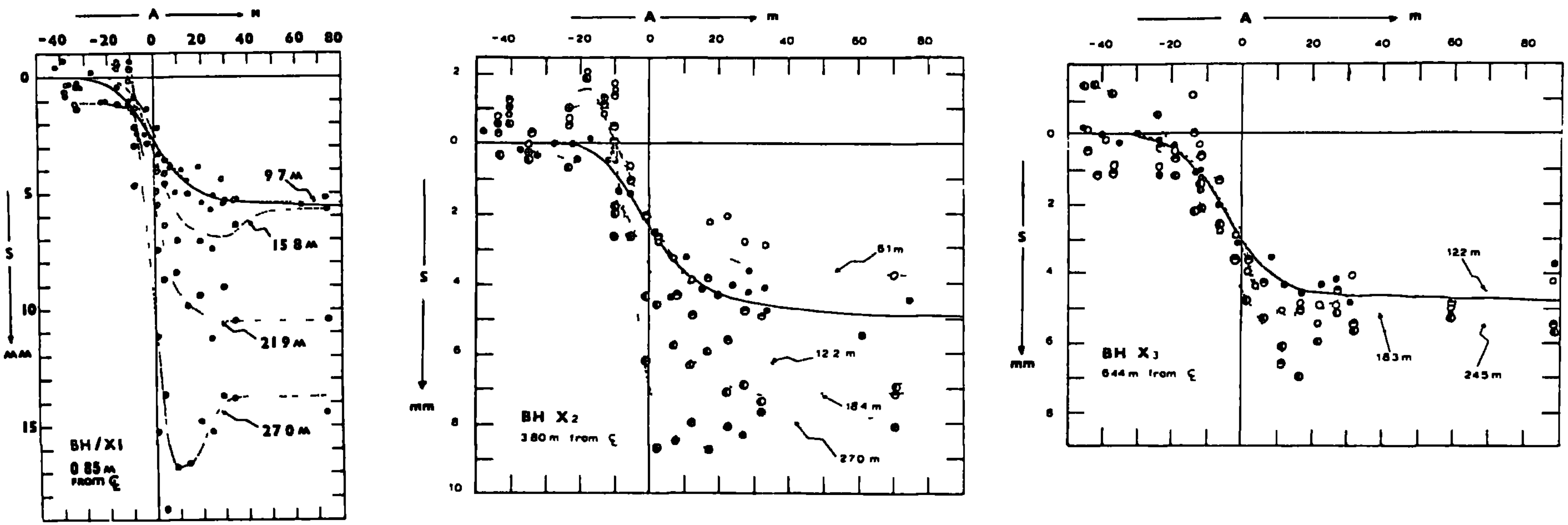

FIG 4.2.1 Vertical settlement profile development in the vertical plane passing through the tunnel center line and at different depths in boreholes X1, X2, X3. The abscissa (A) represents the distance in metres between the borehole and the plane of the tunnel face, in a direction parallel to the tunnel center line. The ordinate (s) represents vertical settlement in millimeters. After, ATTEWELL and FARMER (1972)

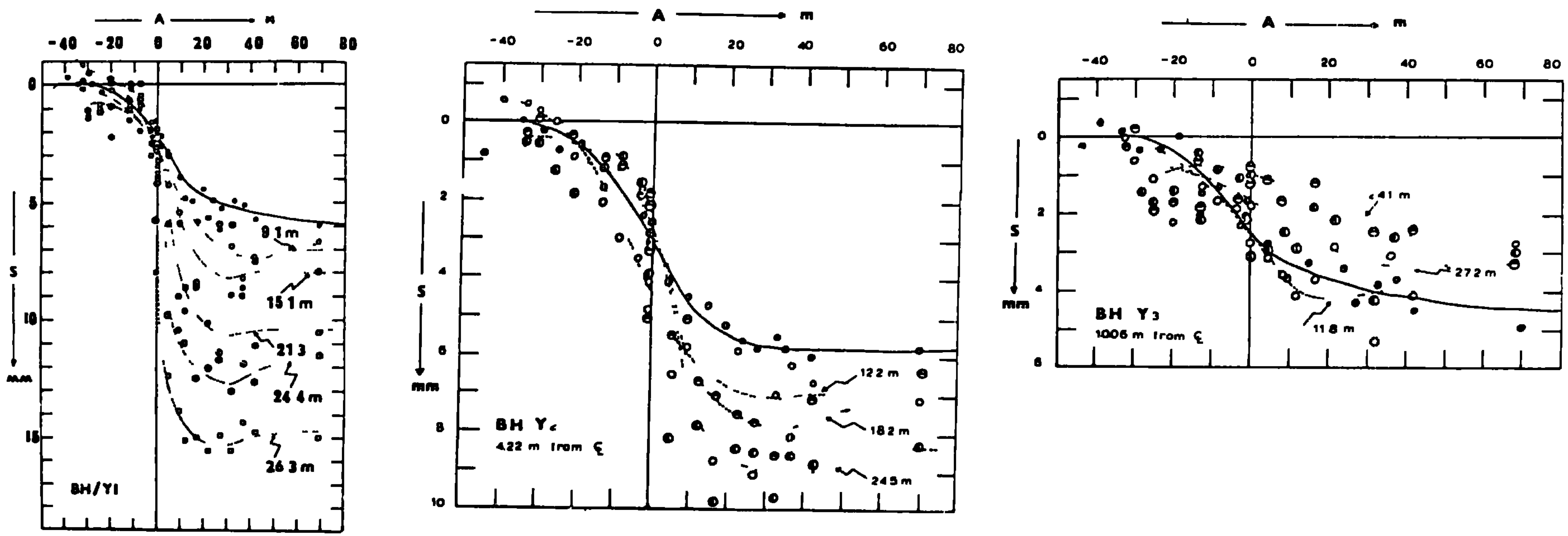

FIG 4.2.2 Vertical settlement profile development in the vertical plane passing through the tunnel center line and at different depths in boreholes Y1, Y2, Y3
After, ATTEWELL and FARMER (1972)

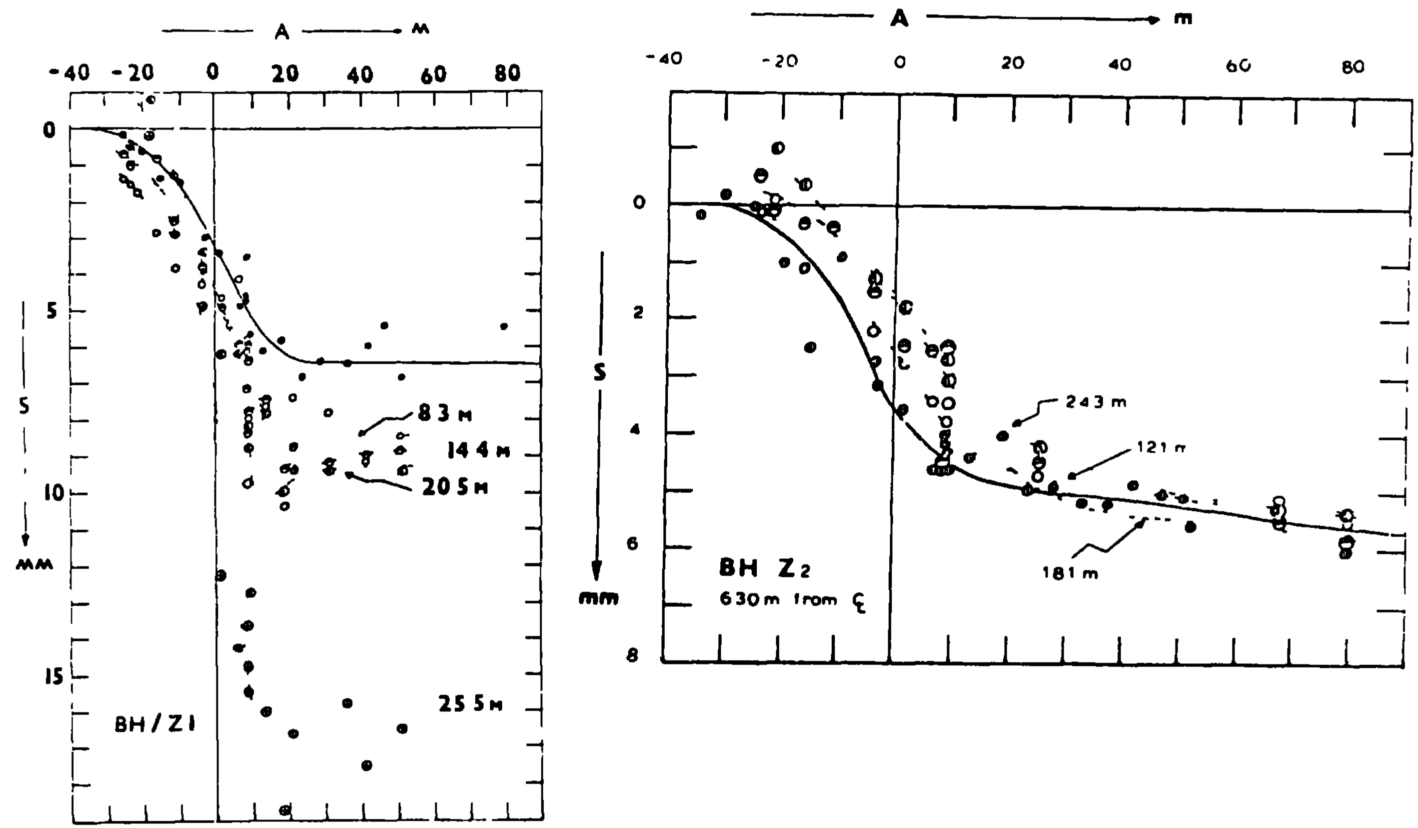

FIG 4 2 3 Vertical settlement profile development in the vertical plane passing through the tunnel center line and at different depths in boreholes Z1, Z2
After ATTEWELL and FARMER (1972)

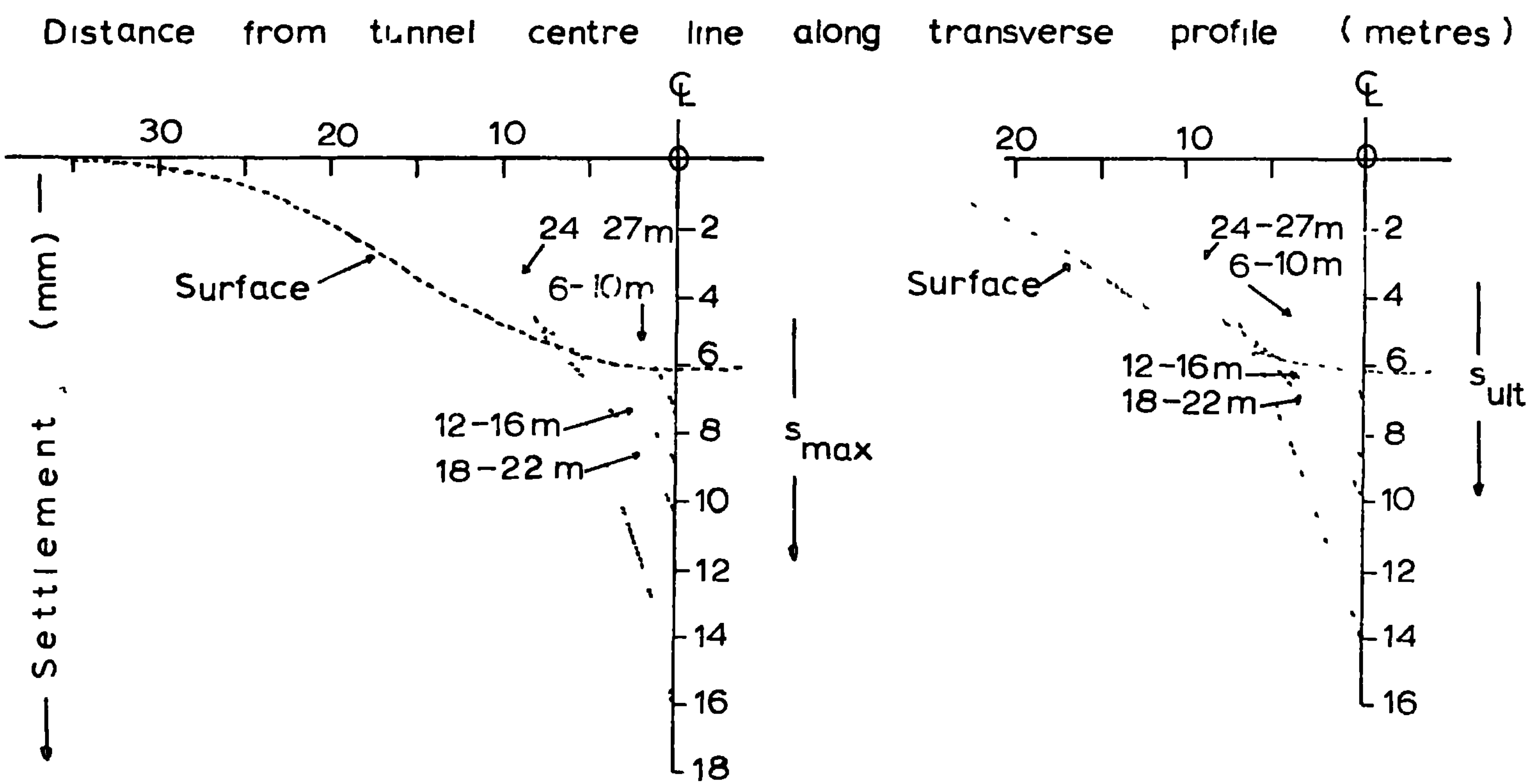

FIG 4.24 Transverse settlement profiles for different subsurface depth ranges After, ATTEWELL and FARMER (1972)

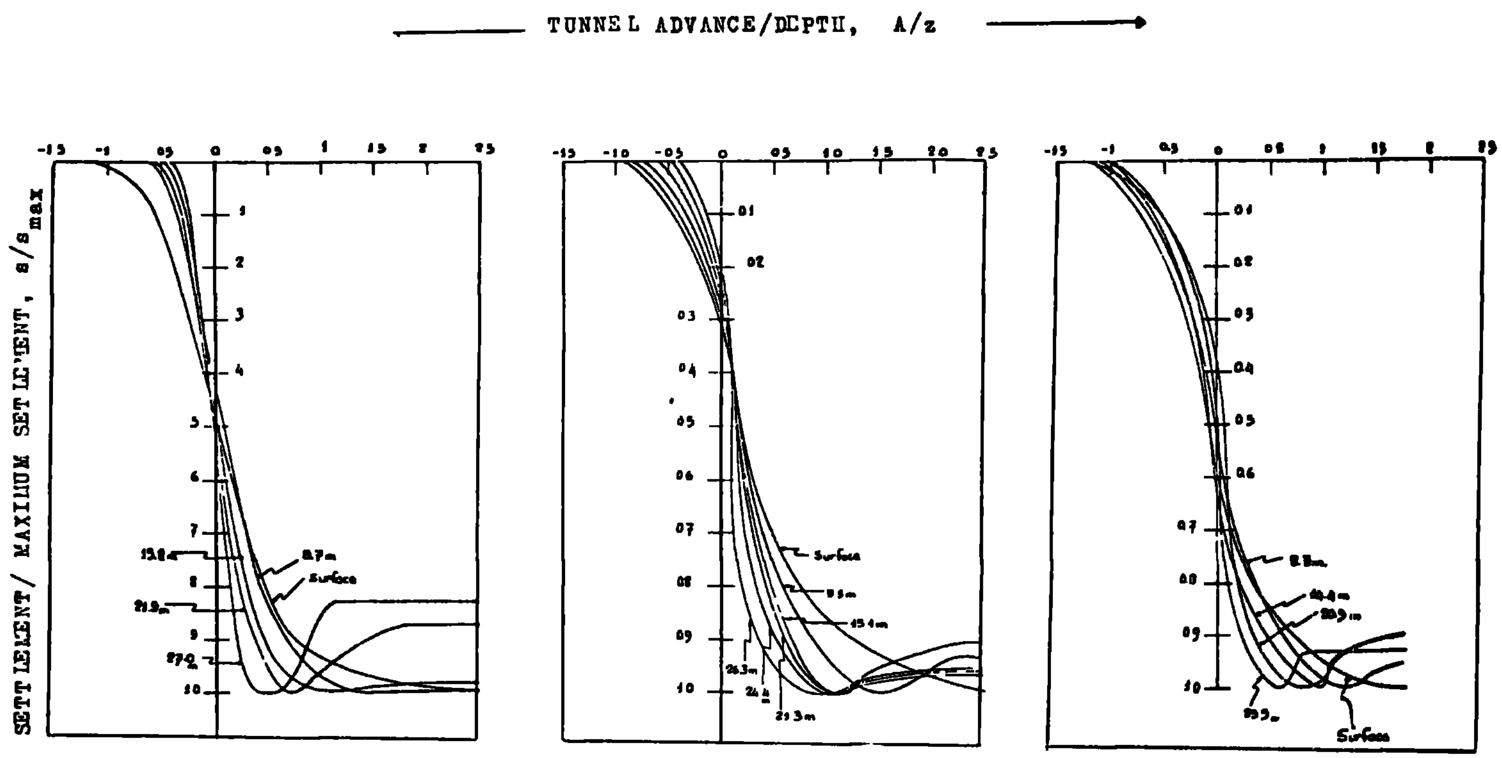

FIG. 4.2.5. Normalised settlement development curves. After, ATTEWELL and FARMER (1972)

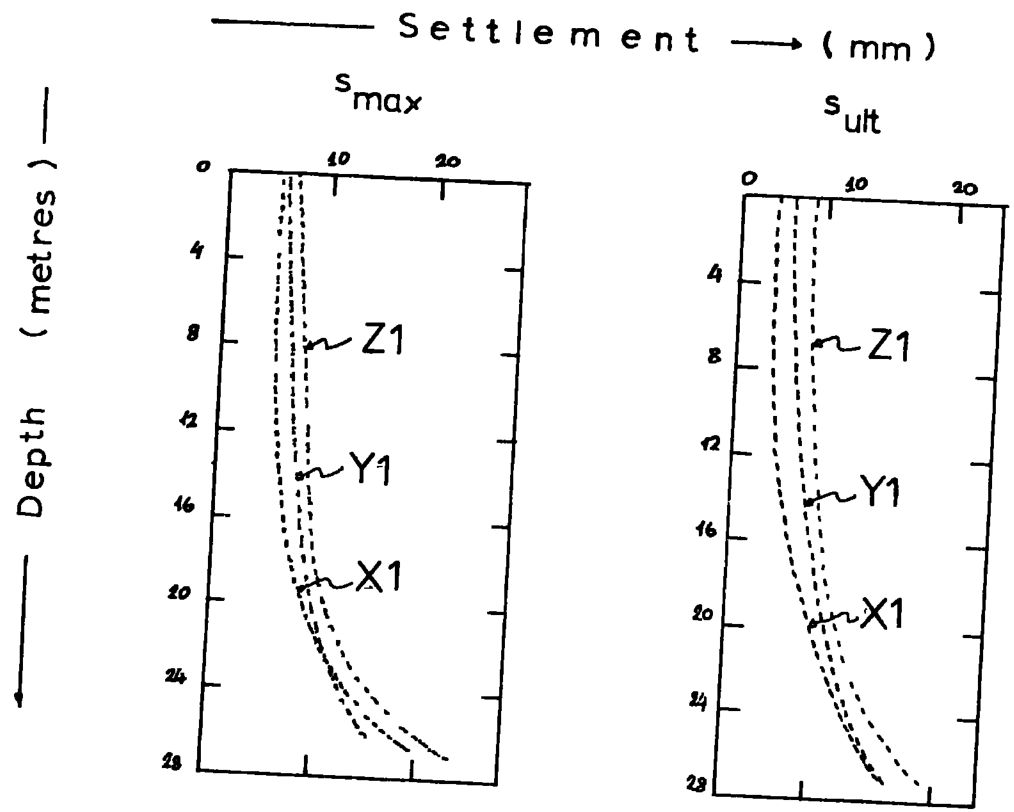

FIG 4 2 6 Development of maximum (s_{max}) and ultimate (s_{ult}) settlement with depth

After, ATTEWELL and FARMER, (1972)

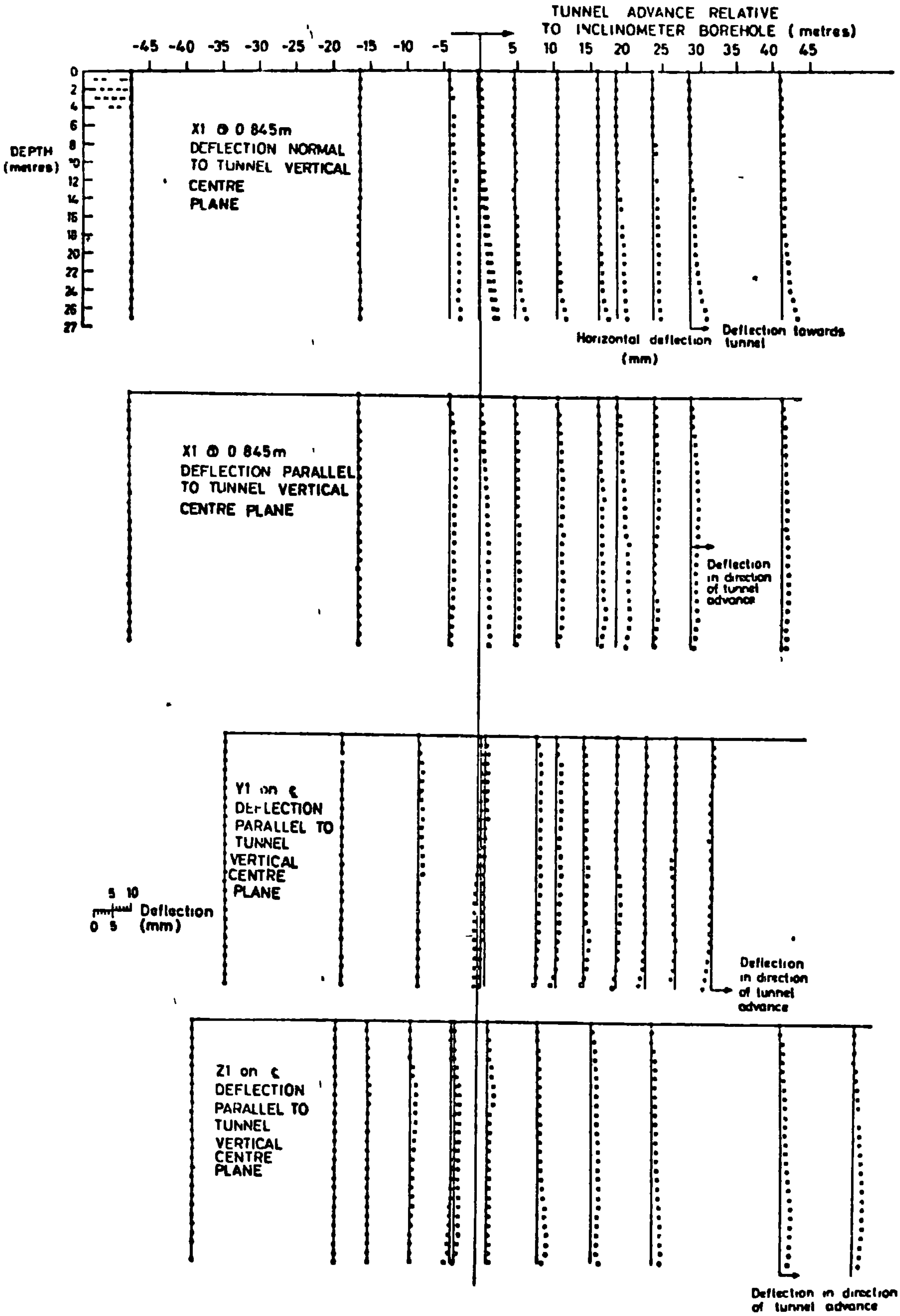

FIG. 4.3.1. Horizontal displacement profiles. Boreholes X1, Y1, Z1. After ATTEWELL and FARMER (1972).

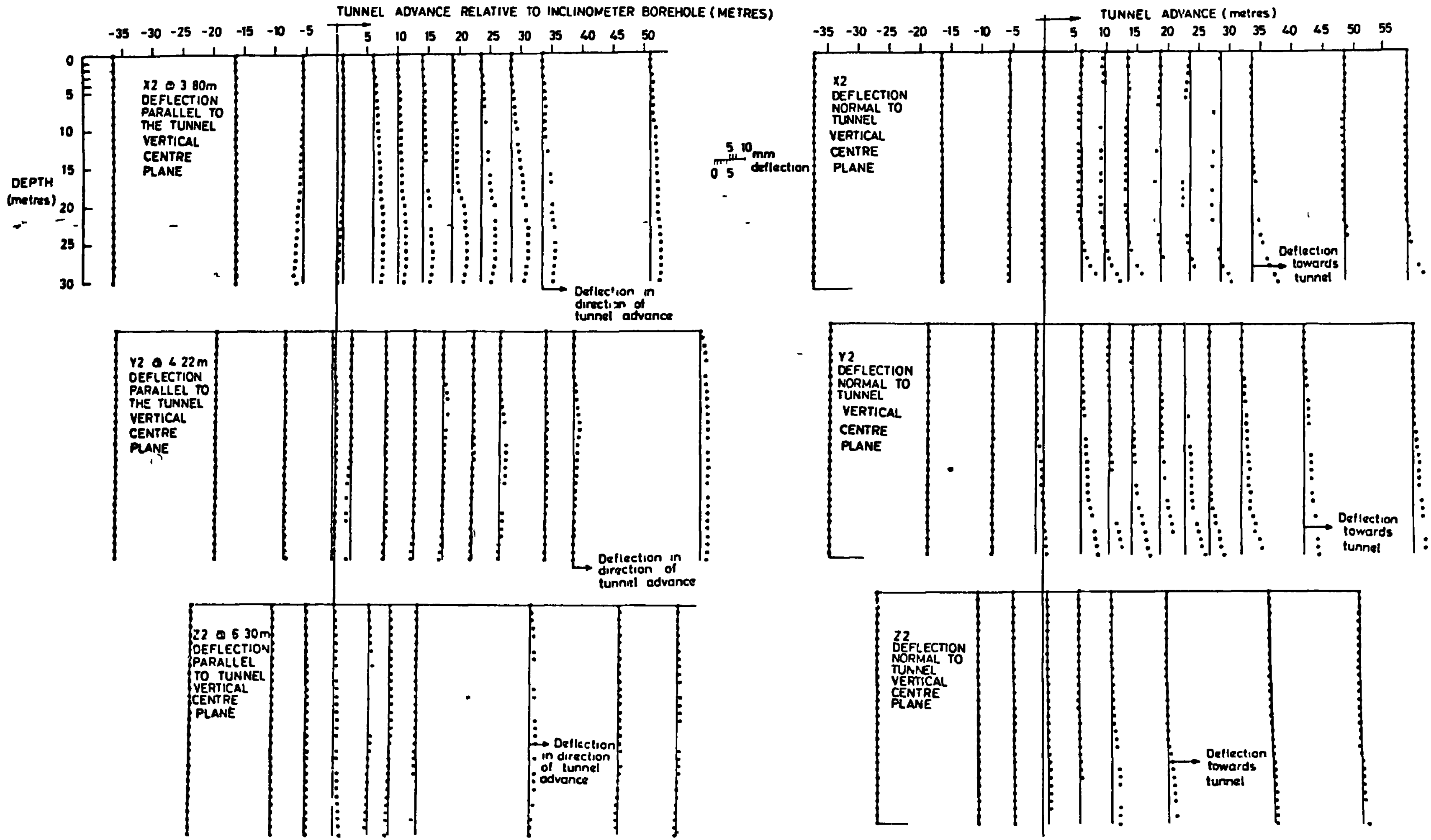

FIG. 4.3.2. Horizontal displacement profiles. Borehole X1, Y1, Z1.
After ATTEWELL and FARMER (1972).

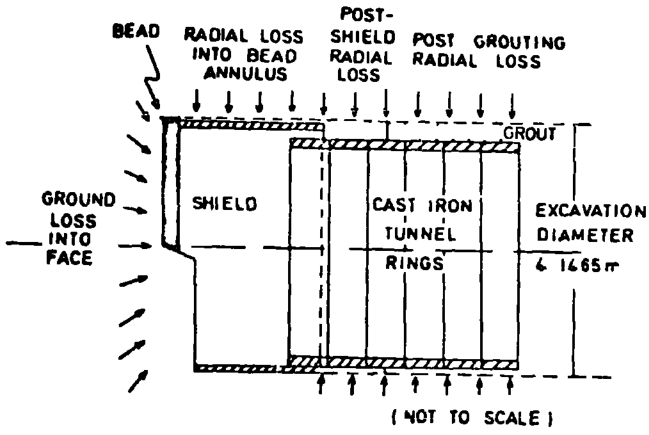

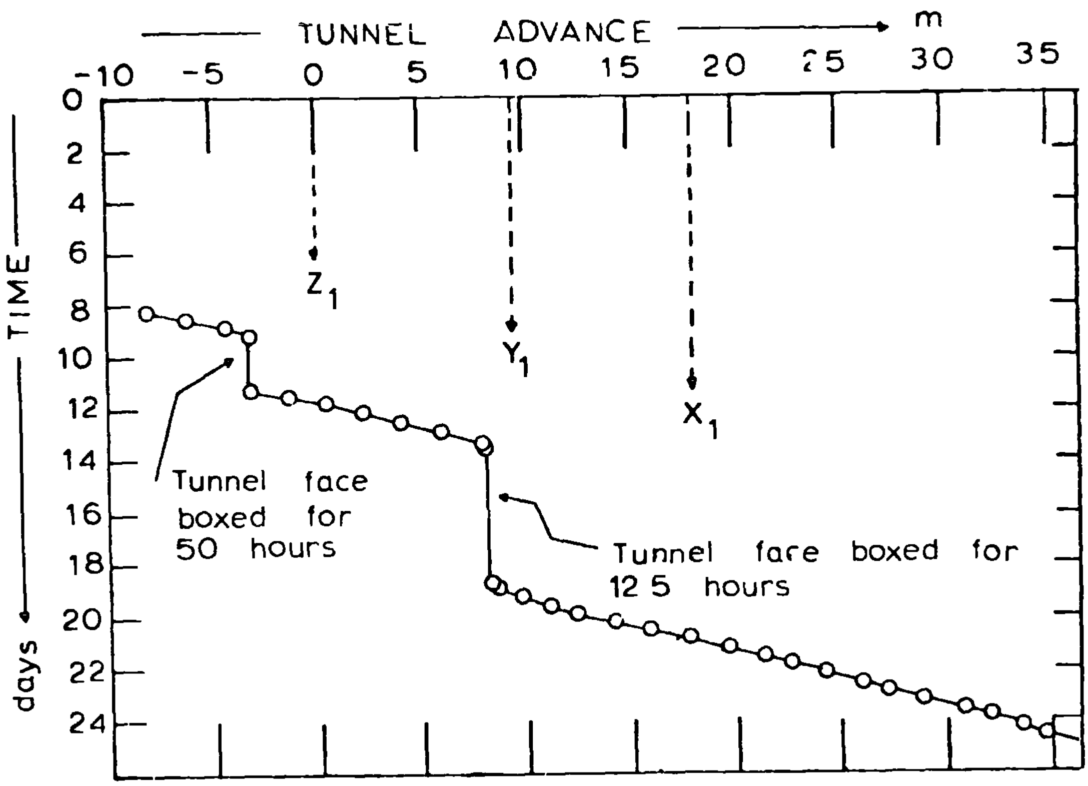

FIG 4 4 1 Ground-loss areas around a shield-driven tunnel

FIG 4 4 2 (Below) Record of tunnel progress

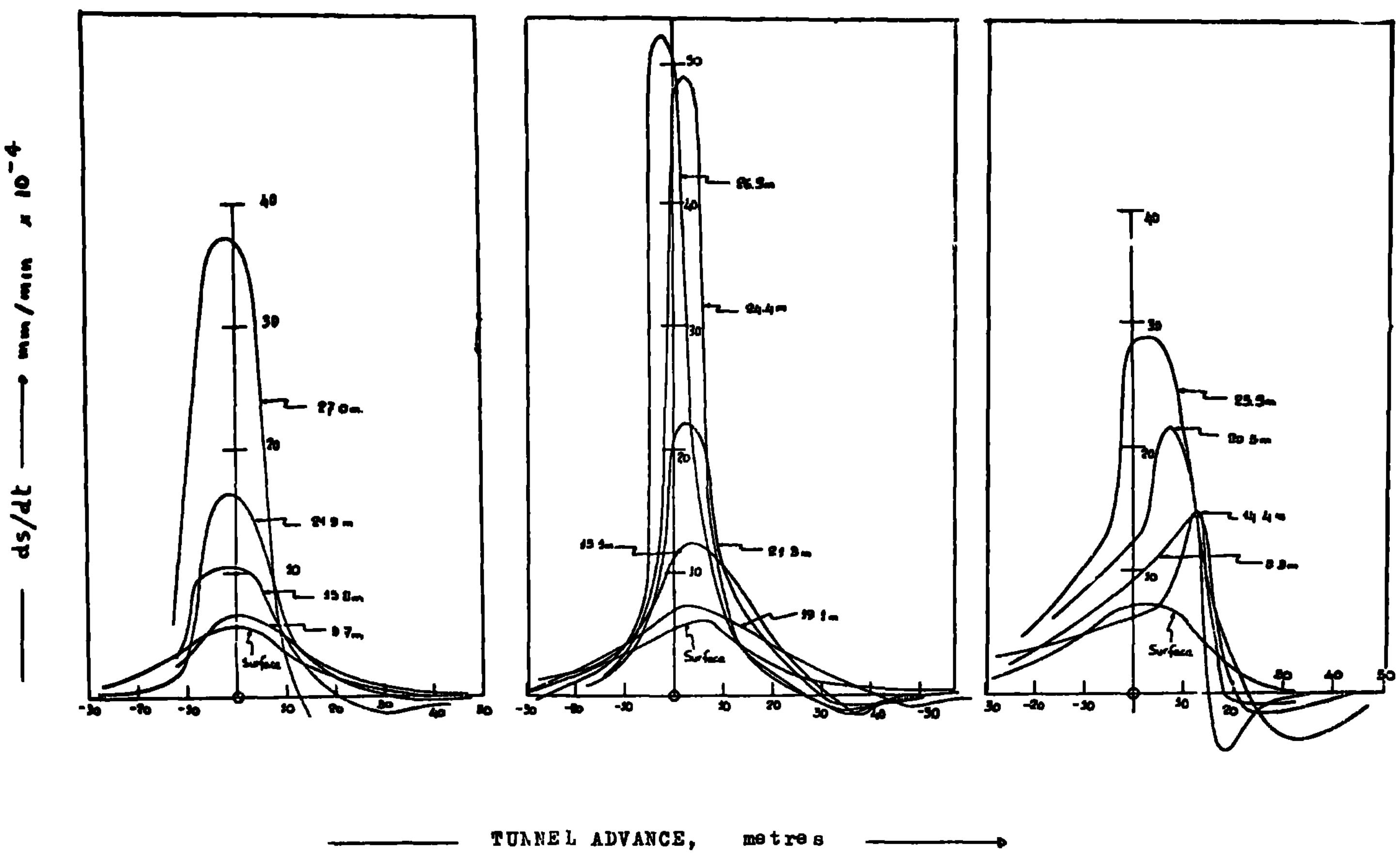

FIG. 4.4.3. Relationship between the rate of settlement (ds/dt) and the tunnel advance (A), for boreholes XI (Left), YI (Medium) and ZI (Right). After, ATTEWELL and FARMER (1972)

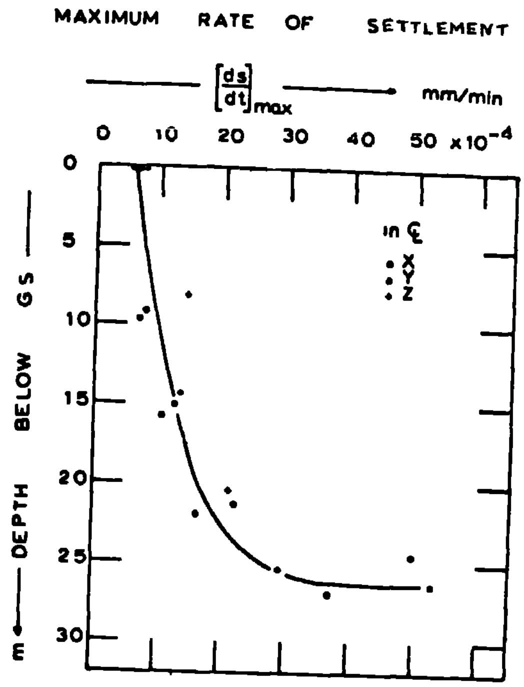

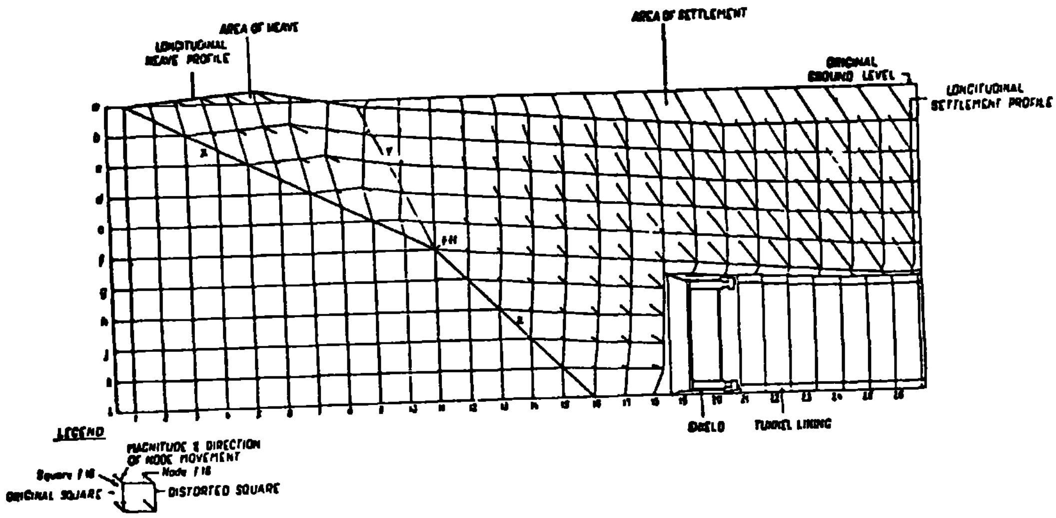

FIG 4.4.4 (Above) The maximum rate of settlement as a function of depth for boreholes X1, Y1, Z1

FIG 4.4.5 (Below) Schematic concept (qualitative) of ground movement ahead of a tunnell shield
After, BARTLETT and BUBBERS, (1970)

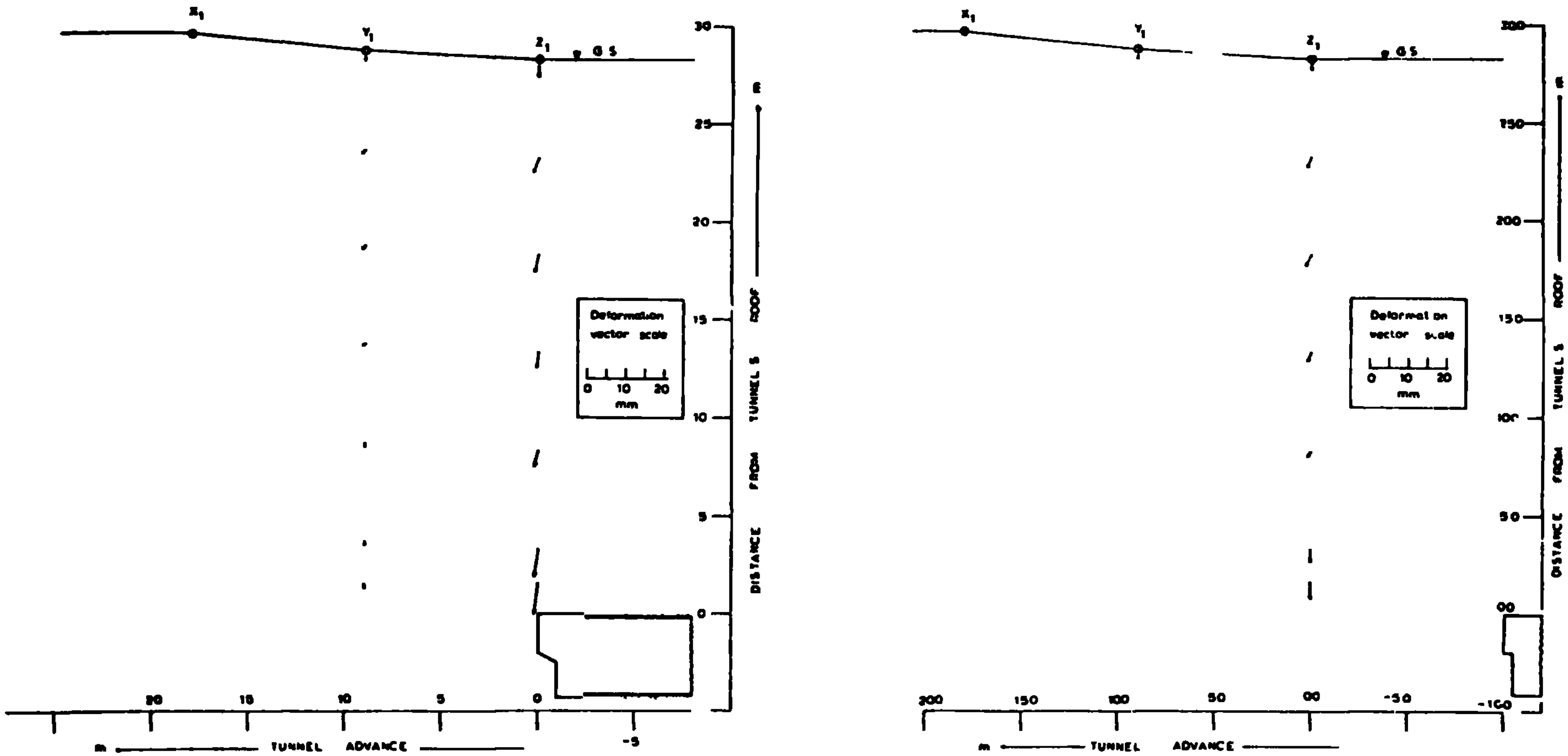

FIG. 4.4.6. Ground deformation in a vertical plane along the tunnel axis.
Tunnel face 10m behind Z1 (right hand side) and at Z1 (left hand side).

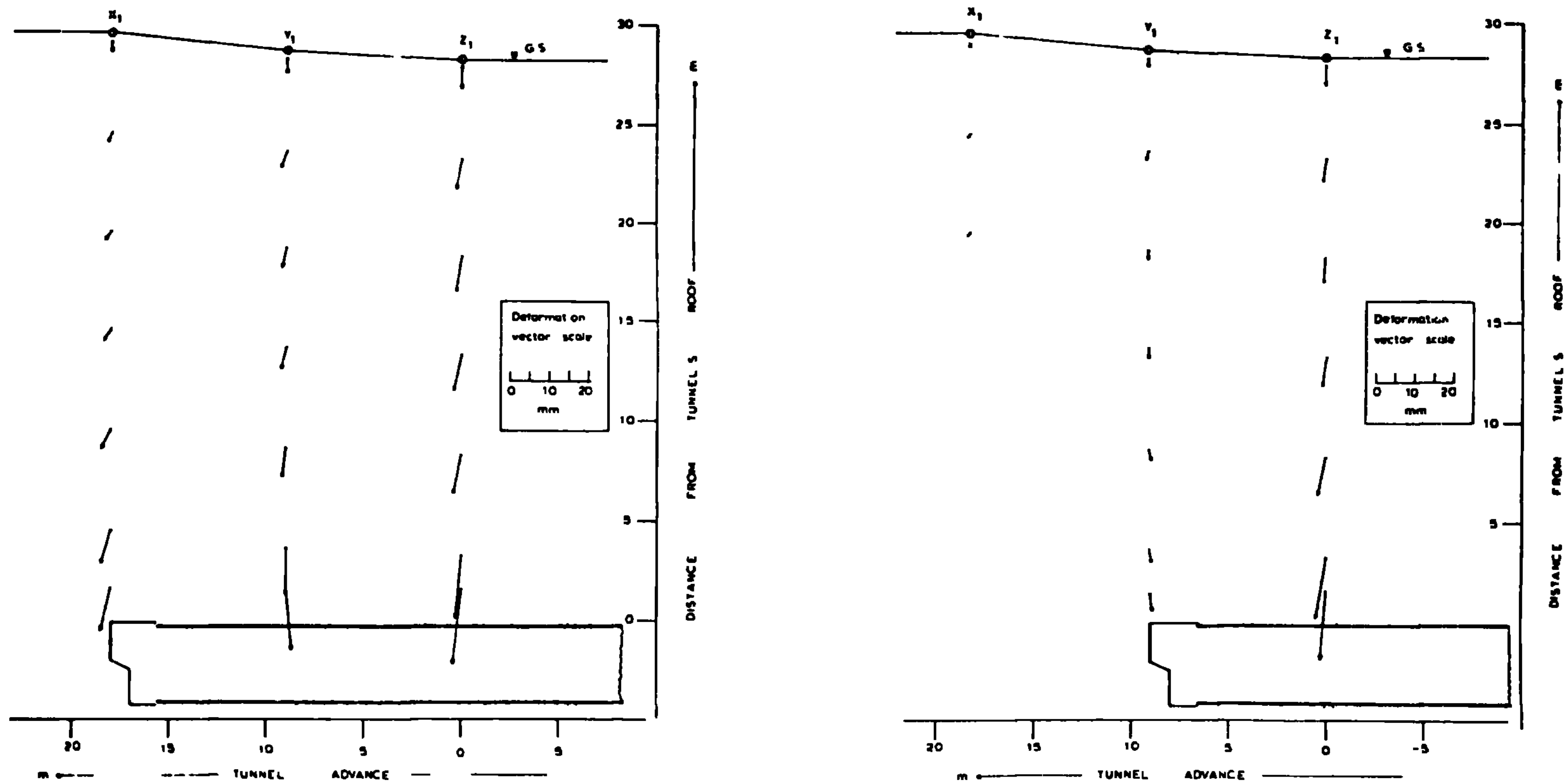

FIG. 4.4.7. Ground deformation in a vertical plane along the tunnel axis. Tunnel face at Y1 (right hand side) and at X1 (left hand side).

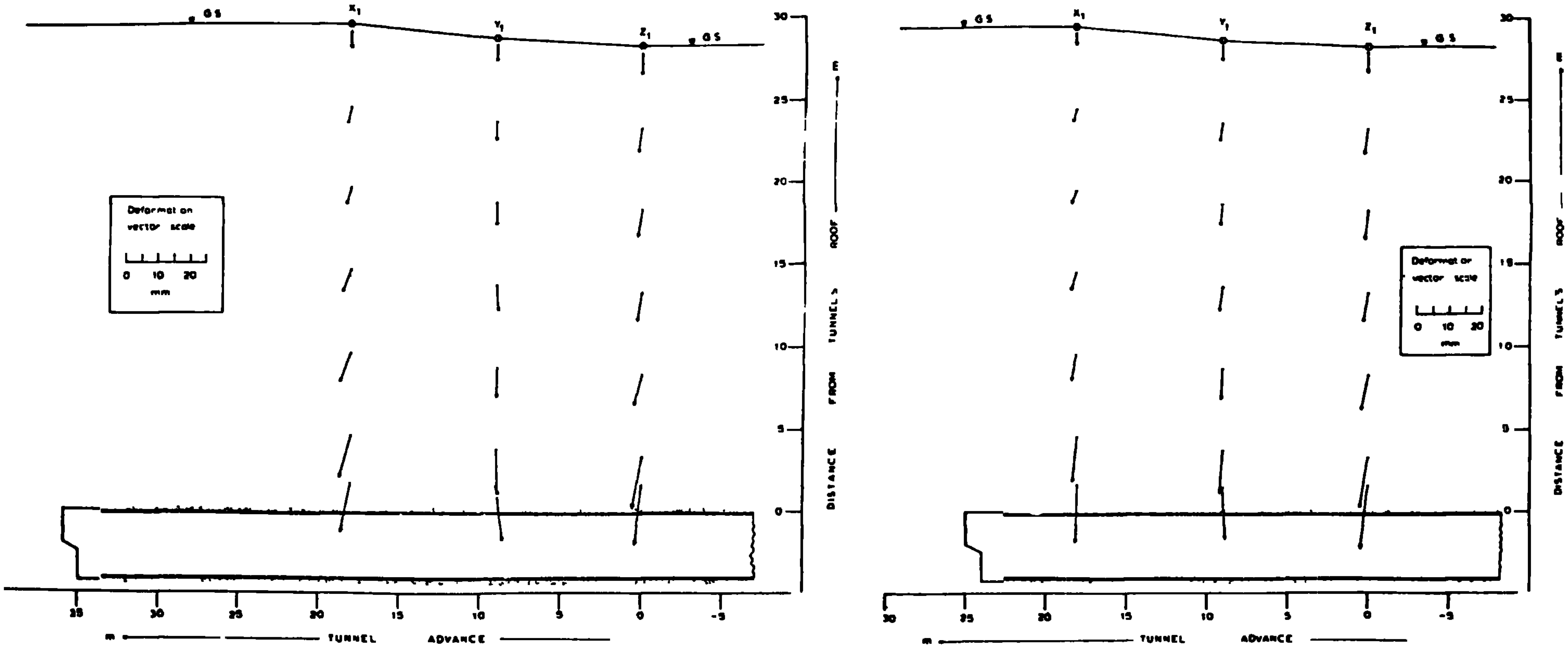

FIG.4.4.8. Ground deformation in a vertical plane along the tunnel axis. Tunnel face ~ 6m ahead of X1 (right hand side) and ~ 17m ahead of X1 (left hand side).

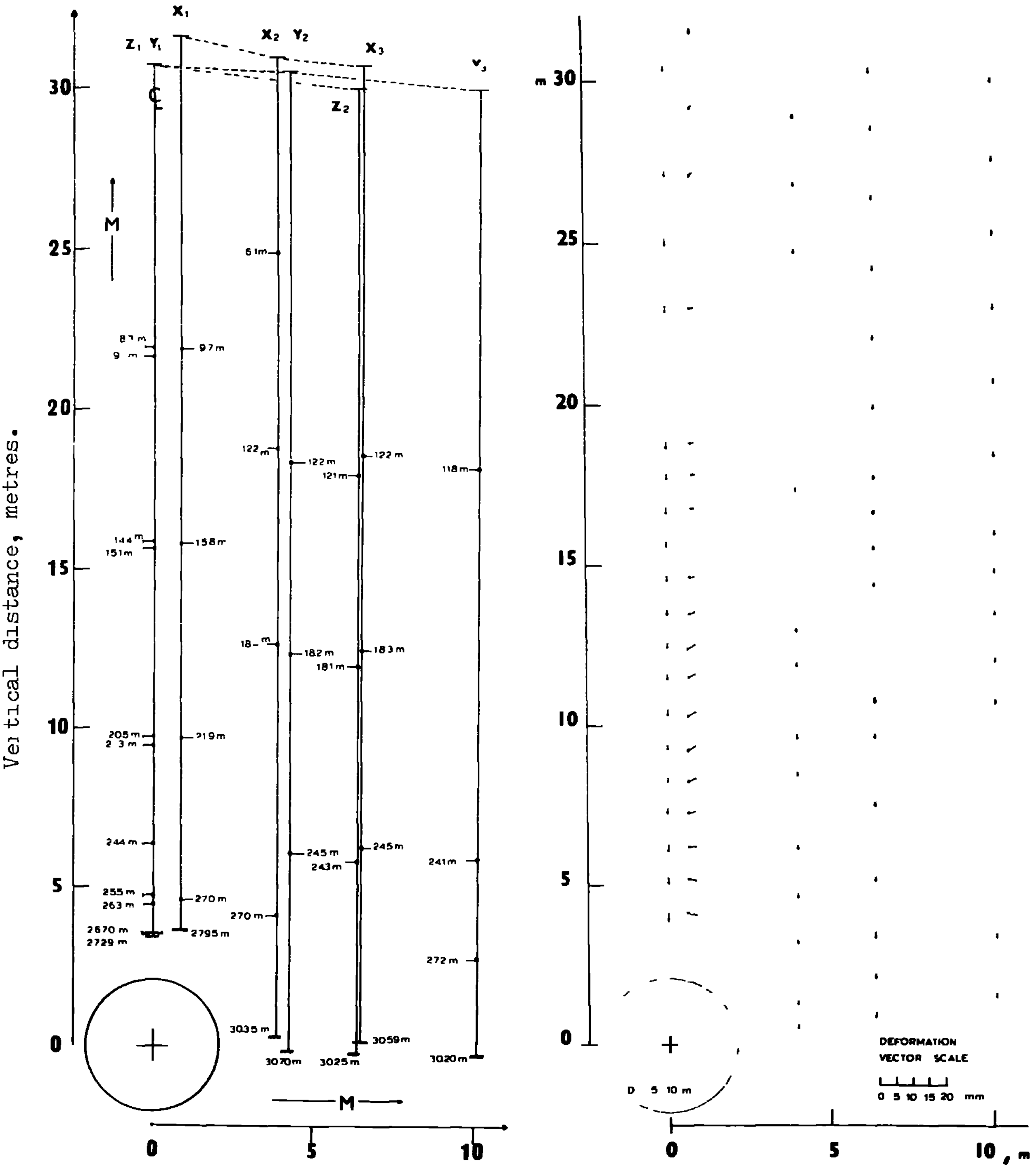

FIG. 4.4.9. Ground deformation at right angles to the tunnel axis. The left hand side illustrates the scaled layout of boreholes with the exact position of magnetic rings. Right hand side shows the state of ground disturbance when the face is 5 to 10 metres behind the cross-section.

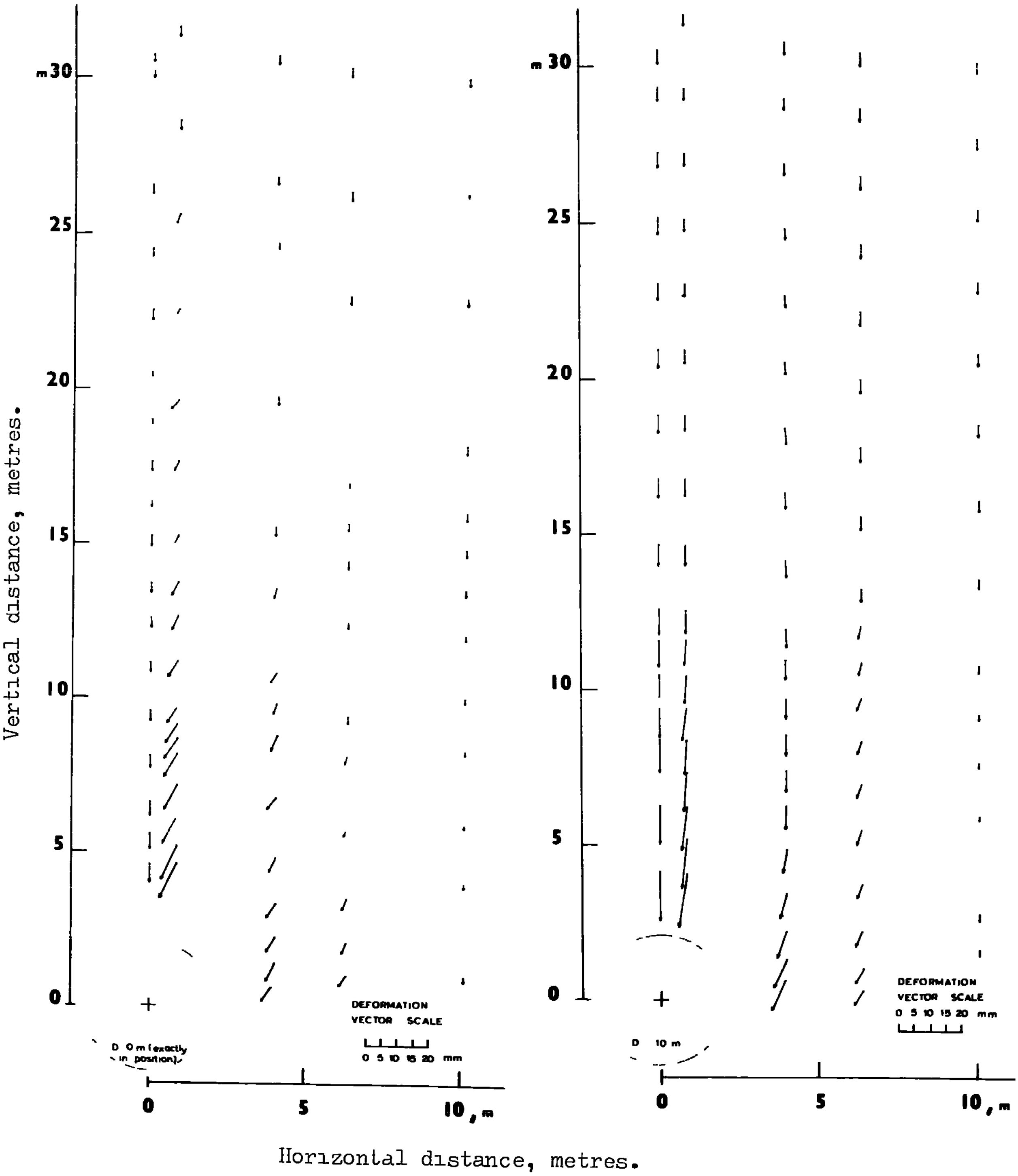

FIG. 4.4.10. Ground deformation at right angles to the tunnel axis. Tunnel face at the cross-section (left hand side) and 10 metres ahead of the cross-section (right hand side).

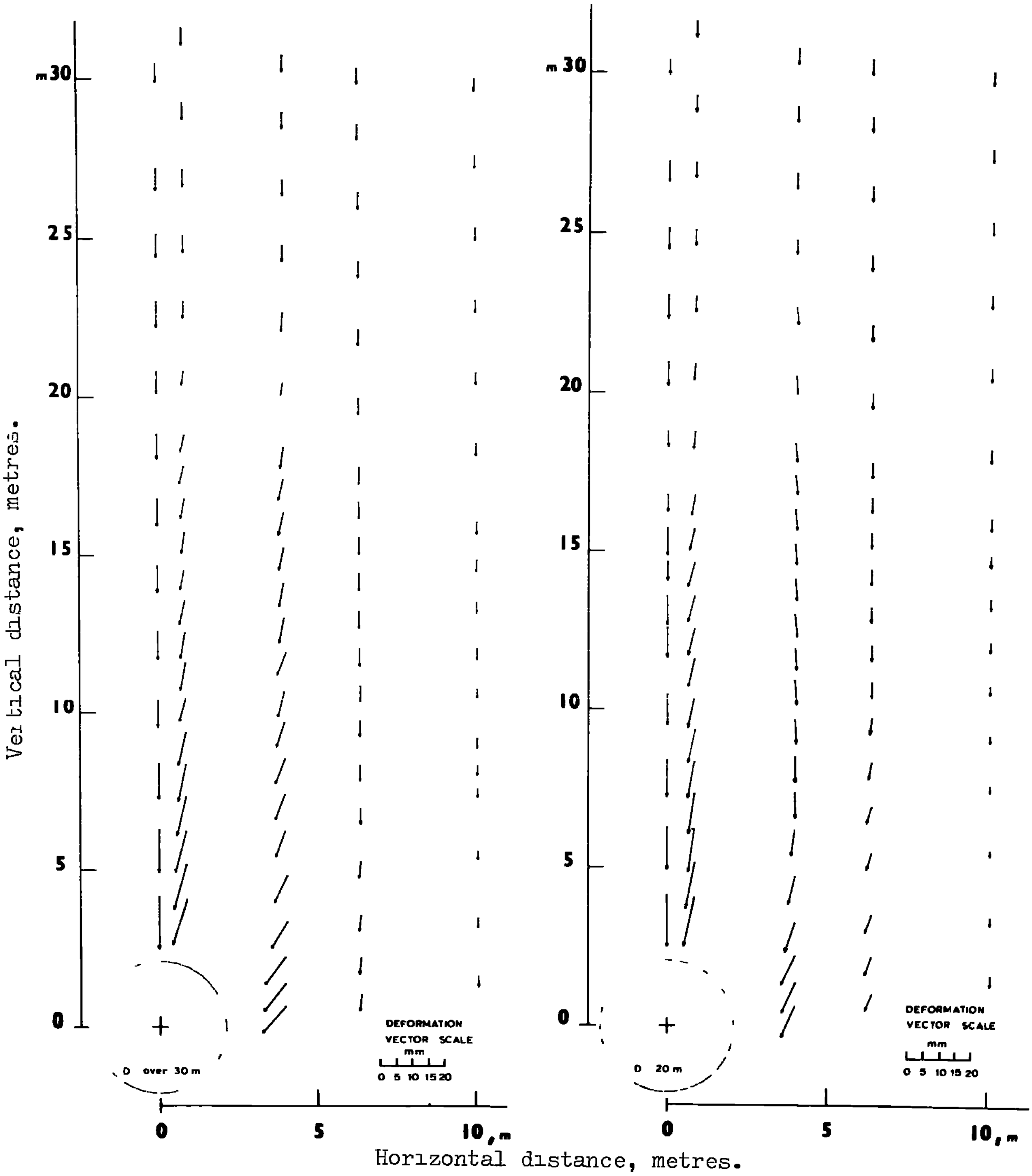

FIG.4.4.11. Ground deformation at right angles to the tunnel axis. Tunnel face 20 metres ahead of the cross-section (right hand side) and 30 metres ahead of the cross-section(left hand side).

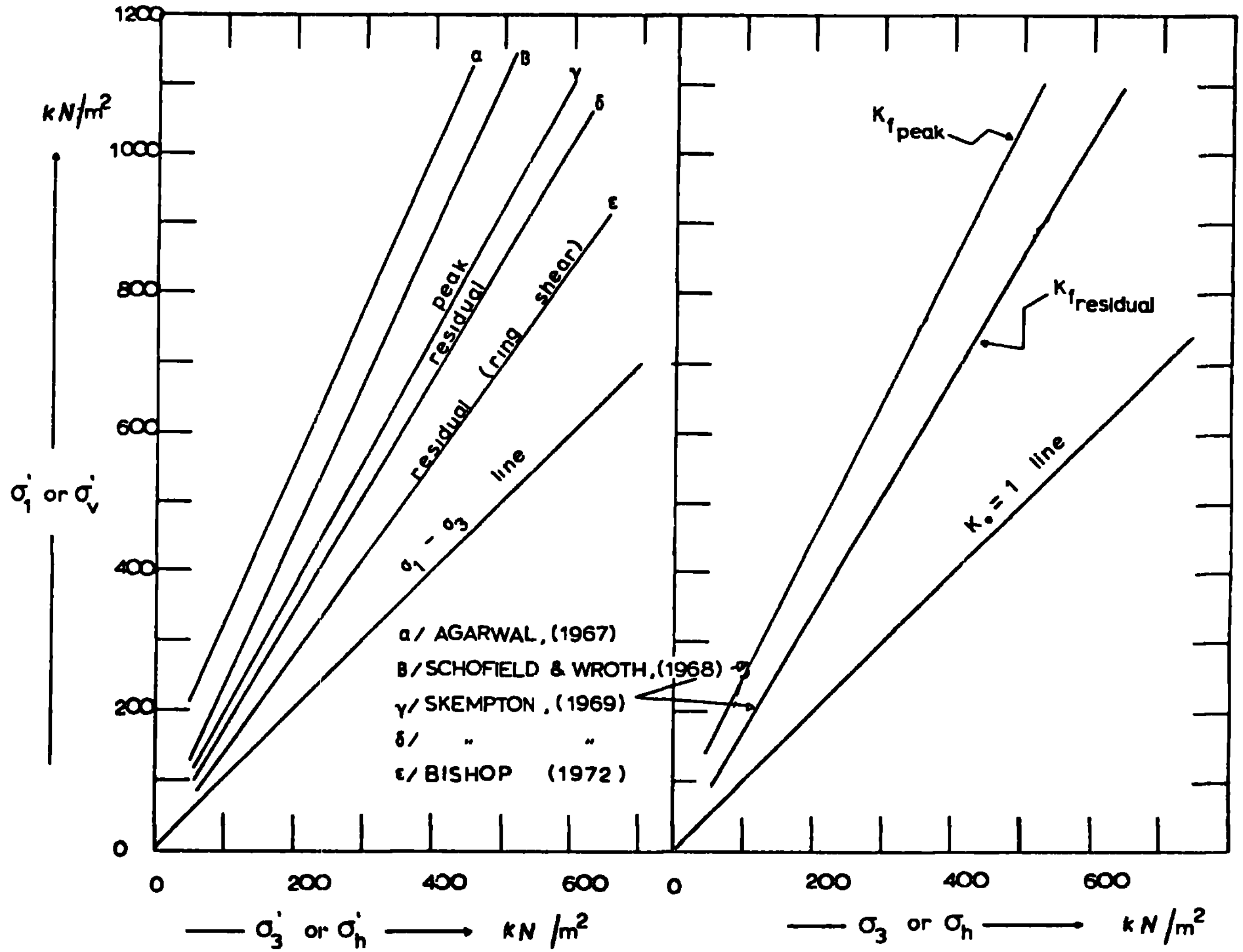

FIG, 5.3.1. Effective (left hand side) and total (right hand side) shear strength parameters for London clay.

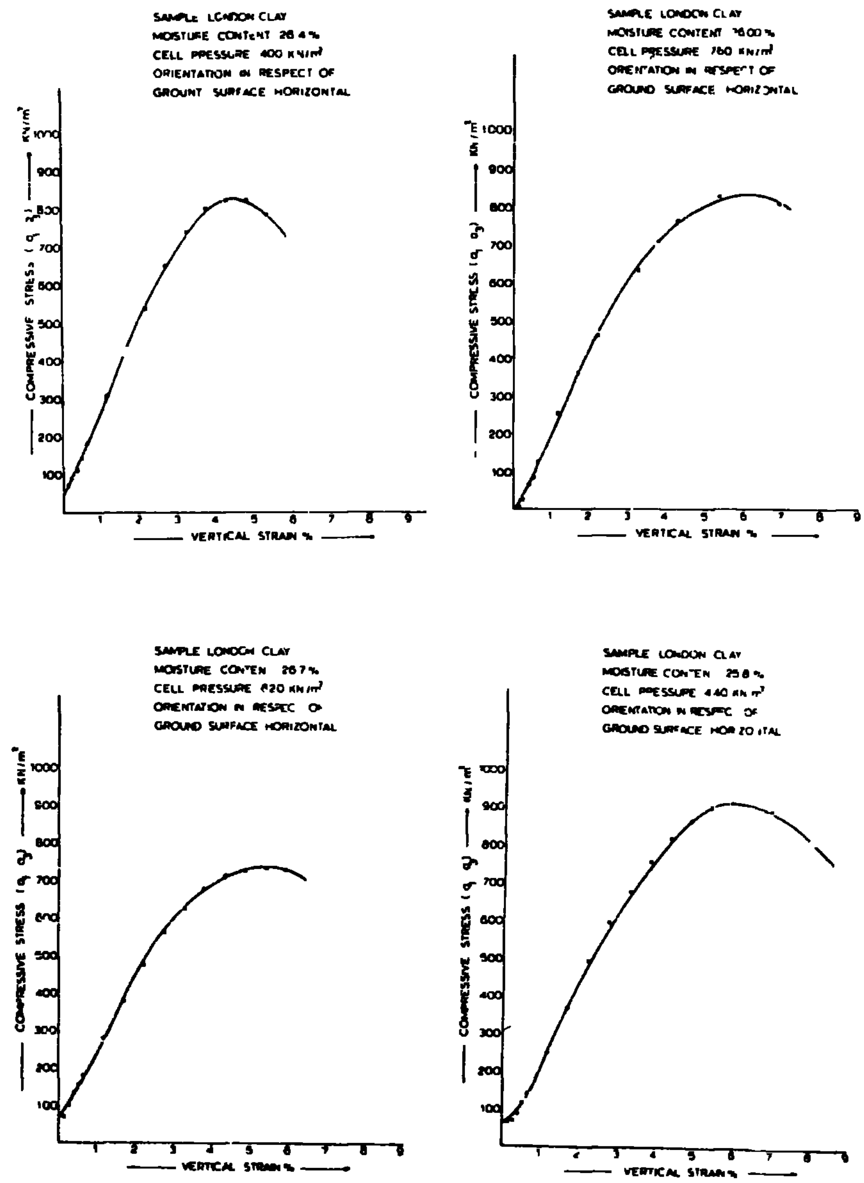

FIG. 5.4.1. Stress-strain relationships for 38mm diameter specimens subject to undrained triaxial tests. Deviator stress applied parallel to the bedding.

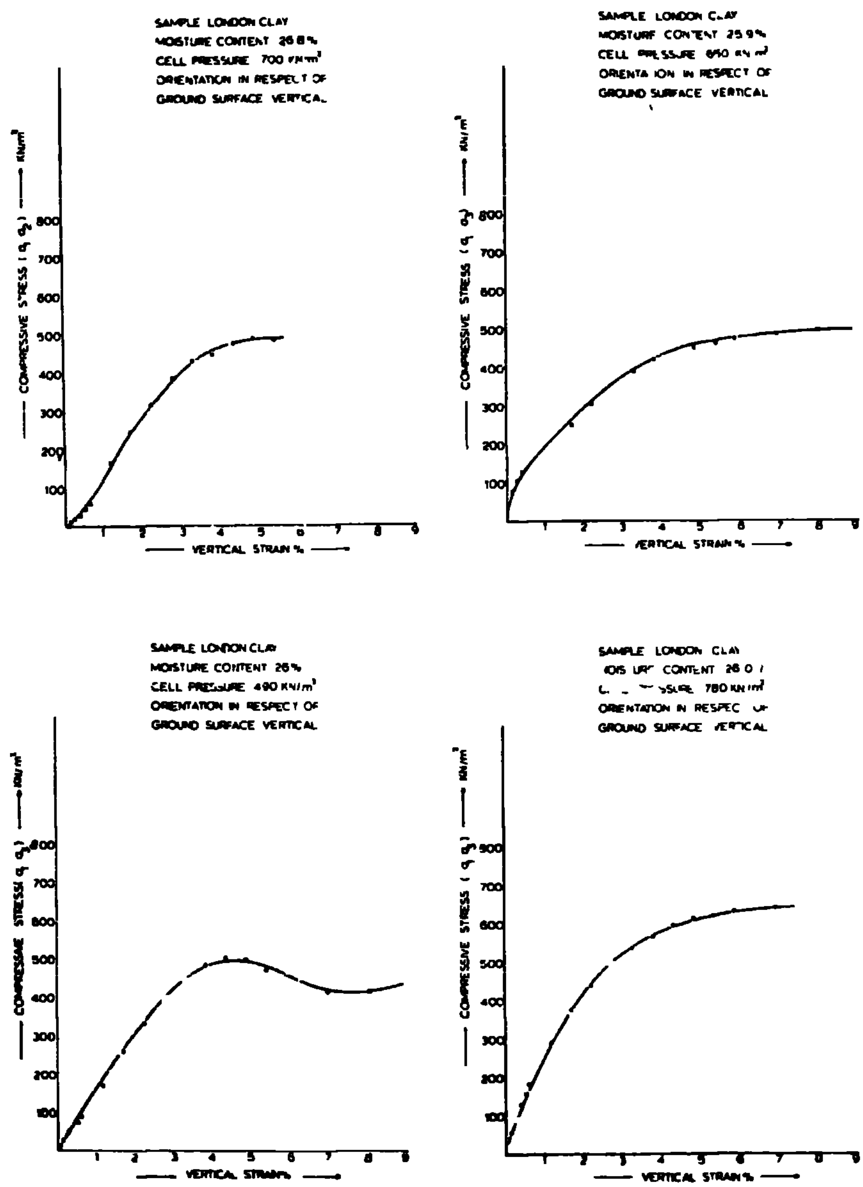

FIG. 5.4.2. Stress-strain relationships for 38mm diameter specimens (London clay) subject to undrained triaxial tests. Deviator stress applied normal to the bedding.

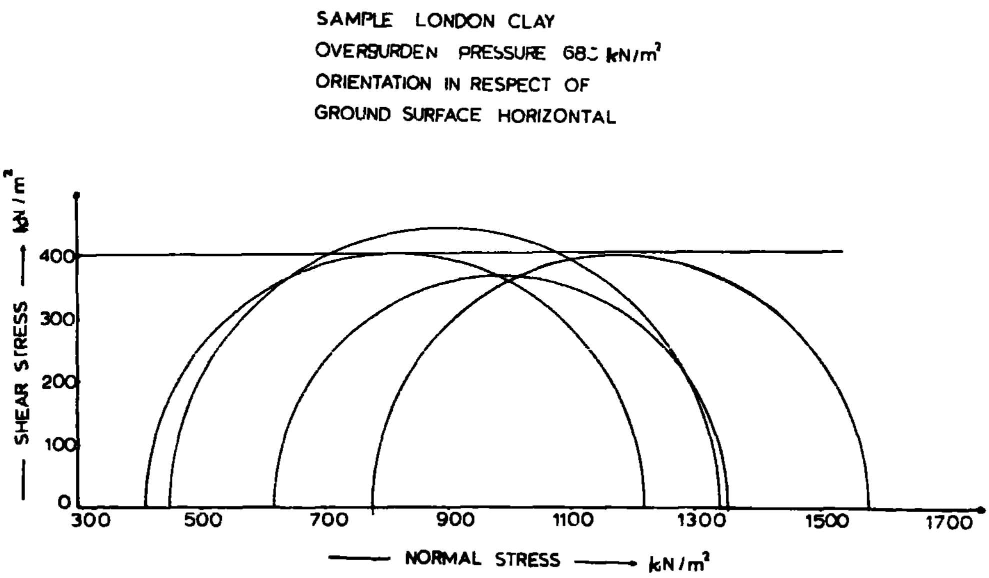

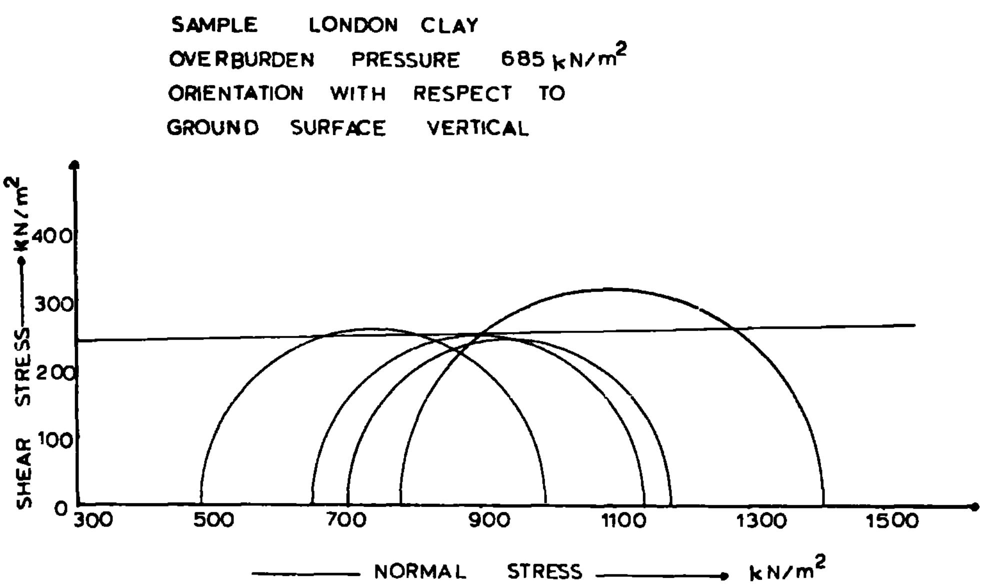

FIG. 5.4.3. Results for undrained triaxial tests on 38mm diameter specimens (London clay). <u>Above</u> deviator stress applied parallel to the bedding, <u>below</u> normal to it.

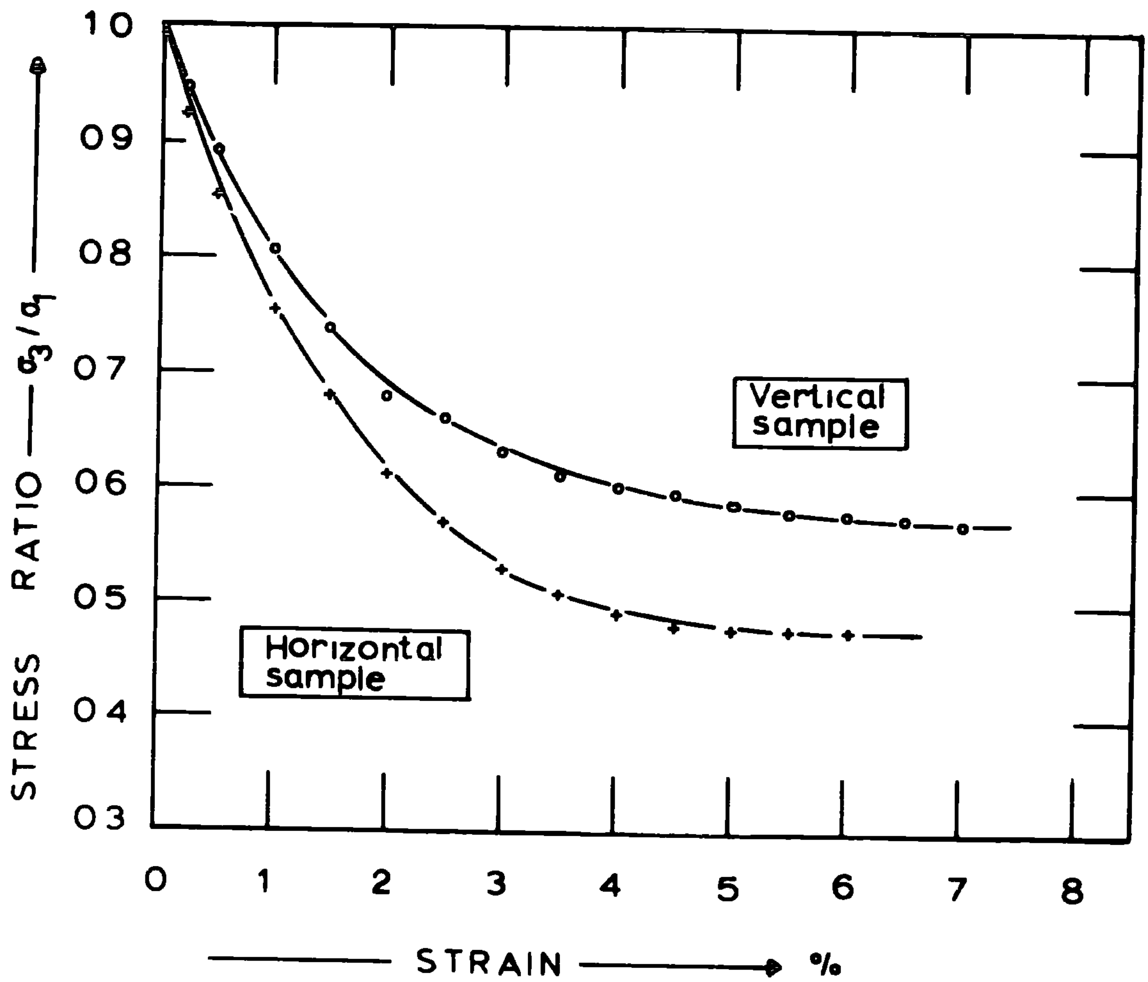

FIG. 5.4.4. Relationship between the principal stress ratio σ_3/σ_1 and the strain for 38mm diameter specimens of London clay subjected to UU triaxial tests.

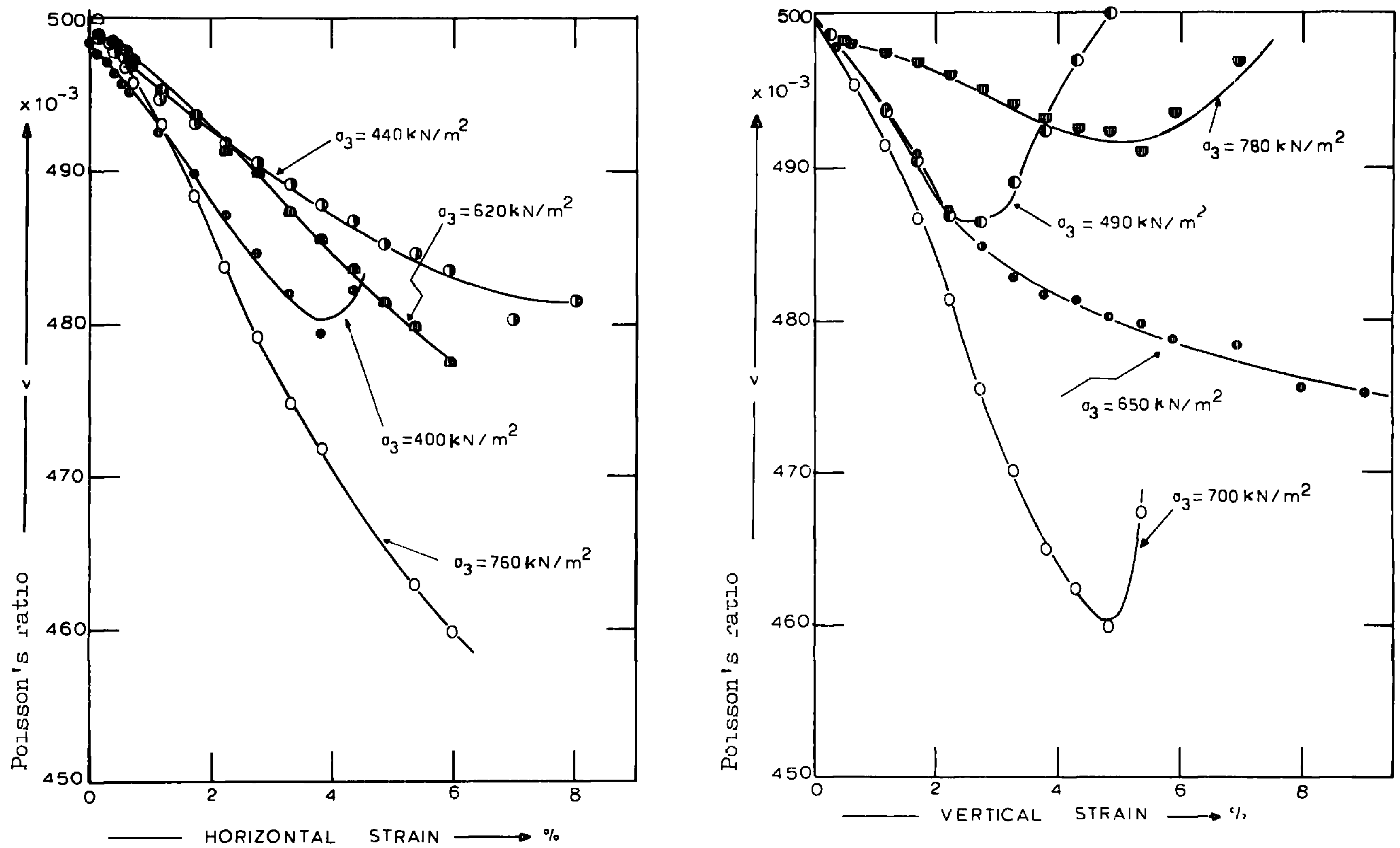

FIG. 5.5.1. Variation of Poisson's ratio with vertical and horizontal strain, during UU triaxial tests on 38mm diameter specimens of London clay.

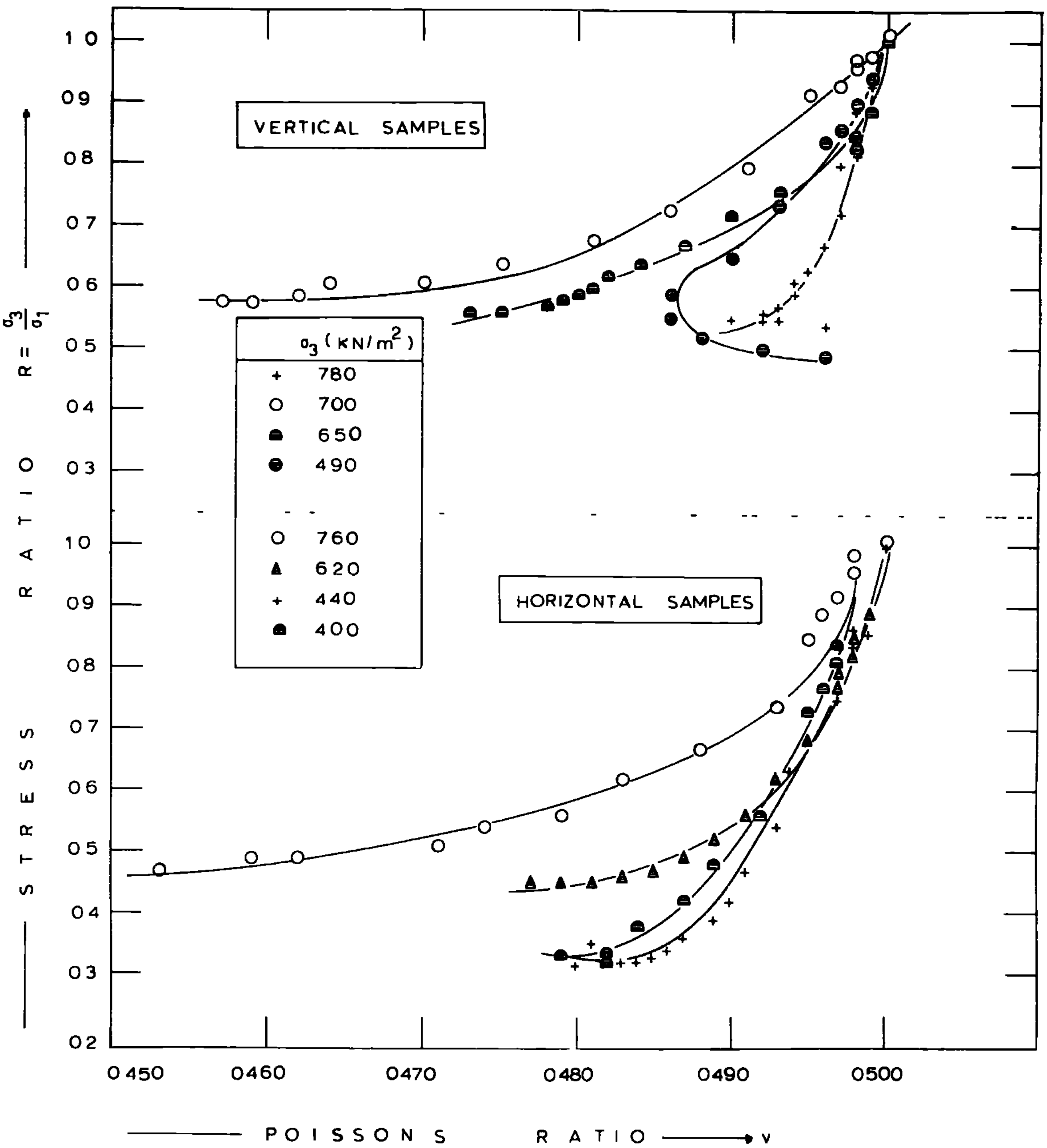

FIG. 5.5.2. Variation of Poisson's ratio with the principal stress ratio σ_3/σ_1 during UU triaxial tests on 38mm diameter specimens of London clay.

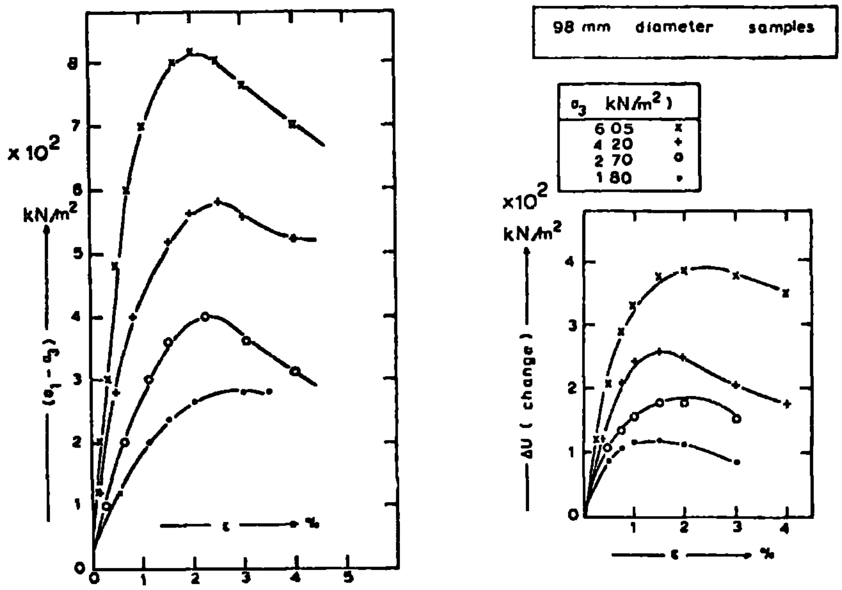

FIG 5.6 1 (Above) Stress-strain relationships for $\overline{UU}$ triaxial tests on 98mm diameter specimen of London clay.

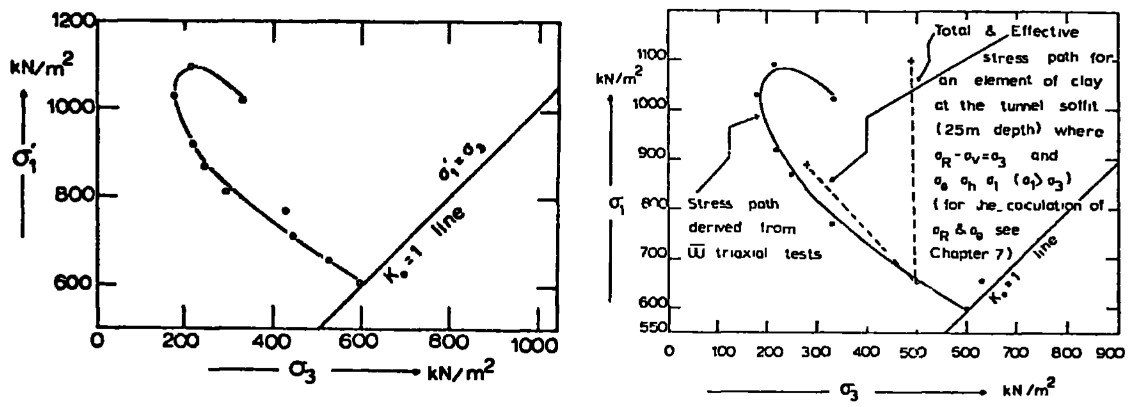

FIG. 5 6 2 (Below) Effective stress paths for $\overline{UU}$ triaxial test on 98mm diameter specimen (London clay) Initial effective stress is equal to 600 kN/m^2.

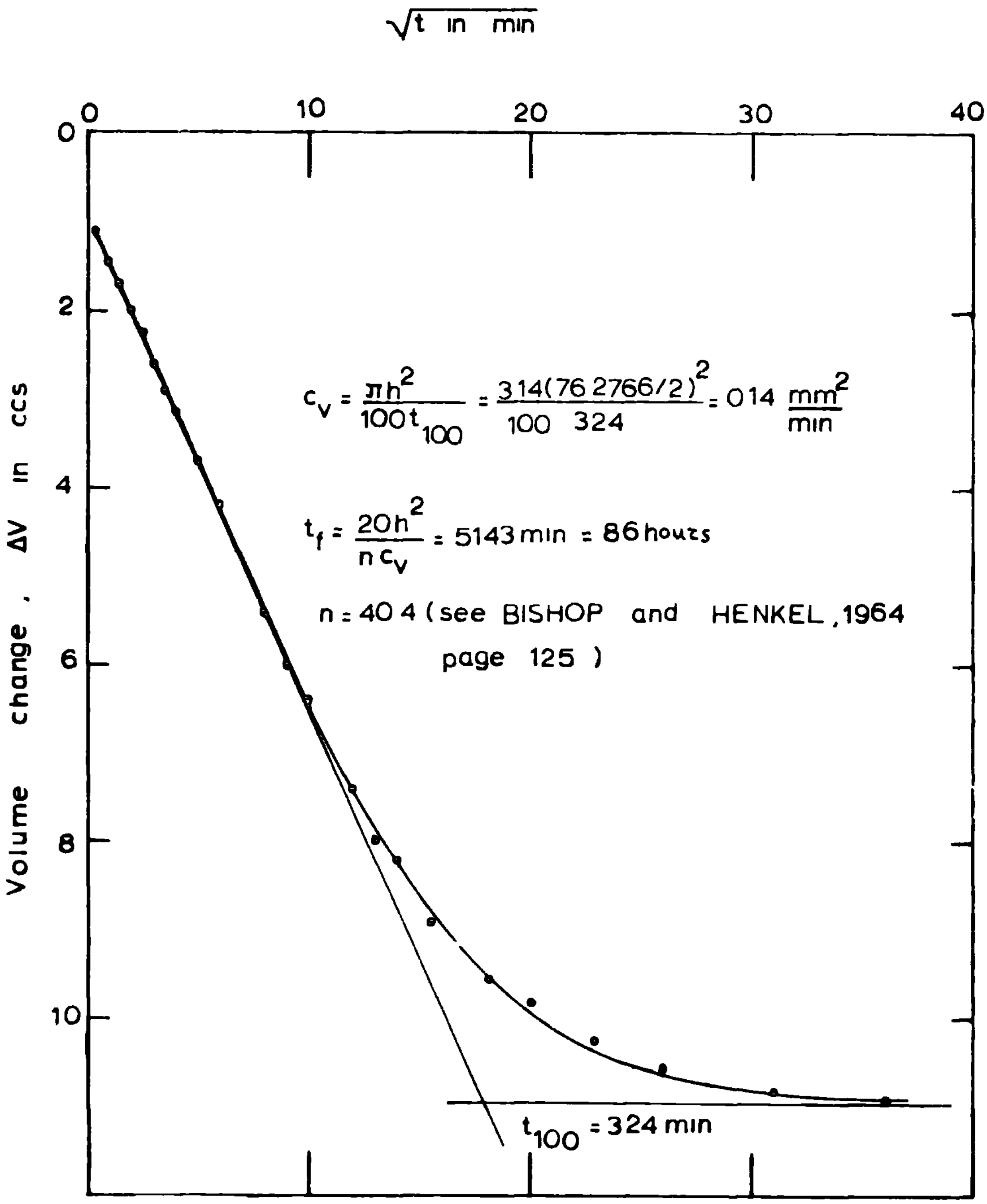

FIG. 5.6.3. Relationship between the volume change and the square root for a 38mm diameter sample of London clay during consolidation under an all around pressure (radial and end drainage).

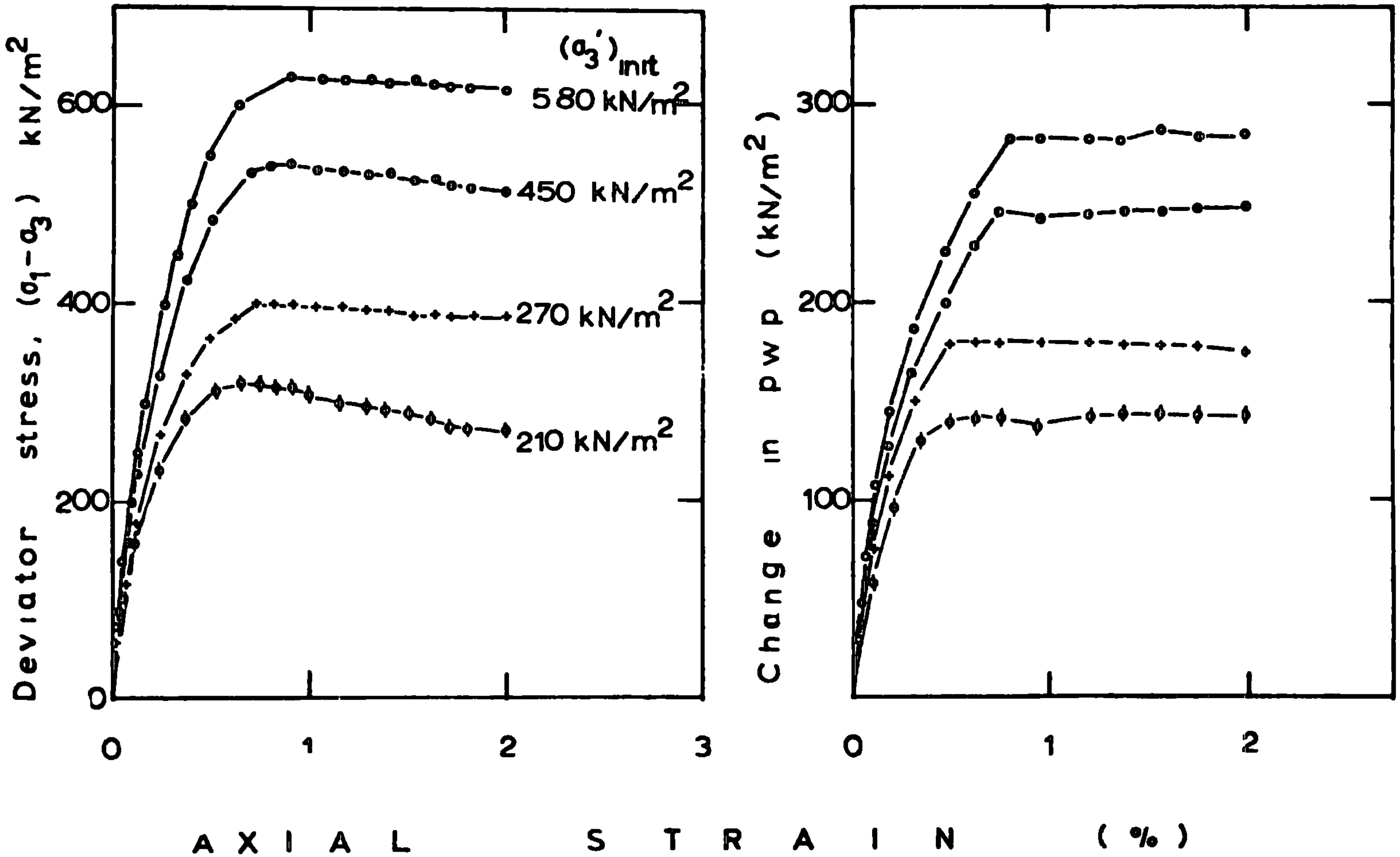

FIG. 5.6.4. Stress-strain relationships for $\overline{CU}$ triaxial tests on 38mm diameter specimens of London clay.

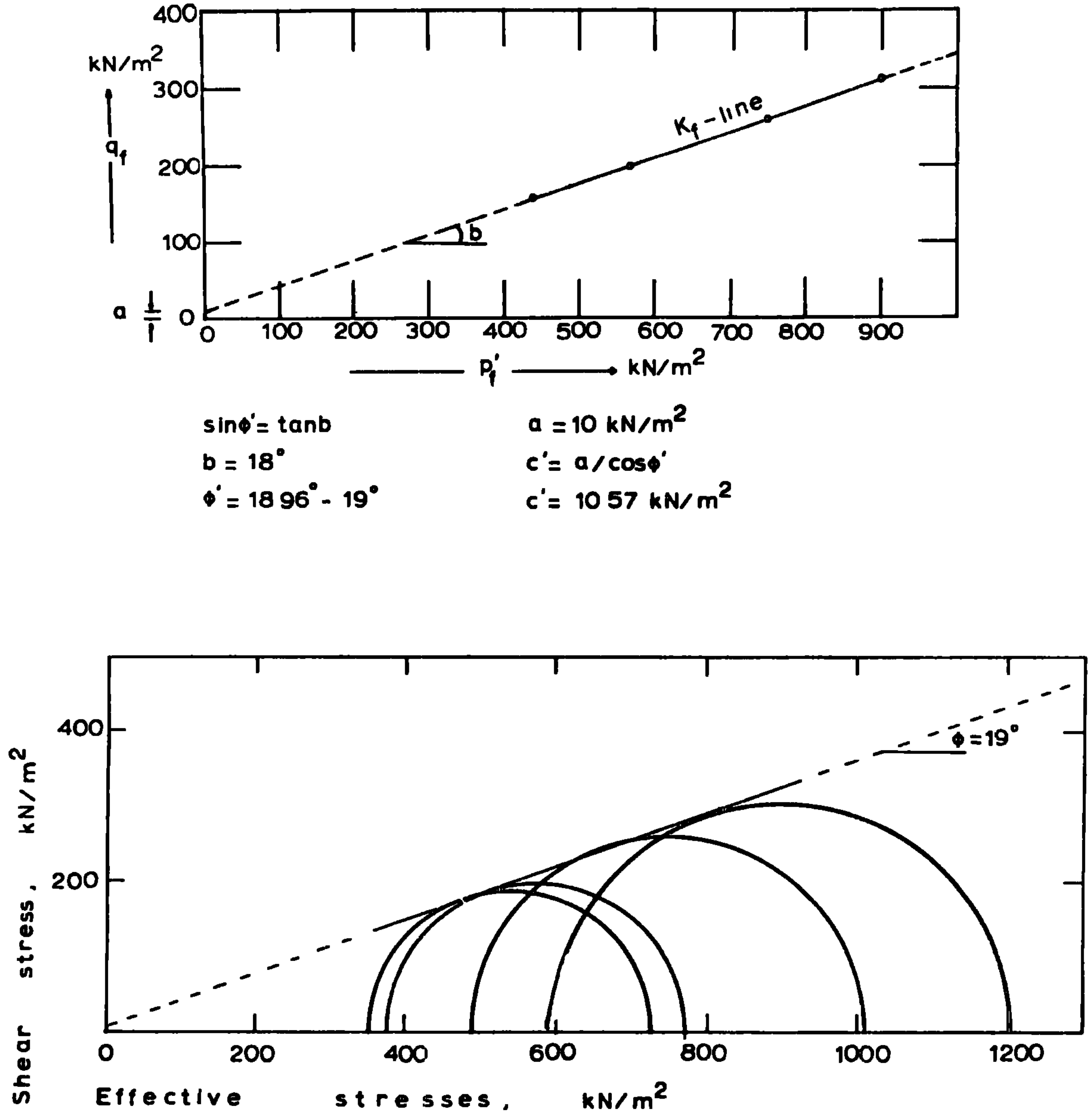

FIG. 5.6.5. Results from $\overline{CU}$ triaxial tests on 38mm diameter specimens of London clay. Above $p'_f - q'_f$ diagram Below Mohr circle representation.

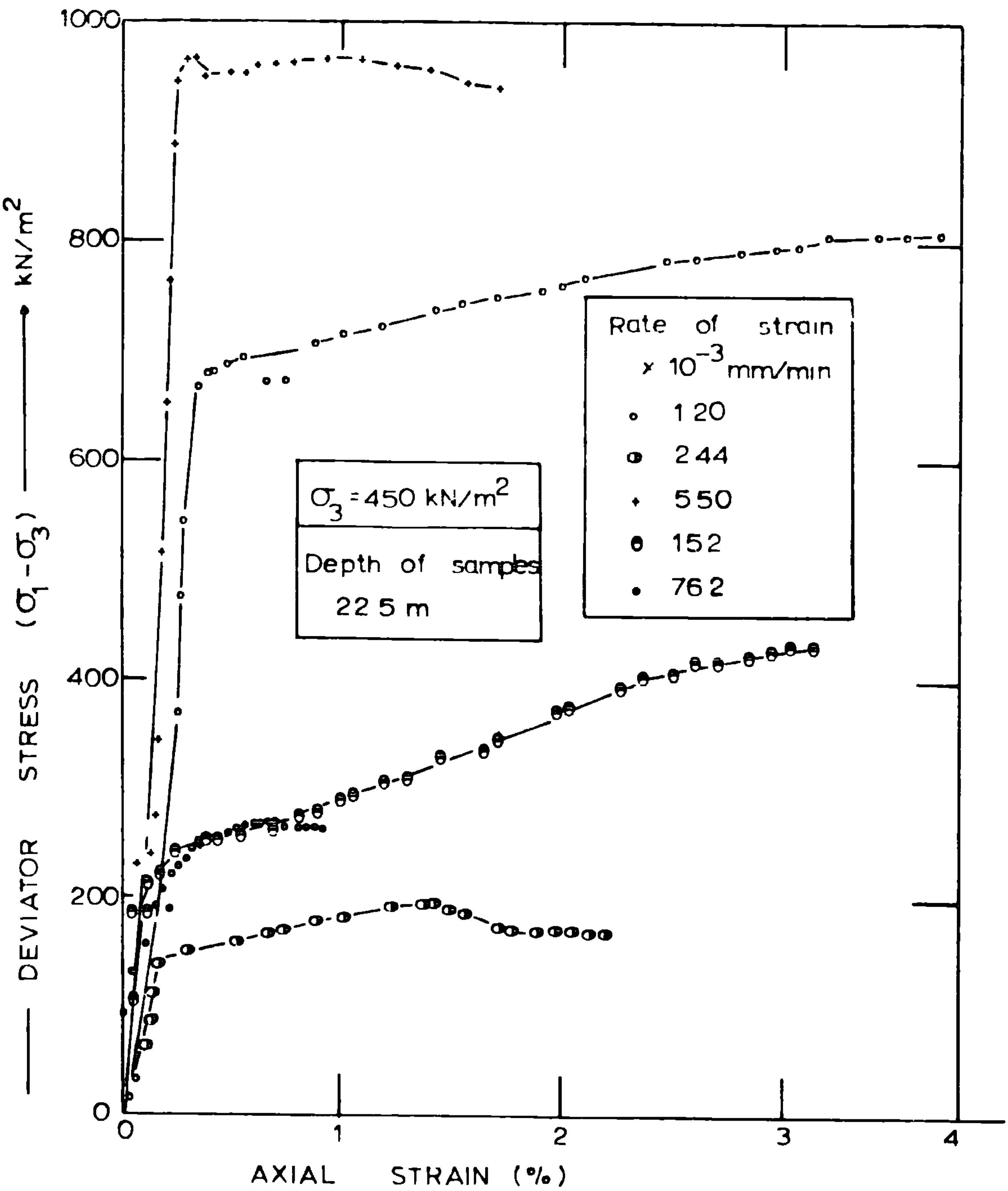

FIG. 5.6.6. Stress-strain relationships for $\overline{CU}$ triaxial tests on 38mm diameter specimens of London clay. Depth of sampling was 22.5m. Each test was carried out under different nominal rate of strain.

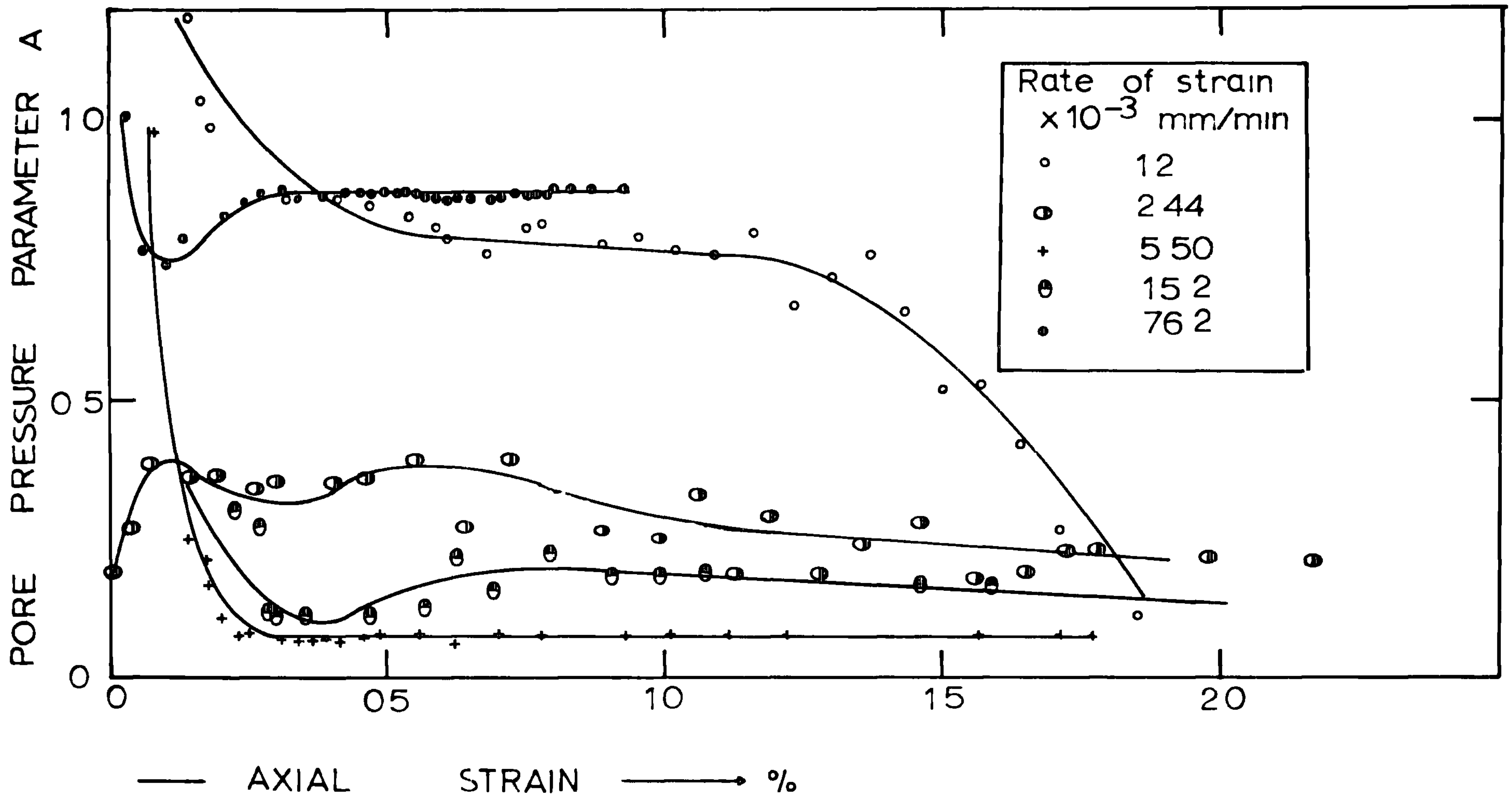

FIG. 5.6.7. Relationship between the pore pressure parameter A and the axial strain, for $\overline{CU}$ triaxial tests on 38mm diameter specimens of London clay. Each test was carried out under different nominal rate of strain.

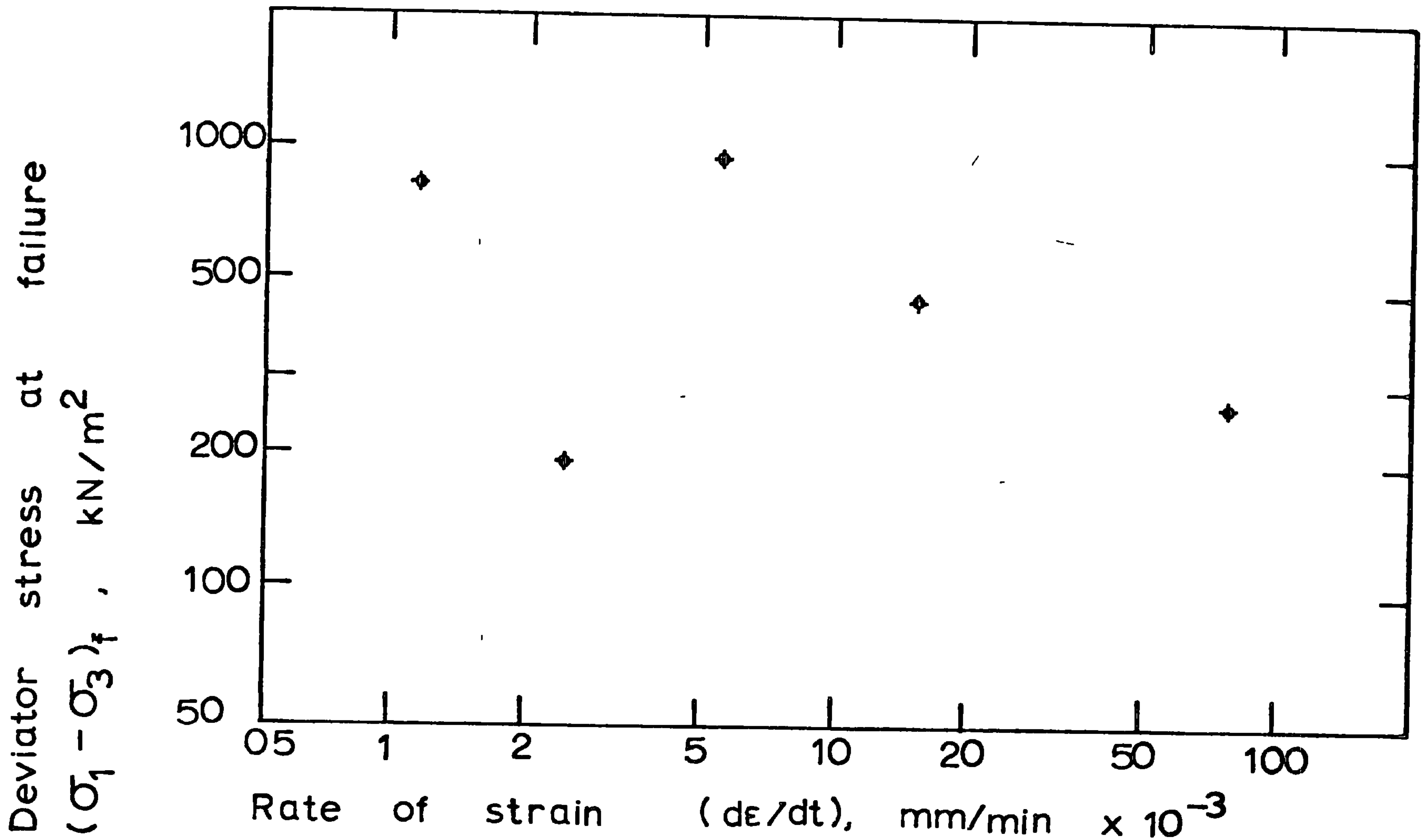

FIG. 5.6.8. Relationship between the deviator stress at failure, and the rate of strain for $\overline{CU}$ triaxial tests on 38mm diameter specimens of London clay.

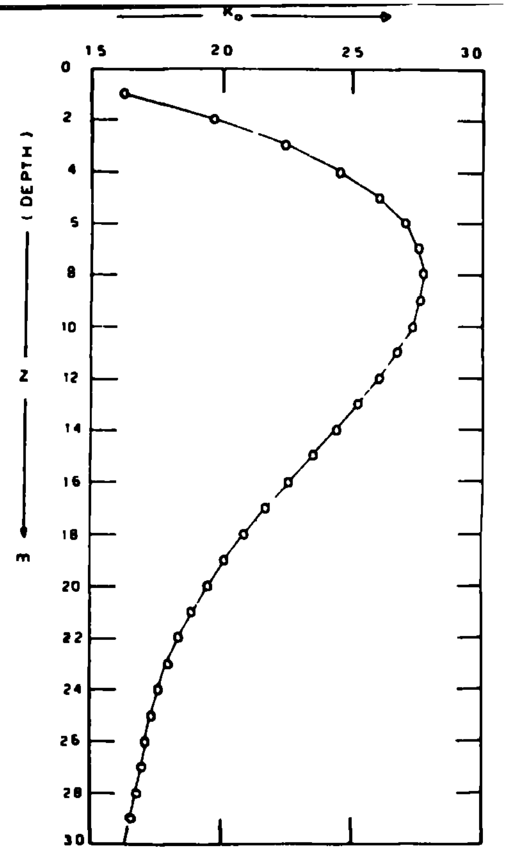

FIG. 6.2.1. Polynomial fitted to Skempton (1961) data relating the variation of K_o with depth in London clay. After Gowland's 1974, private communication.

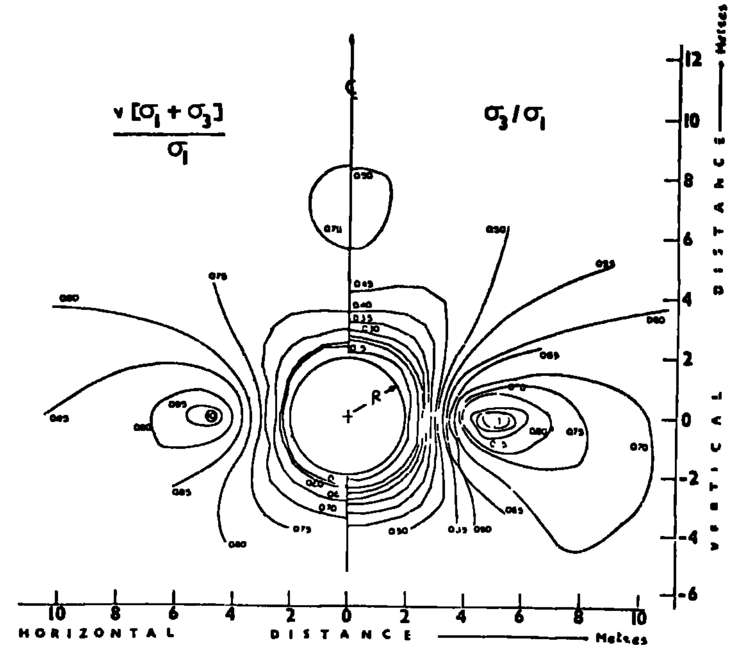

FIG. 6.2.2. Amplitudes of principal stress ratios around the 4m diameter tunnel 30m deep in London clay. Analyses based on elastic equations interrelated with Skempton's K_o function with depth and assuming condition of plane strain (Based on data supplied by Gowland, 1974, private communication).

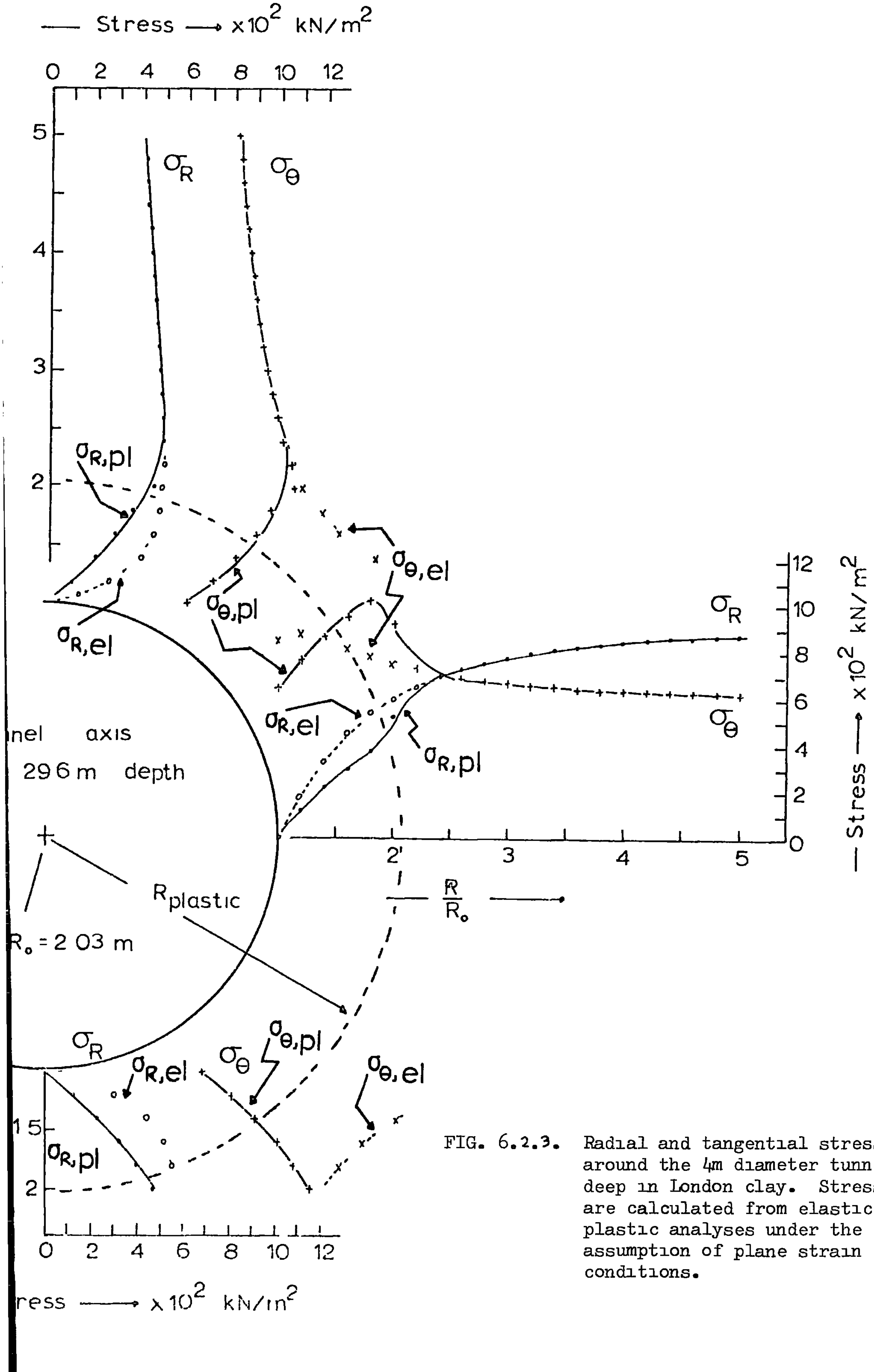

FIG. 6.2.3. Radial and tangential stresses around the 4m diameter tunnel 30m deep in London clay. Stresses are calculated from elastic and plastic analyses under the assumption of plane strain conditions.

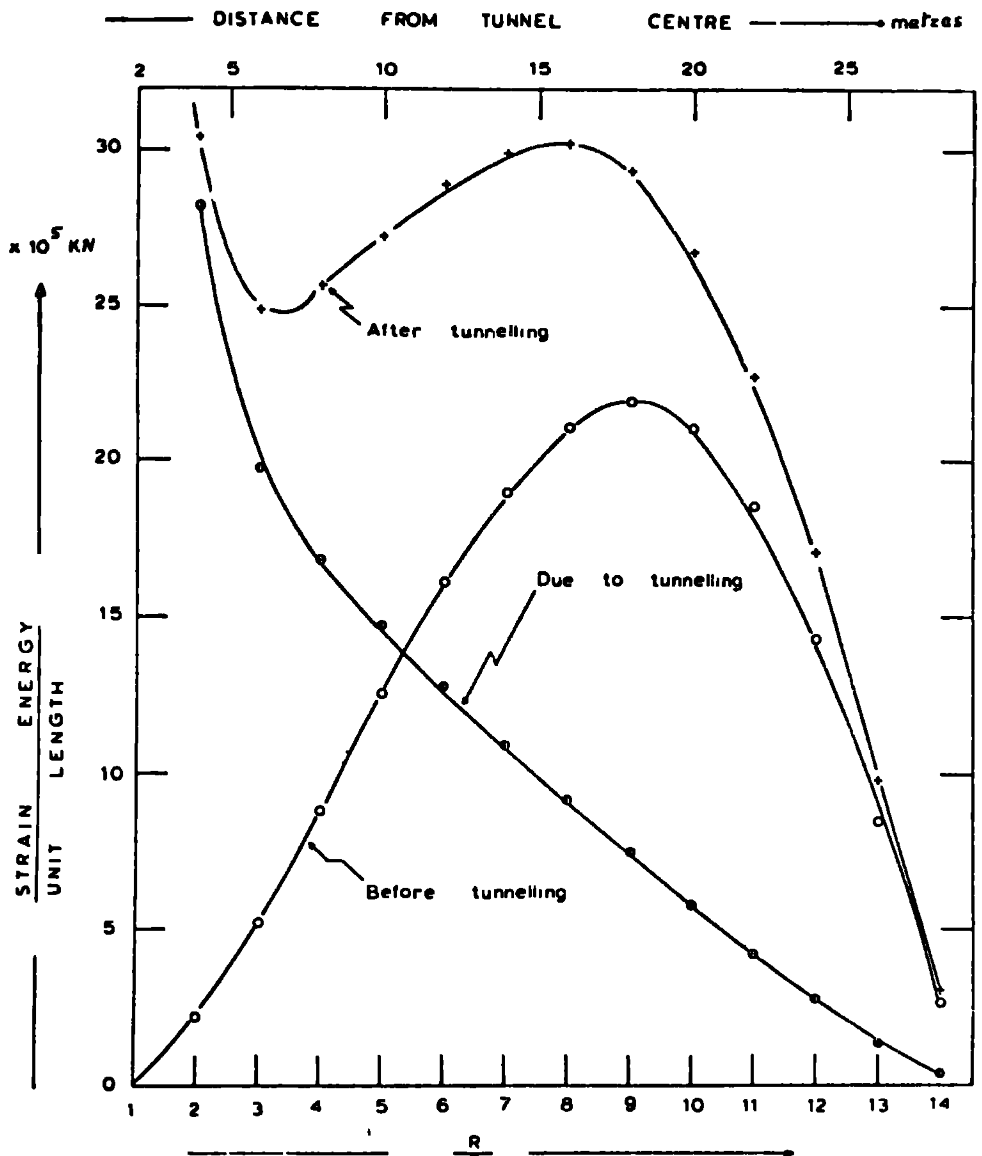

FIG. 6.3.1. Relationship between the strain energy per unit length and the distance from the tunnel centre for the 4m diameter tunnel 30m deep in London clay.

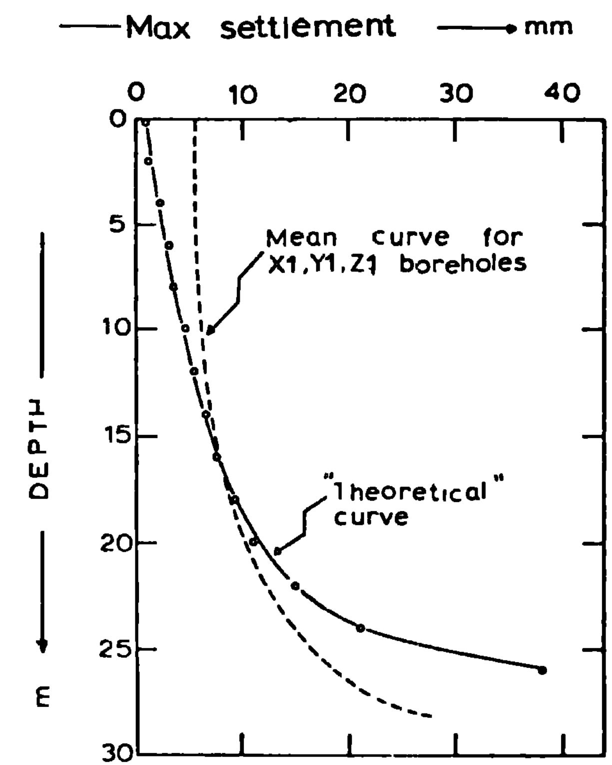

FIG. 6.3.2. The maximum settlement as a function of depth below ground surface. Comparison between the calculated and the actual values.

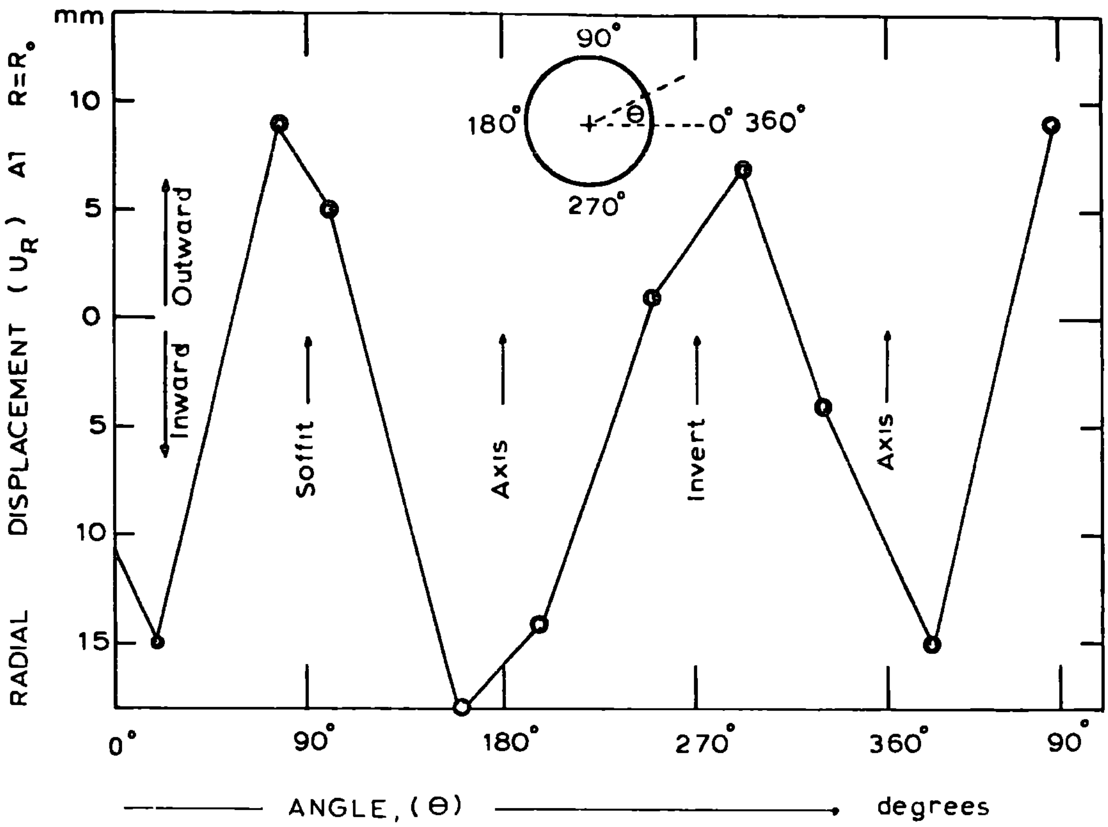

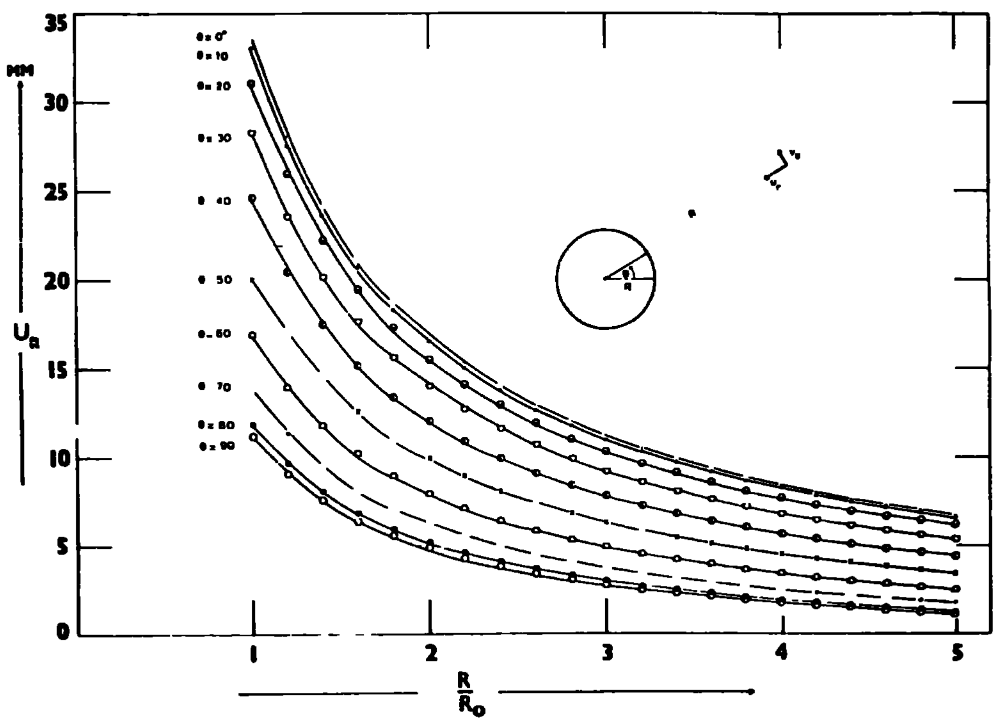

FIG. 6.4.1. (Above) Measured radial displacement as a function of polar co-ordinate angle for the 4m diameter tunnel 30m deep in London clay.

FIG. 6.4.2. (Below) Calculated radial displacement as a function of distance from the tunnel centre taking the polar co-ordinate angle as the main parameter.

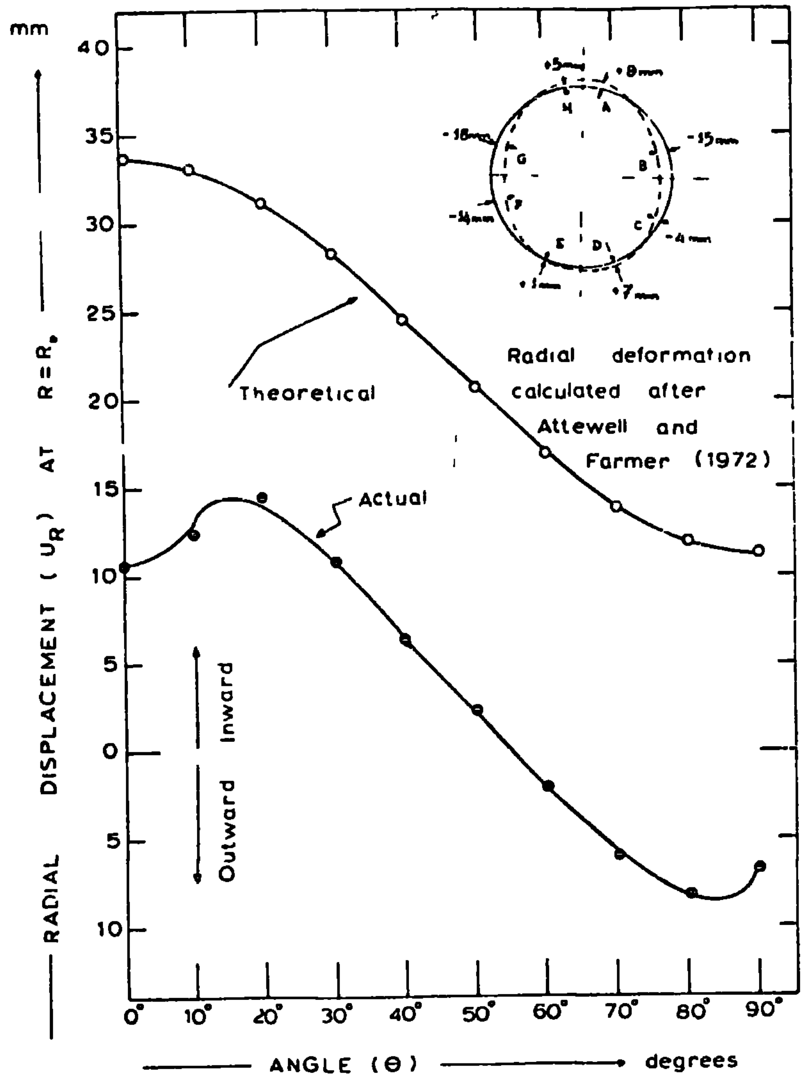

FIG. 6.4.3. Comparison between the actual (after ATTEWELL and FARMER, 1972) and the theoretically predicted radial displacement around the 4m diameter tunnel 30m deep in London clay, for different polar co-ordinate angles

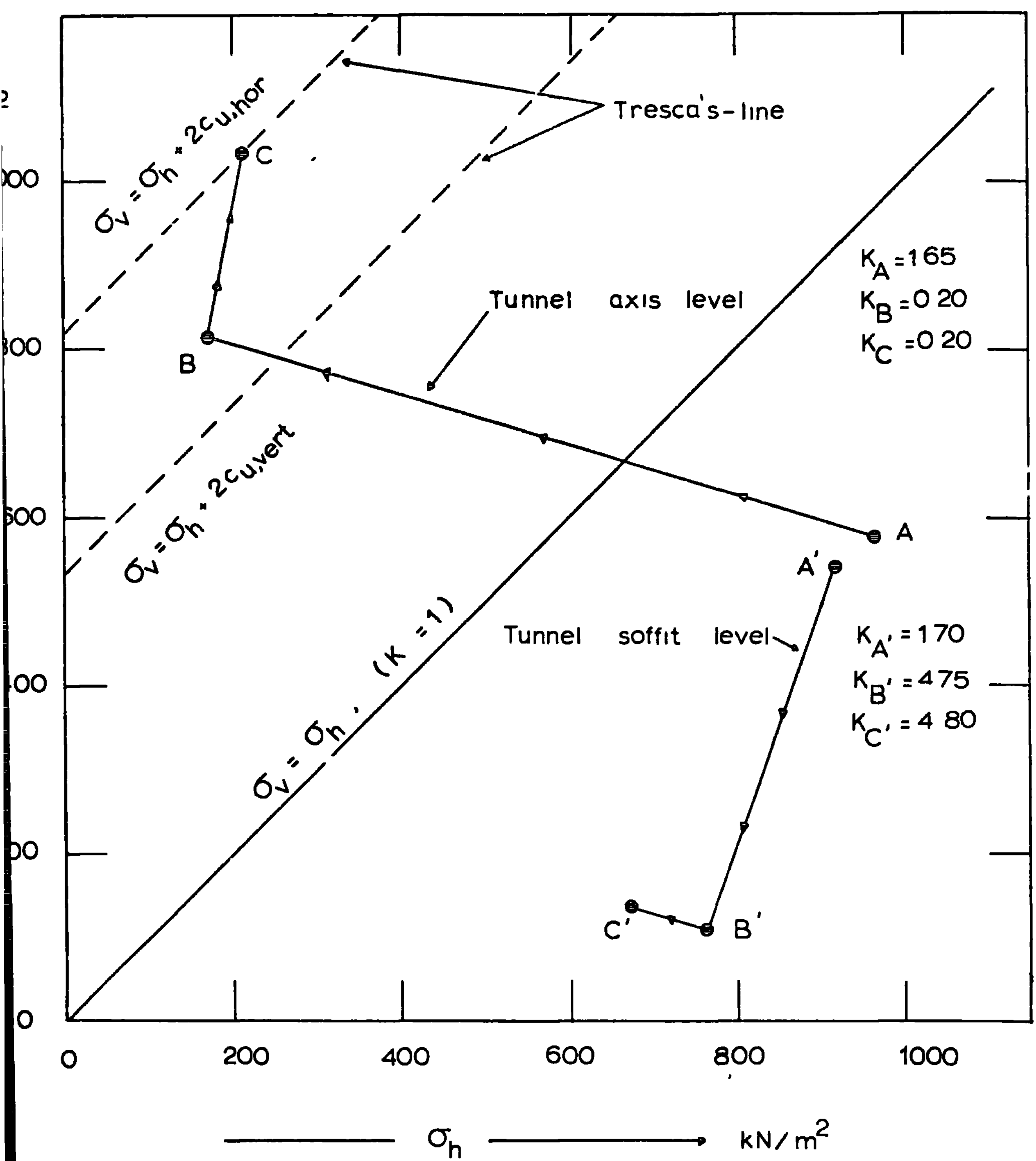

FIG. 7.2.1. Hypothetical stress paths for an element of clay at tunnel soffit and at tunnel axis level. Tresca's lines are defined according to laboratory test results from UU triaxial tests on specimens taken from tunnel axis level in two main directions, parallel and vertical to stratification.

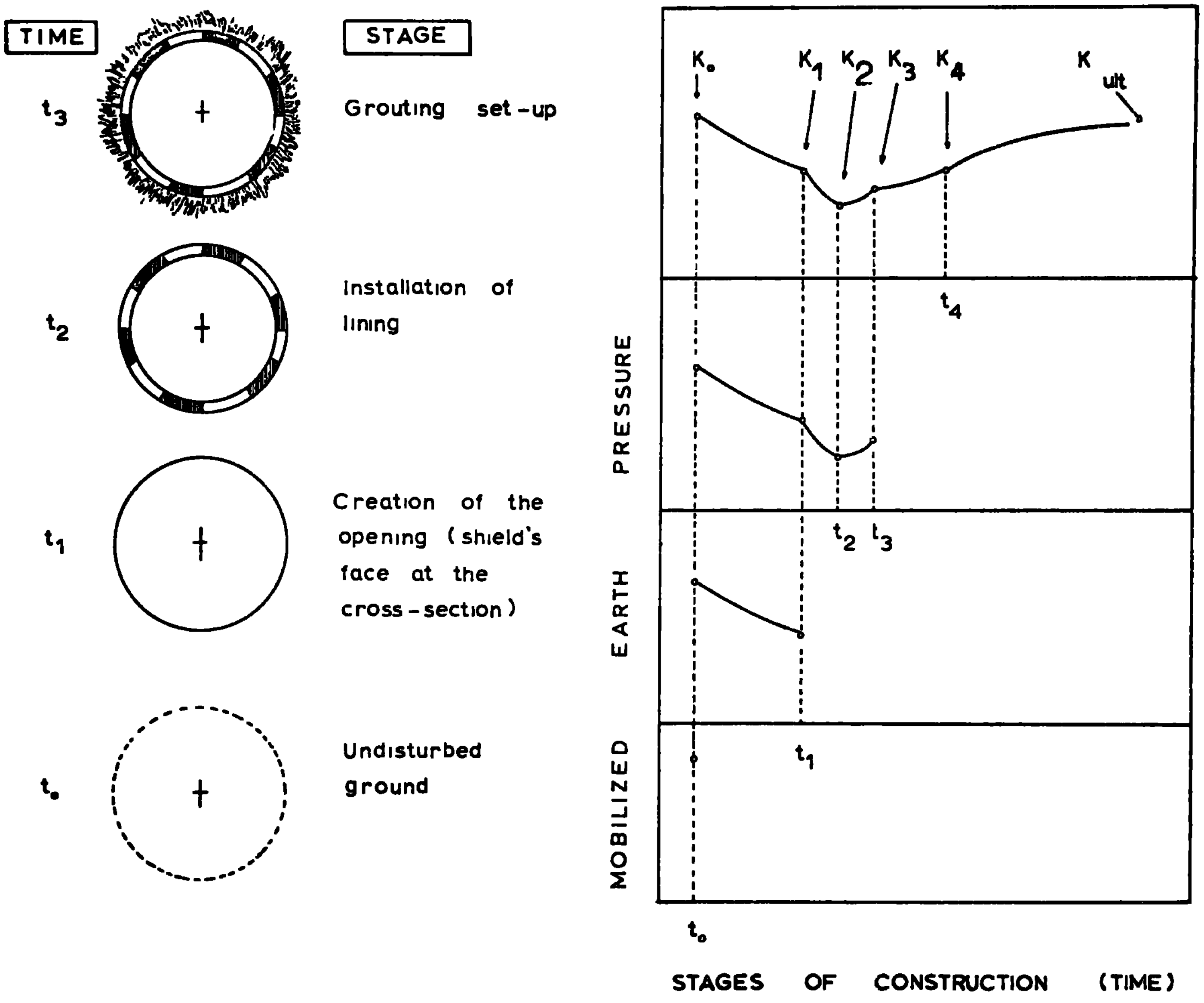

FIG. 7.4.1. Hypothetical mobilization of earth pressure for an element of clay at tunnel axis level during the various stages of construction.

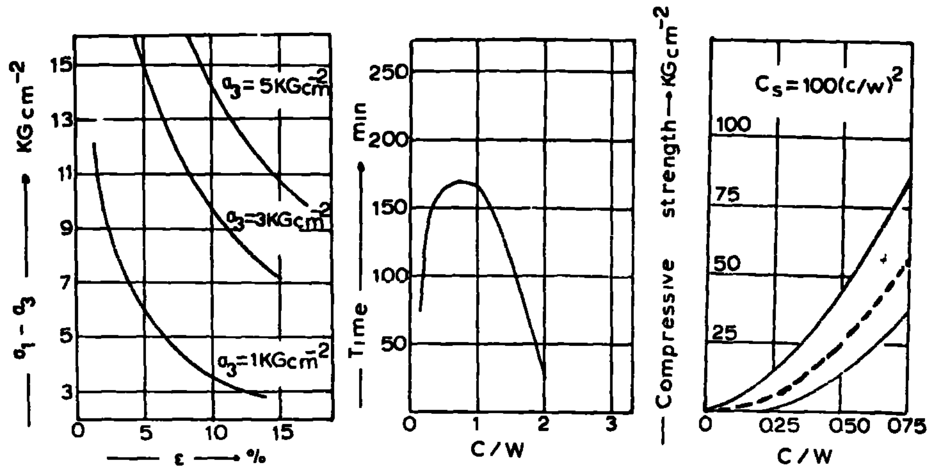

Stress - strain curves for grout being in the plastic state

Solidification time for grout with different cement to water ratios

Compressive strength as a function of the c/w ratio

FIG 811 Some grout properties After CARON (1973)

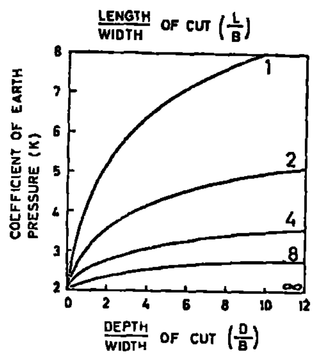

COEFFICIENTS OF EARTH PRESSURE FOR RECTANGULAR CUTS IN CLAY

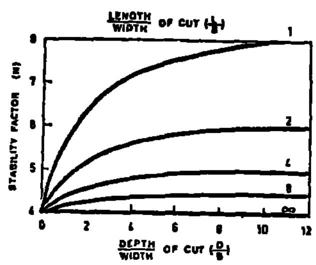

STABILITY FACTORS FOR RECTANGULAR CUTS IN CLAY

FIG 812 a Stability factors of a slurry trench as function of its geometry After, MEYERHOF (1972)

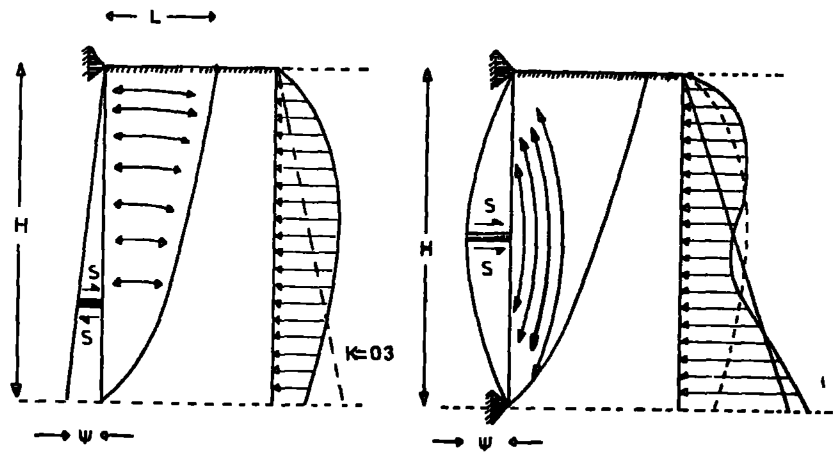

FIG 812 b Horizontal and vertical arching behind flexible retaining structures After TSCHEBOTARIOFF (1951)

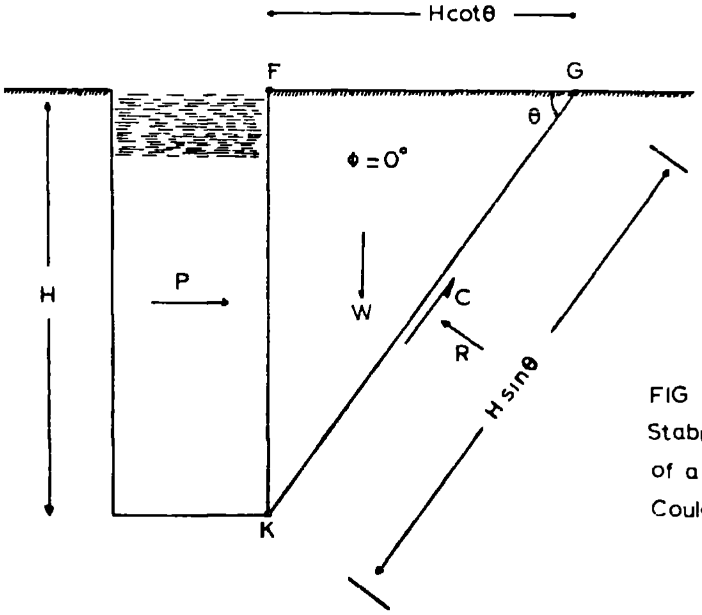

FIG 8 21
Stability analysis of a two-dimensional Coulomb wedge

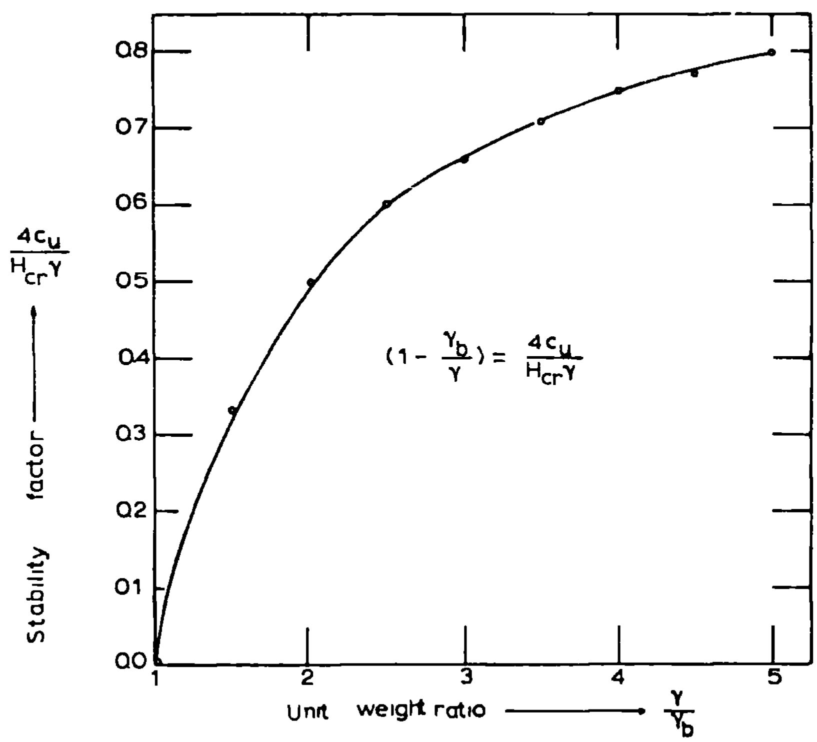

FIG 8 2 2
Relationship between the stability factor and the unit weight ratio

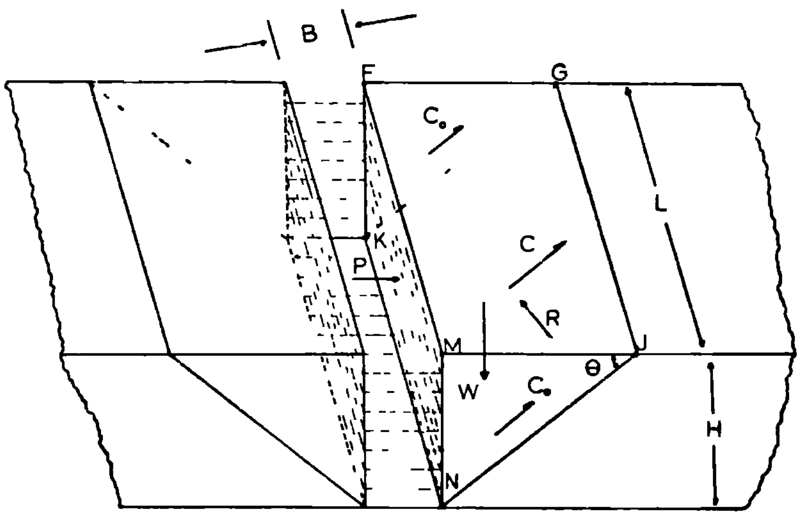

FIG 8.23 Stability analysis of a three-dimensional Coulomb wedge

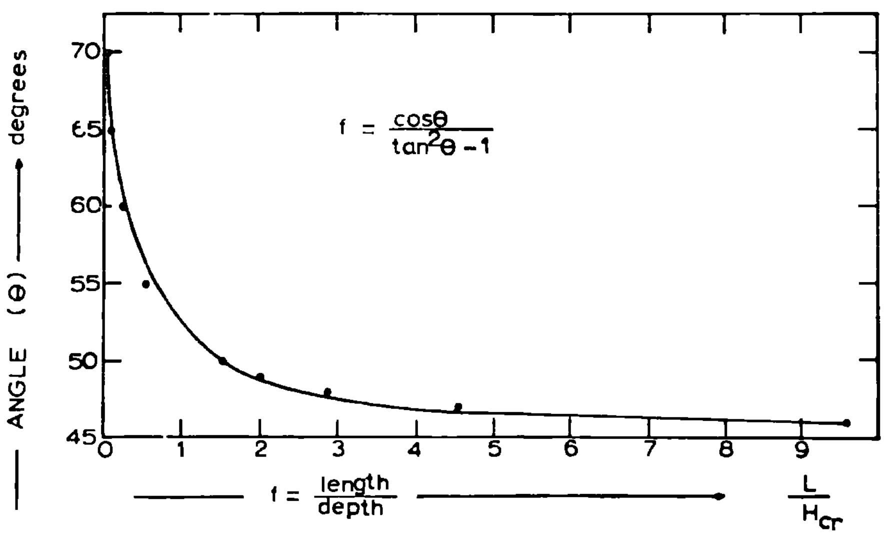

FIG 8.2.4
Relationship between the length/depth ratio, and the angle θ
(after PRATER, 1973)

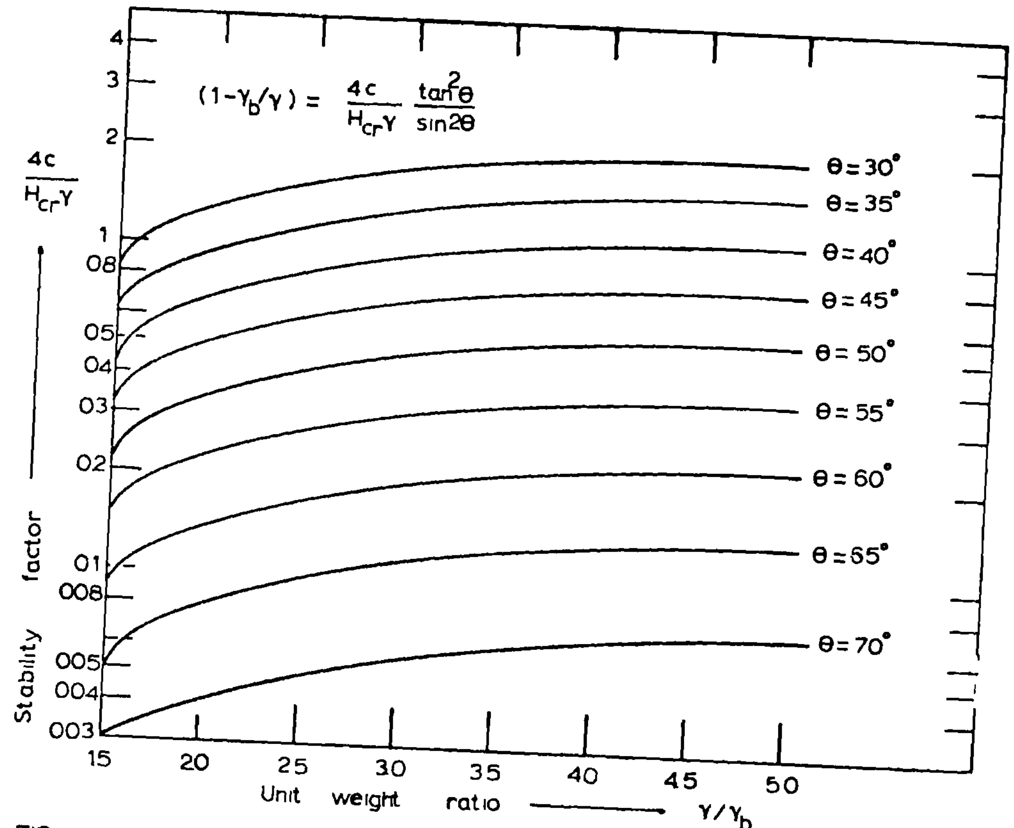

FIG 8 2 5 Relationship between the stability factor and the unit weight ratio, for various values of the angle theta

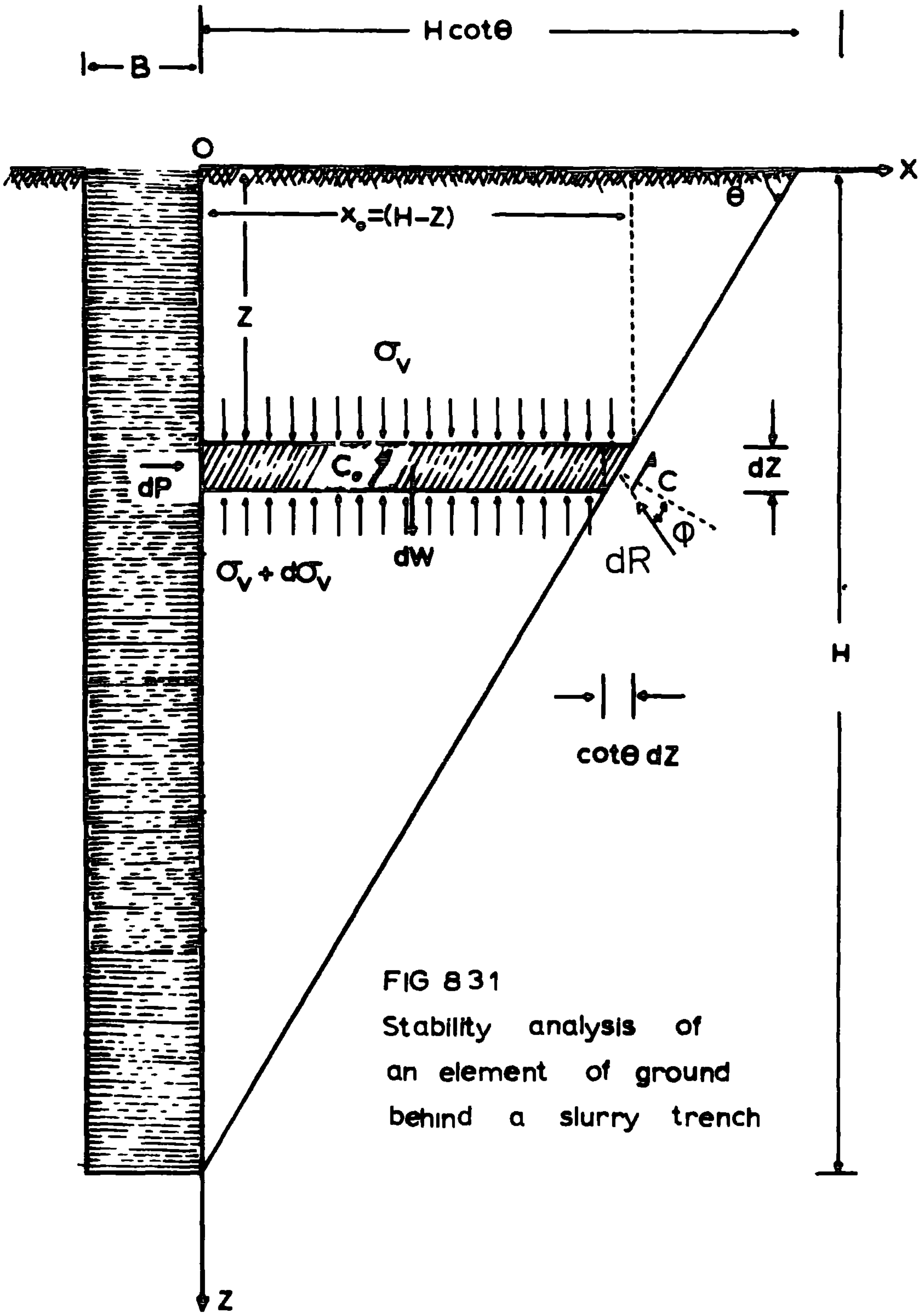

FIG 8.31
Stability analysis of an element of ground behind a slurry trench

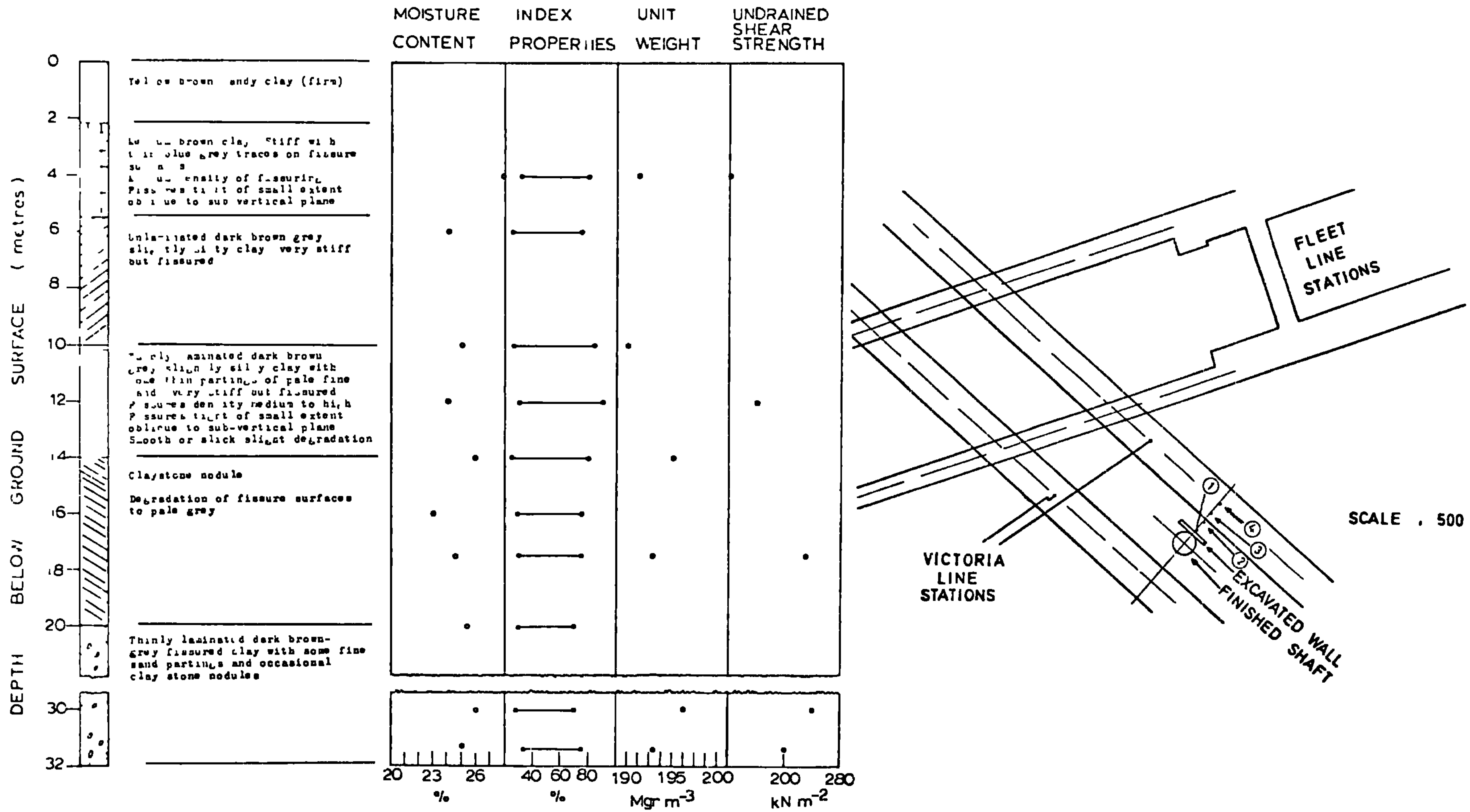

FIG. 9.2.1. Site plan (after ATTEWELL and FARMER, 1972) geology and soil properties as determined by laboratory tests.

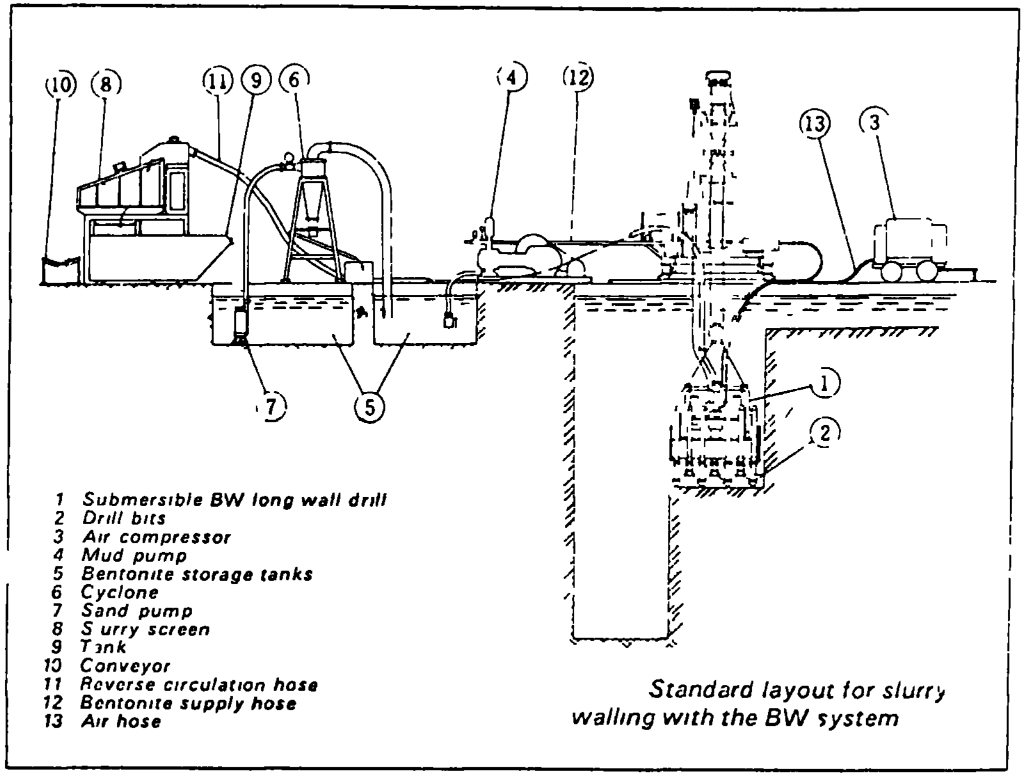

FIG. 9.3.I. Support and excavation System, after "GROUND ENGINEERING", (I977).

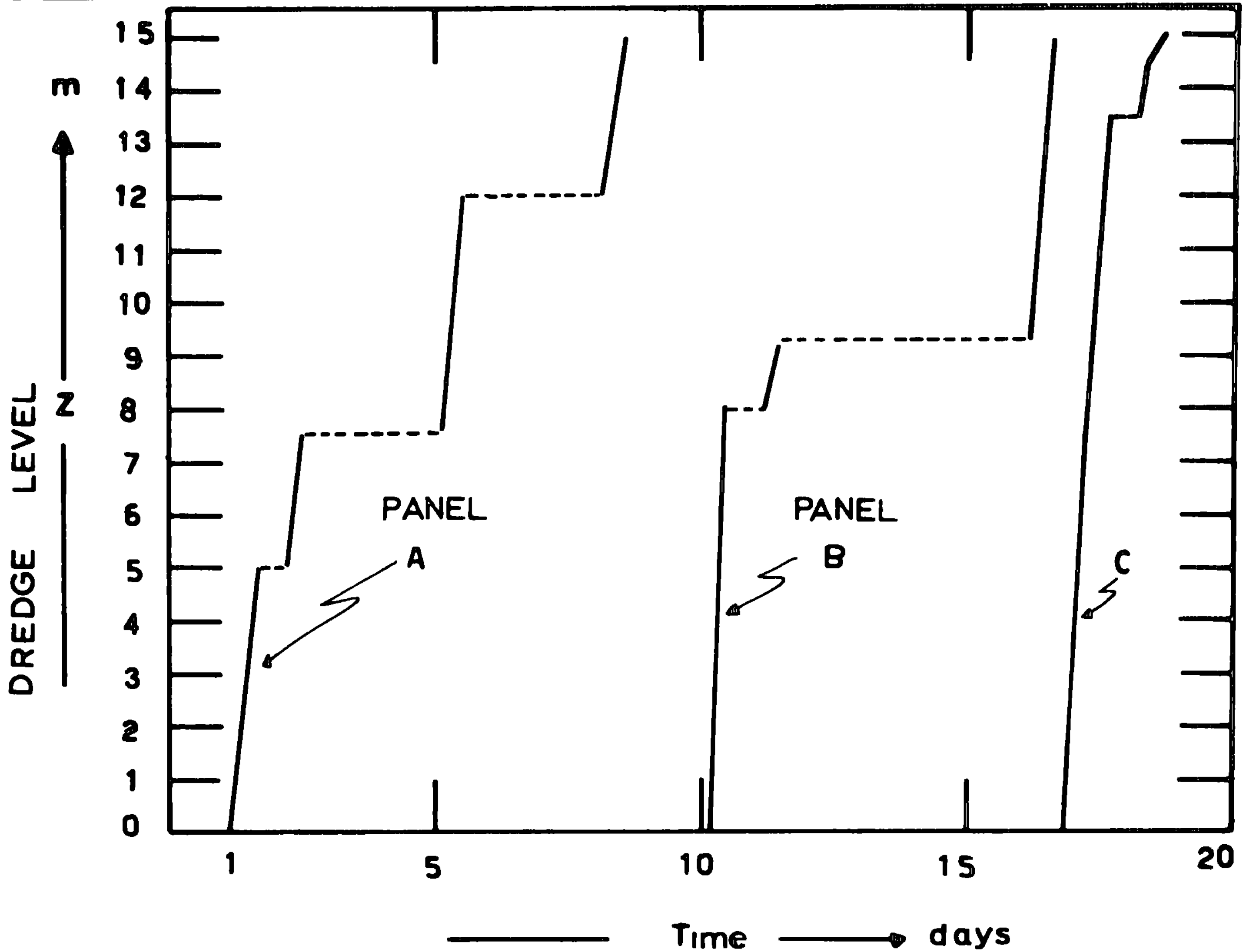

FIG. 9.3.2. Excavation progress. After, ATTEWELL and FARMER, (1972)

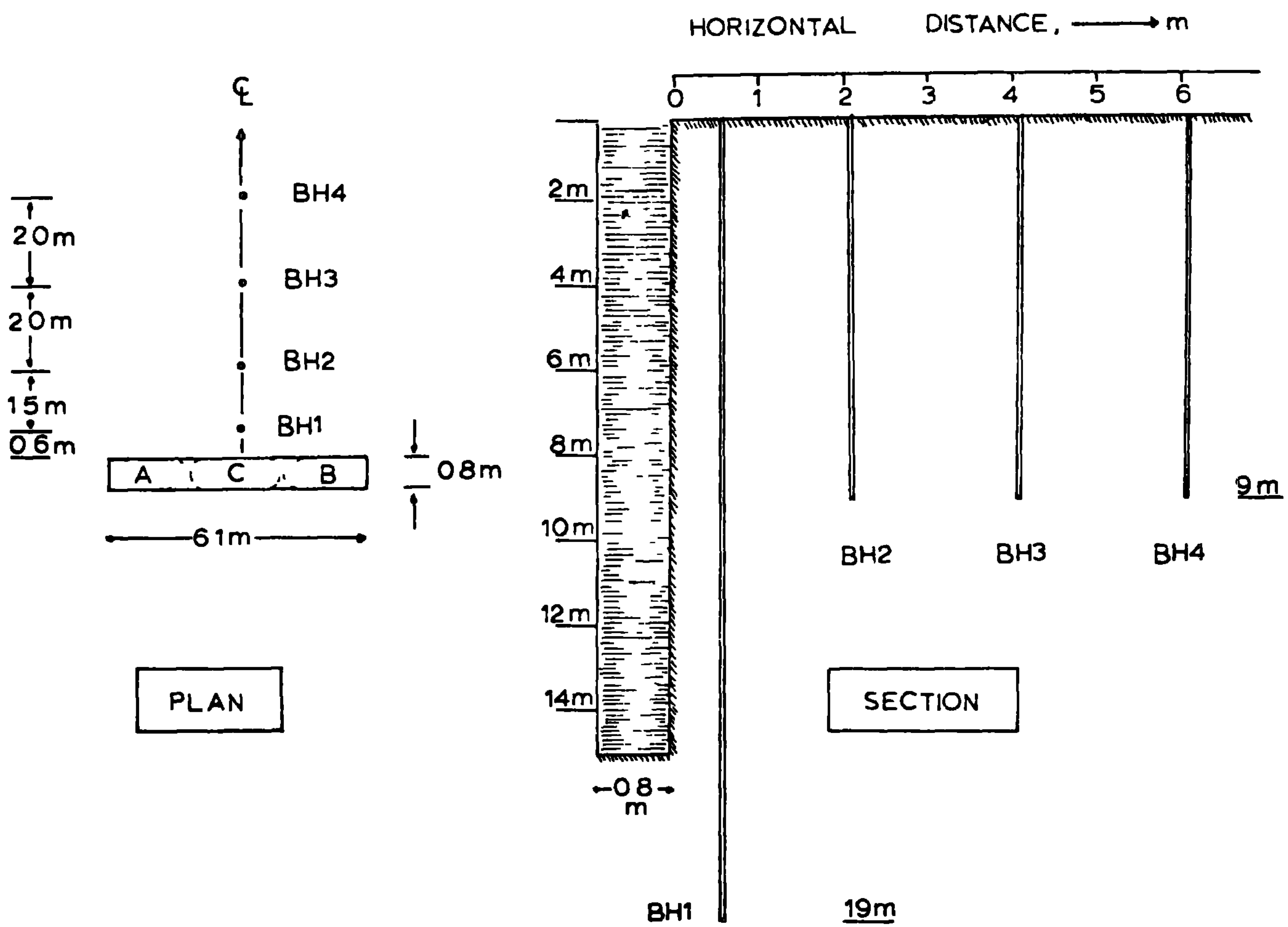

FIG 9 4 1 Boreholes layout.

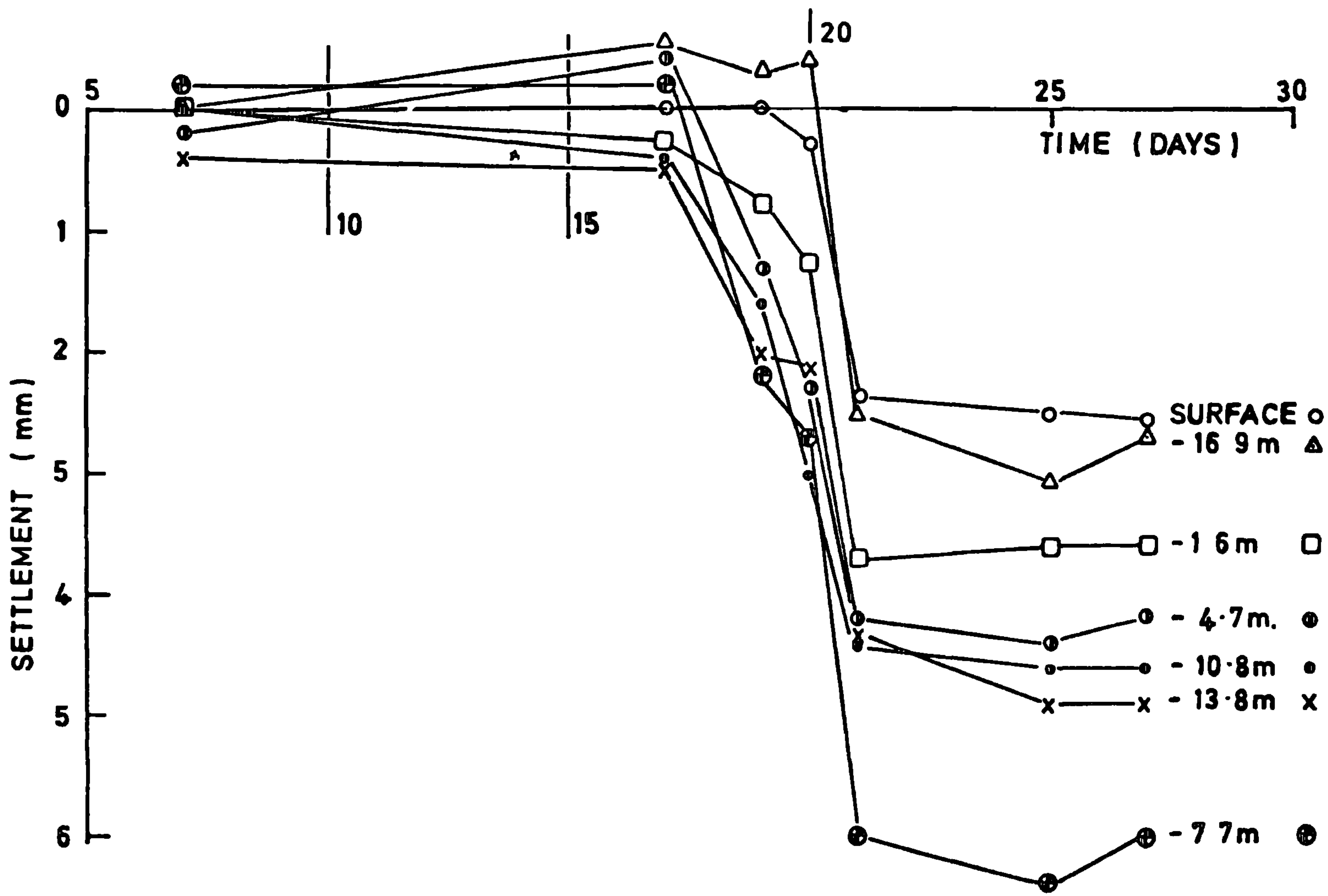

FIG. 9.5.I. Surface and subsurface settlement development curves. After, ATTEWELL and FARMER, (I972)

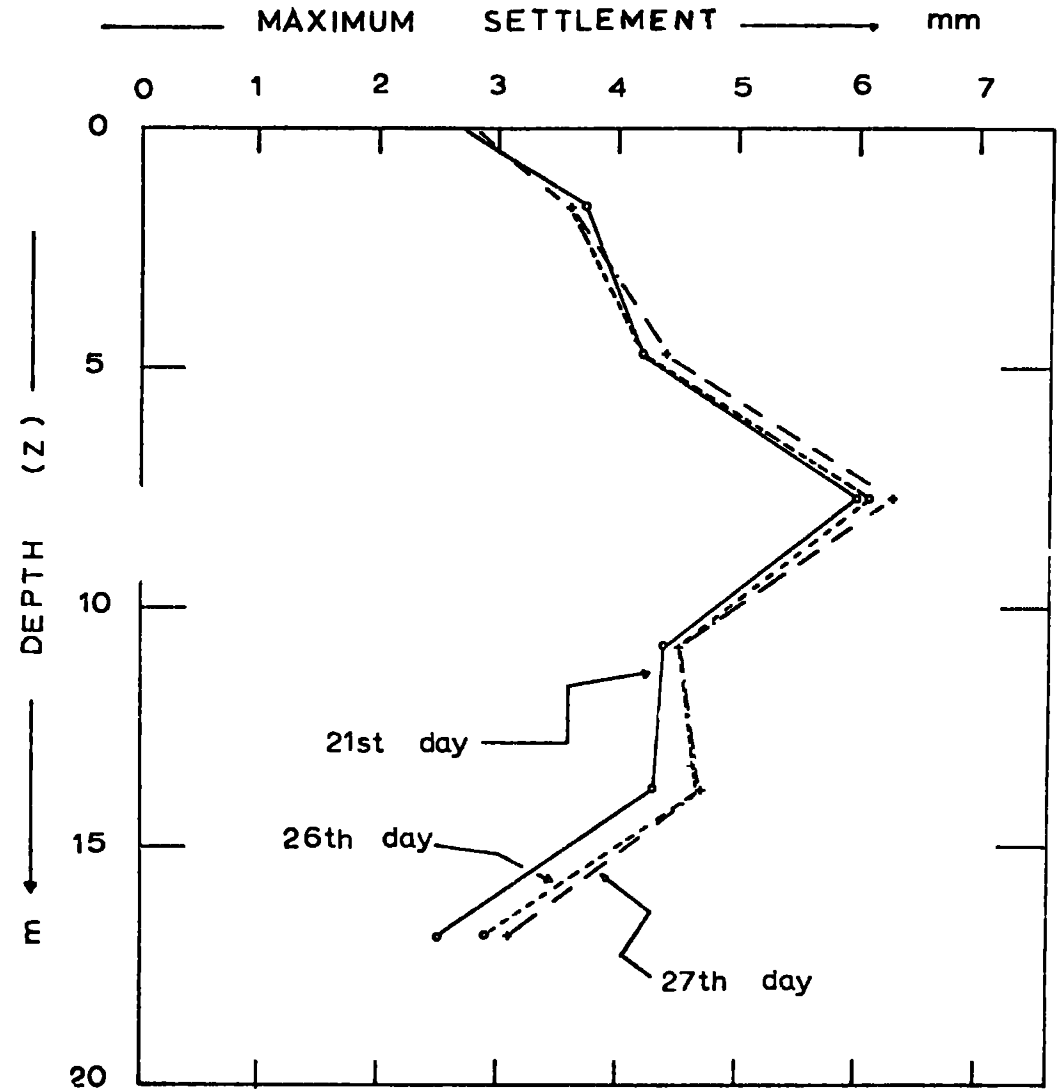

FIG. 9.5.2. Development of maximum settlement with depth below ground surface. Borehole BHI.

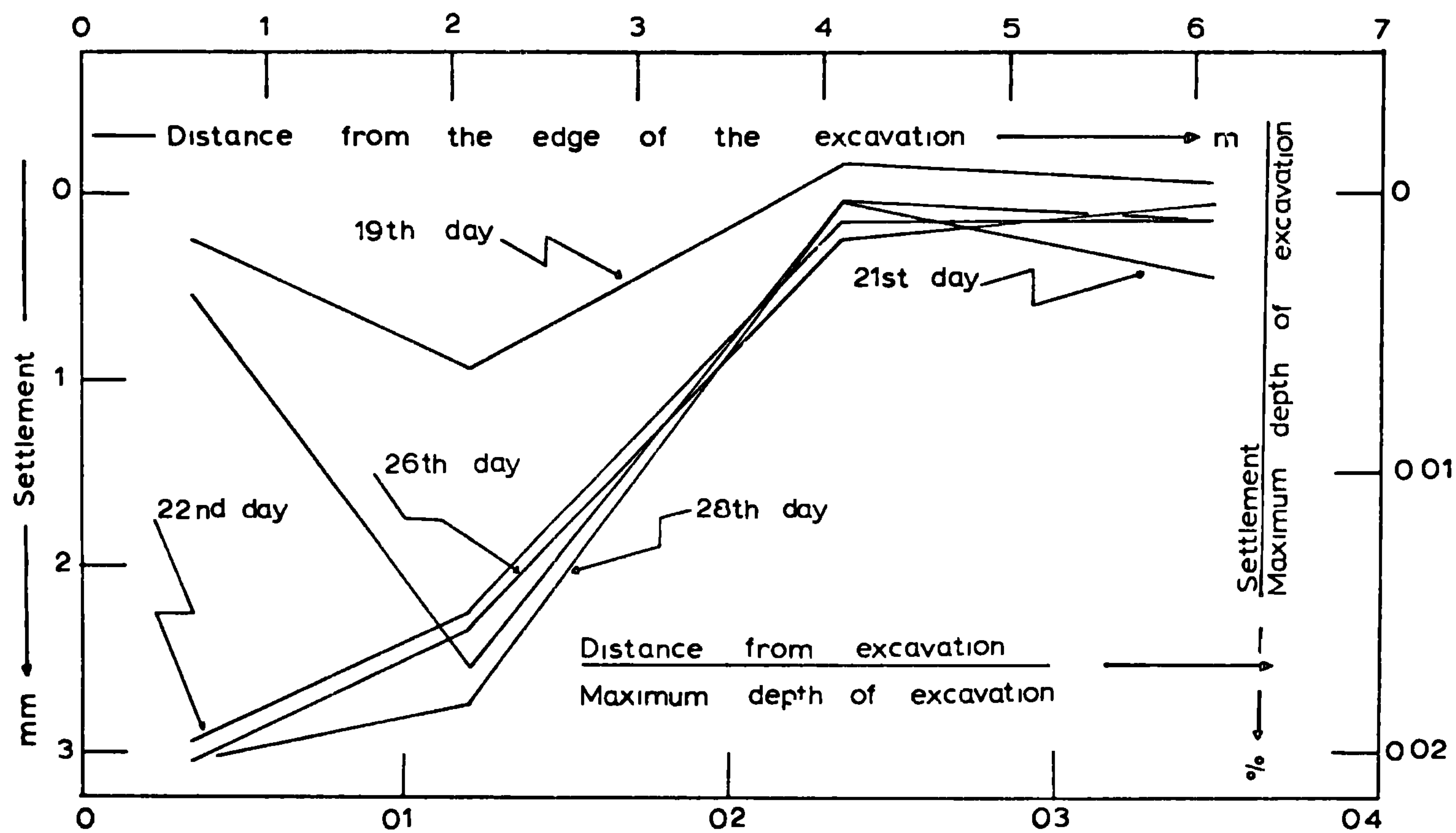

FIG 9 5 3 Transverse surface settlement profile at various times

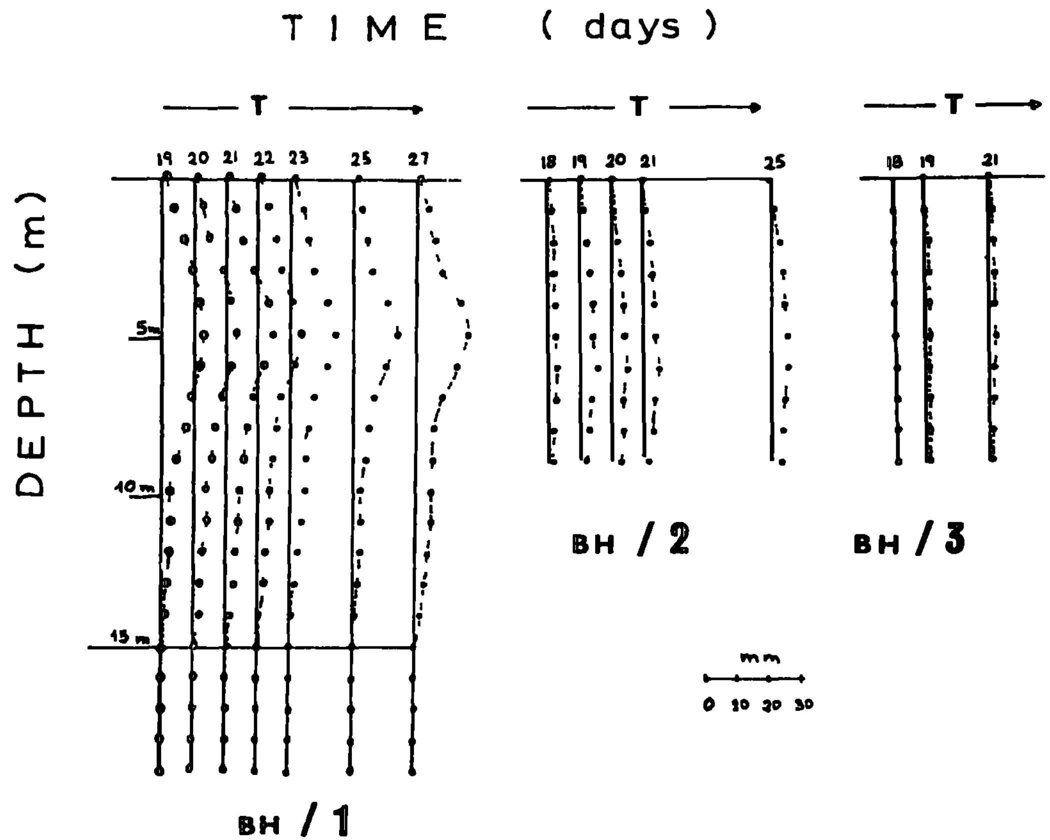

FIG. 9.5.4. Evolution of lateral deflection profiles at various times. After, FARMER and ATTEWELL, (1973)

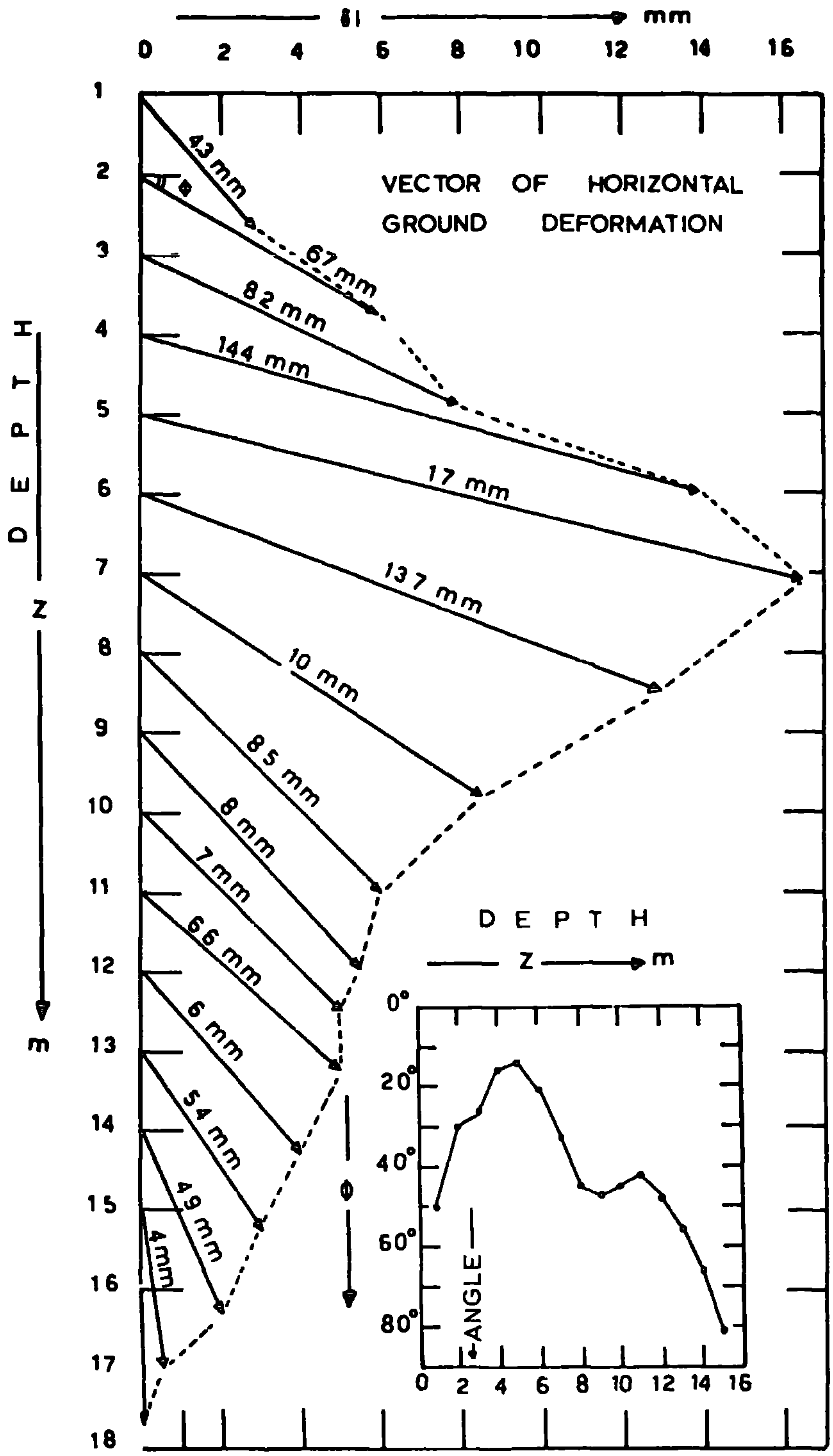

FIG 9 5 5 Two dimensional vector representation of ground movements in borehole BH1

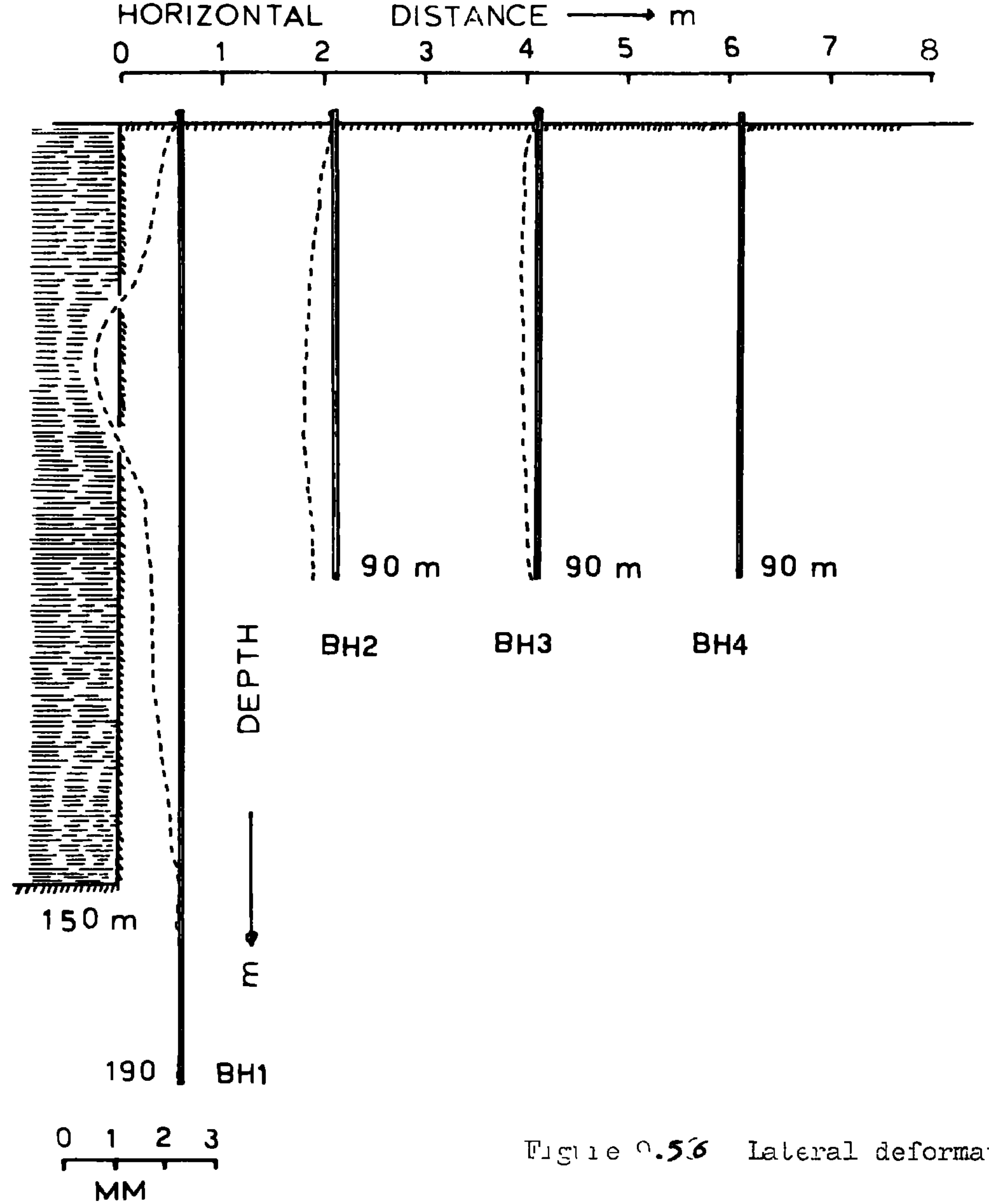

Figure ?.56 Lateral deformation profile

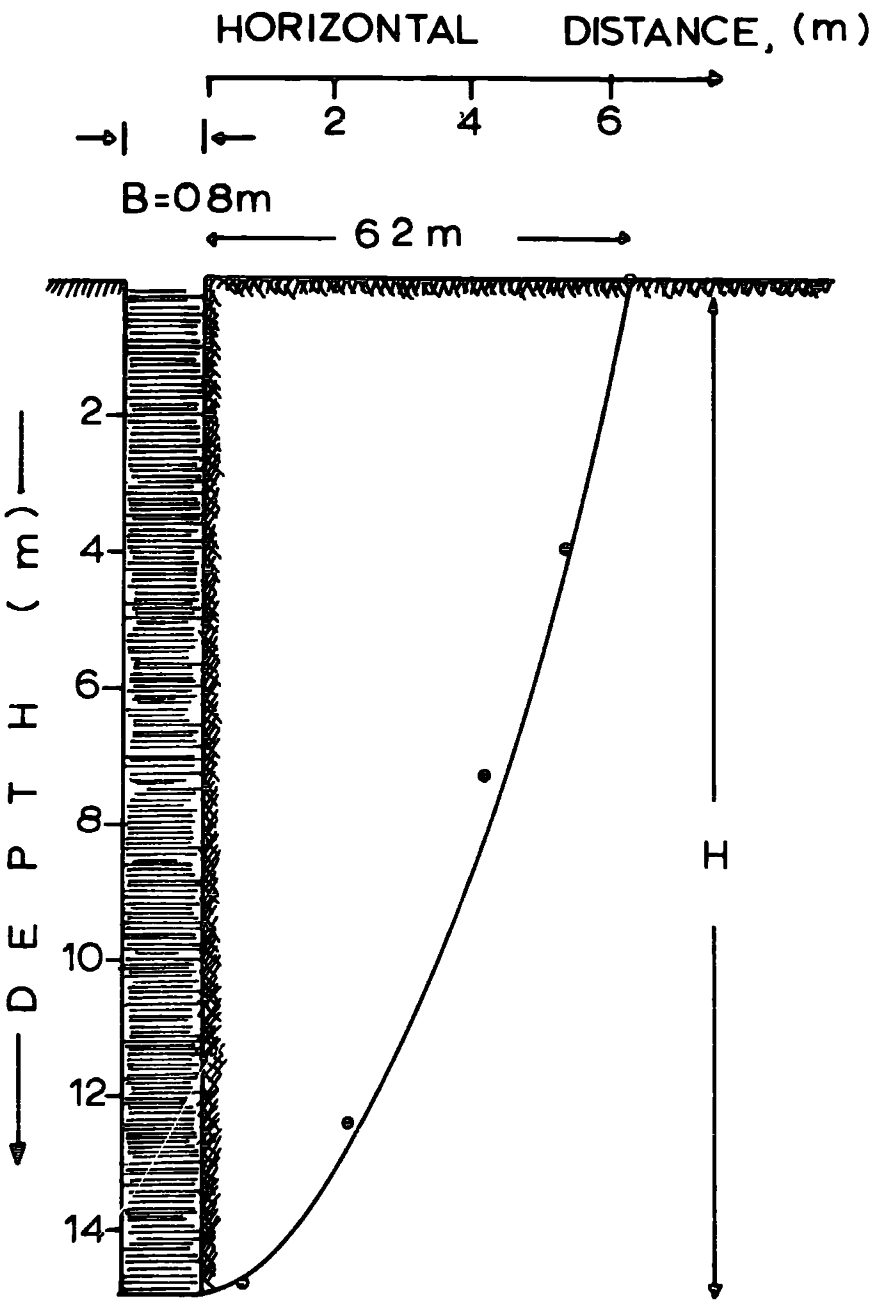

FIG. 9.5.7. Hypothetical shape of the ground affected zone.

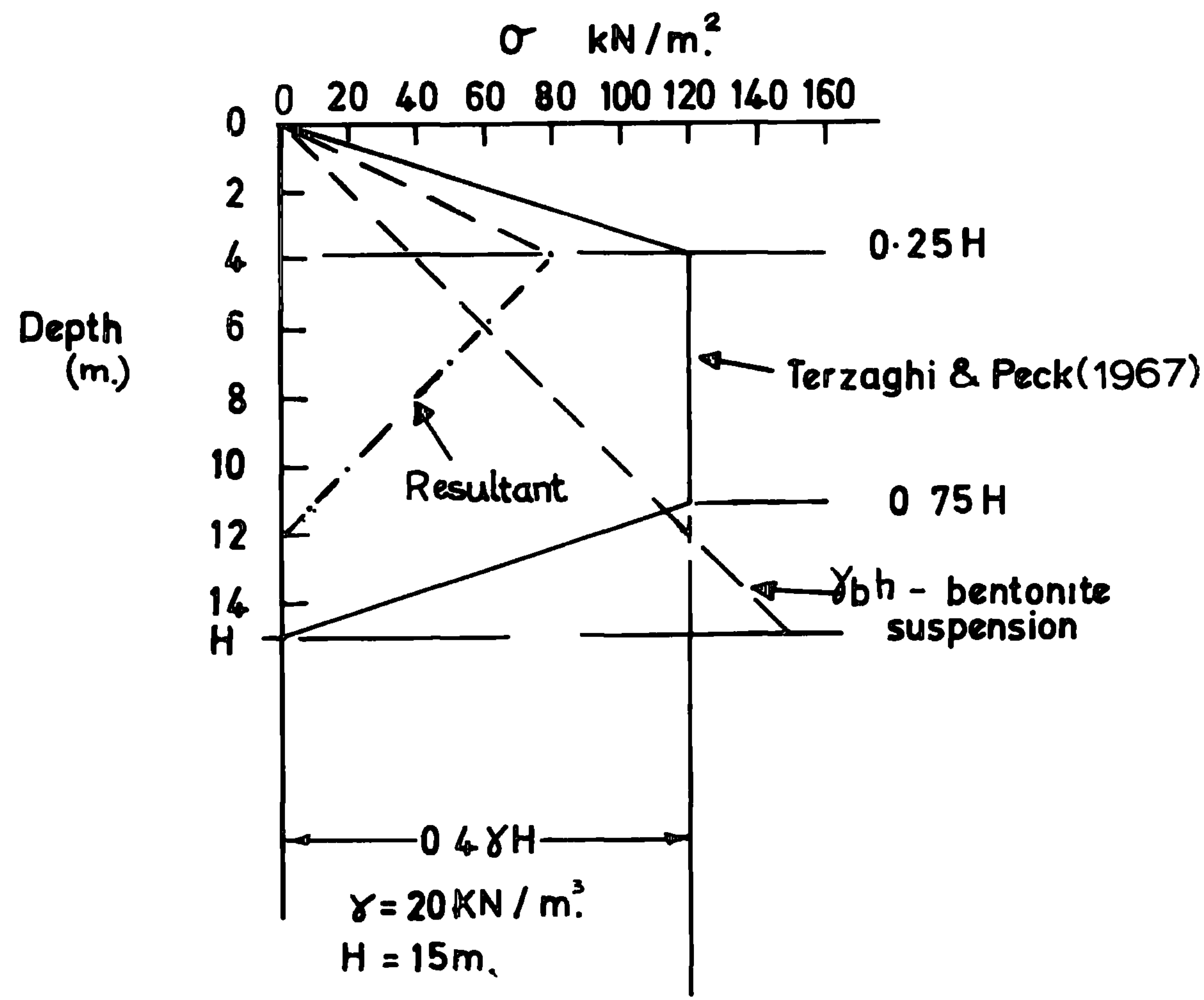

FIG. 9.6.I. Resultant pressure distribution in the excavation sidewall. After, FARMER and ATTEWELL, (1973)

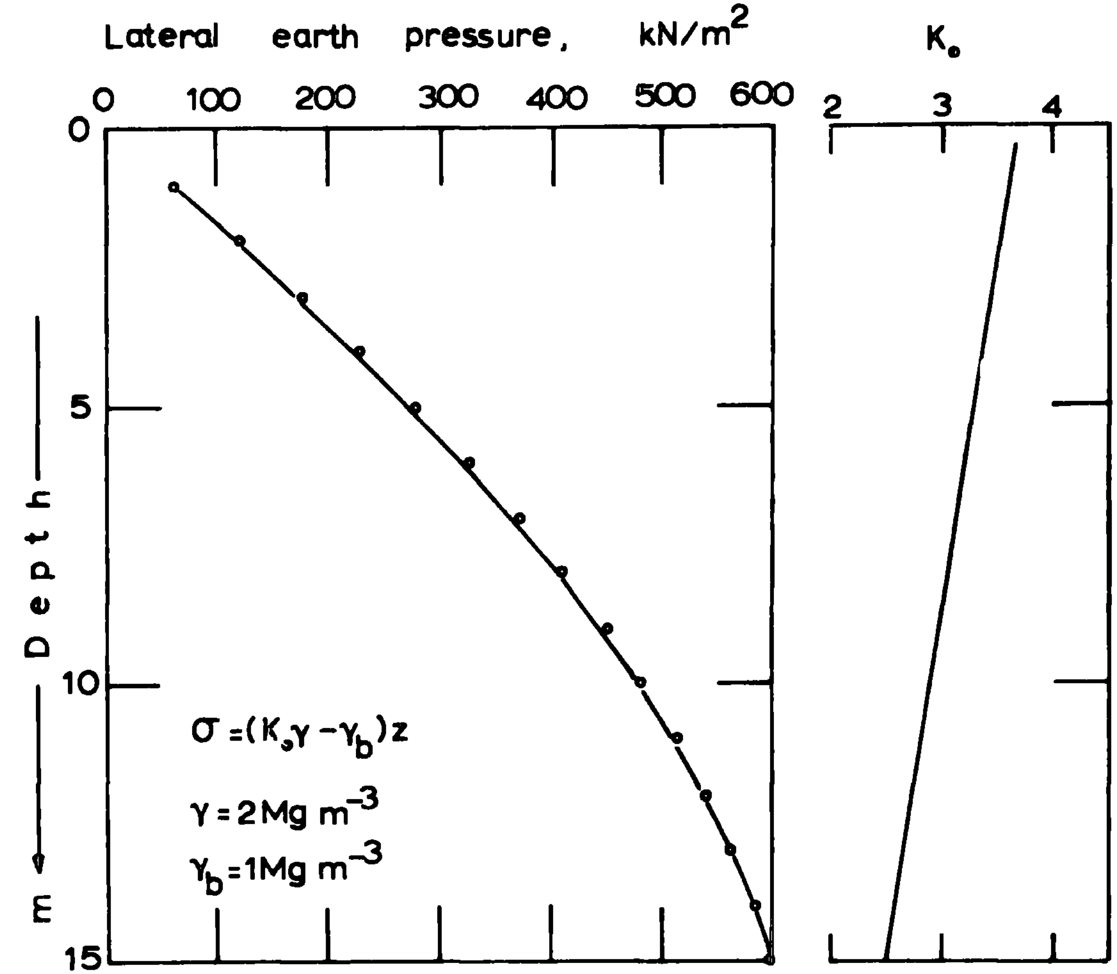

FIG. 9.6.2. Earth pressure distribution calculated from MEYERHOF'S, (1972) approach. The K_o versus depth linear function is taken from COLE and BURLAND, (1972).

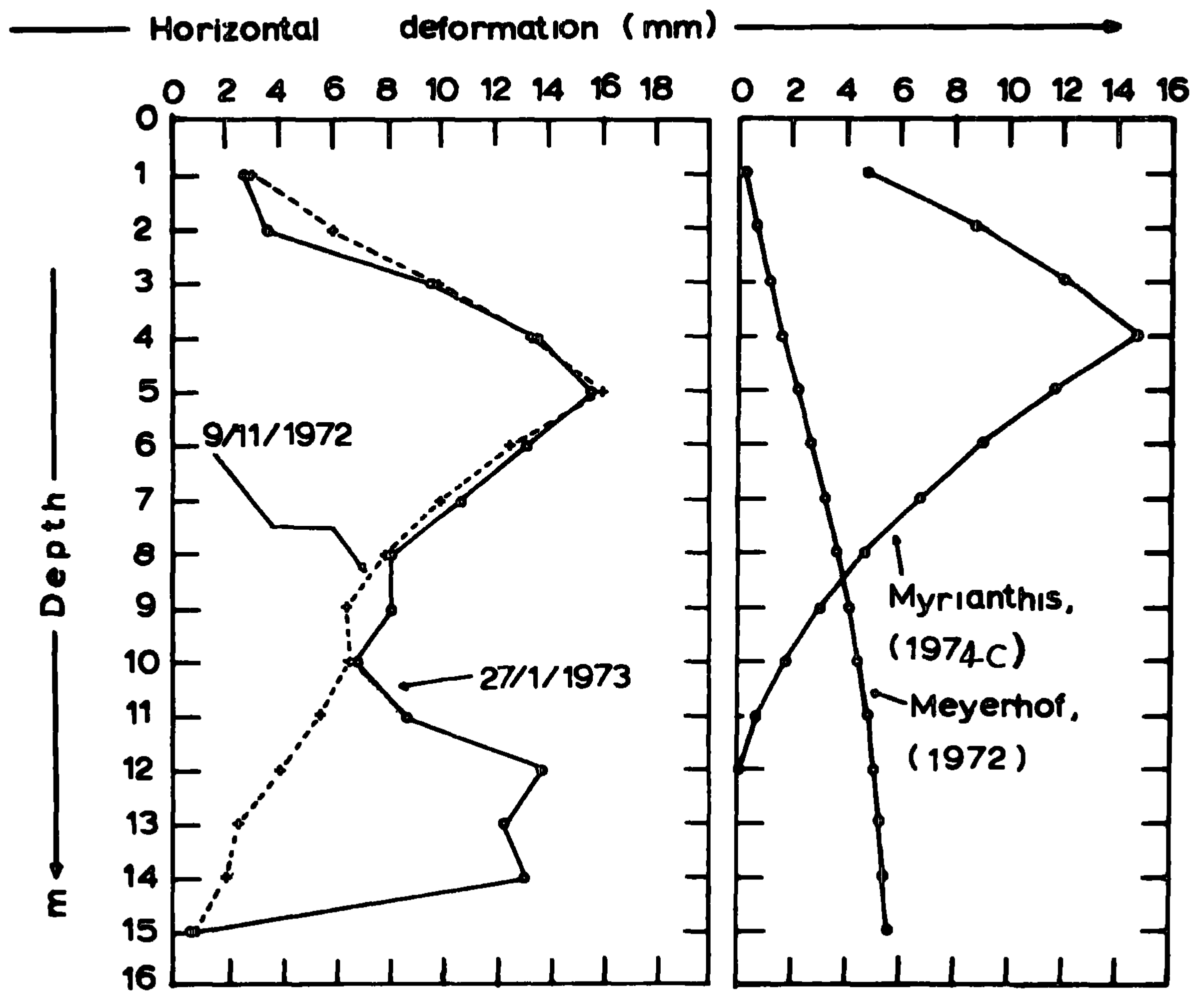

FIG. 9.7.I. Comparison between the actual (left), and the calculated (right) horizontal deformation profile. Borehole BHI.

APPENDICES

(1, 2, 3 & 4)

APPENDIX 1.

PROTODYAKONOV'S DE-COUPLED ARCH

The arching theory developed by PROTODYAKONOV(see SZECHY, 1967) is based on the determination of the natural arching geometry development above a tunnel, neglecting the effect of depth. The stability of such an arch is established when the stresses along the arch are purely compressive and are not associated with bending. Figure A.1.1. illustrates the geometry and the forces acting upon the arch.

SZECHY (1970) presented a detailed analysis from which the calculation of the surface settlements due to shield tunnelling in cohesionless soils was possible. The dominant assumption in the analysis was the equivalence between the volume of the settlement profile and the sum of the volume of material entering at the face, the volume of annular void behind the lining created by the tailskin and the volume resulting from the void created by the material compression within a PROTODYAKONOV de-coupled arch. However, as the shield is advanced and the primary lining is built within the tailskin, there is a loosening of the soil mass as it collapses to fill the void around the lining as the shield moves forward. Very early injection with grout or pea gravel when shoving of the last ring of segments will reduce this value of void thickness, say u_o, by some factor.λ The maximum thickness of the annular void will be due to the thickness of the shield bead plus any slackness between the inner surface of the skin and the lining extrados.

Let the double shield skin thickness be 2δ , and the slackness be Δ. Then $u_o = 2\delta + \Delta$, or taking into account the void reduction factor λ ,

$$u_o = \lambda (2\delta + \Delta) \qquad \text{.....(A.1.1.)}$$

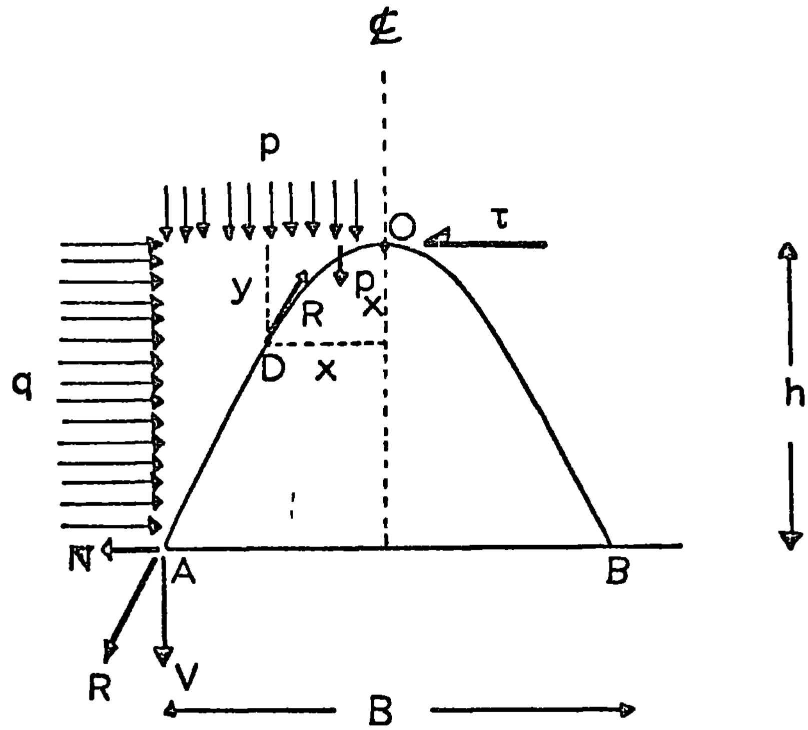

Area of the parabola : $\frac{2}{3}Bh$

Load per unit area : $\frac{1}{3}\frac{\gamma B^2}{\tan\varphi}$

FIG. A 11

Development of Protodyakonov's theory of roof arching.

This void will cause loosening of the soil mass above the tunnel crown and arching effects will develop up to a limiting horizon. The whole transverse profile and settlement geometry due to the pressure arch generation is shown in Figure A.1.2.

The geometric elements of the arch connected with the geometry of the transverse profile are as follows

<u>arch width</u> $$B = 2R(\operatorname{cosec}\beta + \cot\beta) \qquad \text{.....(A.1.2.)}$$

<u>arch height</u> $$h = \frac{2R(\operatorname{cosec}\beta + \cot\beta)}{2\tan\phi} \qquad \text{.....(A.1.3.)}$$

or, $h = \dfrac{\text{arch width}}{\tan\phi}$ for a cohesionless material.

It is possible to calculate the compressive settlement of the detached parabola of soil due to its graviational pressure. The average pressure acting vertically downwards through gravitational self-weight equals $\gamma h/2$. The average strain in the soil is

$$\frac{\text{decrease in height}}{\text{original height}} = \frac{u_1}{h}.$$

Therefore, $$u_1 = \frac{\gamma h^2}{2E} \qquad \text{.....(A.1.4.)}$$

where,

γ is the soil density which is taken as being independent of depth

u_1 is the de-coupled displacement at the crown of the parabola

E is the deformation modulus.

Combining the equations,

$$u_1 = \frac{\gamma R^2(\operatorname{cosec}\beta + \cot\beta)^2}{2E\tan^2\phi} \qquad \text{.....(A.1.5.)}$$

Thus, u_1 defines the boundary of the rupture zone, that is, the boundary delimiting those shear stresses which exceed the shear strength of the mass.

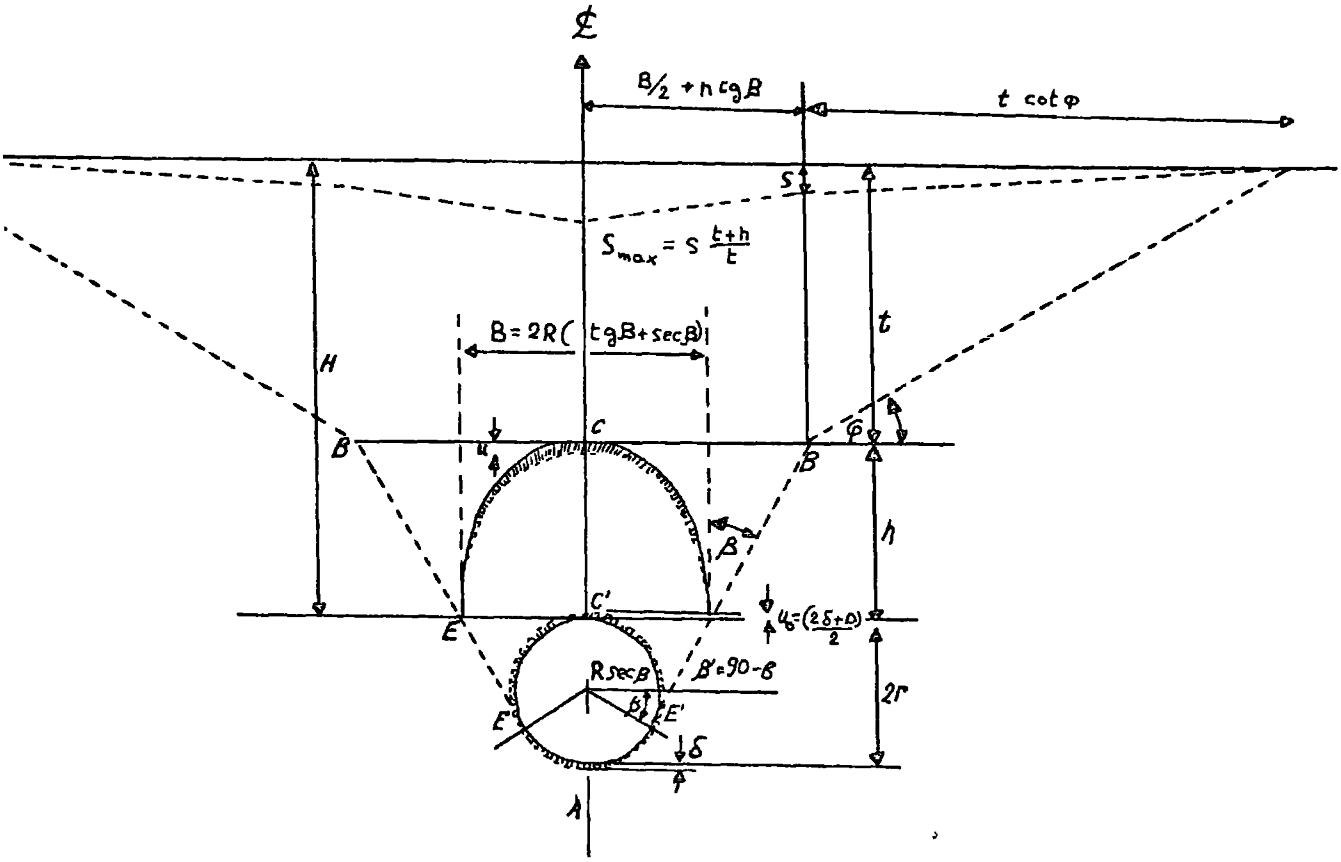

FIG A12
Transverse profile and subsidence due to pressure arch generation above a cavity
(after K SZÉCHY , 1970)

Beyond this parabolic area, the deformations result from shear stresses that are less than the shear strength of the mass. SZECHY, op cit suggests that for a cohesionless material, the deformation zone above the de-coupled arch will be de-limited by the surface rising at an angle Ø degrees from the horizontal. The argument is that the intersection of these surfaces with the ground surface fixes the full extent of the subsidence trough. But it must be appreciated that this form of analysis is rather specific with respect to the particular geology associated with the Metro construction in Budapest.

APPENDIX 2

RELATIONSHIP BETWEEN THE SHEAR STRENGTH AND DEPTH OF A SOIL WITH A LINEAR MOHR ENVELOPE

For a soil with a linear Mohr envelope, shear strength increases linearly with depth from the ground surface. (after SZECHY,1970).

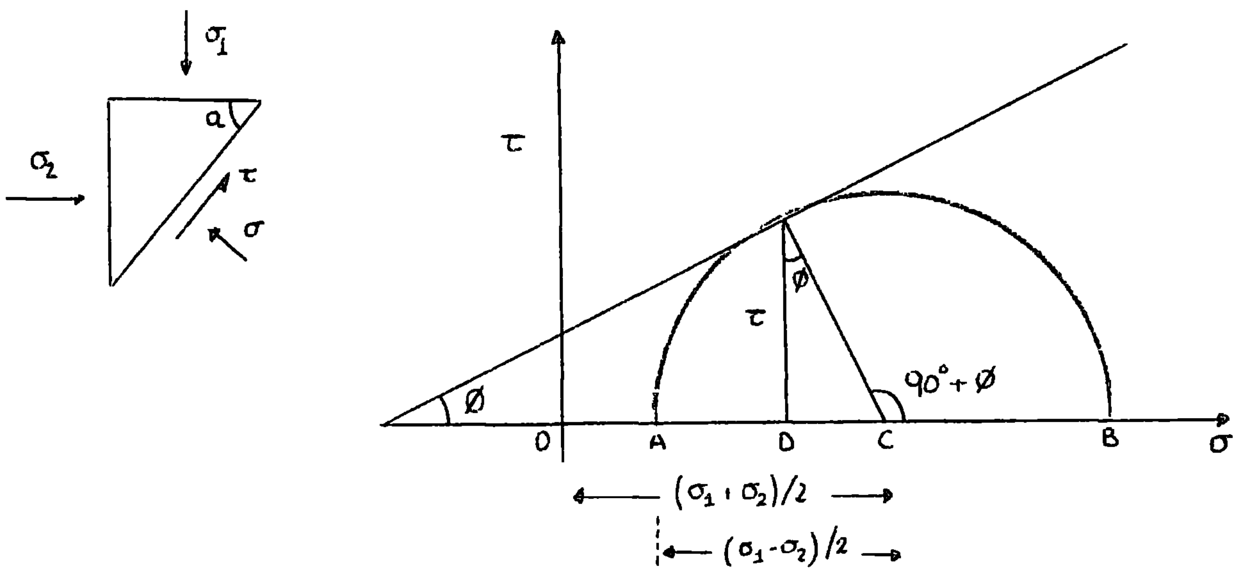

$$\sigma = \overline{OD} = \overline{OC} - \overline{DC} = \frac{\sigma_1 + \sigma_2}{2} - \frac{\sigma_1 - \sigma_2}{2} \sin\phi \qquad .....(A.2.1.)$$

$$\sigma = \sigma_1(1 - \sin\phi) + \sigma_2\,(1 + \sin\phi) \qquad .....(A.2.2.)$$

$$\text{if } \sigma_2 = \sigma_1 \; \frac{1 - \sin\phi}{1 - \sin\phi} \qquad .....(A.2.3.)$$

$$\text{then } \sigma = \sigma_1\,(1 - \sin\phi) \qquad .....(A.2.4.)$$

$$\text{but given that } \sigma_1 = \gamma z \qquad .....(A.2.5.)$$

Thus, from equations 4.2.4. and 4.2.5. it follows that.

$$\sigma = \gamma z\,(1 - \sin\phi) \qquad .....(A.2.6.)$$

and finally,

$$\underline{\underline{\tau = C + \tan\phi\,\gamma z\,(1 - \sin\phi)}} \qquad .....(A.2.7.)$$

This relationship indicates that shear strength is a linear function of depth.

Appendix 3a Tunnelling in stiff plastic clay

CASE	NO	REFERENCE	Z m	2R m	Z/2R	s_{max} mm.	s_{max}/R x 10^{-3}	V_{exc} m^3/m	V_{surf} m^3/m	V %	TUNNELLING METHOD	SOIL CONDITIONS
Fleet Line, London (U.K.)	1	Attewell and Farmer (1972)	30.3	4.14	7.32	6.65	3.21	13.52	0.161	1.19	Hand mined shield	Stiff fissured clay (London clay) c_u = 266 kN/m^2 (vertical sample) c_u = 411 kN/m^2 (horizontal sample)
Ottawa Sewer (Canada)	2	Eden and Bozozuk (1969)	18.3	3.05	6.06	7.00	4.59	7.25	0.116	1.60	Digger-shield, liner segments erected behind the shield	Leda Clay (sensitive) 9_u = 361 kN/m^2, OFS = 1 5
Ottawa Sewer (Canada)	2'	Schmidt (1969)	18.3	3.05	6.06	6.35	4.16	7.30	0.106	1.46	"	Over-consolidated clay c_u= 178 kN/m^2, overc.ratio 2.5 4.3
Victoria Line, London (U.K.)	3	Bartlett and Bubbers (1970)	21.8	4.115	5.297	9.00	4.37	12.54	0.171	1.36	Hooded, hand excavation shield	Over-consolidated clay (London clay) c_u = 170 kN/m^2, W = 25%
"	4	"	21.8	4.115	5.297	10.00	4.86	12.54+	0.190+	1.50	"	"
"	5	"	17.0	4.115	4.131	13.00	6.32	12.54+	0.234	1.87	"	" c_u = 145 kN/m^2
Broadway Oakland (U.S.A)	6	Kuesel (1969)	-	5.79	3.22	25.3	8.74	-	-	-	-	very stiff moist coarse sandy clay, very dense clayey sand
Garrison Dam Tunnel (U.S.A)	7	Burke (1957)	36.9	11.0	3.35	42.6	7.75	95.03	1.49	1.5	Construction by full face blasting, use of ribs and lagging	Hard clay, clay shale, c_u = 488 kN/m^2
Victoria Line, London (U.K.)	8	Bartlett & Bubbers (1970)	17.5	6.02	2.916	37.0	12 29	26.98*	0.421+	1.56	By hand without shield	Overconsolidated clay (London clay) C_u=145 kN/m^2
"	9	"	17.5	6.96	2.514	37.0	10.63	26.98*	0.421+	1.56	Shield tunnel, hand exc.	"
"	10	"	17.5	6.96	2.514	50.0	14.37	25.08*	0.565	2.25	"	"
"	11	"	21.0	9.525	2.201	88.0	18.48	71.25	1.410	1.98	Shield hooded, hand exc	Boulder clay c_u = 250 kN/m^2
Chicago Subway D-3 (U.S.A.)	12	Peck (1969)	23.5	7.32	3.21	81.0	22.5	48.4	1.91	3.95	Hand mined horshoe, face benched ribs and liner plates.	Chicago Glacial clay. c_u = 73.4 kN/m^2
San Francisco Bart, Market str. (U.S.A.)	13	"	18.0	5.34	3 37	79.3	29.7	22.0	1.395	6.20	shield breasted face	Medium to stiff clay
Victoria Line, London (U.K.)	14	Dunton et al (1965)	15.86	3.66	1.54x	61.0	33.0	21.90	1.16	5.50	Shield tunnel	London clay
GNNR, Seattle (U.S.A.)	15	Hussey et al (1915)	36.7	12.0	3.06	25.9	4.32	126.0	3.86	3.06	Hand mined, small drifts with centre core, timbered	Hard clayey till

* combined face area of a complex tunnel
\+ mean value
x $Z/\ 2(R + \frac{cc}{2}) = 1.54$, cc = 6.6m.

Appendix 3b Tunnelling in saturated plastic clay

CASE	NO.	REFERENCE	Z m	2R m	Z/2R	s_{max} mm.	s_{max}/R x 10^{-3}	V_{exc} m^3/m	V_{surf} m^3/m	V %	TUNNELLING METHOD	SOIL CONDITIONS
San Francisco Bart (U S.A.)	26	Peck (1969)	18.0	5.50	3.275	61.0	22.18	23.76	1.022	4.3	Shield, breasted face	Moderately sensitive clay
Tunnel in Poland	27	Knothe (1959)	30.5	6.00	3.33	48.0	16.0	36.0	0.60	1 7	-	Plastic clay
Tokyo Kyoto (Japan)	28	Peck (1969)	22 6	7.00	3 23	183 0	50.29	38 48	1.655	4.3	-	Normally loaded sensitive clay
Tyholt Tunnel (Norway)	29	Hartmark (1964)	20.0	7.8	2.56	650.0	166.67	50 0	15.0	30.0	Shield, Hand-mined.	Sensitive clay with silt layers. 9u = 45 to 60 kN/m^2
Toronto Subway Contract B-4,b (Canada)	30 31	Peck (1969)	12.8	5.19	2 30 2.45	10.4	4.01	22 3	0.13	0.6	Shield, hand-mined.	Silty clay 9u = 55 kN/m^2
Chicago Subway Contract D-5 Station 191-20 (U S A.)	32	Terzaghi (1943)	11.9	6.10	1 95	41.9	13.74	37.2	0.5115	1.4	Hand-mined. Ribs and liner plates.	Glacial clay 9u = 50 kN/m^2
Chicago Subway Contract D-5 Station 192-20 (U S.A.)	33	"	11.9	6.10	1 95	35.6	11.67	37.2	0.437	1.2	"	" 9u = 50 kN/m^2
Chicago Subway Contract S-6 (U.S.A.)	34	"	11.0	6.10	1.80	71.0	23.28	37 2	0.855[x]	2.3	"	" 9u = 40 kN/m^2
Chicago Subway Contract S-5 (U S.A.)	35	"	11.0	6.10	1.80	134.5	44.1	37.2	1.64[x]	4 4	"	"
Tokyo, Teito Rapid transit route s (Japan)	37	Schmidt (1969)	13.5 to 18.5	6.75	0.64 to 0.88 *	68.0	6.50 +	76.0	1.46	1.9	Hand mined, in sections in shield. Face breasted.	Sensitive clay C_u = 30 kN/m^2
Tyneside Tunnel (U.K.)	37'	Attewell (1973) Attewell & Farmer(1975)	7.30	2.02	3.613	7.70	7.62	3.20	0.0774	2.4	Hand shield, concrete segmental linings with contact cement grout	Laminated clay

* $\frac{Z}{B} = \frac{Z}{2(R + \frac{cc}{2})}$

cc = centre to centre distance =13.2 metres

+ $\frac{s_{max}}{(R + \frac{cc}{2})}$

x = estimated

Appendix 3c- Tunnelling in granular soil

CASE	NO.	REFERENCE	Z m	2R m	Z/2R	s_{max} mm.	s_{max}/R x 10^{-3}	V_{exc} m^3/m	V_{surf} m^3/m	V_l %	TUNNELLING METHOD	SOIL CONDITIONS
Toronto Subway (Canada)	16	Peck (1969)	11.3 14.6	5.83	2.25*	93.3	32.01	22.0	0.42	1.9	Hand mined shield	Medium to fine uniform dense sand N= 40 60 above GWL
Toronto Subway II (Canada)	17	"	11.3 14.6	5.66	2.25*	110 0	38.9	-	-	-	"	"
San Francisco Bart Mission Line A (U.S A.)	18	"	12.33	5.83	2.11	13.3	4.56	22.32	0.15	0.15	Mechanical shield De-watering by wells	Cemented sand, peat layer, below GWL
San Francisco Bart Mission Line B (U.S.A)	19	"	12.00	5.83	2.06	10.0	3 4	44.64	0.14	0 7	"	Slightly cemented fine sand
Toronto Subway contract E-1 (Canada)	20	Schmidt (1969)	9 33	5 66	1.65	99.05 193.04	35 0 68.2	22.32	0.56	1.0	Shield, hand-mined	Dry, sand above GWL
Bruxelles Metro (Belgium)	21	Vinel and Herman (1969)	12 1 20.1	9.9	1.63*	150.0*	30.3	82.0	2.41	2.9	Shield, hand-mined	Bruxelles sand, loose calcareous $\bar{\phi} = 35^{o}$, $\bar{c} = 0$, e = 0.71
Tokyo, Haneda I (Japan)	22	Schmidt (1969)	10.8	6 6	1.64	56.0	17.0	34.3	1.15	1 5	Shield, hand-mined	sand, below GWL
Nagoya Utility Tunnel Point A (Japan)	23	"	7.45	4.1	1.82	45.0	22.0	13.25	0.41	3.1	Hand-mined in rect-angular shield	Dry sand
Nagoya Utility Tunnel. Point B (Japan)	24	"	7.45	4.1	1.82	53.0	25.8	13.25	[illegible]	3.8	"	"
Tokyo, Haneda II (Japan)	25	"	10.8*	6.6	1.64	132.0	40.0	34.3	1.56	4.5	Hand mining in shield top half of face breasted in benches.	Layers of loose sand N = 4-12
Toronto Subway Contract B-4 Point A (Canada)	36	Peck (1969)	12.3*	5.66	2.17*	19.3	6.82	22.32	0.45	1.2	Shield hand-mined	Crown in sand
San Francisco Bart (U.S.A.)	38	Peck (1969) Peck et al (1969)	-		2.05	-	-	-	-	0.56		cemented dense sand above GWL
Toronto Subway (Canada)	39	"	-	-	2.29	-	-	-	-	1.9	-	Dense sand, above GWL
Toronto Subway (Canada)	40	"	-	-	2.00	-	-	-	-	1.0	-	Crown in sand, below GWL

* Mean value

APPENDIX 4

EXTRAPOLATED CONVERSION CURVES FOR THE SETTLEMENT VERSUS DEPTH RELATIONSHIPS